AN ASTROPHYSICS DATA PROGRAM INVESTIGATION OF

A SYNOPTIC STUDY OF QUASAR CONTINUA

NASA Grant NAG8-689

FINAL REPORT

For the Period 1 October 1987 through 30 September 1990

Principal Investigator
Martin Elvis

September 1991

Prepared for:

National Aeronautics and Space Administration
George C. Marshall Space Flight Center
Marshall Space Flight Center, Alabama 35812

Smithsonian Institution
Astrophysical Observatory
Cambridge, Massachusetts 02138

The Smithsonian Astrophysical Observatory
is a member of the
Harvard-Smithsonian Center for Astrophysics

The NASA Technical Officer for this grant is Ms. Donna M. Havrisik, Code EM25 George C. Marshall Space Flight Center, Marshall Space Flight Center, Alabama

Final Management Report

ADP: 'Synoptic Study of Quasar Continua'

P.I.: Martin Elvis

This report summarizes the work undertaken on the above ADP grant. The work is now complete, with the submission of the major product, the 'Atlas of Quasar Energy Distributions' (Appendix A) being finalized for submission to the Astrophysical Journal Supplements. Other papers written as a result of this grant are included in Appendix B. The overall themes developed under this grant will be pursued in a Long Term Space Astrophysics Program grant, which will build on the data and methodology established under the ADP. The aim of the Long Term program will be to extend our knowledge of the quasar continuum shapes to high redshifts.

Once the QED (Quasar Energy Distributions) data base became sufficiently complete we began our 'synoptic' (*i.e.* multi-wavelength) analysis. This bore fruit immediately in the study of the 'accretion disk' Big Bump. Our first detailed study of the strength of the opt/uv bump strengths and shapes was undertaken. Four different measures of bump strength were made. These all correlate, albeit with scatter. All the measures clearly showed a range of bump strengths, most of which can be reproduced by reddening. A simple change in normalization of a 'bump' component also cannot reproduce the observed range of shapes. The resulting paper on 'Weak Bump Quasars' was published in Ap. J. Letters. Follow-up work looking at the whole range of 'Big Bump' strengths, and shapes followed.

Accurate Galactic column densities derived from Green Bank 140ft data were published in the Astronomical Journal. These column densities are some 10 times more accurate than those derived from the standard 'Bell Labs' survey of Stark et al. alone, and allow valuable constraints in fitting soft excesses to x-ray spectra. The work also has value for soft x-ray and EUV surveys (eg ROSAT, EUVE). Further work on this subject is planned due to the collapse of the 300ft, which would otherwise have undertaken an all-sky survey to this level of accuracy.

A paper on the variability of the soft excess in PG1211+143 resulted in a paper to the Ap. J. It is clear that the soft excess in PG1211+143 is persistent over 6 years (from an early, serendipitous, Einstein observation through the last EXOSAT observation), yet varies in amplitude on a short (weeks) timescale, demonstrating that it comes from a compact source region. If the variation is intrinsic, ie not due to changing absorption, then the emission cannot be from optically thin plasma.

A visit to Meudon to complete work on the 'soft-excesses' paper with Dr. Masnou was undertaken. The visit, by B. Wilkes, resulted in considerable progress on the 'soft-excesses' paper with J.-L. Masnou. Dr. Wilkes and Dr. Masnou characterized the 'ultra-soft' excesses in a more definitive fashion, modifying the conventional fitting procedure to make the strength of the excess the fitted parameter not the normal 'power law index'. The intercalibration of the Einstein MPC/IPC was investigated (with J-L. Masnou, Meudon, FRANCE) in order to confirm the new X-ray spectral results derived from this instrument combination. A paper on the soft X-ray excesses is in press with Astronomy and Astrophysics.

The EXOSAT ME and LE spectral data on 12 quasars (the complete set of good quality EXOSAT quasar data) were analyzed by A. Comastri (visiting from Univ. Bologna, ITALY). Results show interesting differences from the IPC results and use of the Boron filter suggests in a few cases that the high energy spectral slopes continue down to $\sim$1 keV. The 3LX and AlP filter data show strong excesses in most cases. A paper is in press in the Ap. J.

Our sub-millimeter observations from the JCMT were used in conjunction with the IRAS and other, ground-based, infrared data to constrain synchrotron and dust models for the infrared continuum in radio-quiet active galaxies and quasars. A paper has been published in MNRAS.

X-ray data for the Piccinotti sample were included in the data base. Optical and ultraviolet data, from our collaborators C. Boisson and M.J. Ward, were included for the Piccinotti sample. The data base software was enhanced to include basic model fitting functions (polynomial fitting to the data, integration under a curve, power-law and black body fitting) to allow a more quantitative investigation of the strength of the Big Bump, in particular to define the 'weak bump' quasars more carefully.

The 'TIGER' software was updated to use the new release 2.0 of SMONGO, which allows the use of color plotting. This makes our crowded data plots far easier to examine by distinguishing, e.g. different epoch observations from one another, or data from model fits. The SUN workstation color upgrade arrived and was installed. It has proved valuable in visualizing the multi-epoch data and in comparing data with models.

A Harvard astronomy department graduate student, Olga Kuhn, elected to work on the range of 'Big Bump' strengths and shapes for her research exam. She is concentrating on modeling the optical/ultraviolet 'Big Bump', in particular examining the range of accretion disk properties needed to explain the variety of shapes that are seen. She modified her accretion disk code to incorporate the

effects considered by B. Czerny which will allow more sophisticated modeling of the optical/ultraviolet 'Big Bump' color-color plots. She then made 'mixing curves' of these models with various fractions of power-law slopes with a number of spectral indices. These were compared with the IR/V/UV color-color plot for the data (as in the Weak Bump Quasars paper), and with other color-color plots, e.g. IR/UV/SX. O. Kuhn attended the SAAS-FEE School (Switzerland) on 'Active Galactic Nuclei', a week-long course of lectures given by leaders in the field designed for graduate students. Her research exam is due soon and her write-up for that exam will be recast as a paper for the Ap. J.

The accretion disk modeling code being developed by O. Kuhn and J. McDowell, based on the original code of B. Czerny and was used to generate the model locus described above. The code has shown that the effects of General Relativity and of electron Scattering do not change the shape of this locus, but do strongly affect the derived physical parameters (mass and accretion rate). This implies a degeneracy in these parameters that the present data cannot lift. The effects of inclination and of using a Kerr metric for the black hole are now being explored.

Two summer students, Elisha Polomski and Sally Oey, were employed. Their main task was the reduction of the optical continuum and line data. They made major progress in reducing the optical data that is part of the data base. Many of the optical spectra are now ready to be included in the TIGER data base. Several more optical observing runs remain to be reduced however.

The peculiar object PG1407+265 has an uninterpretable spectrum. We no longer believe that we know its redshift; we are not even certain that it is a quasar. A paper is in preparation describing this unusual object.

A visit to the IUE RDAF at GSFC by J. McDowell resulted in the complete reduction of some 60 IUE spectra of quasars in our sample. This completed our data base. It also added information on time variability in the ultraviolet which is vital to our confidence in our non-simultaneous multi-wavelength energy distributions. The sample of 37 quasars with 'complete' continuum coverage has been analyzed to examine the shapes of the optical/ultraviolet 'Big Bump'. A new color-color diagram was constructed using octave wide near-IR, optical and UV bands. This diagram allows the distribution of the slope/strength and the curvature of the Big Bump to be displayed for the whole sample in a model independent fashion. The locus of points described by accretion disk models can be plotted on this diagram, as can the effects of dust reddening, the inclusion of a galaxian (starlight) component, and of a non-thermal power-law component. The sample objects are restricted to one part of this diagram. The accretion disk locus forms one boundary to this

region, suggesting that it has some physical significance. However the mixing of disk models with reddening, galaxy starlight or power-law components does not naturally reproduce the distribution of data points. This promises to be a valuable technique for understanding this major component of the quasar continuum.

The complete sample of Quasar Energy Distributions has been assembled with care taken over variability and inter-wavelength calibration. Host galaxy contributions to the quasar continuum light have been estimated from the literature and subtracted. The set of QEDs are being made available in digital form via anonymous ftp from SAO.

As a result of this study of quasar energy distributions we find that:

1. The bolometric luminosity of the quasars is a factor of 12.7 ± 4.2 times the monochromatic visual luminosity, using a simple interpolation in the EUV; the more accurately defined 'UVOIR luminosity' is a factor of 8.5 ± 2.9 times the monochromatic visual luminosity.

2. The strength of the 'ultraviolet bump' varies by a factor of 10, but typical objects have an ultraviolet luminosity three times their near infrared luminosity.

3. "The submillimeter break" often occurs at wavelengths of 60μm or shorter. The IR emission can be weak relative to the optical.

4. Objects with weak ultraviolet bumps are luminous in the far infrared.

5. We confirm the near constancy in wavelength of, and ubiquity of, the "1 μm inflection" first noticed by Neugebauer et al (1979) and studied by Elvis et al (1986) and Neugebauer et al (1987).

6. The shape of the ultraviolet bump varies significantly from object to object, rising steeply in the optical for some objects, but remaining flat there for others.

7. The ultraviolet variability of these objects (chosen to exclude strongly optically variable quasars) is typically less than a factor of 2 on a timescale of years, and many vary by less than twenty per cent.

8. While we confirm the correlations found by Kriss (1988), we suspect that they may be induced by host galaxy contamination at low luminosities.

9. The 'infrared to x-ray connection' discussed by Carleton et al (1987) is not present in this sample.

The publication of this Atlas completes the work under the ADP Grant on the 'Synoptic Study of the Quasar Continuum'.

Refereed Papers

1989 Accurate Galactic N_H Values Toward Quasars and AGN (M. Elvis, F.J. Lockman, and B.J. Wilkes), ***Astronomical Journal***, **97**, 777.

1989 Weak Bump Quasars (J.C. McDowell, M. Elvis, B.J. Wilkes, S.P. Willner, M.S. Oey, E. Polomski, J. Bechtold, and R.F. Green), ***Ap.J.Letters***, **345**, L13.

1991 Millimetric Measurements of Hard X-ray Selected Active Galaxies: Implications for the Nature of the Continuous Spectrum (A. Lawrence, M. Rowan-Robinson, A. Efstathiou, M.J. Ward, M. Elvis, J.C. McDowell, M.G. Smith, W. Duncan, and E.I. Robson), ***Mon.Not.R.Astr.Soc.***, **248**, 91.

1991 Persistence and Change in a Quasar X-ray Spectrum (PG1211+143) (M. Elvis, P. Giommi, J. McDowell, and B.J. Wilkes) ***Ap.J.***, in press (Sept. 10).

1991 Soft X-ray Excesses in Einstein Quasar Spectra (J.-L. Masnou, B.J. Wilkes, M. Elvis, K. Arnaud, and J.C. McDowell), ***Astronomy and Astrophysics***, in press.

1991 EXOSAT X-ray Spectra of Quasars (A. Comastri, G. Setti, G. Zamorani, M. Elvis, P. Giommi, B.J. Wilkes, and J. McDowell), ***Ap.J.***, submitted.

1991 An Atlas of Quasar Energy Distribution (M. Elvis, J.C. McDowell, B.J. Wilkes, et al.), in preparation for ***Ap.J. Suppl.***

Papers Presented at Meetings

1989 The Ultraviolet Continua of Active Galactic Nuclei (M. Elvis), ***Comments on Astrophysics***, **14**, no. 3, 177.

1989 Is There a Relation between Optical Emission Line Strengths and Continuum Shapes? (B.J. Wilkes, M. Elvis, and J. McDowell), IAU Symposium 134 "Active Galactic Nuclei", eds. J. Miller and D.E. Osterbrock, [Dordrecht: Reidel], 187.

1989 The Infrared and X-ray Continuum of Quasars: Is There a Connection? (M. Elvis, J. McDowell, and B.J. Wilkes), IAU Symposium 134 "Active Galactic Nuclei", eds. J. Miller and D.E. Osterbrock, [Dordrecht: Reidel], 184.

1990 XUV Excesses in Quasars (M. Elvis, B.J. Wilkes, and J.C. McDowell), in "Extreme Ultraviolet Astronomy", eds. R. Malina and S. Bowyer, [New York: Pergamon], p.238.

1990 The Soft X-ray Excess in ***Einstein*** Quasar Spectra (B.J. Wilkes, J.-L. Masnou, M. Elvis, J. McDowell, and K. Arnaud), in "X-ray Astronomy", proceedings of the 23rd ESLAB Symposium [Noordwijk: ESA], ed. N.E. White, p.1081.

1990 Inclination Effects for Kerr Disks (J. McDowell, O. Kuhn, M. Elvis, and B.

Wilkes), in Proceedings of IAP Conference on Accretion Disk, in press.

1991 Soft X-ray/XUV Excesses in ***Einstein*** Quasar Spectra (B.J. Wilkes, M. Elvis, J. McDowell, J-L. Masnou, and K.A. Arnaud), ***BAAS***, 21, no. 4, 1225.

1989 Ultraviolet and X-ray Energy Distributions of IPC Quasars (J. McDowell, B.J. Wilkes, and M. Elvis), ***BAAS***, 21, no. 4, 1225.

1989 Quasar Accretion Disk Colors (O. Kuhn, J.C. McDowell, M. Elvis, and B.J. Wilkes), ***BAAS***, 21, no. 4, 1131.

1990 An Atlas of Quasar Energy Distributions (J. McDowell, M. Elvis, and B.J. Wilkes), ***BAAS***, 22, 1192.

1990 The Relation Between Radio and X-ray Emission in Quasars (B.J. Wilkes, M. Elvis, J.C. McDowell, and P. Shastri), ***BAAS***, 22, 1193.

1990 Using AGN Colors as Diagnostics for Accretion Disks (O. Kuhn, J. McDowell, M. Elvis and B.J. Wilkes), ***BAAS***, 22, 1193.

Colloquia Given

Univ. Penn., PA (M. Elvis), *Quasar Continua.*

STScI, MD, (M. Elvis), *Constraints on the Continuum Forms of Quasars.*

Penn. State, PA (M. Elvis), *Continuum emission features in Quasars.*

Columbia Univ., NY (J.McDowell),

MSFC, AL (J.McDowell),

Northeastern University, MA (B. Wilkes),

Queen Mary College, London, (B. Wilkes),

'Accretion Disk Workshop', Santa Barbara (M. Elvis0.

'Orientation Effects in AGN and Quasars', Carnegie Observatories, Pasadena(J. McDowell).

Appendix A

ATLAS OF QUASAR ENERGY DISTRIBUTIONS[1]

MARTIN ELVIS[2], BELINDA J. WILKES[2], JONATHAN C. MCDOWELL[2,4], RICHARD F. GREEN[5], JILL BECHTOLD[3], STEVEN P. WILLNER[2], M.S. OEY[2,3] ELISHA POLOMSKI[2], AND ROC CUTRI[3]

Version: August 21, 1991
To be submitted to *Astrophysical Journal Supplement Series*

[1]Based in part on data acquired with the *International Ultraviolet Explorer* satellite, operated at the Goddard Space Flight Center for the National Aeronautics and Space Administration, the Multiple Mirror Telescope (MMT), a joint facility of the Smithsonian Institution and the University of Arizona, and the Infrared Telescope Facility (IRTF), a joint facility of NASA and the University of Hawaii.

[2]Harvard-Smithsonian Center for Astrophysics

[3]Steward Observatory,University of Arizona

[4]NASA Marshall Space Flight Center

[5]Kitt Peak National Observatory, NOAO, operated by the Association of Universities for Research in Astronomy, Inc., under contract with the NSF.

Abstract

We present an atlas of the spectral energy distributions (SEDs) of 33 normal, non-blazar, quasars over the whole available range (radio to 10 keV X-rays) of the electromagnetic spectrum. XX radio-quiet and XX radio-loud quasars are included.

We discuss the effects of the limited dynamic range of flux density in the different parts of the spectrum on the range of SED shapes that are seen.

We present a mean energy distribution for radio-loud and radio-quiet quasars, along with an analytic representation appropriate for theoretical modelling.

ATLAS OF QUASAR ENERGY DISTRIBUTIONS[1]

MARTIN ELVIS[2], BELINDA J. WILKES[2], JONATHAN C. MCDOWELL[2,4], RICHARD F. GREEN[5], JILL BECHTOLD[3], STEVEN P. WILLNER[2], M.S. OEY[2,3] ELISHA POLOMSKI[2], AND ROC CUTRI[3]

Version: September 6, 1991
To be submitted to *Astrophysical Journal Supplement Series*

[1]Based in part on data acquired with the *International Ultraviolet Explorer* satellite, operated at the Goddard Space Flight Center for the National Aeronautics and Space Administration, the Multiple Mirror Telescope (MMT), a joint facility of the Smithsonian Institution and the University of Arizona, and the Infrared Telescope Facility (IRTF), a joint facility of NASA and the University of Hawaii.

[2]Harvard-Smithsonian Center for Astrophysics

[3]Steward Observatory,University of Arizona

[4]NASA Marshall Space Flight Center

[5]Kitt Peak National Observatory, NOAO, operated by the Association of Universities for Research in Astronomy, Inc., under contract with the NSF.

Abstract

We present an atlas of the spectral energy distributions (SEDs) of 33 normal, non-blazar, quasars over the whole available range (radio to 10 keV X-rays) of the electromagnetic spectrum. XX radio-quiet and XX radio-loud quasars are included.

We discuss the effects of the limited dynamic range of flux density in the different parts of the spectrum on the range of SED shapes that are seen.

We present a mean energy distribution for radio-loud and radio-quiet quasars, along with an analytic representation appropriate for theoretical modelling.

1 Introduction

One of the reasons that main sequence stars are much better understood than quasars is that they radiate (almost) black body spectra at between ~4000 and ~30,000 K, so that their black body peak moves conveniently through the optical band. The resulting strong color changes allowed the early recognition of the main sequence in the Hertzprung-Russell diagram. By showing that most starts lay in a restricted band of color and luminosity this diagram provided a crucial input to theories of stellar structure. The current lack of understanding of quasars may similarly be due to the distribution of their continuum light. Because the quasar phenomenon covers an extremely broad range of wavelengths it is hard to see continuum features analogous to the black body peak in normal stars. Quasars seem in fact to emit almost constant power per decade of frequency from 100μm to at least 100keV (see *e.g.* figure 1 of Carleton et al., 1987). While this equipartition is surprising (and may be to some extent an observational artifact, see §6) it contains too little information to constrain theoretical ideas. Overcoming this problem requires the assembly of Spectral Energy Distributions (SEDs) for sizable samples of quasars over the whole accessible range of the electromagnetic spectrum from far-infrared to hard X-rays.

In this paper we present SEDs for a sample of 33 quasars. We concentrate on 'normal', (*i.e.* non-Blazar)quasars. Our primary selection criteria were: existing *Einstein* observations at good signal-to-noise (to ensure good x-ray spectra); an optical magnitude bright enough to make an IUE spectrum obtainable. This combination leads to some IRAS upper limits. We consider the effects of these selection criteria in some detail in section 4.

Several previous studies of quasar SEDs have been published. Each emphasized a particular region, and none considered the X-rays in detail. Infrared to optical for the PG quasars were presented in Sanders et al (1989) with an emphasis on explaining the infrared ; near-infrared to ultraviolet SEDs for IUE observed quasars were presented by Sun and Malkan (1989). Our study is different in that it includes X-ray data for all the objects, divided into three energy bands in many cases, and takes care to include both IUE and IRAS data. The sample is fairly evenly divided between radio-quiet and radio-loud objects.

2 Continuum Features

In Fig. 1 the radio to x-ray rest frame energy distributions of two typical quasars, 3C273 and Mkn586, are shown. All energy distributions are plotted as log νf_ν vs. log ν; such plots give the best indication of the frequency ranges where most energy is released (since νf_ν is the flux per logarithmic frequency interval). The x-ray data are

indicated with a 'bow-tie' symbol representing a power law fit with both the best fit slope and the 90 per cent confidence limit slopes drawn in. No data are available in the extreme ultraviolet 'gap' beyond the Lyman limit where our galaxy is opaque.

In the 1-100 μm infrared both quasars are almost flat (Ward et al. 1987, Neugebauer et al. 1987, hereafter N87). A single, nearly horizontal, power-law fits the IR points reasonably well and intersects the x-ray point at about 1 keV. We will call deviations from this power-law 'continuum features'. There are four prominent features of this kind.

The power output always drops in the millimeter band (the "mm-break", Fig. 1) but the size of the drop varies dramatically from object to object. Quasars in which the drop is only 2 decades are called "radio-loud" (e.g. 3C273). The great majority of quasars have a much stronger mm-break of 5 or even 6 decades (Condon et al 1981, Kellermann et al. 1989) and are called "radio-quiet" (e.g. Mkn586). This distinction between radio-loud and radio-quiet quasars is the oldest in the quasar literature and goes back to the 'blue interlopers' found in early radio source identification work (Sandage 1965). Radio-quiet objects are much the more common, by about a factor 10. The mm-break is the strongest feature in normal quasar continua.

The optical-ultraviolet continuum rises above the infrared and forms a "UV bump" (Shields 1978, Malkan and Sargent 1982, N87). Variability studies show that this is a separate component from the infrared (Cutri et al. 1985) since it varies much more strongly. This big bump is most often interpreted in terms of thermal emission from an accretion disk (e.g. Malkan 1983, Czerny and Elvis 1987). The beginning of the bump is marked by an inflection between 1 and 1.5 μm in the rest frame; this "1 μm inflection" is the only continuum feature whose wavelength is well defined.

X-ray spectra of many radio-loud quasars and high luminosity Seyfert 1 galaxies rise to high frequencies in log νf_ν vs. log ν energy distributions (Mushotzky 1984, Bezler et al. 1984, Turner and Pounds 1989, Williams et al 1991). They cannot then be an extension of a flat, or slightly falling, infrared power-law, as has been suggested for the radio-quiet objects (Carleton et al 1987). A new emission component must be emerging in the x-rays in these objects. This 'hard x-ray component' at $\sim \geq 1$ keV is the third clear feature of normal quasar continua. It is not always seen.

The most recently identified continuum feature is the 'XUV excess' (e.g. Arnaud et al 1985, Wilkes and Elvis 1987, Turner and Pounds 1989, Masnou et al 1991). The 1 keV spectrum of quasars is often fitted with a power law spectrum since the available spectral resolution is very low; studies using the *Einstein* IPC and EXOSAT showed that excess flux above this power law was often present in the ultra-soft (0.3 keV and below) region of the spectrum. It is possible that the XUV excess is the same physical component as the ultraviolet bump since the energy distribution rises towards the EUV from both sides of the unobserved spectral region; it is present in about half of objects (both Seyferts and quasars) studied.

3 The IPC UV sample

We have carried out an extensive program of quasar continuum observations over the past five years, the results of which we present here. Since we believe it to be important to include x-ray observations, we restricted ourselves to objects that had been observed with the Imaging Proportional Counter (IPC, Gorenstein, Harnden and Fabricant 1979) instrument on the *Einstein Observatory* (HEAO 2, Giacconi et al 1979) satellite. We note that this introduces a bias towards objects which are low redshift, moderate luminosity and have strong x-ray to optical flux ratios; the sample is heterogenous and not flux-limited. The objects were selected mainly from the PG and 3C and Parkes catalogs. No single completeness criterion could be used however, because of the quasi-random way in which the original *Einstein* observations were made.

We have selected a subsample of quasars which have sufficient counts in the IPC to give a reasonably constrained power law spectral fit, and which are optically bright enough (V< 17) to be observable with IUE: the 'IPC UV sample'. Approximately half the sample is radio-loud and half radio-quiet. The x-ray and ultraviolet data have been combined with IRAS space-based infrared data and ground-based optical, infrared and radio observations to construct the complete energy distributions.

The 33 quasars in the Einstein UV sample are listed in Table 1(a). The sample has substantial overlap with the work of Elvis et al (1986) and Wilkes and Elvis (1987). The table gives the common name of the quasar as well as its catalog number in the *Einstein Observatory Source Catalog* (Harris et al 1991), and the name of the associated host galaxy where appropriate. Both B1950 and J2000 coordinates are provided, as well as the redshift and typical V magnitude. The estimate of the foreground Galactic hydrogen column density (in units of 10^{20} cm^{-2}) is listed together with a reference. Most of the column estimates are accurate values from Elvis, Lockman and Wilkes (1989). Finally, each object is given a classification. The classifications are as follows: radio-quiet (RQ), broad absorption line (BAL, a subset of RQ), and radio-loud (RL). Radio-loud quasars are further subdivided into superluminal (SL, a subset of RL), flat spectrum compact (FSC), steep spectrum compact (SSC), and Fanaroff-Riley class 2 steep spectrum doubles (FR2). Further, following the convention of Veron-Cetty and Veron (1987) and Schmidt and Green (1983), radio-quiet objects with absolute visual magnitude fainter than -23.0 calculated according to their prescription are designated as Seyfert 1 (Sy1); two objects in the UV sample satisfy this criterion. Table 1(b) lists the corresponding properties of 37 other quasars for which ultraviolet, optical and infrared data is presented in this paper. These other quasars were observed by *Einstein* or EXOSAT but are not included in the main sample either because of poor quality x-ray data, strong optical variability, low luminosity or low optical flux.

Further properties of the quasars in the UV sample are listed in Table 2, and

illustrated as histograms in Fig. 2, with the shaded regions corresponding to the radio-loud objects. The numerical value of the radio-loudness, R_L, is defined to be the logarithm of the ratio of observed core 5 GHz flux to flux in the optical B band, and an object is considered to be radio-loud if $R_L = \log(f_{5GHz}/f_B) > 1$. Note that this definition is based on observed frame fluxes, but corrections to the rest frame do not make an important difference. In each case an attempt has been made to estimate a core flux on arcsecond scales, since we are studying the properties of the compact central source at other wavelengths and wish to neglect the extended radio source, if any. We were unable to find maps of the two most southern sources, and the VLA fails to resolve the core of 3C48 from the compact steep spectrum source in which it is embedded (Spencer et al 1989). For sources where information on the fluxes of individual radio components was available, we have calculated the Browne parameter R_B which gives the ratio of core to extended emission at 5 GHz, and is believed to be correlated with source orientation (Orr and Browne 1982).

Monochromatic luminosities ($\log(\nu L_\nu/\mathrm{erg/s})$) in the visual ($L_V$ at 5400$\AA$ in the rest frame) and x-ray (L_X at 2 keV) are tabulated, as are the bolometric luminosities derived later in this paper. The absolute visual magnitude is also given, derived using the formulae of Veron-Cetty and Veron (1987) but using our chosen cosmological parameters. α_x is the x-ray spectral index derived from the IPC results; the ultraviolet to x-ray two-point spectral slope α_{ox} is defined from 2500$\AA$ to 2 keV in the rest frame. These spectral indices are conventional energy indices, $\alpha = -d\log f_\nu/d\log\nu$.

4 Data

4.1 Overview

To assemble the SEDs for the 33 quasars required observations on 12 different telescopes, using 16 different instruments, in locations from ground-based to space. Because of this diversity of observing techniques it is necessary to describe each data set and the corrections made to it carefully. Table Nof their characteristics (wavelength range, $\Delta\lambda/\lambda$, typical signal to noise ratio). Also noted is the faintest detectable flux for each detector, and the brightest observed flux of an AGN in the band. These will be used in section §XX when discussing selection effects. Figure XX shows the bands covered graphically, and notes the type of detector, observing site, conventional names for the bands, and regions for which interstellar opacity is important. In the following sections each band is discussed in turn.

4.2 X-ray

The 'x-ray band' covers two full decades of the spectrum. Even though most x-ray spectra have low resolution it is still useful to divide the band into three parts: 'hard x-ray', covering 2-10 keV; 'soft x-ray', covering 0.3-2 keV; and 'ultra-soft x-ray' covering 0.1-0.3 keV. All the 33objects in our sample were observed in the soft x-ray band in 1979 or 1980 with the IPC instrument on *Einstein*. The limited spectral resolution of this instrument allows us to characterize the $0.1 - 3.5$ keV spectrum as a single power law modified by foreground absorption. For most of the objects in the sample, the data and spectral fits are presented in Wilkes and Elvis (1987). Although the foreground Galactic absorption is now well determined for our objects, we choose to retain the earlier fits in which the Galactic absorption is allowed to vary freely, since the presence of an ultra-soft excess in the incident spectrum is almost equivalent to a reduction in the absorption, and thus we get a better estimate of the slope in the soft band (beyond the excess) than if the absorption is fixed at its true value.

Ultra-soft excesses were searched for in thirteen of the highest signal-to-noise observations. The data were re-analysed by Masnou et al (1991) using a two power law model and including data out to 10 keV from the MPC instrument, revealing the presence of an ultra-soft x-ray excess component in eight of the objects. This is indicated as a separate data point at 0.2 keV on our energy distribution plots (Fig. 4). In these two power law fits, the foreground absorption was fixed at the known (Elvis, Lockman and Wilkes 1989) value. The object PG1211+143 was studied in a separate paper by Elvis et al (1991). These results are summarized in Table 3 together with several previously unpublished spectral fits. The analysis for the new fits was identical to that of Wilkes and Elvis (1987). Contour plots for the new fits are presented in Fig. XX.

Hard x-ray data are available for about half the sample from EXOSAT ME (Turner and Pounds 1989, Comastri et al 1991), and *Ginga* observations (Williams et al 1991) and the corresponding power law fits are listed in Table 3. The effects of foreground absorption are relatively unimportant in this band.

4.3 Ultraviolet

All of the 33 UV sample objects have been observed with both the long and short wavelength cameras on the *International Ultraviolet Explorer* between 1978 and 1989. A total of 19 exposures were made explicitly for this program, many were long wavelength observations needed to fill in pre-existing short wavelength data. In addition, 108 further spectra were extracted from the Regional Data Analysis Facility archive. Both sets of data were analysed uniformly using the GEX Gaussian extraction algorithm (Urry and Reichert 1988) which is the most effective for our faint targets. Bad data points (reseau marks, cosmic ray hits and microphonic noise in the

LWR) were removed interactively. We then averaged the ultraviolet flux within each of a set of wavelength bands chosen to avoid strong emission lines, converting the somewhat noisy spectra to a small set of relatively well determined continuum flux estimates. The continuum wavelength bands are defined to be fixed in the rest frame of the object (Table 4) and are 50$\AA$ wide shortward of 1900$\AA$, 100$\AA$ wide shortward of 5000$\AA$ and 200$\AA$ wide beyond that wavelength. Bands which overlapped a region of avoidance 8000 km/s to either side of strong broad lines or 2000 km/s to either side of strong narrow lines were omitted. We avoid the lines $L\alpha\lambda1215$, $OIV\lambda1402$, $CIV\lambda1549$, $CIII]\lambda1909$, $MgII\lambda2798$, $NeV\lambda3426$, $[OII]\lambda3727$, $[OIII]\lambda5007/5009$, $NeII\lambda3869/3968$, $OI\lambda6300$, and the Balmer lines $H\alpha$ to $H\delta$. We note that weak lines and the blended [FeII] lines are not avoided and so these are included in our 'continuum' fluxes.

Table 5 lists the IUE exposures and the observed frequencies and fluxes corresponding to each continuum band. Note that the fluxes are given as $\log(\nu f_\nu/\mathrm{Jy\ Hz})$ in the observed frame, and that they are not corrected for foreground extinction. (1Jy Hz $= 10^{-23}$erg cm^{-2} s^{-1}). The first row on each page gives the rest frame wavelengths of each band. Then there is a header line for each object which gives the name of the object and the logarithm of the corresponding observed frequencies in Hz. This is followed by two lines for each observation giving the date of the observation (in the first column) followed by the logarithmic fluxes ($\log(\nu F(\nu)/1$ Jy Hz)) on the first line and the errors in the logarithmic fluxes on the second line. The errors are 1 σ internal statistical errors derived from the scatter in the individual data points prior to binning.

Table 5(a) contains data for the UV sample, while Table 5(b) contains data for other objects observed in the program. The optical spectrophotometry for the probable high redshift object PG1407+265 (see discussion below) is also included in Table 5(a) for convenience, since the rest wavelengths for the observed optical spectrum lie in the ultraviolet.

4.4 Optical

Spectrophotometric observations for 14 objects were obtained with the Red ($\sim 4500-7500\AA$) and Blue ($\sim 3200-6400\AA$) Spectrographs or the FOGS (Faint Object Grism Spectrograph, $\sim 4500-7500\AA$) on the MMT. Blue spectrograph observations were made through a 5" circular aperture at air mass below 1.4 to minimize light lost due to atmospheric dispersion. Objects were then reobserved at highter resolution with a 1x3" aperture. A nearby standard star was observed immediately before or after the quasar observation. For both red spectrographs the large aperture used was 10x20" and the small one was a 1" long slit. In all cases the large aperture observations were used to flux calibrate the accompanying, higher S/N small aperture observations in order to obtain $\sim 5-10\AA$ spectral resolution. The data were reduced

in the standard manner, using IRAF. To ensure the photometric accuracy of these spectra, BVRI CCD photometric data were obtained on the FLWO 24-inch telescope within one week of the MMT observations. Table 7 gives the BVRI photometry values, estimated within a 14 arcsecond beam; Table 8 lists the continuum fluxes observed with FOGS and MMT spectrograph. As with the IUE data, emission lines have been avoided by averaging the logarithmic fluxes in the line-free, rest frame continuum bands listed in Table 4.

Optical spectrophotometry for the 18 PG objects in our program were presented by Neugebauer et al (1987, N87). These data were already corrected for Galactic reddening; this correction is removed here using the same law used by those authors for consistency with our database (Neugebauer, G., private communication). This allows us, and others, to apply a uniform Galactic dereddening to all of our optical, ultraviolet and soft x-ray data. Since the values of $E(B-V)$ used in N87 were not given in that paper, we tabulate them here (Table 6) for all the objects in that paper together with the values obtained using the prescription described below (Section 6.2).

Optical data have also been included in the figures and analysis from Neugebauer et al (1979), Treves et al (1988), Sitko et al (1982), Condon et al (1981), Adam (1978,1985), and McAlary et al (1983).

4.5 Near Infrared (1-3.5μm)

Table 9 records measurements of JHKL ($1.2-3.5\mu m$) photometry obtained at the MMT and the IRTF. The table gives the magnitudes and errors on the Johnson scale, the date of observation and the telescope and aperture used.

We also included infrared photometry from Glass (1982), Rieke (1978), Condon et al (1981), Hyland and Allen (1982), Sitko et al (1982), Rudy, LeVan and Rodriguez (1982), Ward et al (1987), and Neugebauer et al (1987).

4.6 Far Infrared ($\geq 10\mu$m)

Table 10 gives measurements at N and Q (10, 20 μm) made at IRTF and the United Kingdom Infrared Telescope (UKIRT). At the IRTF, the CT1 bolometer was used with a 6" beam and an east-west chopper throw of 30". At UKIRT the UKT8 system was used with an 8" beam and a 20" east-west chopper throw. All magnitudes were derived from comparisons with standard stars (Tokunaga 1984, Elias et al 1982). Magnitudes are listed on the instrumental system, i.e. without color corrections.

The Infrared Astronomical Satellite (IRAS, Neugebauer et al 1984) surveyed the sky in 1983 at far infrared wavelengths ($12-100\mu m$). We have determined fluxes

or upper limits at the positions of each of our sources. Where pointed Additional Observations (AO) were made, these were used; otherwise 'lineadd' (LA) estimates were made from the survey scans. This procedure allows a better estimate of the local background and errors in a particular measurement. The coadded survey maps were used to check for the presence of contaminating cirrus. The results are listed in Table 11; they are consistent *(This is currently a lie!)* with the results of Neugebauer et al (1986) and Sanders et al (1989) where we have objects in common (for the UV sample, 6 objects are previously unpublished). In some cases the 100μm upper limits are rather weak due to the presence of cirrus in the region of the source. Upper limits (3σ) are listed for each source when no detection was made in any of the IRAS bands.

4.7 Radio and Millimetre

We have gathered core radio fluxes at 5 GHz for the UV sample from the literature (Table 12(a)). The PG sample study with the VLA by Kellerman et al (1989) was given preference over other references in the calculation of radio-loudness. By 'core' we mean the flat spectrum compact component which appears to be physically distinct from the steep spectrum diffuse emission. Since this steep spectrum emission can itself be relatively compact in angular size (e.g. 3C48), we do not use a fixed angular size to define the core, although in practice because detailed spectral information is not usually available we often use flux unresolved within a 1 arcsecond beam as our criterion. In the absence of spectral data this is an upper limit on the flat spectrum core flux. Beamsizes are given in the table. In Table 12(a) we also list measurements at other frequencies; and in Table 12(b) we list estimates of the flux of any extended radio source associated with the object.

Millimetre wave data or upper limits are available for about half the sample (Table 13). Only III Zw 2 and 3C 273 are strong millimetre emitters, but four other sources have weak detections.

5 Corrections

5.1 Variability and averaging

One limitation on our dataset is that the observations are typically not simultaneous, although the optical and IR data were generally obtained within about one month. For many of the objects we have observations at at two epochs (rarely more) in a given waveband, so we can make a crude estimate of the degree of variablilty. In table 14 we list the observed range of variablity, F_{max}/F_{min}, and the associated timescale, at rest wavelengths in the near infrared, optical, mid ultraviolet and far ultraviolet. Fig.

XXX. It can be seen that in the optical and infrared variability is not a serious problem for these 'normal' quasars, but that in the ultraviolet the variability is significant on timescales of a few years, although typically (13 out of 18 cases) it is less than a factor of two. These results indicate somewhat less variability found by Kinney et al (1991). *We have to address this problem!*

To generate a single mean energy distribution for each quasar, we have taken an average (in $\log \nu F(\nu)$) of all the data in each frequency bin. However, for the IUE data, we have been selective in the exposures we chose to include in the average. Specifically, where simultaneous data from the long (LWP/LWR) and short (SWP) wavelength cameras were available, we have included them and excluded 'orphan' LWP/LWR or SWP exposures in order to avoid spurious steps in the data due to variability. Objects affected are Q0007+106, Q1100+772, Q1146-037, Q1202+281, and Q1613+658. Further, when one exposure had significantly lower signal-to-noise than the rest available for a given object, it was omitted (Q1545+210, Q1613+658, and Q1721+343).

5.2 Magnitude scales

To include the optical and near infrared photometric data in the energy distributions, we have adopted for each band an effective wavelength and an absolute zero point appropriate for a flat energy distribution. We used the Hayes (1975) calibration of Vega, extended to other wavelengths by matching to a Kurucz (1979) theoretical model (9400K, $\log g = 3.95$). We convolved the Vega energy distribution with filter shapes from Tokunaga (1986) and Johnson (1965) to obtain absolute calibrations, assuming that Vega has a magnitude of +0.03 in all bands. However, we did not include the effects of atmospheric absorption in the calculation. The resulting absolute calibrations are listed in table 15. The color corrections are important for the optical bands but negligible in the infrared.

5.3 Extinction corrections

Corrections for foreground (Galactic) extinction are important in the optical, UV and soft x-ray. The x-ray spectral fits of table 3 already include correction for the line of sight absorption column as discussed above. A single extinction correction is applied to all the rest of the data, using an extinction law based on that of Savage and Mathis (1979) in the visible and ultraviolet, and Rieke and Lebofsky (1985) in the infrared beyond $3\mu m$, Table 16. The magnitude of the correction has been estimated from the Galactic neutral hydrogen column by assuming a fixed conversion of $N(HI)/E(B-V) = 5.0 \times 10^{21} \mathrm{cm}^2\ \mathrm{mag}^{-1}$ (Burstein and Heiles 1978). The Galactic HI column (Table 1) has been accurately measured with a narrow beam and good stray

radiation corrections in all but a few cases using the 140 ft Green Bank radio telescope (Elvis, Lockman and Wilkes 1989). The value for 3C 273 was taken from Dickey, Salpeter and Terzian (1978). In the three remaining cases it has been estimated from Heiles and Cleary (1979) or Stark et al (1984)

5.4 Cosmological model

We have adopted a standard Friedmann-Robertson-Walker cosmological model with $\Omega_0 = 2q_0 = 1$ and $H_0 = 50\text{km s}^{-1}\text{Mpc}^{-1}$. After Galactic reddening corrections were applied, the data were blueshifted to the rest frame. Since in the rest frame we are working with the complete energy distributions, no k-corrections and no assumptions about the intrinsic spectrum are required.

5.5 Host Galaxies

Although the overall energy output of our sample objects is dominated by the active nucleus, in the near infrared and optical the host galaxy can make a significant contribution. In a few cases (Q0049+171, Q1426+015, Q1501+106, Q1613+658) where a strong host galaxy is present in optical images and large aperture photometric data shows a significant excess over the small aperture spectrophotometry, we omit the photometric data from the final energy distributions.

Table 17 gives absolute magnitudes of the host galaxies and central point sources as found in the literature for 17 of the UV sample quasars. In cases where the change in the near infrared energy distribution is more than 5 per cent, we have subtracted a host galaxy template normalized to the quoted host galaxy magnitude. Our host galaxy template is based on the Sab galaxy model of Pence (1976).Fig. XX shows the host galaxy subtracted energy distributions.

5.6 PG 1407+265

The redshift of PG 1407+265 (= 2E 3196) is uncertain; the object has very weak emission lines, the only certain feature coming at 5500$\AA$. An identification of this as Mg II and the weak presence of CIII] led Schmidt and Green (1983) to propose the redshift as z=0.944. The absence of a clear Lyman alpha line in our IUE spectrum caused us to consider lower redshift identifications, including blueshifts, but no choice of redshift allows normal quasar line ratios. We have adopted the high redshift given by Schmidt and Green because of the position of a prominent continuum feature, namely the inflection at the beginning of the ultraviolet bump. The rest wavelength of this feature lies between 1.0 and 1.5 microns for all our other objects, and in this object occurs at an observed wavelength between 2.0 and 2.4 microns, which lends

support to the high redshift estimate. A weak broad line is marginally detected in the LWP spectrum. If this line is Lyman alpha, it peaks at approximately z=0.99, a velocity shift of 15000 km/s with respect to the Mg II line.

We continue to adopt the Schmidt and Green value despite the absence of definitely observed hydrogen lines. We note that the broad width of the line, the overall continuum shape, the lack of strong optical variability and the x-ray to optical flux ratio indicate that the object is indeed a quasar rather than, for instance, a star, a BL Lac object, or some more exotic object. The near infrared to ultraviolet spectrum of PG1407+265 is presented in Fig. 3. We believe that the sharp drop in flux level between the LWP and SWP spectra at $2000 \pm 100\AA$ is likely due to ultraviolet variability rather than a Lyman absorption system (which would be at $z \sim 1.1$, inconsistent with the adopted redshift). Note the good agreement in flux level at the overlap between the two optical spectra and the smooth continuation of the spectrum made by the infrared photometry, implying a lack of variability.

6 Properties of the energy distributions

6.1 Luminosities: Bolometric and individual bands

In Fig. 4 we present two energy distributions for each object, an overall view and a closeup of the infrared to ultraviolet region. The overall view covers a fixed flux range of ten decades and illustrates the radio-loudness and x-ray properties of each quasar. The closeup view covers two decades in flux and illustrates the 1μm inflection, and the strength of the blue bump.

To characterize the large scale distribution of the energy output of the quasars, we calculate integral luminosites in a set of broad bands. The integrals are calculated by running a simple linear interpolation through the data points in $\log \nu L_\nu$ space, i.e. connecting the individual points with a power law. The errors indicated below are estimated by performing the integrals using the one sigma high and one sigma low flux values instead of the nominal values. For upper limits we interpolate between detections on either side. The lower of the interpolated value and the upper limit is used as the nominal flux estimate, but the errors are estimated using zero as the lower error bar and the upper limit as the upper error bar.

1. *Bolometric* The bolometric luminosity is typically well defined except for two regions of the spectrum: the mostly unobservable EUV region and the as yet unobserved hard x-ray and gamma-ray region. Indications are strong that the

0.1-10 mm gap is energetically negligible. As a first crude estimate of the EUV luminosity, we simply make a linear interpolation between the ends of the IUE and *Einstein* ranges. A reasonable upper limit to the EUV luminosity can be made by finding the maximum blackbody curve which does not exceed the observed data; however this limit is not strong, as the luminosity implied is typically 10 to 100 times the luminosity observed in the rest of the spectrum (Fig. 5.)

We perforce neglect the unknown luminosity above 10 keV ($10^{18.4}$Hz).

2. *UVOIR* The three decades between 100μm and 0.1μm (the ultraviolet/ optical/-infrared or 'UVOIR' region) are relatively well sampled, so the corresponding UVOIR luminosity can be much more accurately calculated. This luminosity accounts for most of that which is directly observed, and so is a useful number for quoting as 'the luminosity' of a quasar.

3. *Decades* We also tabulate the luminosity in individual decades across the electromagnetic spectrum. Outside the range $1 - 0.1\mu$m, these are often estimates from only one or two points and the errors are correspondingly large (typically 25 percent in the far IR).

4. *Octaves* In order to describe the shape of the ultraviolet bump component, we define a set of narrower octave wide bands. The four bands we call IR ($1-2\mu$m), VIS ($4000 - 8000\AA$), NUV ($2000 - 4000\AA$) and UV ($1000 - 2000\AA$). The IR band gives the luminosity longward of the 1μm inflection, where there should be little contribution from the bump. The UV band measures the luminosity in the bluest observed part of the bump, while the VIS band samples the early part of the bump's rise. The NUV band covers the near ultraviolet region of the spectrum dominated by the 'small bump' of blended Fe II and Balmer continuum emission (Wills, Netzer and Wills 1985).

The calculated integral luminosities are tabulated in Tables 18 to 20.

6.2 The Mean Energy Distribution and its Dispersion

We use the interpolations obtained in the previous sections to obtain mean energy distributions for the radio-loud and radio-quiet quasars in the sample. Because we believe the $1\mu m$ inflection to be an important feature separating physically different continuum components, we normalize each energy distribution at that wavelength by dividing by L_{Base}. Fig. 8(a) shows the two mean normalized energy distributions. The difference in x-ray slopes between the radio-loud and radio-quiet quasars is immediately apparent, but the most striking feature is the close agreement in the UVOIR region, as also found by Sanders et al (1989). This is true despite the wide

dispersion in shapes of the individual objects. Because of this agreement we feel it is useful to provide an analytic approximation to our mean quasar energy distribution. Fig. 8(b) shows a closeup of the overall mean distribution in the UVOIR region (solid line), together with the extreme envelope found in the sample (dotted lines). Note that the 'small bump' ($\lambda \sim 3500\AA$) is present in the data. Table 22 contains approximate piecewise power law fits to the curves of Figure 8, together with the measured dispersion for each segment.

We have also derived the mean bolometric corrections relative both to our near-infrared baseline normalization and the more usual normalization at V. The mean value of $L_V/L_{Base} = 1.4$ can be used to convert between the two normalizations. We derive an L_{Bol}/L_V and L_{UVOIR}/L_V of 12.7 ± 4.2 and 8.5 ± 2.9 respectively. The mean ultraviolet to infrared color is 3.1 ± 1.3. The details of these and further mean colors are given in Table 23.

Check Sanders et al $10^{12} Lsun$ separation. Redo dispersion rel to UVOIR. Check dispersion is same for RL and RQ. How many objects not in common?

6.3 The Spectral Window Function

While an average spectrum gives a reasonable representation of the quasar continuum, the observed ranges of continuum shapes is quite broad. The observed diversity of the quasars in our sample is a factor of 10 in the UV and at 100μm. This is as extreme as *could* be observed as a result of what we shall call the 'Spectral Window Function'.

Bounding the spectra in figure NN are two solid lines. The lower line is the limiting sensitivity of the telescopes/instruments used in each frequency range. The upper line is the upper envelope of the brightest objects observed at each frequency. This also is a limit to the range of observable continuum shapes. In effect this is a limit imposed by the space density of AGN; were they more common there would likely be one closer to us and brighter. Only AGN lying between these two lines are observable. The region between the two curves we call the 'Spectral Window Function', by analogy with the window function familiar in timing studies. Where this function is narrow all AGN will necessarily have spectra that are similar. Wherever the window function dominates we are unlikely to be seeing the whole range of spectral shapes in the quasar population. A detailed statistical treatment for the effects of the Window Function needs to be developed.

The window function is particularly narrow in the far-infrared and in the X-rays. For the far-infrared the IRAS 12, 25, 60 and 100μm band sensitivities determine the width of the function to be only a factor of $\sim$10. Table NNN lists the width of the window function and the extreme of the dispersion of quasar shapes (normalized to L_{UVOIR}) in our sample.

The similarity of the far-IR spectra of detected quasars seems likely to be a reflection of the narrow accessible range. IRAS upper limits for the 'Weak Infrared' quasars encourage this belief, since some seem to be IR-quiet (*e.g.* PG0026+129, see below). One third of the PG quasar sample was not detected with IRAS. Sanders *et al.* argue reasonably that these are mostly the same as the detected quasars. However some IR-quiet quasars may exist, as discussed below.

7 Discussion

7.1 The 1μm Inflection

The inflection around 1μm noted by Neugebauer et al (1979) is present in 28 of our objects, while in the remaining 5 it is difficult to rule out its presence because of the lack of IR and red observations. Note that in the ultraviolet weak objects, an inflection is still seen.

The lowest point, which we will call the baseline monochromatic luminosity (cf. Carleton et al 1987), is almost always coincident with the photometric H, or sometimes J, band measurement. While the existence of the inflection is independent of the H and K measurements, as in over half the objects the mid IR and the optical have slopes of opposite sign, the precise wavelength and flux of the minimum are dependent on the H and K measurements and therefore also on the adopted calibration at H and K. We have checked our results using a number of other groups' calibrations and find that the existence of the inflection remains clear and is not an artefact of the conversion to absolute fluxes.

The location of the inflection is relatively constant, as noted by Elvis et al (1986). The inflection wavelength always occurs between 0.8 and 1.5 microns, and usually between 1.0 and 1.5 microns, in agreement with Neugebauer et al (1987). The inflection wavelengths and corresponding baseline monochromatic luminosities L_{Base} using our magnitude scale zero points are listed in Table 21.

7.2 Strength and Shape of the Infrared Continuum

The infrared continuum consists in general of a broad bump, with the flux rising from 1μm towards longer wavelengths, peaking and falling by many decades, with very little emission in the submillimeter. Submillimeter observations of our objects are lacking; only four objects have IRAS and IRAM observations which constrain the slope of the mm-break to $d\log S_\nu / d\log \nu > 2$.

Within this overall shape there is substantial variety. We identify three kinds of infrared continuum behaviour: 'normal' objects in which the infrared continuum peak

occurs between 5 and 20 microns, and the flux falls off strongly at longer wavelengths; 'Strong Far Infrared' objects with a more complex continuum in which the flux rises again after the mid infrared peak' and 'Weak Infrared' objects where the spectrum is flat or falls off at near infrared wavelengths.

In the (60 μm/12 μm) versus (1.2 μm/0.36 μm) color-color classification diagram of Ward et al (1987), all of our objects are 'Type A', lying in the optically blue, far-IR weak quadrant corresponding to their 'bare AGN' classification, with the exception of the two far-IR bright objects, 3C 48 and Mkn 876, which lie in their 'empty' quadrant (Fig XX.)

Defining L_{IR} to be the sum of the far and near IR decades of Table 18, and $L_{IRBase} = (2 \ln 10) L_{Base}$ which converts the monochromatic luminosity to an equivalent integrated luminosity over two decades, we construct the color-color diagram of Fig. 7, which replaces the optical/infrared color of the Ward et al diagram with a purely infrared criterion.

Of those 26 of 33 objects in the sample with mid and far infrared detections or useful upper limits, 15 are classified as 'normal', with a single infrared peak between 3 and 20 μm. Five have abnormally weak infrared emission, and a further five have a more complex 'strong far IR' spectrum.

- *Normal Infrared Continuum*

  It is apparent from Fig. 4 that in many of our objects (e.g. Mkn 586) the turnover in the far infrared occurs well shortward of 100μm. The '3 micron bump' seen in 3C 273 peaks at longer wavelengths in most objects, between 5 and 20 microns, and is the principal infrared continuum peak. This range in turnovers suggests a peak defined by a temperature or a size rather than some atomic process.

- *Strong Far Infrared*

  These objects have $\log(L(60\mu m)/L(12\mu m) > -0.1$ because of the extra peak in their spectrum. In only two of our objects (Mkn 876 and 3C 48) is the flux strongly rising out to 100μm; this may be due to the presence of a large starburst in the host galaxy, at least in the former object (Yee and Green 1987). In the milder examples PHL 909 and PKS 2135-147 the flux rises again slightly toward longer wavelengths; these may represent an intermediate case. These four objects (McDowell et al, 1989) are also notable for their weak ultraviolet emission as can be seen in the IR/UV color-color diagram (Fig. 6). 3C 273 is also in the strong far IR group because of its millimetre-loud blazar component

- *Weak Infrared*

  The weak spectra have a low value of L(1-100μm) relative to the infrared baseline flux of Table 20, with $L_{IR} < L_{IRBase}$ (Fig. 7). They are PG0844+349,

PG1116+215, 3C249.1, and the extreme examples Kaz 102 and PG0026+129. In the latter two objects, a small 3μm peak falls away rapidly in the mid infrared.

7.3 The Strength and Shape of the Ultraviolet Bump

In Fig. 9 we use the IR, V and UV integral octave luminosities to construct a color-color diagram illustrating the variation of spectral shape of the bump in our sample. Most of the objects lie in a relatively well defined range of IR to UV color (overall bump strength), but show a wide range of shapes. The width of the distribution is comparable to the width induced by ultraviolet time variability. We note that the locus occupied by the objects begins near the power law line (dotted) and extends to highly concave spectra which are flat in the red but very steeply rising in the blue (i.e. $\log L(IR)/L(V) \sim 0$ but $\log L(V)/L(UV) \sim -0.6$). The solid line represents a pure face on Kerr accretion disk model, marked with logarithmic luminosity values appropriate for Eddington-limited accretion, and the dashed line repesents mixing an accretion disk with $L_{Bol} = 10^{47}$ erg/s with a power law extending from the infrared of unit slope in L_ν. No objects lie outside the region defined by mixing these two components. Such combined models fit the colors well; however, we leave detailed modelling to a future paper (Kuhn et al 1991, in preparation).

A smaller number of objects are significantly redder than the mean. These four 'weak bump' objects (McDowell et al 1989) have normal x-ray to infrared ratios, but their ultraviolet to infrared ratios are unusually low. Judging from the presence of XUV excess emission in some of the objects, it is unlikely that the weakness of the bump is due to internal extinction. There is no correlation of bump strength with luminosity in this sample. The 'weak bump' objects are also moderately, but not exceptionally, weak in their ultraviolet to x-ray ratio.

7.4 Luminosity correlations

We reproduce the results of Kriss (1988).

7.5 The Infrared to X-ray Connection

Following Carleton et al (1987), we studied the connection of the infrared component to the x-ray. Carleton et al found a tighter correlation between the lowest infrared point (the "infrared baseline") and the hard x-ray flux, for their hard x-ray selected sample. For our sample, the scatter in the correlation of the IR baseline with the x-ray was about the same as for the other correlations, in agreement with Sanders et al (1989) and in contrast to the Carleton et al results where a tighter correlation was found. We note that we used 1 keV fluxes rather than 6 keV, and that the mean

luminosity of our sample is a factor of 30 higher. We also note that Brissenden (1989) does find an effect for low luminosity objects found by HEAO-1, suggesting that the effect may hold preferentially for x-ray selected objects.

8 Conclusions

We have collected a set of data useful for many investigations. In particular, these data will serve as a benchmark against which to compare the energy distributions of high redshift quasars. The data are available by anonymous ftp from cfa248.harvard.edu.

We have studied the properties of a large sample of complete quasar energy distributions. We find that

1. The bolometric luminosity of the quasars is a factor of 12.7 ± 4.2 times the monochromatic visual luminosity, using a simple interpolation in the EUV; the more accurately defined 'UVOIR luminosity' is a factor of 8.5 ± 2.9 times the monochromatic visual luminosity;

2. The IR emission can be weak relative to the optical;

3. "The submillimeter break" often occurs at wavelengths of 60μm or shorter;

4. The strength of the 'ultraviolet bump' varies by a factor of 10, but typical objects have an ultraviolet luminosity three times their near infrared luminosity;

5. The shape of the ultraviolet bump varies significantly from object to object, rising steeply in the optical for some objects, but remaining flat there for others;

6. Objects with weak ultraviolet bumps are luminous in the far infrared;

7. We confirm the near constancy in wavelength of, and ubiquity of, the "1 μm inflection" first noticed by Neugebauer et al (1979) and studied by Elvis et al (1986) and Neugebauer et al (1987).

8. The ultraviolet variability of these objects (chosen to exclude strongly optically variable quasars) is typically less than a factor of 2 on a timescale of years, and many vary by less than twenty per cent.

9. While we confirm the correlations found by Kriss (1988), we suspect that they may be induced by host galaxy contamination at low luminosities.

10. The 'infrared to x-ray connection' discussed by Carleton et al (1987) is not present in this sample.

Acknowledgements

This work was carried out as part of NASA Astrophysics Data Program grant NAG8-689 and NAGW-2201, NASA HEAO contract NAS 8-30751, and NASA IUE grants NAG5-87, NAG5-37. We acknowledge useful discussions with [include AAS membership list here, esp.] Richard Barvainis, Ski Antonucci, Nat Carleton, Walter Rice, Olga Kuhn, Aneta Siemegenowska, Bozena Czerny, and Diana Worrall. Data for this paper were obtained from the Einstein Data Bank, the IUE Reduction and Data Analysis Facility, and the IRAS data bank at IPAC, and we thank the staff at those facilities for their support. JCM is a NAS/NRC Associate.

REFERENCES

Adam, G., 1978. Astron. Astrophys. Suppl. 31, 151.

Adam, G., 1985. Astron. Astrophys. Suppl. 61, 225.

Angel J.R.P. and Stockman H.S., 1980, Ann. Rev. Astr. and Astrophys., *18*, 321.

Antonucci, R.R.J., and Barvainis, R., 1988, Ap.J., *325*, L21.

Arnaud, K.A., et al. 1985

Bezler M., Kendziora E., Stubert R., Hasinger G., Pietsch W., Reppin C., Truemper J., Voges W., 1984, Astron. Ap., *136*, 351.

Bolton, J.G., and Butler, P.W., 1975. Aust. J. Phys. Suppl., 34, 33.

Bregman J.N. et al., 1984, Ap.J., *276*, 454.

Brissenden, R.J.V, 1989. Ph.D. Thesis, Australian National University (unpublished).

Burstein, D., and Heiles, C., 1978, Ap.J., *225*, 40.

Carleton N.P.,Elvis M., Fabbiano G., Lawrence A., Ward M.J. and Willner S.P., 1987, Ap.J.,*318*, 595.

Chini, R., Kreysa, E. and Biermann, P.L., 1989. XXX

Clegg, P. et al., 1983. Ap. J. 273, 58.

Comastri, A., Setti, G., Zamorani, G., Elvis, M., Wilkes, B.J., McDowell, J.C., and Giommi, P., 1991, in preparation.

Condon J.J., O'Dell S.L., Puschell J.J. and Stein W., 1981, Ap.J.,*246*, 624.

Cutri R.M., Wisneiewski W.Z., Rieke G.H. and Lebofsky M.J., 1985, Ap.J., *296*, 423.

Czerny, B. and Elvis, M. 1987. Ap. J. *321*, 305.

Dickey J.M., Salpeter, E., and Terzian, Y. 1978, Ap.J. Suppl. *36*,77.

Ekers, J.A., 1969, Aust. J. Phys. Suppl., 7, 1.

Elias, J.H. Frogel, J.A., Matthews, K., and Neugebauer, G., 1982. Astron. J., *87*, 1029.

Ennis, D.J., Neugebauer, G., and Werner, M., 1982. Ap.J. 262, 460

Elvis M., Green R.F., Bechtold J., Schmidt M., Neugebauer G., Soifer B.T., Matthews K. and Fabbiano G., 1986, Ap.J., *310*, 291.

Elvis M. and Lawrence A., 1985,'Astrophysics of Active Galaxies and Quasi-Stellar Objects', ed. J.S. Miller, [Mill Valley,CA:University Science Books], p.289-331.

Elvis, M., Lockman, F., and Wilkes, B.J., 1989. Astron. J. *97*, 777.

Elvis, M., Giommi, P., Wilkes, B.J., and McDowell, J.C, 1991, Ap.J., in press.

Feigelson, E.D., Isobe, T. and Kembhavi, A., 1984. Astron. J., 89, 1464.

Giacconi, R., et al. 1979, Ap.J. *230*, 540.

Glass, I.S., 1986. MNRAS 219, 5P.

Gorenstein, P., Harnden, R.F., and Fabricant, D., 1981, IEEE Trans. Nucl. Sci., NS-28, 869.

Gower, A.C. and Hutchings, J.B., 1984. Astron. J., 89, 1658.

Harris, D.E., et al., 1991, *The Einstein Observatory Catalog of IPC X-ray Sources*, in press.

Hayes, D.S., 1985. IAU Symposium 111, eds. Hayes, D.S. et al., p. 225.

Hewitt, A., and Burbidge, G., 1986, Ap. J. Suppl. Ser., *63*, 1.

Heiles. C., and Cleary, M.N., 1979. Aust.J.Phys. Suppl., *47*, 1.

Hintzen, P., Ulvestad, J., and Owen, F., 1983. Astron. J., 88, 709.

Hutchings, J.B., and Gower, A.C., 1985. Astron. J., 90, 405.

Hyland, A.R., and Allen, D.A., 1982. MNRAS 199, 943.

Johnson, H.L., 1965. Ap. J., *141*, 923.

Kellermann, K.I., Sramek, R., Shaffer, D., Green, R., and Schmidt, M., 1989, Astron. J., *98*, 1195.

Kriss , G. 1988. Ap.J, 324, 809.

Kurucz, R.L., 1979, Ap.J. Suppl. *40*, 1.

Landau R., Epstein, E.E., and Rather, J.D.G, 1980, Astron. J., 85. 363.

Landau R., et al, 1986, Ap.J., *308*, 78.

Lawrence A., 1987. PASP *99*, 309.

Lawrence A. and Elvis M., 1982, Ap.J., *256*, 410.

Malkan M.A., 1983, Ap.J., *268*, 582.

Malkan M.A. and Sargent W.L.W., 1982, Ap.J., *254*, 22.

Masnou J-L, Wilkes, B.J., Elvis, M., McDowell, J.C., and Arnaud, K.A., 1991. Astron. Astrophys., in press.

McAlary, C.W., McLaren, R.A., McGonegal, R.J., and Maza, J., 1983. Ap.J. Suppl., 52, 341.

McDowell, J.C., Elvis, M., Wilkes, B.J., Willner, S.P., Oey, M.S., Polomski, E., Bechtold, J., and Green, R.F., 1989, Ap.J., *345*, L13.

Miley, G.K., and Hartsuijker, A.P., 1978. Astron. Astrophys. Suppl., 34, 129.

Mushotzky R.F., 1984, Advances in Space Research, *3*, no. 10-13, 312.

Neugebauer, G., Oke, J.B., Becklin, E.E., and Mathews, K., 1979. Ap.J., 230, 79.

Neugebauer, G., et. al., 1984. Ap.J. 278, L1.

Neugebauer, G., Miley, G.K., Soifer, B.T., and Clegg, P.E., 1986, Ap.J. 308, 815.

Neugebauer G., Green R.F., Matthews K., Schmidt M., Soifer B.T. and Bennett J., 1987. Ap.J.Suppl., 63, 615.

O'Dell, S.L., et al. ,1978. Ap.J. Suppl., 38, 267.

Orr, M.J.L., and Browne, I.W.A, 1982, MNRAS, *200*, 1067.

Osterbrock D.E., 1985,'Astrophysics of Active Galaxies and Quasi-Stellar Objects', ed. J.S. Miller, [Mill Valley,CA:University Science Books], p.111-155.

Owen, F., Porcas, R.W., and Neff, S.G., 1978, Astron. J., 83, 1009.

Owen, F., Porcas, R.W., Mufson, S.L., and Moffett, T.J., 1978. Astron. J., 83, 685.

Owen, F., and Puschell, J., 1982, Astron. J., 87, 595.

Perley, R.A., 1982. Astron. J., 87, 859.

Pooley, G.G., and Henbest, S.N., 1974. MNRAS 169, 477.

Preston, R.A., et al. 1985. Astron.J., 90, 1599.

Price, R.M., and Milne, D.K., 1965. Australian J. Phys, 18, 329.

Rieke, G.H., 1978. Ap.J. 226, 550.

Rieke, G.H., and Lebofsky, M.J., 1985. Ap.J. *288*, 618.

Robson, E.I., Gear, W.K., Smith, M.G., Ade, P.A.R., and Nolt, I.G., 1985. MNRAS 213, 355.

Rudnick, L., Sitko, M.L., and Stein, W.A., 1984. Astron. J., 89, 753.

Rudy, R.J., LeVan, P.D. and Rodriguez-Espinoza, J.M., 1982. Astron. J., 87, 598.

Sandage A., 1965, Ap.J., *141*, 1560.

Sanders, D.B., et al., 1989. Ap.J. *347*, 29.

Savage, B.D., and Mathis, J.S., 1979, Ann. Rev. Astron. Astrophys, *17*, 73.

Schmidt M. and Green R.F., 1983, Ap.J., *269*, 352.

Shields G.A., 1978, Nature, *272*, 706.

Shimmins, A.J., and Bolton, J.G., 1972a. Australian J. Phys. Ap. Suppl, 23, 1.

Shimmins, A.J., and Bolton, J.G., 1972b. Australian J. Phys. Ap. Suppl, 26, 1.

Shimmins, A.J., and Bolton, J.G., 1981. Australian J. Phys. Ap. Suppl, XXX, 1.

Sitko, M.L., Stein, W.A., Zhang, Y-X, and Wisniewski, W.Z., 1982. Ap.J. 259, 486.

Spencer, R.E., McDowell, J.C., Charlesworth, M., Fanti, C., Parma, P., and Peacock, J.A., 1989, MNRAS **240**,657.

Stark, A.A., Heiles, C., Bally, J., and Linke, R., 1984. Privately distributed magnetic tape.

Stein W.A. and O'Dell S.L., 1985,'Astrophysics of Active Galaxies and Quasi-Stellar Objects', ed. J.S. Miller, [Mill Valley,CA:University Science Books], p.381-410.

Swarup, Sinha, and Hilldrup, 1978. XXX

Tokunaga, A., 1984. Astron. J., *89*, 172.

Tokunaga, A., 1986. *IRTF Photometry Manual.*

Treves, A., Bouchet, P., Chiapetti, L, Ciapi, A., Falomo, R., Maraschi, L., and Tanzi, E.G., 1988, Ap.J., *330*, 178.

Turner, M.J.L., Williams, O.R., Saxton, R., Stewart, G.C., Courvoisier, T.J-L., Ohashi, T., Makishima, K, Kli, T., and Inoue, H., 1990, in *Proceedings of the 23rd ESLAB Symposium,* ESA SP-296, eds. Hunt, J. and Battrick, B., p 769.

Turner, T.J. and Pounds, K.A., 1989. MNRAS 232, 463.

Unger, S.W., Lawrence, A., Wilson, A.S., Elvis, M., and Wright, A.E., 1987. MNRAS, *228*, 521.

Urry C.M., Mushotzky R.F., Kondo Y., Hackney K.R.H. and Hackney R.L., 1982, Ap.J., *261*,12.

Urry, C.M., and Reichert, G. 1988, NASA IUE Newsletter no.34, p.95.

Veron-Cetty, M.P., and Veron, P., 1987, *ESO Scientific Report,* No. 5.

Ward, M., Elvis, M., Fabbiano, G., Carleton, N.P., Willner, S.P., and Lawrence, A., 1987. Ap.J. *315*, 74.

Wilkes, B.J., and Elvis, M., 1987. Ap.J. *323*, 343.

Williams, O.R., et al., 1991. Ap. J., in press.

Wills B.J., Netzer H. and Wills D., 1985, Ap.J., *237*, 319.

Wills, D., 1975, XXX

Wills, D., 1979, Ap.J. Suppl., *39*. 291.

Worrall D.M., Puschell J.J., Jones B., Bruhweiler F.C., Aller M., Aller H.D., Hodge P.E., Sitko M.L., Stein W.A., Zhang Y.X. and Ku W. H-M., 1982, Ap.J., *261*,403.

Yee, H.K.C., and Green, R.F., 1987, Astron. J., 94, 618.

Figure captions

Fig. 1. Examples of radio-loud (3C 273, top) and radio-quiet (Mkn 586, bottom) quasar energy distributions, illustrating the main continuum features. The energy distributions show the logarithm of the energy per unit logarithmic frequency interval, in the rest frame.

Fig. 2. Histograms of sample properties. Shaded bins correspond to radio-loud objects, $R_L > 1$. The absolute magnitude is calculated using the corrections of Veron and Veron (1987), but with our value of Ω_0. The bolometric luminosity is derived from the observed energy distributions as described in the text. The monochromatic x-ray luminosity is $\nu L(\nu)$ at 2 keV in the rest frame, estimated from the IPC spectral fits. R_B, the ratio of radio core to extended luminosity (Orr and Browne 1982), is an indicator of the source orientation; it was only possible to estimate this for a subset of the sources.

Fig 3. The observed energy distribution of PG1407+265 from the near infrared to the far ultraviolet. The expected positions of prominent quasar emission lines are indicated for an assumed redshift $z = 0.94$. The short and long wavelength IUE observations are not contemporaneous and the low level of the short wavelength data may be due to variability.

Fig 4 (a-ag). Rest frame, dereddened continuum energy distributions of the quasar sample. For each object, the left hand panel shows the overall radio to x-ray energy distribution, and the right hand panel shows the details of the UVOIR (100μm to 1000$\AA$) region.

Fig 5. The maximum black body in the EUV region, compared with the power law interpolation, for the quasar Mkn 586. This shows that the total energy in the EUV is not well constrained by the observations.

Fig 6. Infrared-ultraviolet color-color diagram, plotting the far IR color $L(60\mu m)/L(12\mu m)$ against the UV bump strength $L(1-2\mu m)/L(0.1-0.2\mu m)$. The objects with weak ultraviolet bumps are also luminous in the far infared.

Fig 7. Infrared color-color diagram, plotting the far IR color $L(60\mu m)/L(12\mu m)$ against the IR bump strength $L(1-100\mu m)/L_{Base}$. The dashed lines indicate the regions corresponding to the different spectral classifications.

Fig 8. (a) Mean energy distributions for radio-loud and radio-quiet quasars.
(b). Overall mean energy distribution in UVOIR region. Dashed lines indicate the extreme departures observed from the mean distribution.

Fig 9. Ultraviolet-optical-near infrared color-color diagram, indicating the shape of the ultraviolet bump.

TABLE 1(a)

EINSTEIN UV SAMPLE QUASARS

Object	Name	2E Name	Host Galaxy	RA(B1950)	Dec(B1950)	RA(J2000)	Dec(J2000)	Redshift	V mag	N_H	Ref	Class
Q0007+106	PG0007+106	2E 29	Zw 2A	00 07 56.7	+10 41 47.8	00 10 31.0	+10 58 29.2	0.0890	15.16	6.09	1	FSC
Q0026+129	PG0026+129	2E 93	PGC 1790	00 26 38.1	+12 59 29.6	00 29 13.8	+13 16 04.4	0.1420	15.32	4.93	1	RQ
Q0049+171	PG0049+171	2E 200	Mkn 1148	00 49 16.5	+17 09 41.0	00 51 54.8	+17 25 58.9	0.0640	15.88	4.26	1	Sy1
Q0052+251	PG0052+251	2E 217	PGC 3237	00 52 11.1	+25 09 24.0	00 54 52.2	+25 25 38.9	0.1550	15.42	4.50	1	RQ
Q0054+144	PHL 909	2E 233		00 54 31.9	+14 29 58.6	00 57 09.9	+14 46 11.2	0.1710	16.70	4.20	1	RQ
Q0121−590	2E 378	2E 378	Fairall 9	01 21 51.2	−59 03 58.9	01 23 45.7	−58 48 21.1	0.0450	13.23	2.25	2	RQ
Q0134+329	3C 48	2E 444		01 34 49.8	+32 54 20.2	01 37 41.3	+33 09 35.2	0.3670	16.00	4.35	1	SSC
Q0205+024	NAB0205+024	2E 526	Mkn 586	02 05 14.5	+02 28 42.7	02 07 49.8	+02 42 56.1	0.1550	15.40	2.99	1	RQ
Q0312−770	PKS0312−770	2E 746		03 12 55.7	−77 03 01.0	03 11 54.7	−76 51 51.4	0.2230	15.90	7.31	2	? (RL)
Q0637−752	PKS0637−752	2E 1720		06 37 23.4	−75 13 37.8	06 35 46.5	−75 16 17.1	0.6510	15.75	8.16	2	? (RL)
Q0837−120	3C 206	2E 2028		08 37 27.9	−12 03 54.2	08 39 50.6	−12 14 33.9	0.1980	15.76	5.85	1	FR2
Q0844+349	PG0844+349	2E 2048	PGC 24702	08 44 33.9	+34 56 09.0	08 47 42.5	+34 45 04.6	0.0640	14.00	3.39	1	RQ
Q1028+313	B2 1028+313	2E 2291		10 28 09.8	+31 18 20.6	10 30 59.1	+31 02 55.5	0.1770	16.71	1.98	1	FSC
Q1100+772	3C 249.1	2E 2389		11 00 27.4	+77 15 09.0	11 04 13.8	+76 58 58.6	0.3110	15.72	2.93	1	FR2
Q1116+215	PG1116+215	2E 2443		11 16 30.1	+21 35 43.0	11 19 08.9	+21 19 17.8	0.1770	15.17	1.44	1	RQ
Q1137+660	3C 263	2E 2503		11 37 09.3	+66 04 27.0	11 39 57.0	+65 47 49.4	0.6520	16.32	0.82	1	FR2/SL
Q1146−037	PKS1146−037	2E 2537		11 46 23.9	−03 47 30.0	11 48 57.4	−04 04 10.8	0.3410	16.90	2.79	1	FR2
Q1202+281	GQ Comae	2E 2584	PGC 38224	12 02 08.9	+28 10 53.4	12 04 42.1	+27 54 11.4	0.1650	15.51	1.72	1	RQ
Q1211+143	PG1211+143	2E 2620	PGC 39086	12 11 44.8	+14 19 53.0	12 14 17.6	+14 03 12.5	0.0850	14.63	2.83	1	RQ
Q1219+755	Mkn 205 AGN	2E 2677	Mkn 205	12 19 33.8	+75 35 18.0	12 21 44.4	+75 18 40.1	0.0700	15.24	2.74	1	RQ
Q1226+023	3C 273	2E 2729	PGC 41121	12 26 33.2	+02 19 43.2	12 29 06.7	+02 03 08.4	0.1580	12.86	1.80	3	FSC/SL
Q1307+085	PG1307+085	2E 2978	PGC 45656	13 07 16.2	+08 35 47.0	13 09 47.0	+08 19 49.3	0.1550	15.28	2.20	1	RQ
Q1407+265	PG1407+265	2E 3196		14 07 07.7	+26 32 30.0	14 09 23.8	+26 18 20.8	0.94	15.73	1.38	1	RQ
Q1416−129	PG1416−129	2E 3238	PGC 51142	14 16 21.3	−12 56 58.0	14 19 03.8	−13 10 44.8	0.1290	15.40	7.20	1	BAL
Q1426+015	PG1426+015	2E 3280	Mkn 1383	14 26 33.8	+01 30 27.0	14 29 06.6	+01 17 06.2	0.0860	15.05	2.64	1	RQ
Q1501+106	Mkn 841 AGN	2E 3372	Mkn 841	15 01 36.4	+10 37 57.0	15 04 01.3	+10 26 17.1	0.0360	15.09	2.23	1	Sy1
Q1545+210	3C 323.1	2E 3500		15 45 31.1	+21 01 28.0	15 47 43.5	+20 52 17.2	0.2660	16.05	4.04	1	FR2
Q1613+658	PG1613+658	2E 3624	Mkn 876	16 13 36.3	+65 50 38.0	16 13 57.2	+65 43 10.1	0.1290	15.37	2.66	1	RQ
Q1704+608	3C 351	2E 3828		17 04 03.5	+60 48 31.1	17 04 41.4	+60 44 30.4	0.3710	15.28	2.26	1	FR2
Q1721+343	4C 34.47	2E 3896		17 21 32.0	+34 20 41.8	17 23 20.8	+34 17 58.4	0.2060	16.50	3.06	1	FSC/SL
Q1803+676	2E 4008	2E 4008	Kazaryan 102	18 03 37.4	+67 37 53.9	18 03 28.9	+67 38 09.5	0.1360	16.00	5.00	1	RQ
Q2130+099	PG2130+099	2E 4486	II Zw 136	21 30 01.3	+09 54 59.0	21 32 27.9	+10 08 17.4	0.0610	14.62	4.20	1	RQ
Q2135−147	PHL 1657	2E 4497		21 35 01.2	−14 46 27.3	21 37 45.2	−14 32 55.4	0.2000	15.53	4.45	1	FR2

References to NH: (1) Elvis,Lockman and Wilkes 1989; (2) Heiles and Cleary 1979; (3) Dickey, Salpeter, and Terzian 1978; (4) Stark et al, 1991

TABLE 1(b)

OTHER "IPC" QUASARS

Object	Name	2E Name	Host Galaxy	RA(B1950)	Dec(B1950)	RA(J2000)	Dec(J2000)	Redshift	V mag	N_H	Ref	Class
Q0003+199	PG 0003+199		Mkn 335	00 03 45.0	+19 55 30.0	00 06 19.3	+20 12 11.9	0.025	13.75	3.98	4	Sy1
Q0003+158	PHL 658	2E 12		00 03 25.1	+15 53 07.4	00 05 59.2	+16 09 49.4	0.450	16.40	3.94	1	RL
Q0050+124	PG 0050+124	2E 209	I Zw 1	00 50 57.8	+12 25 20.0	00 53 34.9	+12 41 36.3	0.061	14.07	5.07	1	RQ
Q0112−017	PKS 0112−017	2E 335		01 12 43.9	−01 42 54.8	01 15 17.1	−01 27 04.3	1.365	17.41	5.37	1	RL
Q0133+207	3C 47	2E 437		01 33 20.4	+20 42 10.6	01 36 24.4	+20 57 27.8	0.425	18.10	5.41	4	RL
Q0219+428	3C 66A	2E 558		02 19 30.0	+42 48 30.4	02 22 39.6	+43 02 08.5	0.444	15.50	7.48	4	BL
Q0323+022	H			03 23 38.0	+02 14 47.2	03 26 13.9	+02 25 14.8	0.147	16.50	8.68	1	BL
Q0414−060	3C 110	2E 962		04 14 49.2	−06 01 04.3	04 17 16.7	−05 53 45.1	0.781	15.94	5.12	4	RL
Q0424−131	PKS 0424−131	2E 1048		04 24 47.8	−13 09 33.4	04 27 07.3	−13 02 53.5	2.165	17.50	3.95	4	RL
Q0804+761	PG 0804+761	2E 1919		08 04 35.4	+76 11 32.0	08 10 58.5	+76 02 41.8	0.100	15.15	3.12	1	RQ
Q0915+165	Mkn 704 AGN	2E 2116	Mkn 704	09 15 39.4	+16 30 59.0	09 18 26.0	+16 18 19.7	0.029	14.20	3.15	1	Sy1
Q0923+129	Mkn 705 AGN	2E 2139	Mkn 705	09 23 20.0	+12 57 04.0	09 26 03.3	+12 44 03.3	0.028	14.60	4.03	1	Sy1
Q0923+392	4C 39.25	2E 2141		09 23 55.3	+39 15 23.5	09 27 03.0	+39 02 20.7	0.699	17.86	1.69	1	FSC/SL
Q1012+008	PG 1012+008			10 12 20.8	+00 48 33.0	10 14 54.9	+00 33 36.8	0.185	16.00	3.22	1	RQ
Q1121+422	PG 1121+422			11 21 52.1	+42 16 54.0	11 24 35.5	+42 00 24.9	0.234	16.02	2.33	1	RQ
Q1217+023	PKS 1217+023	2E 2661		12 17 38.4	+02 20 20.9	12 20 11.9	+02 03 42.1	0.240	16.53	1.97	1	RL
Q1244+026	PG 1244+026	2E 2854		12 44 02.1	+02 38 31.0	12 46 35.3	+02 22 08.3	0.048	16.15	1.93	1	Sy1
Q1253−055	3C 279	2E 2900		12 53 35.9	−05 31 08.4	12 56 11.2	−05 47 22.1	0.538	17.75	2.22	1	FSC/SL
Q1318+290	Ton 155			13 18 53.7	+29 03 30.3	13 21 14.8	+28 47 48.8	1.703	16.90	1.14	4	RQ
Q1346−036	Q1346−036			13 46 08.3	−03 38 30.5	13 48 44.0	−03 53 24.6	2.344	17.27	2.49	4	RQ
Q1351+640	PG 1351+640			13 51 46.3	+64 00 28.4	13 53 15.8	+63 45 44.8	0.088	14.84	2.29	4	RQ
Q1351+695	Mkn 279 AGN	2E 3147	Mkn 279	13 51 53.6	+69 33 13.0	13 53 03.5	+69 18 29.4	0.031	14.46	1.64	1	Sy1
Q1352+183	PG 1352+183	2E 3148		13 52 11.5	+18 20 58.0	13 54 34.8	+18 06 16.0	0.152	15.50	1.84	1	RQ
Q1435−067	PG 1435−067	2E 3305		14 35 37.5	−06 45 22.0	14 38 16.4	−06 58 18.3	0.129	15.54	5.08	4	RQ
Q1517+239	LB 9612			15 17 08.2	+23 56 52.6	15 19 19.5	+23 46 02.6	1.898	16.40	3.91	4	RQ
Q1635+119	MC2 1635+119	2E 3737		16 35 25.9	+11 55 46.4	16 37 46.5	+11 49 49.8	0.146	16.50	4.29	1	RL
Q2112+059	PG 2112+059			21 12 23.6	+05 55 12.0	21 14 52.7	+06 07 41.6	0.466	15.52	6.49	4	RQ
Q2120+168	3C 432	1E 2120+168		21 20 25.5	+16 51 46.4	21 22 46.3	+17 04 38.6	1.805	17.96	7.39	4	RL
Q2126−158	PKS 2126−158	2E 4479		21 26 26.7	−15 51 51.5	21 29 12.1	−15 38 42.1	3.260	17.30	4.85	1	RL
Q2128−123	PKS 2128−123	2E 4484		21 28 52.7	−12 20 20.1	21 31 35.3	−12 07 04.3	0.501	15.46	4.83	1	RL
Q2209+184	PG 2209+184	2E 4579		22 09 30.2	+18 27 01.0	22 11 53.7	+18 41 51.4	0.070	15.86	4.82	1	Sy1
Q2214+139	Mkn 304 AGN	2E 4585	Mkn 304	22 14 45.8	+13 59 20.0	22 17 12.2	+14 14 20.8	0.067	14.66	5.23	1	RQ
Q2233+134	PG 2233+134	2E 4626		22 33 39.8	+13 28 21.0	22 36 07.7	+13 43 54.9	0.325	16.04	4.89	4	BAL
Q2251+113	4C 11.72			22 51 40.6	+11 20 39.6	22 54 10.4	+11 36 39.2	0.323	15.77	5.53	1	RL
Q2251−178	MR 2251−178	2E 4645		22 51 25.9	−17 50 54.2	22 54 05.8	−17 34 54.6	0.068	14.36	2.84	1	RQ
Q2254+024	PKS 2254+024	2E 4661		22 54 44.6	+02 27 13.8	22 57 17.6	+02 43 17.3	2.090	18.00	5.88	1	RL
Q2304+042	PG 2304+042			23 04 30.1	+04 16 41.0	23 07 02.7	+04 32 55.3	0.042	15.44	5.52	1	Sy1

TABLE 2

MORE SAMPLE PROPERTIES

Object	$\log L_V$	$\log L_X$	$\log L_{Bol}$	M_V	R_L	R_B	α_x	α_{ox}
Q0007+106	44.93	44.39	46.02	−23.46	1.83	0.88	0.40	1.33
Q0026+129	45.18	44.53	46.15	−24.25	−1.05	0.04	0.88	1.35
Q0049+171	44.11	44.07	45.15	−21.50	−0.16	3.30	0.60	1.16
Q0052+251	45.16	44.59	46.38	−24.20	−0.76	1.31	1.10	1.36
Q0054+144	45.23	44.37	46.28	−24.32	−0.26	1.60	0.41	1.35
Q0121−590	44.82	44.33	45.92	−23.43	<0.03		0.90	1.32
Q0134+329	45.69	44.96	47.00	−25.63	3.68?		0.70	1.29
Q0205+024	45.10	44.14	46.24	−24.33	−0.42		1.20	1.53
Q0312−770	45.29	44.64	46.35	−24.19	2.81?		0.10	1.21
Q0637−752	46.50	45.78	47.58	−27.08	3.60?		0.46	1.33
Q0837−120	45.05	44.97	46.24	−23.54	2.44	0.24	0.70	1.14
Q0844+349	44.79	43.45	45.56	−23.41	< −1.29		0.60	1.60
Q1028+313	45.00	44.39	46.12	−24.17	1.91		0.76	1.91
Q1100+772	45.61	44.90	46.50	−25.40	1.57	0.05	1.00	1.37
Q1116+215	45.53	44.38	46.61	−25.36	−0.39	2.3	1.00	1.58
Q1137+660	46.11	45.60	47.17	−26.89	2.01	0.18	0.70	1.31
Q1146−037	44.94	45.01	46.16	−23.97	2.42	1.4	0.30	1.20
Q1202+281	44.86	44.54	46.20	−23.69	−0.24	3.6	1.10	1.22
Q1211+143	45.13	44.37	46.23	−24.27	−0.75	0.01	2.00	1.40
Q1219+755	44.74	44.13	45.58	−23.17	−0.40		0.78	1.21
Q1226+023	46.18	45.64	47.24	−27.15	2.96	2.5	0.47	1.34
Q1307+085	45.21	44.36	46.19	−24.70	< −0.95		0.90	1.37
Q1407+265	46.44	45.74	47.59	−27.85	0.27	0.58	1.20	1.40
Q1416−129	44.77	44.62	45.93	−23.32	−0.15	0.29	0.90	1.26
Q1426+015	44.82	44.34	46.10	−23.39	−0.56	3.3	1.12	1.40
Q1501+106	44.16	43.78	45.43	−21.76	−0.88	0.5	0.93	1.28
Q1545+210	45.48	45.00	46.53	−24.94	1.34	0.05	0.80	1.32
Q1613+658	45.06	44.36	46.24	−24.09	−0.49	0.35	1.10	1.37
Q1704+608	45.83	44.48	46.86	−25.93	0.69	0.01	0.10	1.61
Q1721+343	45.35	45.08	46.56	−24.95	2.18		0.50	1.29
Q1803+676	44.91	44.12	45.85	−23.64	−0.58		-0.2	1.45
Q2130+099	44.68	43.61	45.80	−23.09	−0.49	1.73	0.81	1.52
Q2135−147	45.31	44.76	46.38	−24.64	1.73	0.09	0.71	1.26

TABLE 3

X-RAY POWER LAW FITS

Object	0.2 keV flux (μJy)	1 keV Energy index	1 keV flux (μJy)	Ref	4 keV Energy index	4 keV flux (μJy)	Ref
Q0007+106		$0.4\pm^{1.2}_{0.4}$	$1.97\pm^{2.49}_{0.52}$	2	$0.66\pm^{0.09}_{0.14}$	2.08	6
Q0026+129	$5.9\pm^{1.4}_{1.1}$	$0.88\pm^{0.05}_{0.05}$	$1.41\pm^{0.03}_{0.03}$	3	$0.86\pm^{0.39}_{0.38}$	0.43	5
Q0049+171		$0.60\pm^{3.50}_{0.10}$	$2.09\pm^{14.02}_{0.28}$	1	$1.03\pm^{0.29}_{0.29}$	0.57	5
Q0052+251		$1.10\pm^{2.30}_{0.68}$	$1.53\pm^{0.46}_{0.48}$	1	$0.84\pm^{0.53}_{0.53}$	0.28	5
Q0054+144	$5.18\pm^{1.6}_{1.6}$	$0.41\pm^{0.22}_{0.22}$	$0.52\pm^{0.04}_{0.04}$	3			
Q0121-590		$0.90\pm^{0.20}_{0.20}$	$9.29\pm^{0.78}_{0.90}$	1	$1.07\pm^{0.07}_{0.07}$	0.91	6
Q0134+329		$0.7\pm^{0.6}_{0.4}$	$0.50\pm^{0.14}_{0.10}$	2			
Q0205+024	$18.8\pm^{4.5}_{5.0}$	$1.2\pm^{0.35}_{0.35}$	$0.58\pm^{0.06}_{0.06}$	3			
Q0312-770		$0.1\pm^{1.3}_{0.4}$	$0.49\pm^{0.59}_{0.09}$	2			
Q0637-752	<34.8	$0.46\pm^{0.10}_{0.10}$	$0.98\pm^{0.05}_{0.05}$	3	$0.93\pm^{0.64}_{0.60}$	0.31	5
					$0.84\pm^{0.22}_{0.22}$	0.55	7
Q0837-120		$0.70\pm^{0.30}_{0.30}$	$1.82\pm^{0.37}_{0.33}$	1	$0.83\pm^{0.37}_{0.37}$	0.35	7
Q0844+349		$0.60\pm^{0.90}_{0.50}$	$0.50\pm^{0.24}_{0.06}$	1			
Q1028+313	$7.5\pm^{2.0}_{2.1}$	$0.62\pm^{0.2}_{0.2}$	$0.76\pm^{0.07}_{0.07}$	3			
Q1100+772		$1.0\pm^{0.6}_{0.6}$	$0.69\pm^{0.19}_{0.13}$	2			
Q1116+215		$1.0\pm^{0.6}_{0.2}$	$0.68\pm^{0.12}_{0.06}$	2			
Q1137+660		$0.7\pm^{0.5}_{0.2}$	$0.39\pm^{0.08}_{0.02}$	2			
Q1146-037		$0.3\pm^{0.8}_{0.3}$	$0.56\pm^{0.26}_{0.07}$	2			
Q1202+281		$1.1\pm^{0.5}_{0.5}$	$1.19\pm^{0.27}_{0.25}$	2			
Q1211+143		$2.0\pm^{1.7}_{0.6}$	$5.5\pm^{0.8}_{0.7}$	4	$1.02\pm^{0.23}_{0.22}$	0.64	5
					$1.10\pm^{0.20}_{0.20}$	0.40	7
Q1219+755	$16.7\pm^{2.4}_{2.5}$	$0.78\pm^{0.1}_{0.1}$	$2.24\pm^{0.08}_{0.08}$	3	$1.17\pm^{0.67}_{0.60}$	0.45	5
Q1226+023	$48.9\pm^{3.3}_{3.3}$	$0.45\pm^{0.05}_{0.05}$	$9.8\pm^{0.2}_{0.2}$	3	$0.53\pm^{0.03}_{0.03}$	5.05	5
					$0.45\pm^{0.02}_{0.02}$	5.86	7
Q1307+085		$0.9\pm^{0.7}_{0.2}$	$0.81\pm^{0.12}_{0.06}$	2			
Q1407+265		$1.2\pm^{1.7}_{0.4}$	$0.44\pm^{0.17}_{0.05}$	2			
Q1416-129		$0.9\pm^{1.3}_{0.6}$	$2.15\pm^{3.50}_{0.70}$	2	$0.05\pm^{0.15}_{0.15}$	0.39	7
Q1426+015	<50.4	$1.12\pm^{0.1}_{0.1}$	$3.05\pm^{0.09}_{0.09}$	3	$0.46\pm^{0.25}_{0.25}$	0.62	5
Q1501+106	$49.3\pm^{8.3}_{9.3}$	$0.93\pm^{0.19}_{0.19}$	$4.2\pm^{0.3}_{0.3}$	3	$0.42\pm^{0.16}_{0.16}$	1.04	5
Q1545+210		$0.8\pm^{0.6}_{0.7}$	$1.10\pm^{0.43}_{0.29}$	2			
Q1613+658	<20.3	$1.10\pm^{0.2}_{0.2}$	$1.40\pm^{0.04}_{0.04}$	3			
Q1704+608		$0.10\pm^{0.90}_{0.30}$	$0.13\pm^{0.10}_{0.02}$	1			
Q1721+343		$0.5\pm^{0.6}_{0.3}$	$1.93\pm^{0.73}_{0.20}$	2			
Q1803+676		$-0.2\pm^{0.6}_{0.4}$	$0.33\pm^{0.20}_{0.06}$	2			
Q2130+099	$22.8\pm^{5.4}_{5.3}$	$0.81\pm^{0.29}_{0.29}$	$0.91\pm^{0.08}_{0.08}$	3	$1.27\pm^{0.36}_{0.36}$	0.36	5
Q2135-147	<9.7	$0.73\pm^{0.05}_{0.05}$	$1.10\pm^{0.02}_{0.02}$	3	$0.83\pm^{0.33}_{0.31}$	0.57	5
					$0.86\pm^{0.20}_{0.02}$	0.78	7

1) This paper; 2) Wilkes and Elvis (1987); 3) Masnou et al (1991); 4) Elvis et al (1991)
5) Comastri et al (1991); 6) Turner and Pounds (1989); 7) Turner et al (1990)

TABLE 4

ADOPTED CONTINUUM BANDS

Central Wavelength	Wavelength Range (A)	Central Wavelength	Wavelength Range (A)
725	700-750	2600	2550-2650
775	750-800	2675	2650-2700
825	800-850	2950	2900-3000
875	850-900	3050	3000-3100
925	900-950	3150	3100-3200
975	950-1000	3250	3200-3300
1025	1000-1050	3600	3550-3650
1075	1050-1100	3800	3750-3850
1125	1100-1150	4500	4450-4550
1300	1275-1325	4600	4550-4650
1350	1325-1375	5200	5100-5300
1475	1450-1500	5400	5300-5500
1625	1600-1650	5600	5500-5700
1675	1650-1700	5800	5700-5900
1725	1700-1750	6000	5900-6100
1775	1750-1800	6175	6100-6250
1825	1800-1850	6875	6850-6900
2000	1950-2050	7000	6900-7100
2100	2050-2150	7200	7100-7300
2200	2150-2250	7400	7300-7500
2300	2250-2350	7600	7500-7700
2400	2350-2450	7800	7700-7900
2500	2450-2550	8000	7900-8100

TABLE 5(a)

ULTRAVIOLET CONTINUUM FLUXES: UV sample quasars

			$\lambda_{rest}(\AA)$	725	775	825	875	925	975	1025	1075	1125	1300	1350	1475	1625
Q0007+106			$\log(\nu_o)$	15.58	15.55	15.52	15.50	15.47	15.45	15.43	15.41	15.39	15.33	15.31	15.27	15.23
1978 Jun	LWR1687	SWP1806	$\log(\nu_o F_{\nu_0})$	-	-	-	-	-	-	-	-	12.17	12.27	12.37	12.27	12.38
				-	-	-	-	-	-	-	-	0.07	0.07	0.07	0.11	0.05
1980 Oct		SWP10281	$\log(\nu_o F_{\nu_0})$	-	-	-	-	-	-	-	-	12.02	12.20	12.19	12.17	12.27
				-	-	-	-	-	-	-	-	0.07	0.06	0.06	0.07	0.07
1981 Jan		SWP11060	$\log(\nu_o F_{\nu_0})$	-	-	-	-	-	-	-	-	11.83	11.86	12.02	11.83	11.92
				-	-	-	-	-	-	-	-	0.21	0.18	0.28	0.22	0.08
1982 May		SWP16957	$\log(\nu_o F_{\nu_0})$	-	-	-	-	-	-	-	-	11.47	11.79	11.76	11.64	11.73
				-	-	-	-	-	-	-	-	0.30	0.21	0.17	0.30	0.23
1984 Jun	LWP3560	SWP23248	$\log(\nu_o F_{\nu_0})$	-	-	-	-	-	-	-	-	12.10	12.25	12.20	12.21	12.31
				-	-	-	-	-	-	-	-	0.06	0.10	0.10	0.11	0.05
1985 Jan	LWP5246		$\log(\nu_o F_{\nu_0})$	-	-	-	-	-	-	-	-	-	-	-	-	-
				-	-	-	-	-	-	-	-	-	-	-	-	-
Q0026+129			$\log(\nu_o)$	15.56	15.53	15.50	15.48	15.45	15.43	15.41	15.39	15.37	15.31	15.29	15.25	15.21
1981 Jan	LWR9629	SWP10953	$\log(\nu_o F_{\nu_0})$	-	-	-	-	-	-	-	12.22	12.16	12.20	12.11	12.16	12.35
				-	-	-	-	-	-	-	0.13	0.14	0.16	0.14	0.09	0.16
1984 Jul	LWP3758		$\log(\nu_o F_{\nu_0})$	-	-	-	-	-	-	-	-	-	-	-	-	-
				-	-	-	-	-	-	-	-	-	-	-		-
1987 Aug	LWP11533		$\log(\nu_o F_{\nu_0})$	-	-	-	-	-	-	-	-	-	-	-	-	-
				-	-	-	-	-	-	-	-	-	-	-	-	-
Q0049+171			$\log(\nu_o)$	15.59	15.56	15.53	15.51	15.48	15.46	15.44	15.42	15.40	15.34	15.32	15.28	15.24
1985	LWP6541	SWP26506	$\log(\nu_o F_{\nu_0})$	-	-	-	-	-	-	-	-	11.89	11.80	11.81	11.83	11.92
				-	-	-	-	-	-	-	-	0.00	0.03	0.10	0.02	0.04
Q0052+251			$\log(\nu_o)$	15.55	15.53	15.50	15.47	15.45	15.43	15.40	15.38	15.36	15.30	15.28	15.25	15.20
1983 Feb	LWR15214	SWP19224	$\log(\nu_o F_{\nu_0})$	-	-	-	-	-	-	12.91	12.60	12.36	12.42	12.40	12.32	12.36
				-	-	-	-	-	-	0.00	0.18	0.02	0.02	0.07	0.03	0.00
Q0054+144			$\log(\nu_o)$	15.55	15.52	15.49	15.47	15.44	15.42	15.40	15.38	15.36	15.29	15.28	15.24	15.20
1987	LWP11207	SWP30040	$\log(\nu_o F_{\nu_0})$	-	-	-	-	-	-	-	11.67	11.62	11.74	11.70	11.61	11.72
				-	-	-	-	-	-	-	0.02	0.05	0.02	0.06	0.09	0.08
Q0121-590			$\log(\nu_o)$	15.60	15.57	15.54	15.52	15.49	15.47	15.45	15.43	15.41	15.34	15.33	15.29	15.25
1978 Jun	LWR1685	SWP1804	$\log(\nu_o F_{\nu_0})$	-	-	-	-	-	-	-	-	-	13.37	13.33	13.32	13.36
				-	-	-	-	-	-	-	-	-	0.03	0.03	0.04	0.03
1982 Jul	LWR13801	SWP17521	$\log(\nu_o F_{\nu_0})$	-	-	-	-	-	-	-	-	-	13.10	13.08	13.08	13.12
				-	-	-	-	-	-	-	-	-	0.05	0.05	0.08	0.05
Q0134+329			$\log(\nu_o)$	15.48	15.45	15.42	15.40	15.38	15.35	15.33	15.31	15.29	15.23	15.21	15.17	15.13
1982 Oct	LWR14436	SWP18328	$\log(\nu_o F_{\nu_0})$	-	-	-	12.92	12.14	11.60	11.51	11.53	11.61	11.68	11.69	12.05	11.85
				-	-	-	0.13	0.66	0.01	0.03	0.01	0.09	0.11	0.05	0.20	0.24

TABLE 5(a) (continued)

			$\lambda_{rest}(\AA)$	725	775	825	875	925	975	1025	1075	1125	1300	1350	1475	1625
Q0205+024			$\log(\nu_o)$	15.55	15.53	15.50	15.47	15.45	15.43	15.40	15.38	15.36	15.30	15.28	15.25	15.20
1982 Dec	LWR14813	SWP18772	$\log(\nu_o F_{\nu_0})$	-	-	-	-	-	-	13.14	12.76	12.21	12.24	12.29	12.21	12.31
				-	-	-	-	-	-	0.05	0.46	0.05	0.03	0.05	0.02	0.03
Q0312-770			$\log(\nu_o)$	15.53	15.50	15.47	15.45	15.42	15.40	15.38	15.36	15.34	15.28	15.26	15.22	15.18
1981 Jul		SWP14485	$\log(\nu_o F_{\nu_0})$	-	-	-	-	-	-	12.39	12.34	12.28	12.26	12.30	12.21	12.25
				-	-	-	-	-	-	0.09	0.06	0.04	0.06	0.06	0.03	0.02
1982 Feb		SWP16423	$\log(\nu_o F_{\nu_0})$	-	-	-	-	-	-	12.24	12.09	12.01	12.03	12.02	12.01	12.17
				-	-	-	-	-	-	0.14	0.10	0.09	0.11	0.08	0.05	0.07
1982 Apr		SWP16816	$\log(\nu_o F_{\nu_0})$	-	-	-	-	-	-	12.14	11.98	11.94	11.93	11.93	11.94	12.02
				-	-	-	-	-	-	0.10	0.10	0.08	0.08	0.07	0.06	0.06
1987 Jan	LWP9887		$\log(\nu_o F_{\nu_0})$	-	-	-	-	-	-	-	-	-	-	-	-	11.75
				-	-	-	-	-	-	-	-	-	-	-	-	0.25
Q0637-752			$\log(\nu_o)$	15.40	15.37	15.34	15.32	15.29	15.27	15.25	15.23	15.21	15.15	15.13	15.09	15.05
1980 Dec		SWP10832	$\log(\nu_o F_{\nu_0})$	-	11.82	11.86	11.94	11.97	11.98	12.03	12.01	11.98	-	-	-	-
				-	0.02	0.03	0.05	0.05	0.04	0.03	0.04	0.02	-	-	-	-
1981 Aug		SWP14867	$\log(\nu_o F_{\nu_0})$	11.77	11.85	11.91	11.98	12.01	12.07	12.11	12.10	12.05	-	-	-	-
				0.06	0.07	0.08	0.09	0.11	0.09	0.08	0.06	0.06	-	-	-	-
1987 Nov	LWP13016		$\log(\nu_o F_{\nu_0})$	-	-	-	-	-	-	-	-	-	12.12	12.16	12.05	12.02
				-	-	-	-	-	-	-	-	-	0.18	0.13	0.14	0.11
1988 Apr	LWP13022		$\log(\nu_o F_{\nu_0})$	-	-	-	-	-	-	-	-	-	12.24	12.07	12.02	12.02
				-	-	-	-	-	-	-	-	-	0.22	0.27	0.20	0.09
Q0837-120			$\log(\nu_o)$	15.54	15.51	15.48	15.46	15.43	15.41	15.39	15.37	15.35	15.28	15.27	15.23	15.19
1979	LWR4214	SWP4292	$\log(\nu_o F_{\nu_0})$	-	-	-	-	-	-	13.02	11.89	11.76	11.85	11.74	11.83	11.91
				-	-	-	-	-	-	0.74	0.02	0.03	0.11	0.15	0.08	0.12
Q0844+349			$\log(\nu_o)$	15.59	15.56	15.53	15.51	15.48	15.46	15.44	15.42	15.40	15.34	15.32	15.28	15.24
1986	LWP7652	SWP25827	$\log(\nu_o F_{\nu_0})$	-	-	-	-	-	-	-	-	-	12.32	12.38	12.38	12.45
				-	-	-	-	-	-	-	-	-	0.08	0.21	0.07	0.04
1987 Nov	LWP12206	SWP32433	$\log(\nu_o F_{\nu_0})$	-	-	-	-	-	-	-	-	-	12.46	12.51	12.54	12.55
				-	-	-	-	-	-	-	-	-	0.06	0.07	0.08	0.05
1987	LWP12207	SWP32434	$\log(\nu_o F_{\nu_0})$	-	-	-	-	-	-	-	-	-	12.46	12.45	12.47	12.57
				-	-	-	-	-	-	-	-	-	0.07	0.09	0.08	0.08
Q1028+313			$\log(\nu_o)$	15.55	15.52	15.49	15.46	15.44	15.42	15.40	15.37	15.36	15.29	15.28	15.24	15.20
1987	LWP12386	SWP28214	$\log(\nu_o F_{\nu_0})$	-	-	-	-	-	-	-	12.22	12.07	12.16	12.11	12.11	12.18
				-	-	-	-	-	-	-	0.04	0.02	0.08	0.04	0.03	0.05
Q1100+772			$\log(\nu_o)$	15.50	15.47	15.44	15.42	15.39	15.37	15.35	15.33	15.31	15.25	15.23	15.19	15.15
1978 Jul	LWR1776	SWP1903	$\log(\nu_o F_{\nu_0})$	-	-	-	-	-	11.58	11.74	11.65	11.66	11.67	11.67	11.58	11.56
				-	-	-	-	-	0.03	0.07	0.08	0.06	0.02	0.04	0.10	0.07

TABLE 5(a) (continued)

			$\lambda_{rest}(\AA)$	725	775	825	875	925	975	1025	1075	1125	1300	1350	1475	1625
1984 Jun	SWP23149	SWP23144	$\log(\nu_o F_{\nu_0})$	-	-	-	-	12.35	12.36	12.42	12.35	12.36	12.34	12.35	12.29	-
				-	-	-	-	0.05	0.05	0.07	0.06	0.06	0.04	0.04	0.04	-
Q1116+215			$\log(\nu_o)$	15.55	15.52	15.49	15.46	15.44	15.42	15.40	15.37	15.36	15.29	15.28	15.24	15.20
1980 May		SWP8898	$\log(\nu_o F_{\nu_0})$	-	-	-	-	-	-	12.98	12.93	12.91	12.89	12.89	12.87	12.88
				-	-	-	-	-	-	0.05	0.06	0.05	0.07	0.06	0.06	0.04
1980 May		SWP8899	$\log(\nu_o F_{\nu_0})$	-	-	-	-	-	-	12.98	12.96	12.95	12.95	12.95	12.94	12.93
				-	-	-	-	-	-	0.03	0.04	0.04	0.03	0.04	0.04	0.02
1982 Jul	LWP13669	SWP17416	$\log(\nu_o F_{\nu_0})$	-	-	-	-	-	-	13.52	13.00	12.75	12.77	12.77	12.75	12.82
				-	-	-	-	-	-	0.03	0.21	0.02	0.02	0.05	0.01	0.04
Q1137+660			$\log(\nu_o)$	15.40	15.37	15.34	15.32	15.29	15.27	15.25	15.23	15.21	15.15	15.13	15.09	15.05
1980 Dec		SWP10763	$\log(\nu_o F_{\nu_0})$	12.12	12.12	12.10	12.12	12.18	12.17	12.27	12.17	12.14	-	-	-	-
				0.09	0.07	0.08	0.10	0.09	0.08	0.11	0.09	0.06	-	-	-	-
1982 Apr	LWR13083		$\log(\nu_o F_{\nu_0})$	-	-	-	-	-	-	-	-	-	12.15	12.36	12.21	12.23
				-	-	-	-	-	-	-	-	-	0.33	0.27	0.24	0.08
Q1146-037			$\log(\nu_o)$	15.49	15.46	15.43	15.41	15.38	15.36	15.34	15.32	15.30	15.24	15.22	15.18	15.14
1981 Jul	LWR11083		$\log(\nu_o F_{\nu_0})$	-	-	-	-	-	-	-	-	-	-	-	-	11.79
				-	-	-	-	-	-	-	-	-	-	-	-	0.07
1981 Jul	LWR11098		$\log(\nu_o F_{\nu_0})$	-	-	-	-	-	-	-	-	-	-	-	11.57	11.65
				-	-	-	-	-	-	-	-	-	-	-	0.22	0.19
1981 Dec	LWR12158		$\log(\nu_o F_{\nu_0})$	-	-	-	-	-	-	-	-	-	-	-	11.54	11.60
				-	-	-	-	-	-	-	-	-	-	-	0.34	0.25
1988 Jan		SWP32758	$\log(\nu_o F_{\nu_0})$	-	-	-	-	11.08	11.21	11.16	11.50	11.16	11.16	11.04	10.69	-
				-	-	-	-	0.26	0.30	0.30	0.56	0.27	0.30	0.25	0.18	-
Q1202+281			$\log(\nu_o)$	15.55	15.52	15.49	15.47	15.44	15.42	15.40	15.38	15.36	15.30	15.28	15.24	15.20
1980 May		SWP8900	$\log(\nu_o F_{\nu_0})$	-	-	-	-	-	-	-	-	11.94	11.99	11.97	11.82	-
				-	-	-	-	-	-	-	-	0.03	0.00	0.01	0.05	-
1983 Jan	LWR15078	SWP19049	$\log(\nu_o F_{\nu_0})$	-	-	-	-	-	-	-	12.17	12.07	12.17	12.05	12.02	12.09
				-	-	-	-	-	-	-	0.17	0.15	0.18	0.17	0.19	0.12
1984 Nov	LWP4904	SWP24580	$\log(\nu_o F_{\nu_0})$	-	-	-	-	-	-	-	11.81	11.74	11.87	11.84	11.87	11.97
				-	-	-	-	-	-	-	0.12	0.09	0.13	0.12	0.11	0.08
1985 Nov		SWP27193	$\log(\nu_o F_{\nu_0})$	-	-	-	-	-	-	-	11.75	11.61	11.59	11.60	11.46	11.35
				-	-	-	-	-	-	-	0.28	0.41	0.40	0.35	0.41	0.29
1986 Jul		SWP28604	$\log(\nu_o F_{\nu_0})$	-	-	-	-	-	-	-	11.96	11.97	12.02	11.98	12.05	12.04
				-	-	-	-	-	-	-	0.10	0.09	0.11	0.10	0.13	0.07
Q1211+143			$\log(\nu_o)$	15.58	15.55	15.53	15.50	15.48	15.45	15.43	15.41	15.39	15.33	15.31	15.27	15.23
1985 Dec	LWP7223	SWP27210	$\log(\nu_o F_{\nu_0})$	-	-	-	-	-	-	-	-	12.71	12.78	12.80	-	12.87
				-	-	-	-	-	-	-	-	0.04	0.04	0.04	-	0.05
1987 Feb	LWP10115	SWP30302	$\log(\nu_o F_{\nu_0})$	-	-	-	-	-	-	-	-	12.54	12.58	12.60	12.60	12.71
				-	-	-	-	-	-	-	-	0.05	0.06	0.07	0.07	0.09

TABLE 5(a) (continued)

			$\lambda_{rest}(\AA)$	725	775	825	875	925	975	1025	1075	1125	1300	1350	1475	1625
Q1219+755			$\log(\nu_o)$	15.59	15.56	15.53	15.51	15.48	15.46	15.44	15.42	15.40	15.33	15.32	15.28	15.24
1978 Jul	LWR1773	SWP1894	$\log(\nu_o F_{\nu_0})$	-	-	-	-	-	-	-	-	-	12.02	12.06	12.04	12.02
				-	-	-	-	-	-	-	-	-	0.14	0.11	0.15	0.17
1983 Feb	LWP1799	SWP19238	$\log(\nu_o F_{\nu_0})$	-	-	-	-	-	-	-	-	-	12.27	12.24	12.28	12.36
				-	-	-	-	-	-	-	-	-	0.07	0.06	0.07	0.06
Q1226+023			$\log(\nu_o)$	15.55	15.52	15.50	15.47	15.45	15.42	15.40	15.38	15.36	15.30	15.28	15.24	15.20
1978 May	LWR1565	SWP1642	$\log(\nu_o F_{\nu_0})$	-	-	-	-	-	-	-	13.45	13.44	13.46	13.45	13.40	13.45
				-	-	-	-	-	-	-	0.03	0.02	0.02	0.02	0.02	0.01
1979 May	LWR4454	SWP5116	$\log(\nu_o F_{\nu_0})$	-	-	-	-	-	-	-	13.38	13.36	13.43	13.42	13.40	13.44
				-	-	-	-	-	-	-	0.05	0.03	0.05	0.05	0.03	0.02
1982 Apr	LWR13056	SWP16803	$\log(\nu_o F_{\nu_0})$	-	-	-	-	-	-	-	13.57	13.58	13.58	13.58	13.54	13.55
				-	-	-	-	-	-	-	0.04	0.03	0.04	0.03	0.03	0.02
1982 Jun	LWR15364	SWP17302	$\log(\nu_o F_{\nu_0})$	-	-	-	-	-	-	-	13.64	13.65	13.68	13.65	13.62	13.64
				-	-	-	-	-	-	-	0.04	0.03	0.03	0.03	0.02	0.02
1983 Apr	LWR15739	SWP19731	$\log(\nu_o F_{\nu_0})$	-	-	-	-	-	-	-	13.40	13.41	13.42	13.41	13.37	13.43
				-	-	-	-	-	-	-	0.07	0.05	0.07	0.04	0.05	0.03
1984 Jul	LWP3757	SWP23444	$\log(\nu_o F_{\nu_0})$	-	-	-	-	-	-	-	13.34	13.34	13.36	13.35	13.32	13.36
				-	-	-	-	-	-	-	0.04	0.03	0.03	0.03	0.04	0.02
1985 May	LWP6010	SWP25974	$\log(\nu_o F_{\nu_0})$	-	-	-	-	-	-	-	13.44	13.46	13.51	13.52	13.45	13.50
				-	-	-	-	-	-	-	0.04	0.03	0.03	0.03	0.04	0.01
1986 Dec	LWP9679	SWP29843	$\log(\nu_o F_{\nu_0})$	-	-	-	-	-	-	-	13.47	13.45	13.49	13.49	13.44	13.47
				-	-	-	-	-	-	-	0.04	0.03	0.04	0.02	0.03	0.02
1986 Dec	LWP9680	SWP29844	$\log(\nu_o F_{\nu_0})$	-	-	-	-	-	-	-	13.48	13.49	13.49	13.50	13.45	13.46
				-	-	-	-	-	-	-	0.04	0.04	0.02	0.03	0.03	0.02
1987 Jun	LWP10892	SWP31077	$\log(\nu_o F_{\nu_0})$	-	-	-	-	-	-	-	13.30	13.27	13.33	13.31	13.27	13.33
				-	-	-	-	-	-	-	0.06	0.05	0.04	0.04	0.03	0.02
1987 Jun	LWP10893	SWP31078	$\log(\nu_o F_{\nu_0})$	-	-	-	-	-	-	-	13.27	13.27	13.32	13.31	13.28	13.32
				-	-	-	-	-	-	-	0.05	0.04	0.04	0.03	0.03	0.02
1988 Jun	LWP13357	SWP33704	$\log(\nu_o F_{\nu_0})$	-	-	-	-	-	-	-	13.46	13.47	13.46	13.45	13.41	13.43
				-	-	-	-	-	-	-	0.04	0.04	0.03	0.03	0.03	0.02
1989 Feb	LWP14957	SWP35471	$\log(\nu_o F_{\nu_0})$	-	-	-	-	-	-	-	13.35	13.35	13.38	13.37	13.32	13.36
				-	-	-	-	-	-	-	0.03	0.03	0.04	0.04	0.03	0.03
Q1229+204			$\log(\nu_o)$	15.59	15.56	15.53	15.51	15.48	15.46	15.44	15.42	15.40	15.34	15.32	15.28	15.24
1982 May	LWR13136	SWP16880	$\log(\nu_o F_{\nu_0})$	-	-	-	-	-	-	-	-	13.26	12.58	12.63	12.54	12.59
				-	-	-	-	-	-	-	-	0.54	0.02	0.08	0.01	0.02
Q1307+085			$\log(\nu_o)$	15.55	15.53	15.50	15.47	15.45	15.43	15.40	15.38	15.36	15.30	15.28	15.25	15.20
1980 May		SWP8915	$\log(\nu_o F_{\nu_0})$	-	-	-	-	-	-	13.54	13.04	12.42	12.44	12.46	12.37	12.42
				-	-	-	-	-	-	0.01	0.59	0.01	0.01	0.04	0.04	0.00
1984 Feb	LWP2826		$\log(\nu_o F_{\nu_0})$	-	-	-	-	-	-	-	-	-	-	-	-	-
				-	-	-	-	-	-	-	-	-	-	-	-	-

TABLE 5(a) (continued)

			$\lambda_{rest}(\AA)$	725	775	825	875	925	975	1025	1075	1125	1300	1350	1475	1625
Q1407+265			$\log(\nu_o)$	15.33	15.30	15.27	15.25	15.22	15.20	15.18	15.16	15.14	15.07	15.06	15.02	14.98
1983 Apr		SWP19858	$\log(\nu_o F_{\nu_0})$	11.95	11.94	11.97	12.01	12.07	11.95	11.99	-	-	-	-	-	-
				0.08	0.09	0.13	0.10	0.13	0.07	0.04	-	-	-	-	-	-
1986 Dec	LWP9733		$\log(\nu_o F_{\nu_0})$	-	-	-	-	-	-	12.23	12.27	12.21	12.14	12.13	12.12	12.91
				-	-	-	-	-	-	0.16	0.15	0.17	0.06	0.05	0.03	0.18
1988 Sep	MMT/FOGS		$\log(\nu_o F_{\nu_0})$	-	-	-	-	-	-	-	-	-	-	-	-	-
				-	-	-	-	-	-	-	-	-	-	-	-	-
1988 Jun	MMT/Blue		$\log(\nu_o F_{\nu_0})$	-	-	-	-	-	-	-	-	-	-	-	-	-
				-	-	-	-	-	-	-	-	-	-	-	-	-
Q1416-129			$\log(\nu_o)$	15.56	15.54	15.51	15.48	15.46	15.44	15.41	15.39	15.37	15.31	15.29	15.26	15.21
1980 Jul		SWP8916	$\log(\nu_o F_{\nu_0})$	-	-	-	-	-	-	-	-	-	11.95	11.92	11.84	-
				-	-	-	-	-	-	-	-	-	0.02	0.07	0.13	-
1983 Jun	LWR16072		$\log(\nu_o F_{\nu_0})$	-	-	-	-	-	-	-	-	-	-	-	-	-
				-	-	-	-	-	-	-	-	-	-	-	-	-
1988 Mar		SWP33030	$\log(\nu_o F_{\nu_0})$	-	-	-	-	-	-	-	11.67	11.68	11.82	11.92	11.90	11.92
				-	-	-	-	-	-	-	0.10	0.13	0.17	0.22	0.17	0.06
Q1426+015			$\log(\nu_o)$	15.58	15.55	15.52	15.50	15.48	15.45	15.43	15.41	15.39	15.33	15.31	15.27	15.23
1983	LWR16015	SWP19214	$\log(\nu_o F_{\nu_0})$	-	-	-	-	-	-	-	-	-	12.94	-	12.95	-
				-	-	-	-	-	-	-	-	-	0.00	-	0.01	-
1983 May	LWR16020	SWP20076	$\log(\nu_o F_{\nu_0})$	-	-	-	-	-	-	-	-	12.74	12.71	12.69	12.68	12.79
				-	-	-	-	-	-	-	-	0.08	0.09	0.09	0.09	0.05
1983 Aug	LWR16611	SWP20708	$\log(\nu_o F_{\nu_0})$	-	-	-	-	-	-	-	-	12.83	12.85	12.86	12.83	12.91
				-	-	-	-	-	-	-	-	0.06	0.04	0.05	0.05	0.05
1985 Mar	LWP5446	SWP25338	$\log(\nu_o F_{\nu_0})$	-	-	-	-	-	-	-	-	12.98	12.94	12.94	12.93	12.93
				-	-	-	-	-	-	-	-	0.02	0.03	0.02	0.03	0.02
Q1501+106			$\log(\nu_o)$	15.60	15.57	15.55	15.52	15.50	15.47	15.45	15.43	15.41	15.35	15.33	15.29	15.25
1983 Feb	LWR15200	SWP19213	$\log(\nu_o F_{\nu_0})$	-	-	-	-	-	-	-	-	-	12.70	12.67	12.66	12.74
				-	-	-	-	-	-	-	-	-	0.05	0.05	0.06	0.03
Q1545+210			$\log(\nu_o)$	15.51	15.49	15.46	15.43	15.41	15.39	15.36	15.34	15.32	15.26	15.24	15.21	15.16
1983 Jun	LWR16665	SWP20764	$\log(\nu_o F_{\nu_0})$	-	-	-	-	-	-	12.00	11.93	11.90	11.95	11.91	11.91	11.95
				-	-	-	-	-	-	0.02	0.04	0.00	0.12	0.07	0.05	0.02
1983 Aug	LWR16677	SWP20816	$\log(\nu_o F_{\nu_0})$	-	-	-	-	-	12.12	12.16	12.06	12.10	12.13	12.03	12.12	12.21
				-	-	-	-	-	0.08	0.09	0.11	0.11	0.12	0.10	0.08	0.29
Q1613+658			$\log(\nu_o)$	15.56	15.54	15.51	15.48	15.46	15.44	15.41	15.39	15.37	15.31	15.29	15.26	15.21
1981 Sep	LWR11477		$\log(\nu_o F_{\nu_0})$	-	-	-	-	-	-	-	-	-	-	-	-	12.05
				-	-	-	-	-	-	-	-	-	-	-	-	0.05
1983 May		SWP20073	$\log(\nu_o F_{\nu_0})$	-	-	-	-	-	-	-	-	12.28	12.27	12.25	12.20	12.31
				-	-	-	-	-	-	-	-	0.10	0.04	0.01	0.09	0.02

TABLE 5(a) (continued)

			$\lambda_{rest}(\AA)$	725	775	825	875	925	975	1025	1075	1125	1300	1350	1475	1625
1983 Aug	LWR16673	SWP20801	$\log(\nu_o F_{\nu_0})$	-	-	-	-	-	-	-	12.26	12.27	12.33	12.34	12.30	12.39
				-	-	-	-	-	-	-	0.06	0.05	0.06	0.07	0.08	0.03
1984 Jan	LWP2615	SWP21962	$\log(\nu_o F_{\nu_0})$	-	-	-	-	-	-	-	12.33	12.28	12.30	12.26	12.23	12.35
				-	-	-	-	-	-	-	0.06	0.07	0.06	0.07	0.07	0.04
1984 Jun	LWP3561	SWP23249	$\log(\nu_o F_{\nu_0})$	-	-	-	-	-	-	-	12.35	12.44	12.44	12.31	12.38	12.29
				-	-	-	-	-	-	-	0.18	0.19	0.20	0.15	0.18	0.14
Q1704+608			$\log(\nu_o)$	15.48	15.45	15.42	15.40	15.37	15.35	15.33	15.31	15.29	15.23	15.21	15.17	15.13
1979	LWR6208	SWP1376	$\log(\nu_o F_{\nu_0})$	-	-	-	12.21	12.13	12.18	12.20	12.15	12.21	12.22	12.21	11.99	12.11
				-	-	-	0.04	0.09	0.11	0.08	0.11	0.10	0.06	0.06	0.13	0.12
1983 Dec		SWP21654	$\log(\nu_o F_{\nu_0})$	-	-	-	12.07	12.08	12.14	12.18	12.17	12.15	12.17	12.14	-	-
				-	-	-	0.07	0.08	0.07	0.09	0.06	0.07	0.06	0.04	-	-
1986 Dec	LWP9624		$\log(\nu_o F_{\nu_0})$	-	-	-	-	-	-	-	-	-	-	-	12.08	12.16
				-	-	-	-	-	-	-	-	-	-	-	0.12	0.16
Q1721+343			$\log(\nu_o)$	15.54	15.51	15.48	15.45	15.43	15.41	15.39	15.36	15.34	15.28	15.27	15.23	15.18
1983 Aug	LWR16678	SWP20817	$\log(\nu_o F_{\nu_0})$	-	-	-	-	-	-	12.72	12.58	12.50	12.51	12.45	12.45	12.57
				-	-	-	-	-	-	0.09	0.07	0.09	0.12	0.12	0.06	0.15
1986 May	LWP8171	SWP28261	$\log(\nu_o F_{\nu_0})$	-	-	-	-	-	-	12.58	12.40	12.36	12.47	12.39	12.38	12.47
				-	-	-	-	-	-	0.13	0.07	0.08	0.08	0.11	0.04	0.07
Q1803+676			$\log(\nu_o)$	15.56	15.53	15.51	15.48	15.46	15.43	15.41	15.39	15.37	15.31	15.29	15.25	15.21
1987 May	LWP10810	SWP31032	$\log(\nu_o F_{\nu_0})$	-	-	-	-	-	-	11.93	12.86	11.97	12.06	12.00	12.04	12.11
				-	-	-	-	-	-	0.29	0.74	0.09	0.07	0.07	0.10	0.06
Q2130+099			$\log(\nu_o)$	15.59	15.56	15.54	15.51	15.49	15.46	15.44	15.42	15.40	15.34	15.32	15.28	15.24
1978 Jul	LWR1774	SWP1909	$\log(\nu_o F_{\nu_0})$	-	-	-	-	-	-	-	-	-	12.66	12.68	12.76	12.80
				-	-	-	-	-	-	-	-	-	0.04	0.03	0.04	0.04
1979 May	LWR4610	SWP5389	$\log(\nu_o F_{\nu_0})$	-	-	-	-	-	-	-	-	12.91	12.56	12.56	12.74	12.48
				-	-	-	-	-	-	-	-	0.29	0.07	0.05	0.18	0.00
1985	LWP7205	SWP27211	$\log(\nu_o F_{\nu_0})$	-	-	-	-	-	-	-	-	-	12.43	12.45	12.43	12.51
				-	-	-	-	-	-	-	-	-	0.11	0.11	0.12	0.09
Q2135-147			$\log(\nu_o)$	15.54	15.51	15.48	15.46	15.43	15.41	15.39	15.37	15.35	15.28	15.27	15.23	15.19
1979 Apr	LWR4280	SWP4935	$\log(\nu_o F_{\nu_0})$	-	-	-	-	-	-	12.01	11.90	11.85	11.87	11.82	11.85	11.89
				-	-	-	-	-	-	0.11	0.10	0.08	0.13	0.09	0.08	0.07
1982 Dec	LWP1739	SWP18741	$\log(\nu_o F_{\nu_0})$	-	-	-	-	-	-	11.98	11.72	11.75	11.83	11.69	11.83	11.99
				-	-	-	-	-	-	0.14	0.13	0.13	0.18	0.11	0.07	0.16

TABLE 5(a)

ULTRAVIOLET CONTINUUM FLUXES: UV sample quasars

	$\lambda_{rest}(\AA)$	1675	1725	1775	1825	2000	2100	2200	2300	2400	2500	2600	2675	2950	3050	3150
Q0007+106	$\log(\nu_o)$	15.22	15.20	15.19	15.18	15.14	15.12	15.10	15.08	15.06	15.04	15.03	15.01	14.97	14.96	14.94
1978 Jun	$\log(\nu_o F_{\nu_0})$	12.38	12.31	12.32	12.24	12.21	12.24	12.23	12.34	12.39	12.43	12.43	12.43	12.23	-	-
		0.05	0.03	0.05	0.05	0.04	0.01	0.03	0.01	0.03	0.02	0.01	0.02	0.10	-	-
1980 Oct	$\log(\nu_o F_{\nu_0})$	12.28	12.15	12.13	12.13	-	-	-	-	-	-	-	-	-	-	-
		0.08	0.06	0.06	0.04	-	-	-	-	-	-	-	-	-	-	-
1981 Jan	$\log(\nu_o F_{\nu_0})$	11.92	11.81	11.92	11.82	-	-	-	-	-	-	-	-	-	-	-
		0.16	0.08	0.10	0.08	-	-	-	-	-	-	-	-	-	-	-
1982 May	$\log(\nu_o F_{\nu_0})$	11.61	11.44	11.46	11.70	-	-	-	-	-	-	-	-	-	-	-
		0.21	0.18	0.18	0.22	-	-	-	-	-	-	-	-	-	-	-
1984 Jun	$\log(\nu_o F_{\nu_0})$	12.29	12.22	12.25	12.22	12.17	12.21	12.22	12.27	12.33	12.37	12.37	12.36	12.34	-	-
		0.07	0.05	0.06	0.09	0.11	0.10	0.09	0.07	0.04	0.03	0.03	0.02	0.07	-	-
1985 Jan	$\log(\nu_o F_{\nu_0})$	-	-	12.27	12.19	12.22	12.26	12.18	12.30	12.34	12.40	12.39	12.38	12.37	-	-
		-	-	0.17	0.43	0.20	0.23	0.12	0.07	0.06	0.04	0.04	0.05	0.06	-	-
Q0026+129	$\log(\nu_o)$	15.20	15.18	15.17	15.16	15.12	15.10	15.08	15.06	15.04	15.02	15.00	14.99	14.95	14.94	14.92
1981 Jan	$\log(\nu_o F_{\nu_0})$	12.31	12.29	12.26	12.31	12.16	12.25	12.29	12.19	12.22	12.24	12.18	12.18	-	-	-
		0.08	0.14	0.24	0.17	0.20	0.23	0.24	0.16	0.16	0.12	0.18	0.21	-	-	-
1984 Jul	$\log(\nu_o F_{\nu_0})$	-	12.42	12.30	12.38	12.30	12.20	12.17	12.21	12.22	12.24	12.24	12.27	-	-	-
		-	0.28	0.22	0.24	0.24	0.16	0.15	0.09	0.07	0.06	0.07	0.11	-	-	-
1987 Aug	$\log(\nu_o F_{\nu_0})$	-	12.17	12.12	12.15	12.13	12.17	12.20	12.23	12.26	12.30	12.24	12.21	-	-	-
		-	0.17	0.15	0.18	0.13	0.10	0.09	0.06	0.04	0.06	0.06	0.06	-	-	-
Q0049+171	$\log(\nu_o)$	15.23	15.21	15.20	15.19	15.15	15.13	15.11	15.09	15.07	15.05	15.04	15.02	14.98	14.97	14.95
1985	$\log(\nu_o F_{\nu_0})$	11.85	11.80	11.75	11.81	11.84	11.78	11.93	11.95	11.99	11.96	12.06	12.05	-	-	-
		0.11	0.07	0.09	0.17	0.08	0.05	0.04	0.02	0.07	0.03	0.08	0.06	-	-	-
Q0052+251	$\log(\nu_o)$	15.19	15.18	15.17	15.15	15.11	15.09	15.07	15.05	15.03	15.02	15.00	14.99	14.94	14.93	14.92
1983 Feb	$\log(\nu_o F_{\nu_0})$	12.34	12.22	12.26	12.24	12.19	12.16	12.20	12.27	-	-	-	-	-	-	-
		0.07	0.09	0.09	0.07	0.08	0.04	0.07	0.07	-	-	-	-	-	-	-
Q0054+144	$\log(\nu_o)$	15.18	15.17	15.16	15.15	15.11	15.09	15.07	15.05	15.03	15.01	14.99	14.98	14.94	14.92	14.91
1987	$\log(\nu_o F_{\nu_0})$	11.85	11.97	11.94	11.93	11.79	11.83	11.79	11.87	11.92	11.96	11.99	12.00	-	-	-
		0.22	0.22	0.20	0.25	0.16	0.12	0.10	0.07	0.05	0.05	0.08	0.10	-	-	-
Q0121-590	$\log(\nu_o)$	15.23	15.22	15.21	15.20	15.16	15.14	15.12	15.10	15.08	15.06	15.04	15.03	14.99	14.97	14.96
1978 Jun	$\log(\nu_o F_{\nu_0})$	13.35	13.30	13.29	13.28	13.25	13.21	13.19	13.20	13.22	13.22	13.23	13.21	13.22	13.22	-
		0.03	0.02	0.02	0.02	0.04	0.03	0.03	0.03	0.03	0.03	0.03	0.03	0.03	0.04	-
1982 Jul	$\log(\nu_o F_{\nu_0})$	13.07	13.01	13.03	12.99	12.96	12.95	12.92	12.95	12.97	13.00	12.97	12.95	13.00	12.95	-
		0.04	0.03	0.03	0.02	0.05	0.07	0.05	0.05	0.05	0.04	0.03	0.03	0.08	0.07	-
Q0134+329	$\log(\nu_o)$	15.12	15.10	15.09	15.08	15.04	15.02	15.00	14.98	14.96	14.94	14.93	14.91	14.87	14.86	14.84
1982 Oct	$\log(\nu_o F_{\nu_0})$	11.79	11.87	11.81	11.71	11.72	11.78	11.88	12.08	-	-	-	-	-	-	-
		0.23	0.25	0.26	0.23	0.19	0.18	0.28	0.39	-	-	-	-	-	-	-

TABLE 5(a) (continued)

	$\lambda_{rest}(\AA)$	1675	1725	1775	1825	2000	2100	2200	2300	2400	2500	2600	2675	2950	3050	3150
Q0205+024	$\log(\nu_o)$	15.19	15.18	15.17	15.15	15.11	15.09	15.07	15.05	15.03	15.02	15.00	14.99	14.94	14.93	14.92
1982 Dec	$\log(\nu_o F_{\nu_0})$	12.23	12.41	12.34	12.29	12.26	12.33	12.31	12.31	12.32	12.34	12.34	12.30	-	-	-
		0.09	0.15	0.13	0.14	0.10	0.09	0.09	0.06	0.08	0.08	0.09	0.12	-	-	-
Q0312-770	$\log(\nu_o)$	15.17	15.15	15.14	15.13	15.09	15.07	15.05	15.03	15.01	14.99	14.97	14.96	14.92	14.91	14.89
1981 Jul	$\log(\nu_o F_{\nu_0})$	-	-	-	-	-	-	-	-	-	-	-	-	-	-	-
		-	-	-	-	-	-	-	-	-	-	-	-	-	-	-
1982 Feb	$\log(\nu_o F_{\nu_0})$	-	-	-	-	-	-	-	-	-	-	-	-	-	-	-
		-	-	-	-	-	-	-	-	-	-	-	-	-	-	-
1982 Apr	$\log(\nu_o F_{\nu_0})$	-	-	-	-	-	-	-	-	-	-	-	-	-	-	-
		-	-	-	-	-	-	-	-	-	-	-	-	-	-	-
1987 Jan	$\log(\nu_o F_{\nu_0})$	11.82	11.65	11.81	11.71	11.21	11.28	11.19	11.27	11.41	11.29	11.85	-	-	-	-
		0.34	0.31	0.37	0.35	0.28	0.20	0.23	0.19	0.29	0.30	0.41	-	-	-	-
Q0637-752	$\log(\nu_o)$	15.04	15.02	15.01	15.00	14.96	14.94	14.92	14.90	14.88	14.86	14.84	14.83	14.79	14.78	14.76
1980 Dec	$\log(\nu_o F_{\nu_0})$	-	-	-	-	-	-	-	-	-	-	-	-	-	-	-
		-	-	-	-	-	-	-	-	-	-	-	-	-	-	-
1981 Aug	$\log(\nu_o F_{\nu_0})$	-	-	-	-	-	-	-	-	-	-	-	-	-	-	-
		-	-	-	-	-	-	-	-	-	-	-	-	-	-	-
1987 Nov	$\log(\nu_o F_{\nu_0})$	12.01	11.97	11.93	11.99	-	-	-	-	-	-	-	-	-	-	-
		0.11	0.07	0.09	0.11	-	-	-	-	-	-	-	-	-	-	-
1988 Apr	$\log(\nu_o F_{\nu_0})$	12.03	11.92	11.98	12.02	-	-	-	-	-	-	-	-	-	-	-
		0.15	0.09	0.11	0.15	-	-	-	-	-	-	-	-	-	-	-
Q0837-120	$\log(\nu_o)$	15.17	15.16	15.15	15.14	15.10	15.08	15.06	15.04	15.02	15.00	14.98	14.97	14.93	14.91	14.90
1979	$\log(\nu_o F_{\nu_0})$	11.88	11.73	11.80	11.83	11.78	11.77	11.80	11.84	11.83	11.80	11.83	11.75	-	-	-
		0.10	0.06	0.09	0.08	0.11	0.08	0.07	0.09	0.07	0.06	0.13	0.11	-	-	-
Q0844+349	$\log(\nu_o)$	15.23	15.21	15.20	15.19	15.15	15.13	15.11	15.09	15.07	15.05	15.04	15.02	14.98	14.97	14.95
1986	$\log(\nu_o F_{\nu_0})$	12.37	12.44	12.38	12.55	12.66	12.64	12.59	12.66	12.69	12.67	12.66	12.65	12.67	12.69	-
		0.11	0.04	0.01	0.20	0.13	0.11	0.08	0.06	0.06	0.04	0.05	0.03	0.06	0.02	-
1987 Nov	$\log(\nu_o F_{\nu_0})$	12.51	12.51	12.51	12.45	12.56	12.49	12.50	12.53	12.50	12.55	12.54	12.53	12.58	12.72	-
		0.06	0.05	0.03	0.06	0.18	0.13	0.14	0.09	0.05	0.04	0.05	0.02	0.06	0.04	-
1987	$\log(\nu_o F_{\nu_0})$	12.53	12.48	12.47	12.45	12.53	12.50	12.44	12.52	12.55	12.54	12.52	12.53	12.52	12.41	-
		0.06	0.04	0.06	0.06	0.15	0.16	0.15	0.09	0.06	0.05	0.04	0.04	0.08	0.01	-
Q1028+313	$\log(\nu_o)$	15.18	15.17	15.16	15.15	15.11	15.08	15.06	15.04	15.03	15.01	14.99	14.98	14.94	14.92	14.91
1987	$\log(\nu_o F_{\nu_0})$	12.08	12.11	12.08	12.13	12.08	12.06	12.03	12.08	12.08	12.11	12.08	12.05	-	-	-
		0.13	0.12	0.10	0.12	0.08	0.07	0.05	0.05	0.05	0.03	0.06	0.08	-	-	-
Q1100+772	$\log(\nu_o)$	15.14	15.12	15.11	15.10	15.06	15.04	15.02	15.00	14.98	14.96	14.94	14.93	14.89	14.88	14.86
1978 Jul	$\log(\nu_o F_{\nu_0})$	11.50	11.44	11.52	11.50	11.54	11.52	11.52	11.57	11.64	-	-	-	-	-	-
		0.02	0.01	0.04	0.06	0.02	0.02	0.02	0.03	0.04	-	-	-	-	-	-

TABLE 5(a) (continued)

	$\lambda_{rest}(\AA)$	1675	1725	1775	1825	2000	2100	2200	2300	2400	2500	2600	2675	2950	3050	3150
1984 Jun	$\log(\nu_o F_{\nu_0})$	-	-	-	-	-	-	-	-	-	-	-	-	-	-	-
		-	-	-	-	-	-	-	-	-	-	-	-	-	-	-
Q1116+215	$\log(\nu_o)$	15.18	15.17	15.16	15.15	15.11	15.08	15.06	15.04	15.03	15.01	14.99	14.98	14.94	14.92	14.91
1980 May	$\log(\nu_o F_{\nu_0})$	12.93	-	-	-	-	-	-	-	-	-	-	-	-	-	-
		0.03	-	-	-	-	-	-	-	-	-	-	-	-	-	-
1980 May	$\log(\nu_o F_{\nu_0})$	12.92	-	-	-	-	-	-	-	-	-	-	-	-	-	-
		0.03	-	-	-	-	-	-	-	-	-	-	-	-	-	-
1982 Jul	$\log(\nu_o F_{\nu_0})$	12.71	12.62	12.61	12.63	12.56	12.62	12.59	12.62	12.63	12.67	12.69	12.84	-	-	-
		0.06	0.00	0.01	0.05	0.03	0.02	0.01	0.01	0.02	0.00	0.04	0.04	-	-	-
Q1137+660	$\log(\nu_o)$	15.04	15.02	15.01	15.00	14.96	14.94	14.92	14.90	14.88	14.86	14.84	14.83	14.79	14.77	14.76
1980 Dec	$\log(\nu_o F_{\nu_0})$	-	-	-	-	-	-	-	-	-	-	-	-	-	-	-
		-	-	-	-	-	-	-	-	-	-	-	-	-	-	-
1982 Apr	$\log(\nu_o F_{\nu_0})$	12.14	12.16	12.11	12.06	-	-	-	-	-	-	-	-	-	-	-
		0.08	0.10	0.11	0.21	-	-	-	-	-	-	-	-	-	-	-
Q1146-037	$\log(\nu_o)$	15.13	15.11	15.10	15.09	15.05	15.03	15.01	14.99	14.97	14.95	14.93	14.92	14.88	14.87	14.85
1981 Jul	$\log(\nu_o F_{\nu_0})$	11.61	11.54	11.50	11.51	11.44	11.42	11.47	11.58	11.62	-	-	-	-	-	-
		0.06	0.00	0.07	0.04	0.05	0.03	0.07	0.13	0.07	-	-	-	-	-	-
1981 Jul	$\log(\nu_o F_{\nu_0})$	11.61	11.49	11.42	11.46	11.41	11.42	11.50	11.58	11.61	-	-	-	-	-	-
		0.20	0.20	0.18	0.17	0.15	0.13	0.15	0.22	0.23	-	-	-	-	-	-
1981 Dec	$\log(\nu_o F_{\nu_0})$	11.36	11.29	11.12	11.27	11.15	11.22	11.41	11.63	11.89	-	-	-	-	-	-
		0.24	0.32	0.21	0.27	0.18	0.16	0.19	0.30	0.44	-	-	-	-	-	-
1988 Jan	$\log(\nu_o F_{\nu_0})$	-	-	-	-	-	-	-	-	-	-	-	-	-	-	-
		-	-	-	-	-	-	-	-	-	-	-	-	-	-	-
Q1202+281	$\log(\nu_o)$	15.19	15.17	15.16	15.15	15.11	15.09	15.07	15.05	15.03	15.01	15.00	14.98	14.94	14.93	14.91
1980 May	$\log(\nu_o F_{\nu_0})$	-	-	-	-	-	-	-	-	-	-	-	-	-	-	-
		-	-	-	-	-	-	-	-	-	-	-	-	-	-	-
1983 Jan	$\log(\nu_o F_{\nu_0})$	12.08	12.10	12.10	12.11	12.13	12.14	12.10	12.10	-	11.98	-	-	-	-	-
		0.14	0.01	0.01	0.02	0.01	0.02	0.06	0.05	-	0.05	-	-	-	-	-
1984 Nov	$\log(\nu_o F_{\nu_0})$	11.92	11.87	12.05	11.92	11.86	11.85	11.84	11.90	11.91	11.94	11.87	11.88	-	-	-
		0.17	0.27	0.37	0.26	0.23	0.22	0.13	0.09	0.08	0.07	0.09	0.10	-	-	-
1985 Nov	$\log(\nu_o F_{\nu_0})$	11.32	-	-	-	-	-	-	-	-	-	-	-	-	-	-
		0.40	-	-	-	-	-	-	-	-	-	-	-	-	-	-
1986 Jul	$\log(\nu_o F_{\nu_0})$	11.92	-	-	-	-	-	-	-	-	-	-	-	-	-	-
		0.07	-	-	-	-	-	-	-	-	-	-	-	-	-	-
Q1211+143	$\log(\nu_o)$	15.22	15.20	15.19	15.18	15.14	15.12	15.10	15.08	15.06	15.04	15.03	15.01	14.97	14.96	14.94
1985 Dec	$\log(\nu_o F_{\nu_0})$	12.78	12.73	12.69	12.69	12.71	12.73	12.69	12.75	12.77	12.79	12.76	12.76	12.78	-	-
		0.04	0.03	0.05	0.08	0.12	0.11	0.06	0.05	0.04	0.03	0.03	0.03	0.06	-	-
1987 Feb	$\log(\nu_o F_{\nu_0})$	12.65	12.58	12.55	12.58	12.60	12.67	12.64	12.71	12.72	12.72	12.70	12.71	12.72	-	-
		0.06	0.03	0.04	0.09	0.12	0.10	0.08	0.05	0.04	0.03	0.04	0.03	0.06	-	-

TABLE 5(a) (continued)

	$\lambda_{rest}(\AA)$	1675	1725	1775	1825	2000	2100	2200	2300	2400	2500	2600	2675	2950	3050	3150
Q1219+755	$\log(\nu_o)$	15.22	15.21	15.20	15.19	15.15	15.13	15.11	15.09	15.07	15.05	15.03	15.02	14.98	14.96	14.95
1978 Jul	$\log(\nu_o F_{\nu_0})$	12.10	12.00	11.98	12.00	11.75	11.85	11.80	11.99	11.96	12.02	12.01	12.01	12.00	-	-
		0.08	0.11	0.10	0.11	0.09	0.03	0.05	0.03	0.01	0.01	0.01	0.00	0.17	-	-
1983 Feb	$\log(\nu_o F_{\nu_0})$	12.31	12.28	12.25	12.25	12.30	12.24	12.25	12.32	12.34	12.40	12.39	12.40	12.39	-	-
		0.07	0.03	0.04	0.05	0.10	0.08	0.07	0.06	0.04	0.03	0.04	0.06	0.04	-	-
Q1226+023	$\log(\nu_o)$	15.19	15.18	15.16	15.15	15.11	15.09	15.07	15.05	15.03	15.02	15.00	14.99	14.94	14.93	14.92
1978 May	$\log(\nu_o F_{\nu_0})$	13.41	13.35	13.35	13.33	13.32	13.31	13.31	13.35	13.35	13.38	13.34	13.32	-	-	-
		0.04	0.03	0.04	0.04	0.03	0.03	0.03	0.05	0.04	0.03	0.03	0.03	-	-	-
1979 May	$\log(\nu_o F_{\nu_0})$	13.41	13.38	13.38	13.37	13.37	13.34	13.33	13.38	13.43	13.41	13.38	13.37	-	-	-
		0.03	0.03	0.04	0.04	0.04	0.04	0.04	0.04	0.05	0.04	0.03	0.06	-	-	-
1982 Apr	$\log(\nu_o F_{\nu_0})$	13.51	13.50	13.51	13.47	13.43	13.44	13.42	13.45	13.45	13.46	13.44	13.45	-	-	-
		0.02	0.04	0.05	0.04	0.04	0.05	0.05	0.04	0.04	0.03	0.03	0.05	-	-	-
1982 Jun	$\log(\nu_o F_{\nu_0})$	13.61	13.55	13.54	13.54	13.50	13.50	13.47	13.51	13.49	13.51	13.50	13.50	-	-	-
		0.02	0.03	0.01	0.00	0.00	0.01	0.01	0.01	0.01	0.00	0.02	0.01	-	-	-
1983 Apr	$\log(\nu_o F_{\nu_0})$	13.39	13.40	13.38	13.43	13.37	13.43	13.38	13.40	13.43	13.44	13.41	13.37	-	-	-
		0.04	0.07	0.08	0.07	0.08	0.07	0.05	0.05	0.04	0.04	0.05	0.07	-	-	-
1984 Jul	$\log(\nu_o F_{\nu_0})$	13.32	13.27	13.31	13.30	13.24	13.28	13.27	13.28	13.28	13.31	13.32	13.29	-	-	-
		0.04	0.05	0.06	0.05	0.06	0.05	0.04	0.03	0.03	0.02	0.03	0.03	-	-	-
1985 May	$\log(\nu_o F_{\nu_0})$	13.46	13.38	13.33	13.34	13.35	13.36	13.36	13.37	13.38	13.39	13.38	13.38	-	-	-
		0.05	0.05	0.04	0.04	0.03	0.03	0.03	0.03	0.02	0.02	0.02	0.03	-	-	-
1986 Dec	$\log(\nu_o F_{\nu_0})$	13.43	13.43	13.46	13.43	13.41	13.42	13.39	13.42	13.42	13.43	13.42	13.40	-	-	-
		0.03	0.07	0.06	0.08	0.05	0.04	0.04	0.03	0.02	0.03	0.03	0.03	-	-	-
1986 Dec	$\log(\nu_o F_{\nu_0})$	13.44	13.46	13.47	13.44	13.42	13.42	13.39	13.42	13.42	13.43	13.42	13.41	-	-	-
		0.03	0.06	0.06	0.06	0.05	0.05	0.03	0.03	0.03	0.02	0.02	0.03	-	-	-
1987 Jun	$\log(\nu_o F_{\nu_0})$	13.29	13.28	13.31	13.28	13.25	13.30	13.28	13.30	13.33	13.33	13.32	13.29	-	-	-
		0.04	0.08	0.08	0.07	0.06	0.05	0.04	0.04	0.03	0.02	0.03	0.04	-	-	-
1987 Jun	$\log(\nu_o F_{\nu_0})$	13.27	13.27	13.30	13.27	13.25	13.30	13.28	13.31	13.32	13.34	13.33	13.28	-	-	-
		0.04	0.06	0.08	0.07	0.05	0.06	0.05	0.03	0.04	0.03	0.02	0.02	-	-	-
1988 Jun	$\log(\nu_o F_{\nu_0})$	13.42	13.42	13.40	13.41	13.38	13.38	13.35	13.37	13.39	13.40	13.39	13.37	-	-	-
		0.03	0.06	0.06	0.06	0.06	0.05	0.03	0.03	0.03	0.02	0.03	0.03	-	-	-
1989 Feb	$\log(\nu_o F_{\nu_0})$	13.31	13.32	13.27	13.31	13.26	13.30	13.26	13.29	13.31	13.35	13.33	13.30	-	-	-
		0.04	0.10	0.08	0.12	0.09	0.07	0.06	0.04	0.03	0.03	0.02	0.04	-	-	-
Q1229+204	$\log(\nu_o)$	15.23	15.21	15.20	15.19	15.15	15.13	15.11	15.09	15.07	15.05	15.04	15.02	14.98	14.97	14.95
1982 May	$\log(\nu_o F_{\nu_0})$	12.54	12.49	12.46	12.43	12.42	12.40	12.42	12.48	12.49	12.50	12.48	12.51	12.53	-	-
		0.08	0.01	0.05	0.05	0.04	0.02	0.01	0.04	0.02	0.01	0.01	0.02	0.02	-	-
Q1307+085	$\log(\nu_o)$	15.19	15.18	15.17	15.15	15.11	15.09	15.07	15.05	15.03	15.02	15.00	14.99	14.94	14.93	14.92
1980 May	$\log(\nu_o F_{\nu_0})$	12.36	-	-	-	-	-	-	-	-	-	-	-	-	-	-
		0.04	-	-	-	-	-	-	-	-	-	-	-	-	-	-
1984 Feb	$\log(\nu_o F_{\nu_0})$	12.25	12.21	12.19	12.17	12.10	12.14	12.12	12.13	12.13	12.16	12.16	12.16	-	-	-
		0.01	0.01	0.00	0.03	0.07	0.02	0.03	0.01	0.01	0.01	0.02	0.01	-	-	-

TABLE 5(a) (continued)

	$\lambda_{rest}(\AA)$	1675	1725	1775	1825	2000	2100	2200	2300	2400	2500	2600	2675	2950	3050	3150
Q1407+265	$\log(\nu_o)$	14.96	14.95	14.94	14.93	14.89	14.87	14.85	14.83	14.81	14.79	14.77	14.76	14.72	14.70	14.69
1983 Apr	$\log(\nu_o F_{\nu_0})$	-	-	-	-	-	-	-	-	-	-	-	-	-	-	-
		-	-	-	-	-	-	-	-	-	-	-	-	-	-	-
1986 Dec	$\log(\nu_o F_{\nu_0})$	-	-	-	-	-	-	-	-	-	-	-	-	-	-	-
		-	-	-	-	-	-	-	-	-	-	-	-	-	-	-
1988 Sep	$\log(\nu_o F_{\nu_0})$	-	-	-	-	-	-	-	12.06	12.08	12.06	12.04	12.01	12.03	11.97	11.98
		-	-	-	-	-	-	-	0.04	0.01	0.01	0.01	0.01	0.01	0.02	0.01
1988 Jun	$\log(\nu_o F_{\nu_0})$	12.08	12.07	12.06	12.09	12.06	12.06	12.04	12.05	12.06	12.04	12.03	12.00	12.00	11.95	11.95
		0.01	0.02	0.00	0.01	0.01	0.01	0.01	0.01	0.00	0.01	0.01	0.00	0.01	0.01	0.02
Q1416-129	$\log(\nu_o)$	15.20	15.19	15.18	15.16	15.12	15.10	15.08	15.06	15.04	15.03	15.01	15.00	14.95	14.94	14.93
1980 Jul	$\log(\nu_o F_{\nu_0})$	-	11.90	-	-	-	-	-	-	-	-	-	-	-	-	-
		-	0.00	-	-	-	-	-	-	-	-	-	-	-	-	-
1983 Jun	$\log(\nu_o F_{\nu_0})$	-	11.89	11.99	12.03	11.92	11.81	11.94	11.99	12.03	12.08	12.06	12.01	-	-	-
		-	0.27	0.23	0.18	0.23	0.20	0.15	0.12	0.12	0.08	0.12	0.14	-	-	-
1988 Mar	$\log(\nu_o F_{\nu_0})$	11.89	11.71	11.70	-	-	-	-	-	-	-	-	-	-	-	-
		0.11	0.11	0.03	-	-	-	-	-	-	-	-	-	-	-	-
Q1426+015	$\log(\nu_o)$	15.22	15.20	15.19	15.18	15.14	15.12	15.10	15.08	15.06	15.04	15.03	15.01	14.97	14.96	14.94
1983	$\log(\nu_o F_{\nu_0})$	-	13.00	12.92	12.62	12.78	12.57	12.63	12.69	12.68	12.68	12.66	12.69	12.81	-	-
		-	0.15	0.36	0.32	0.33	0.28	0.29	0.17	0.13	0.16	0.21	0.17	0.40	-	-
1983 May	$\log(\nu_o F_{\nu_0})$	12.75	12.69	12.63	12.63	12.65	12.65	12.60	12.68	12.69	12.71	12.70	12.70	12.75	-	-
		0.04	0.05	0.06	0.08	0.06	0.07	0.06	0.05	0.05	0.04	0.03	0.05	0.07	-	-
1983 Aug	$\log(\nu_o F_{\nu_0})$	12.85	12.81	12.77	12.81	12.69	12.71	12.62	12.62	12.74	12.77	12.78	12.76	13.05	-	-
		0.04	0.03	0.08	0.17	0.19	0.16	0.14	0.14	0.13	0.14	0.10	0.10	0.24	-	-
1985 Mar	$\log(\nu_o F_{\nu_0})$	12.88	12.86	12.83	12.86	12.81	12.80	12.79	12.80	12.81	12.80	12.79	12.79	12.89	-	-
		0.02	0.02	0.02	0.07	0.05	0.04	0.04	0.04	0.03	0.02	0.03	0.02	0.04	-	-
Q1501+106	$\log(\nu_o)$	15.24	15.22	15.21	15.20	15.16	15.14	15.12	15.10	15.08	15.06	15.05	15.03	14.99	14.98	14.96
1983 Feb	$\log(\nu_o F_{\nu_0})$	12.71	12.65	12.64	12.64	12.57	12.60	12.52	12.57	12.61	12.65	12.65	12.63	12.65	12.63	-
		0.05	0.03	0.02	0.02	0.08	0.11	0.10	0.10	0.06	0.07	0.05	0.05	0.08	0.10	-
Q1545+210	$\log(\nu_o)$	15.15	15.14	15.13	15.11	15.07	15.05	15.03	15.01	14.99	14.98	14.96	14.95	14.90	14.89	14.88
1983 Jun	$\log(\nu_o F_{\nu_0})$	11.97	11.93	11.95	12.02	12.10	-	-	-	-	-	-	-	-	-	-
		0.00	0.01	0.01	0.03	0.01	-	-	-	-	-	-	-	-	-	-
1983 Aug	$\log(\nu_o F_{\nu_0})$	12.19	12.16	12.20	12.07	11.95	11.94	12.03	11.99	12.10	12.50	-	-	-	-	-
		0.27	0.27	0.27	0.27	0.20	0.19	0.19	0.17	0.25	0.25	-	-	-	-	-
Q1613+658	$\log(\nu_o)$	15.20	15.19	15.18	15.16	15.12	15.10	15.08	15.06	15.04	15.03	15.01	15.00	14.95	14.94	14.93
1981 Sep	$\log(\nu_o F_{\nu_0})$	12.19	12.12	12.02	12.02	12.09	12.17	-	-	-	-	-	-	-	-	-
		0.04	0.03	0.03	0.03	0.03	0.03	-	-	-	-	-	-	-	-	-
1983 May	$\log(\nu_o F_{\nu_0})$	12.23	12.03	-	-	-	-	-	-	-	-	-	-	-	-	-
		0.08	0.11	-	-	-	-	-	-	-	-	-	-	-	-	-

TABLE 5(a) (continued)

	$\lambda_{rest}(\AA)$	1675	1725	1775	1825	2000	2100	2200	2300	2400	2500	2600	2675	2950	3050	3150
1983 Aug	$\log(\nu_o F_{\nu_0})$	12.34	12.27	12.27	12.20	12.29	12.20	12.20	12.23	12.31	12.33	12.25	12.24	-	-	-
		0.05	0.08	0.20	0.18	0.21	0.24	0.14	0.13	0.11	0.11	0.11	0.09	-	-	-
1984 Jan	$\log(\nu_o F_{\nu_0})$	12.29	12.27	12.23	12.31	12.23	12.21	12.23	12.27	12.31	12.33	12.31	12.30	-	-	-
		[illegible]	0.08	0.11	0.13	0.12	0.08	0.05	0.04	0.03	0.03	0.03	0.03	-	-	-
1984 Jun	$\log(\nu_o F_{\nu_0})$	12.3	12.32	12.49	12.49	12.48	12.49	12 44	12.30	12.31	12.34	12.30	12.30	-	-	-
		0.12	0.18	0.26	0.28	0.29	0.29	0.23	0.21	0.16	0.14	0.16	0.16	-	-	-
Q1704+608	$\log(\nu_o)$	15.12	15.10	15.09	15.08	15.04	15.02	15.00	14.98	14.96	14.94	14.93	14.91	14.87	14.86	14.84
1979	$\log(\nu_o F_{\nu_0})$	12.05	12.04	12.10	12.04	11.99	12.05	12.00	12.06	-	-	-	-	-	-	-
		0.11	0.12	0.10	0.09	0.07	0.07	0.08	0.11	-	-	-	-	-	-	-
1983 Dec	$\log(\nu_o F_{\nu_0})$	-	-	-	-	-	-	-	-	-	-	-	-	-	-	-
		-	-	-	-	-	-	-	-	-	-	-	-	-	-	-
1986 Dec	$\log(\nu_o F_{\nu_0})$	12.07	12.03	12.06	12.07	12.04	12.04	12.06	12.11	-	-	-	-	-	-	-
		0.11	0.10	0.09	0.07	0.05	0.04	0.05	0.09	-	-	-	-	-	-	-
Q1721+343	$\log(\nu_o)$	15.17	15.16	15.15	15.13	15.09	15.07	15.05	15.03	15.02	15.00	14.98	14.97	14.93	14.91	14.90
1983 Aug	$\log(\nu_o F_{\nu_0})$	12.63	12.59	12.66	12.60	12.46	12.33	12.37	12.40	12.31	12.37	12.61	12.96	-	-	-
		0.29	0.20	0.28	0.25	0.22	0.20	0.20	0.18	0.21	0.27	0.37	0.38	-	-	-
1986 May	$\log(\nu_o F_{\nu_0})$	12.47	12.39	12.42	12.43	12.31	12.31	12.30	12.34	12.36	12.40	12.39	12.52	-	-	-
		0.10	0.08	0.08	0.09	0.06	0.06	0.04	0.04	0.04	0.04	0.07	0.02	-	-	-
Q1803+676	$\log(\nu_o)$	15.20	15.18	15.17	15.16	15.12	15.10	15.08	15.06	15.04	15.02	15.01	14.99	14.95	14.94	14.92
1987 May	$\log(\nu_o F_{\nu_0})$	12.08	11.99	11.99	12.17	11.97	11.98	12.03	12.07	12.11	12.14	12.09	12.07	-	-	-
		0.16	0.27	0.52	0.28	0.15	0.11	0.08	0.05	0.04	0.05	0.05	0.18	-	-	-
Q2130+099	$\log(\nu_o)$	15.23	15.21	15.20	15.19	15.15	15.13	15.11	15.09	15.07	15.05	15.04	15.02	14.98	14.97	14.95
1978 Jul	$\log(\nu_o F_{\nu_0})$	12.76	12.74	12.78	12.75	12.44	12.50	12.47	12.55	12.54	12.56	12.53	12.51	12.57	12.63	-
		0.05	0.02	0.03	0.13	0.09	0.11	0.08	0.09	0.07	0.06	0.06	0.05	0.10	0.06	-
1979 May	$\log(\nu_o F_{\nu_0})$	12.42	12.43	-	-	12.43	12.44	12.46	12.47	12.50	12.54	12.51	12.49	12.51	12.38	-
		0.03	0.01	-	-	0.02	0.05	0.03	0.03	0.02	0.02	0.02	0.00	0.02	0.02	-
1985	$\log(\nu_o F_{\nu_0})$	12.48	12.42	12.41	12.39	12.42	12.45	12.39	12.47	12.48	12.51	12.49	12.45	12.51	12.45	-
		0.11	0.07	0.05	0.09	0.16	0.14	0.08	0.09	0.07	0.04	0.06	0.03	0.07	0.05	-
Q2135-147	$\log(\nu_o)$	15.17	15.16	15.15	15.14	15.10	15.08	15.06	15.04	15.02	15.00	14.98	14.97	14.93	14.91	14.90
1979 Apr	$\log(\nu_o F_{\nu_0})$	11.89	11.76	11.80	11.79	11.81	11.75	11.77	11.88	11.95	11.92	11.99	12.03	-	-	-
		0.13	0.08	0.07	0.12	0.13	0.11	0.07	0.10	0.07	0.09	0.14	0.14	-	-	-
1982 Dec	$\log(\nu_o F_{\nu_0})$	11.96	11.88	11.96	11.85	11.83	11.83	11.86	11.89	11.96	12.00	11.99	12.00	-	-	-
		0.17	0.15	0.18	0.15	0.13	0.10	0.07	0.05	0.04	0.04	0.09	0.11	-	-	-

TABLE 5(b)

ULTRAVIOLET CONTINUUM FLUXES: Other IPC quasars

			$\lambda_{rest}(\AA)$	725	775	825	875	925	975	1025	1075	1125	1300	1350	1475	1625
Q0804+761			$\log(\nu_o)$	15.58	15.55	15.52	15.49	15.47	15.45	15.43	15.40	15.38	15.32	15.31	15.27	15.22
1982	LWR16666?	SWP17393	$\log(\nu_o F_{\nu_0})$	-	-	-	-	-	-	-	12.62	12.61	12.63	12.73	12.58	12.66
				-	-	-	-	-	-	-	0.00	0.01	0.03	0.09	0.02	0.03
Q0915+165			$\log(\nu_o)$	15.60	15.58	15.55	15.52	15.50	15.48	15.45	15.43	15.41	15.35	15.33	15.30	15.25
1983 Jun	LWR16188	SWP20255	$\log(\nu_o F_{\nu_0})$	-	-	-	-	-	-	-	-	-	12.12	12.13	12.12	12.23
				-	-	-	-	-	-	-	-	-	0.09	0.13	0.12	0.13
1986 Apr	LWP7964	SWP28101	$\log(\nu_o F_{\nu_0})$	-	-	-	-	-	-	-	-	-	11.99	11.99	12.04	12.18
				-	-	-	-	-	-	-	-	-	0.09	0.07	0.07	0.09
Q0923+129			$\log(\nu_o)$	15.60	15.58	15.55	15.52	15.50	15.48	15.45	15.43	15.41	15.35	15.33	15.30	15.25
1985 May		SWP25826	$\log(\nu_o F_{\nu_0})$	-	-	-	-	-	-	-	-	-	-	-	-	-
				-	-	-	-	-	-	-	-	-	-	-	-	-
Q1012+008			$\log(\nu_o)$	15.54	15.51	15.49	15.46	15.44	15.41	15.39	15.37	15.35	15.29	15.27	15.23	15.19
1985 Nov		SWP27189	$\log(\nu_o F_{\nu_0})$	-	-	-	-	-	-	11.78	11.51	11.44	11.71	11.66	11.51	11.38
				-	-	-	-	-	-	0.49	0.28	0.31	0.37	0.29	0.32	0.30
Q1217+023			$\log(\nu_o)$	15.52	15.49	15.47	15.44	15.42	15.39	15.37	15.35	15.33	15.27	15.25	15.21	15.17
1981 Jul		SWP14476	$\log(\nu_o F_{\nu_0})$	-	-	-	-	-	11.91	12.03	11.89	11.85	11.84	11.86	11.81	-
				-	-	-	-	-	0.07	0.13	0.08	0.12	0.09	0.11	0.06	-
1981 Jul		SWP14484	$\log(\nu_o F_{\nu_0})$	-	-	-	-	-	11.95	12.18	12.07	12.01	12.00	11.99	12.01	-
				-	-	-	-	-	0.12	0.18	0.07	0.12	0.09	0.09	0.08	-
1987 Jul	LWP11206		$\log(\nu_o F_{\nu_0})$	-	-	-	-	-	-	-	-	-	-	-	-	12.21
				-	-	-	-	-	-	-	-	-	-	-	-	0.15
Q1244+026			$\log(\nu_o)$	15.60	15.57	15.54	15.51	15.49	15.47	15.45	15.43	15.41	15.34	15.33	15.29	15.25
1983 Feb	LWR15213	SWP19223	$\log(\nu_o F_{\nu_0})$	-	-	-	-	-	-	-	-	-	11.91	11.89	11.87	-
				-	-	-	-	-	-	-	-	-	0.03	0.02	0.00	-
Q1351+695			$\log(\nu_o)$	15.60	15.57	15.55	15.52	15.50	15.47	15.45	15.43	15.41	15.35	15.33	15.30	15.25
1981 Jun		SWP14225	$\log(\nu_o F_{\nu_0})$	-	-	-	-	-	-	-	-	-	12.56	12.56	12.60	12.64
				-	-	-	-	-	-	-	-	-	0.04	0.04	0.06	0.04
1987 Feb	LWP10116	SWP30303	$\log(\nu_o F_{\nu_0})$	-	-	-	-	-	-	-	-	-	12.16	12.14	12.18	12.33
				-	-	-	-	-	-	-	-	-	0.12	0.10	0.14	0.12
Q1635+119			$\log(\nu_o)$	15.56	15.53	15.50	15.48	15.45	15.43	15.41	15.39	15.37	15.30	15.29	15.25	15.21
1988 Apr		SWP33232	$\log(\nu_o F_{\nu_0})$	-	-	-	-	-	-	-	11.84	12.02	11.96	11.76	11.74	11.74
				-	-	-	-	-	-	-	0.36	0.25	0.25	0.30	0.31	0.29

TABLE 5(b) (continued)

		$\lambda_{rest}(\AA)$	725	775	825	875	925	975	1025	1075	1125	1300	1350	1475	1625
Q2304+042		$\log(\nu_o)$	15.60	15.57	15.54	15.52	15.49	15.47	15.45	15.43	15.41	15.35	15.33	15.29	15.25
1985 Aug	LWP6542	$\log(\nu_o F_{\nu_0})$	-	-	-	-	-	-	-	-	-	-	-	-	-
			-	-	-	-	-	-	-	-	-	-	-	-	-

TABLE 5(b)

ULTRAVIOLET CONTINUUM FLUXES: Other IPC quasars

	$\lambda_{rest}(\AA)$	1675	1725	1775	1825	2000	2100	2200	2300	2400	2500	2600	2675	2950	3050	3150
Q0804+761	$\log(\nu_o)$	15.21	15.20	15.19	15.17	15.13	15.11	15.09	15.07	15.06	15.04	15.02	15.01	14.97	14.95	14.94
1982	$\log(\nu_o F_{\nu_0})$	12.66	12.62	12.81	12.74	12.61	12.62	12.59	12.64	12.62	12.69	12.66	12.67	12.96	-	-
		0.05	0.17	0.12	0.04	0.06	0.08	0.07	0.03	0.03	0.03	0.02	0.00	0.09	-	-
Q0915+165	$\log(\nu_o)$	15.24	15.23	15.22	15.20	15.16	15.14	15.12	15.10	15.08	15.07	15.05	15.04	14.99	14.98	14.97
1983 Jun	$\log(\nu_o F_{\nu_0})$	12.16	12.07	12.16	12.15	12.26	12.48	12.28	12.38	12.43	12.36	12.44	12.39	12.44	12.54	12.85
		0.09	0.08	0.07	0.08	0.26	0.37	0.28	0.28	0.24	0.17	0.15	0.18	0.22	0.27	0.28
1986 Apr	$\log(\nu_o F_{\nu_0})$	12.08	12.08	12.10	12.05	12.17	12.09	12.10	12.11	12.16	12.24	12.29	12.32	12.55	13.11	13.43
		0.06	0.05	0.05	0.05	0.17	0.20	0.14	0.13	0.07	0.06	0.04	0.04	0.08	0.21	0.03
Q0923+129	$\log(\nu_o)$	15.24	15.23	15.22	15.20	15.16	15.14	15.12	15.10	15.08	15.07	15.05	15.04	15.00	14.98	14.97
1985 May	$\log(\nu_o F_{\nu_0})$	-	-	-	-	12.77	12.45	12.28	12.39	12.37	12.53	12.67	12.39	12.35	12.32	12.40
		-	-	-	-	0.08	0.15	0.02	0.12	0.02	0.13	0.27	0.01	0.04	0.02	0.07
Q1012+008	$\log(\nu_o)$	15.18	15.17	15.15	15.14	15.10	15.08	15.06	15.04	15.02	15.01	14.99	14.98	14.93	14.92	14.91
1985 Nov	$\log(\nu_o F_{\nu_0})$	11.27	-	-	-	-	-	-	-	-	-	-	-	-	-	-
		0.18	-	-	-	-	-	-	-	-	-	-	-	-	-	-
Q1217+023	$\log(\nu_o)$	15.16	15.15	15.13	15.12	15.08	15.06	15.04	15.02	15.00	14.99	14.97	14.96	14.91	14.90	14.89
1981 Jul	$\log(\nu_o F_{\nu_0})$	-	-	-	-	-	-	-	-	-	-	-	-	-	-	-
		-	-	-	-	-	-	-	-	-	-	-	-	-	-	-
1981 Jul	$\log(\nu_o F_{\nu_0})$	-	-	-	-	-	-	-	-	-	-	-	-	-	-	-
		-	-	-	-	-	-	-	-	-	-	-	-	-	-	-
1987 Jul	$\log(\nu_o F_{\nu_0})$	12.16	12.15	12.05	12.10	12.03	12.04	12.01	12.02	12.08	12.12	12.18	-	-	-	-
		0.15	0.15	0.13	0.17	0.09	0.06	0.05	0.06	0.05	0.06	0.10	-	-	-	-
Q1244+026	$\log(\nu_o)$	15.23	15.22	15.21	15.20	15.16	15.13	15.11	15.10	15.08	15.06	15.04	15.03	14.99	14.97	14.96
1983 Feb	$\log(\nu_o F_{\nu_0})$	-	11.84	11.86	11.86	11.85	11.98	11.93	11.90	11.91	11.94	11.89	-	-	-	-
		-	0.02	0.03	0.00	0.07	0.04	0.06	0.08	0.03	0.03	0.02	-	-	-	-
Q1351+695	$\log(\nu_o)$	15.24	15.23	15.21	15.20	15.16	15.14	15.12	15.10	15.08	15.07	15.05	15.04	14.99	14.98	14.97
1981 Jun	$\log(\nu_o F_{\nu_0})$	12.62	12.54	12.58	12.62	-	-	-	-	-	-	-	-	-	-	-
		0.04	0.03	0.02	0.03	-	-	-	-	-	-	-	-	-	-	-
1987 Feb	$\log(\nu_o F_{\nu_0})$	12.23	12.16	12.19	12.15	12.28	12.22	12.30	12.34	12.41	12.41	12.38	12.36	12.38	12.32	12.47
		0.08	0.08	0.06	0.11	0.23	0.25	0.25	0.16	0.10	0.07	0.05	0.04	0.06	0.10	0.02
Q1635+119	$\log(\nu_o)$	15.19	15.18	15.17	15.16	15.12	15.10	15.08	15.06	15.04	15.02	15.00	14.99	14.95	14.93	14.92
1988 Apr	$\log(\nu_o F_{\nu_0})$	11.70	11.40	-	-	-	-	-	-	-	-	-	-	-	-	-
		0.36	0.41	-	-	-	-	-	-	-	-	-	-	-	-	-

TABLE 5(b) (continued)

	$\iota(\AA)$	1675	1725	1775	1825	2000	2100	2200	2300	2400	2500	2600	2675	2950	3050	3150
Q2304+042	$\log(\nu_o)$	15.24	15.22	15.21	15.20	15.16	15.14	15.12	15.10	15.08	15.06	15.04	15.03	14.99	14.97	14.96
1985 Aug	$\log(\nu_o F_{\nu_0})$	-	-	-	-	12.35	12.15	12.13	11.96	11.88	11.83	11.80	11.70	11.78	11.66	-
		-	-	-	-	0.33	0.38	0.34	0.23	0.25	0.20	0.17	0.16	0.25	0.17	-

TABLE 6

ADOPTED E(B-V) VALUES FOR PG QUASARS

Object PG	E(B-V) (N87)	E(B-V) (This paper)	Object PG	E(B-V) (N87)	E(B-V) (This paper)	Object PG	E(B-V) (N87)	E(B-V) (This paper)
0002+05	0.18	0.08	1115+40	−0.04	0.04	1407+26	−0.02	0.03
0003+15	0.10	0.06	1116+21	−0.02	0.03	1411+44	−0.07	0.02
0007+10	0.17	0.12	1119+12	−0.03	0.05	1415+45	−0.07	0.02
0014+16	0.21	0.08	1121+42	−0.01	0.05	1416−12	0.35	0.14
0026+12	0.16	0.10	1126−04	0.07	0.09	1426+01	0.16	0.05
0043+03	0.03	0.06	1138+04	0.05	0.04	1427+48	0.00	0.04
0044+03	0.03	0.06	1148+54	0.01	0.02	1435−06	0.18	0.10
0049+17	0.11	0.09	1151+11	−0.04	0.05	1440+35	0.00	0.02
0052+25	0.11	0.09	1202+28	0.00	0.03	1444+40	0.00	0.03
0117+21	0.11	0.10	1206+45	−0.05	0.03	1448+27	0.00	0.05
0157+00	0.08	0.05	1211+14	0.03	0.06	1501+10	0.13	0.04
0804+76	0.12	0.06	1216+06	−0.05	0.03	1512+37	0.03	0.03
0832+25	0.11	0.07	1222+22	0.04	0.04	1519+22	0.04	0.08
0838+77	0.04	0.05	1226+02	0.03	0.04	1522+10	0.10	0.06
0844+34	0.07	0.07	1229+20	0.02	0.05	1534+58	0.01	0.05
0906+48	0.03	0.04	1241+17	0.03	0.04	1535+54	0.01	0.03
0923+19	0.07	0.08	1244+02	0.05	0.04	1543+48	0.03	0.03
0931+43	0.04	0.03	1247+26	0.05	0.02	1545+21	0.11	0.08
0935+41	0.04	0.03	1248+40	−0.12	0.03	1552+08	0.07	0.07
0946+30	0.04	0.04	1254+04	0.02	0.04	1612+26	0.07	0.08
0947+39	0.04	0.03	1259+59	0.03	0.03	1613+65	0.00	0.05
0953+41	0.04	0.03	1302−10	0.11	0.07	1617+17	0.18	0.09
1001+05	0.07	0.04	1307+08	0.05	0.04	1626+55	−0.02	0.04
1004+13	0.04	0.07	1309+35	0.00	0.02	1630+37	0.05	0.02
1008+13	0.12	0.08	1310−10	0.06	0.06	1634+70	0.14	0.11
1011−04	0.03	0.07	1329+41	−0.05	0.02	1700+51	0.02	0.05
1012+00	0.04	0.06	1333+17	0.00	0.04	1704+60	0.04	0.05
1048−09	0.11	0.06	1338+41	−0.05	0.02	1718+48	0.07	0.05
1048+34	0.01	0.04	1351+23	0.00	0.03	2112+05	0.26	0.13
1049−00	0.07	0.08	1351+64	0.03	0.05	2130+09	0.13	0.08
1100+77	0.09	0.06	1352+18	0.00	0.04	2209+18	0.16	0.10
1103−00	0.06	0.08	1352+01	0.14	0.04	2233+13	0.11	0.10
1112+43	0.01	0.03	1354+21	−0.04	0.04	2251+11	0.15	0.11
1114+44	−0.04	0.04	1402+26	−0.02	0.03	2302+02	0.25	0.10
1115+08	0.04	0.07	1404+22	−0.02	0.04	2344+09	0.26	0.10
						2349−01	0.11	0.07

TABLE 7(a)

OPTICAL CCD PHOTOMETRY: UV sample Quasars

Object	V	B-V	V-R	R-I	Date
Q0007+106	15.155 ±0.071	0.507 ±0.041	0.582 ±0.035	0.489 ±0.039	1986 Sep 28
Q0026+129	15.314 ±0.040	0.363 ±0.027	0.243 ±0.017	0.624 ±0.064	1985 Sep 16
	15.325 ±0.053	0.395 ±0.061	0.253 ±0.035	0.603 ±0.018	1986 Sep 26
Q0054+144	11.726 ±0.040	0.280 ±0.027	0.209 ±0.017	0.209 ±0.064	1985 Sep 16
	11.811 ±0.053	0.291 ±0.061	0.252 ±0.035	0.201 ±0.018	1986 Sep 26
Q0134+329	16.007 ±0.040	0.403 ±0.027	0.452 ±0.017	0.223 ±0.064	1985 Sep 16
Q0205+024	15.549 ±0.053	0.276 ±0.061	0.163 ±0.011	0.582 ±0.047	1986 Sep 25
Q0844+349	14.500 ±0.053	0.334 ±0.061	0.479 ±0.035	0.247 ±0.018	1986 Sep 26
Q1028+313	15.920 ±0.055	0.316 ±0.027	0.240 ±0.020	0.679 ±0.016	1985 May 13
Q1116+215	14.725 ±0.069	0.129 ±0.028	0.135 ±0.027	0.606 ±0.023	1986 May 13
Q1137+660	15.951 ±0.030	0.121 ±0.037	0.187 ±0.026	0.215 ±0.029	1986 May 14
Q1146–037	18.115 ±0.030	-0.181 ±0.037	0.687 ±0.026		1986 May 14
Q1202+281	15.918 ±0.055	0.254 ±0.027	0.126 ±0.020	0.631 ±0.016	1985 May 13
Q1211+143	14.252 ±0.052	0.267 ±0.045	0.386 ±0.020	0.274 ±0.012	1985 May 14
Q1219+755	14.828 ±0.041	0.410 ±0.032	0.518 ±0.028	0.359 ±0.058	1985 May 11
	15.032 ±0.069	0.464 ±0.028	0.550 ±0.027	0.365 ±0.023	1986 May 13
Q1226+023	12.810 ±0.069	0.176 ±0.028	0.096 ±0.027	0.584 ±0.023	1986 May 13
Q1307+085	15.115 ±0.069	0.208 ±0.028	0.139 ±0.027	0.555 ±0.023	1986 May 13
Q1407+265	15.740 ±0.030	0.334 ±0.037	0.197 ±0.026	0.196 ±0.029	1986 May 14
Q1416–129	16.101 ±0.052	0.319 ±0.045	0.235 ±0.020	0.902 ±0.012	1985 May 14
Q1426+015	14.547 ±0.055	0.313 ±0.027	0.426 ±0.020	0.432 ±0.016	1985 May 13
	14.670 ±0.069	0.349 ±0.028	0.473 ±0.027	0.432 ±0.023	1986 May 13
Q1501+106	14.265 ±0.069	0.345 ±0.028	0.559 ±0.027	0.193 ±0.023	1986 May 13
Q1545+210	16.023 ±0.041	0.257 ±0.032	0.350 ±0.028	0.519 ±0.058	1985 May 11
	16.015 ±0.069	-0.023 ±0.028	0.390 ±0.027	0.551 ±0.023	1986 May 13
Q1613+658	14.915 ±0.055	0.436 ±0.027	0.292 ±0.020	0.759 ±0.016	1985 May 13
Q1721+343	15.465 ±0.055	0.120 ±0.027	0.212 ±0.020	0.597 ±0.016	1985 May 13
Q1803+676	15.892 ±0.041	0.345 ±0.032	0.248 ±0.028	0.783 ±0.058	1985 May 11
Q2130+099	14.743 ±0.041	0.366 ±0.032	0.540 ±0.028		1985 May 11
	14.674 ±0.053	0.296 ±0.061	0.477 ±0.035	0.219 ±0.018	1986 Sep 26
Q2135–147	15.648 ±0.040	0.376 ±0.027	0.266 ±0.017	0.679 ±0.064	1985 Sep 16
	15.775 ±0.053	0.031 ±0.061	0.460 ±0.035	0.705 ±0.018	1986 Sep 26

TABLE 7(b)

OPTICAL CCD PHOTOMETRY: Other IPC Quasars

Object	V	B-V	V-R	R-I	Date
Q0003+199	13.838 ±0.040	0.290 ±0.027	0.532 ±0.017	0.178 ±0.064	1985 Sep 16
Q0050+124	14.083 ±0.071	0.509 ±0.041	0.470 ±0.035	0.336 ±0.039	1986 Sep 28
Q0133+207	17.438 ±0.071	0.267 ±0.041	0.314 ±0.035	0.502 ±0.039	1986 Sep 28
Q0414−060	16.095 ±0.032	0.287 ±0.009	0.132 ±0.017	0.138 ±0.013	1986 Feb 03
Q0804+762	14.708 ±0.032	0.321 ±0.009	0.318 ±0.017	0.481 ±0.013	1986 Feb 03
Q0923+129	14.615 ±0.069	0.569 ±0.028	0.581 ±0.027	0.435 ±0.023	1986 May 13
Q0923+392	17.015 ±0.052	0.057 ±0.045	0.226 ±0.020	0.417 ±0.012	1985 May 14
Q1012+008	15.586 ±0.069	0.425 ±0.028	0.261 ±0.027	0.648 ±0.023	1986 May 13
Q1121+422	16.252 ±0.030	0.331 ±0.037	0.221 ±0.026	0.416 ±0.029	1986 May 14
Q1217+023	16.754 ±0.052	0.163 ±0.045	0.414 ±0.020	0.854 ±0.012	1985 May 14
Q1435−067	16.009 ±0.069	0.123 ±0.028	0.236 ±0.027	0.758 ±0.023	1986 May 13
Q1635+119	16.796 ±0.052	0.478 ±0.045	0.418 ±0.020	0.735 ±0.012	1985 May 14
Q2112+059	15.774 ±0.056	0.288 ±0.021	0.414 ±0.011	0.260 ±0.047	1986 Sep 25
	15.854 ±0.027	0.167 ±0.037	0.396 ±0.004	0.375 ±0.059	1986 Sep 29
Q2120+168	18.283 ±0.027	0.296 ±0.037	-1.303 ±0.035	0.333 ±0.039	1986 Sep 28
Q2128−123	15.965 ±0.071	0.180 ±0.041	0.172 ±0.035	0.282 ±0.039	1986 Sep 28
Q2209+184	15.444 ±0.052	0.652 ±0.045	0.545 ±0.020		1985 May 14
	15.457 ±0.040	0.650 ±0.027	0.616 ±0.017	0.295 ±0.064	1985 Sep 16
	15.405 ±0.053	0.603 ±0.061	0.592 ±0.035	0.404 ±0.018	1986 Sep 26
Q2214+139	14.982 ±0.056	0.613 ±0.021	0.610 ±0.011	0.310 ±0.047	1986 Sep 25
	15.066 ±0.027	0.584 ±0.037	0.635 ±0.004	0.380 ±0.059	1986 Sep 29
Q2233+134	16.707 ±0.071	-0.011 ±0.041	0.284 ±0.035	0.408 ±0.039	1986 Sep 28
	16.747 ±0.027	0.025 ±0.037	0.272 ±0.011	0.106 ±0.047	1986 Sep 25
Q2251+113	15.739 ±0.056	0.209 ±0.021	0.423 ±0.011	0.517 ±0.047	1986 Sep 25
Q2254+024	17.959 ±0.027	0.083 ±0.037	0.456 ±0.035	0.463 ±0.039	1986 Sep 28
Q2304+042	15.496 ±0.053	0.825 ±0.061	0.743 ±0.035	0.441 ±0.018	1986 Sep 26

TABLE 8(a)

OPTICAL CONTINUUM FLUXES: UV sample quasars

		$\lambda_{rest}(\AA)$	2675	2950	3050	3150	3250	3600	3800	4500	4600	5200
Q0837-120		$\log(\nu_o)$	14.97	14.93	14.91	14.90	14.89	14.84	14.82	14.75	14.74	14.68
1988 Aug	MMT/FOGS	$\log(\nu_o F_{\nu_0})$	-	-	-	-	-	-	11.79	11.70	11.72	11.68
			-	-	-	-	-	-	0.01	0.01	0.02	0.01
Q0844+349		$\log(\nu_o)$	15.02	14.98	14.97	14.95	14.94	14.89	14.87	14.80	14.79	14.73
1988 Sep	MMT/FOGS	$\log(\nu_o F_{\nu_0})$	-	-	-	-	-	-	-	12.54	12.55	12.51
			-	-	-	-	-	-	-	0.02	0.01	0.02
Q1028+313		$\log(\nu_o)$	14.98	14.94	14.92	14.91	14.89	14.85	14.83	14.75	14.74	14.69
1988 Sep	MMT/FOGS	$\log(\nu_o F_{\nu_0})$	-	-	-	-	-	-	11.93	11.86	11.86	11.80
			-	-	-	-	-	-	0.06	0.01	0.01	0.01
Q1116+215		$\log(\nu_o)$	14.98	14.94	14.92	14.91	14.89	14.85	14.83	14.75	14.74	14.69
1988 Sep	MMT/FOGS	$\log(\nu_o F_{\nu_0})$	-	-	-	-	-	-	12.57	12.49	12.48	12.40
			-	-	-	-	-	-	0.12	0.01	0.01	0.02
Q1211+143		$\log(\nu_o)$	15.01	14.97	14.96	14.94	14.93	14.89	14.86	14.79	14.78	14.73
1988 Sep	MMT/FOGS	$\log(\nu_o F_{\nu_0})$	-	-	-	-	-	-	-	12.57	12.54	12.52
			-	-	-	-	-	-	-	0.01	0.01	0.02
1988 Jun	MMT/Blue	$\log(\nu_o F_{\nu_0})$	-	12.64	12.67	12.69	12.69	12.63	12.58	12.55	12.55	12.52
			-	0.02	0.00	0.01	0.00	0.01	0.01	0.01	0.01	0.02
Q1226+023		$\log(\nu_o)$	14.99	14.94	14.93	14.92	14.90	14.86	14.83	14.76	14.75	14.70
1988 Sep	MMT/FOGS	$\log(\nu_o F_{\nu_0})$	-	-	-	-	-	-	-	13.17	13.17	13.11
			-	-	-	-	-	-	-	0.02	0.01	0.02
1988 Jun	MMT/Blue	$\log(\nu_o F_{\nu_0})$	-	13.28	13.28	13.30	13.29	13.23	13.21	13.13	13.12	13.05
			-	0.01	0.01	0.01	0.01	0.01	0.01	0.01	0.02	0.02
Q1307+085		$\log(\nu_o)$	14.99	14.94	14.93	14.92	14.90	14.86	14.83	14.76	14.75	14.70
1988 Sep	MMT/FOGS	$\log(\nu_o F_{\nu_0})$	-	-	-	-	-	-	-	12.23	12.24	12.17
			-	-	-	-	-	-	-	0.01	0.01	0.01
1988 Jun	MMT/Blue	$\log(\nu_o F_{\nu_0})$	-	12.44	12.41	12.42	12.41	12.37	12.31	12.20	12.19	12.13
			-	0.01	0.01	0.01	0.00	0.00	0.01	0.01	0.01	0.01
Q1407+265		$\log(\nu_o)$	14.76	14.72	14.70	14.69	14.68	14.63	14.61	14.54	14.53	14.47
1988 Sep	MMT/FOGS	$\log(\nu_o F_{\nu_0})$	12.01	12.03	11.97	11.98	11.97	11.91	11.87	-	-	-
			0.01	0.01	0.02	0.01	0.01	0.01	0.02	-	-	-
1988 Jun	MMT/Blue	$\log(\nu_o F_{\nu_0})$	12.00	12.00	11.95	11.95	11.99	-	-	-	-	-
			0.00	0.01	0.01	0.02	0.00	-	-	-	-	-

TABLE 8(a) (continued)

		$\lambda_{rest}(\AA)$	2675	2950	3050	3150	3250	3600	3800	4500	4600	5200
Q1416-129		$\log(\nu_o)$	15.00	14.95	14.94	14.93	14.91	14.87	14.84	14.77	14.76	14.71
1988 Sep	MMT/FOGS	$\log(\nu_o F_{\nu_0})$	-	-	-	-	-	-	-	11.61	11.61	11.61
			-	-	-	-	-	-	-	0.01	0.01	0.01
1988 Jun	MMT/Blue	$\log(\nu_o F_{\nu_0})$	-	11.81	11.77	11.83	11.83	11.82	11.79	11.66	11.65	11.61
			-	0.01	0.00	0.02	0.01	0.00	0.01	0.00	0.01	0.02
Q1426+015		$\log(\nu_o)$	15.01	14.97	14.96	14.94	14.93	14.88	14.86	14.79	14.78	14.73
1988 Sep	MMT/FOGS	$\log(\nu_o F_{\nu_0})$	-	-	-	-	-	-	-	12.38	12.36	12.31
			-	-	-	-	-	-	-	0.01	0.01	0.01
1988 Jun	MMT/Blue	$\log(\nu_o F_{\nu_0})$	-	12.48	12.45	12.47	12.47	12.40	12.35	12.29	12.28	12.21
			-	0.01	0.03	0.01	0.01	0.01	0.02	0.01	0.01	0.01
Q1501+106		$\log(\nu_o)$	15.03	14.99	14.98	14.96	14.95	14.91	14.88	14.81	14.80	14.75
1988 Sep	MMT/FOGS	$\log(\nu_o F_{\nu_0})$	-	-	-	-	-	-	-	12.31	12.33	12.29
			-	-	-	-	-	-	-	0.02	0.01	0.01
1988 Jun	MMT/Blue	$\log(\nu_o F_{\nu_0})$	-	-	-	12.50	12.45	12.41	12.33	12.28	12.29	12.22
			-	-	-	0.01	0.01	0.00	0.02	0.02	0.00	0.01
Q1613+658		$\log(\nu_o)$	15.00	14.95	14.94	14.93	14.91	14.87	14.84	14.77	14.76	14.71
1988 Sep	MMT/FOGS	$\log(\nu_o F_{\nu_0})$	-	-	-	-	-	-	-	12.20	12.19	12.17
			-	-	-	-	-	-	-	0.01	0.01	0.01
1988 Jun	MMT/Blue	$\log(\nu_o F_{\nu_0})$	-	12.40	12.36	12.39	12.39	12.32	12.29	12.21	12.21	12.16
			-	0.01	0.01	0.01	0.02	0.00	0.01	0.00	0.01	0.01
Q1704+608		$\log(\nu_o)$	14.91	14.87	14.86	14.84	14.83	14.78	14.76	14.69	14.68	14.62
1988 Sep	MMT/FOGS	$\log(\nu_o F_{\nu_0})$	-	-	-	-	12.00	12.00	11.99	11.99	11.98	11.99
			-	-	-	-	0.06	0.01	0.01	0.00	0.01	0.01
1988 Jun	MMT/Blue	$\log(\nu_o F_{\nu_0})$	12.01	11.98	11.96	11.99	11.99	11.95	11.94	11.96	11.91	-
			0.02	0.01	0.01	0.01	0.01	0.00	0.01	0.01	0.01	-
Q1803+676		$\log(\nu_o)$	14.99	14.95	14.94	14.92	14.91	14.87	14.84	14.77	14.76	14.71
1988 Sep	MMT/FOGS	$\log(\nu_o F_{\nu_0})$	-	-	-	-	-	-	-	11.95	11.97	11.92
			-	-	-	-	-	-	-	0.01	0.01	0.01
1988 Jun	MMT/Blue	$\log(\nu_o F_{\nu_0})$	-	12.07	12.06	12.11	12.10	12.07	12.03	11.90	11.91	11.85
			-	0.01	0.01	0.01	0.02	0.00	0.01	0.00	0.01	0.01

TABLE 8(a)

OPTICAL CONTINUUM FLUXES: UV sample quasars

	$\lambda_{rest}(\AA)$	5400	5600	5800	6000	6175	6875	7000	7200	7400	7600	7800	8000
Q0837-120	$\log(\nu_o)$	14.67	14.65	14.64	14.62	14.61	14.56	14.55	14.54	14.53	14.52	14.51	14.50
1988 Aug	$\log(\nu_o F_{\nu_0})$	11.66	11.65	11.69	11.69	11.69	11.63	11.66	-	-	-	-	-
		0.01	0.01	0.02	0.02	0.02	0.02	0.05	-	-	-	-	-
Q0844+349	$\log(\nu_o)$	14.72	14.70	14.69	14.67	14.66	14.61	14.61	14.59	14.58	14.57	14.56	14.55
1988 Sep	$\log(\nu_o F_{\nu_0})$	12.49	12.46	12.47	12.46	12.47	12.45	12.47	12.45	12.40	12.38	12.36	-
		0.02	0.01	0.02	0.01	0.01	0.01	0.01	0.01	0.02	0.02	0.02	-
Q1028+313	$\log(\nu_o)$	14.67	14.66	14.64	14.63	14.62	14.57	14.56	14.55	14.54	14.53	14.51	14.50
1988 Sep	$\log(\nu_o F_{\nu_0})$	11.79	11.77	11.80	11.81	11.78	11.75	11.73	11.70	-	-	-	-
		0.01	0.01	0.02	0.01	0.02	0.02	0.02	0.02	-	-	-	-
Q1116+215	$\log(\nu_o)$	14.67	14.66	14.64	14.63	14.62	14.57	14.56	14.55	14.54	14.53	14.51	14.50
1988 Sep	$\log(\nu_o F_{\nu_0})$	12.34	12.31	12.35	12.34	12.32	12.25	12.27	12.23	-	-	-	-
		0.02	0.01	0.03	0.01	0.01	0.01	0.02	0.02	-	-	-	-
Q1211+143	$\log(\nu_o)$	14.71	14.69	14.68	14.66	14.65	14.60	14.60	14.58	14.57	14.56	14.55	14.54
1988 Sep	$\log(\nu_o F_{\nu_0})$	12.47	12.44	12.45	12.43	12.43	12.43	12.43	12.37	12.34	12.33	12.30	-
		0.02	0.01	0.03	0.02	0.01	0.00	0.02	0.02	0.01	0.01	0.02	-
1988 Jun	$\log(\nu_o F_{\nu_0})$	12.48	12.44	12.45	-	-	-	-	-	-	-	-	-
		0.02	0.02	0.04	-	-	-	-	-	-	-	-	-
Q1226+023	$\log(\nu_o)$	14.68	14.67	14.65	14.64	14.62	14.58	14.57	14.56	14.54	14.53	14.52	14.51
1988 Sep	$\log(\nu_o F_{\nu_0})$	13.06	13.02	13.02	13.03	13.04	12.95	12.95	12.93	-	-	-	-
		0.03	0.01	0.02	0.01	0.01	0.01	0.01	0.02	-	-	-	-
1988 Jun	$\log(\nu_o F_{\nu_0})$	13.01	-	-	-	-	-	-	-	-	-	-	-
		0.03	-	-	-	-	-	-	-	-	-	-	-
Q1307+085	$\log(\nu_o)$	14.68	14.67	14.65	14.64	14.62	14.58	14.57	14.56	14.55	14.53	14.52	14.51
1988 Sep	$\log(\nu_o F_{\nu_0})$	12.14	12.12	12.15	12.15	12.15	12.07	12.08	12.08	-	-	-	-
		0.01	0.01	0.02	0.01	0.01	0.01	0.01	0.03	-	-	-	-
1988 Jun	$\log(\nu_o F_{\nu_0})$	12.13	12.19	-	-	-	-	-	-	-	-	-	-
		0.01	0.01	-	-	-	-	-	-	-	-	-	-
Q1407+265	$\log(\nu_o)$	14.46	14.44	14.42	14.41	14.40	14.35	14.34	14.33	14.32	14.31	14.30	14.29
1988 Sep	$\log(\nu_o F_{\nu_0})$	-	-	-	-	-	-	-	-	-	-	-	-
		-	-	-	-	-	-	-	-	-	-	-	-
1988 Jun	$\log(\nu_o F_{\nu_0})$	-	-	-	-	-	-	-	-	-	-	-	-
		-	-	-	-	-	-	-	-	-	-	-	-

TABLE 8(a) (continued)

	$\lambda_{rest}(\AA)$	5400	5600	5800	6000	6175	6875	7000	7200	7400	7600	7800	8000
Q1416-129	$\log(\nu_o)$	14.69	14.68	14.66	14.65	14.63	14.59	14.58	14.57	14.56	14.54	14.53	14.52
1988 Sep	$\log(\nu_o F_{\nu_0})$	11.58	11.57	11.62	11.64	11.63	11.63	11.59	11.57	11.58	-	-	-
		0.01	0.01	0.03	0.01	0.01	0.02	0.02	0.03	0.04	-	-	-
1988 Jun	$\log(\nu_o F_{\nu_0})$	11.56	11.56	-	-	-	-	-	-	-	-	-	-
		0.02	0.03	-	-	-	-	-	-	-	-	-	-
Q1426+015	$\log(\nu_o)$	14.71	14.69	14.68	14.66	14.65	14.60	14.60	14.58	14.57	14.56	14.55	14.54
1988 Sep	$\log(\nu_o F_{\nu_0})$	12.27	12.25	12.29	12.28	12.25	12.27	12.26	12.21	12.20	12.19	12.16	-
		0.02	0.00	0.03	0.02	0.01	0.01	0.01	0.02	0.01	0.02	0.01	-
1988 Jun	$\log(\nu_o F_{\nu_0})$	12.17	12.18	12.24	-	-	-	-	-	-	-	-	-
		0.02	0.02	0.05	-	-	-	-	-	-	-	-	-
Q1501+106	$\log(\nu_o)$	14.73	14.71	14.70	14.68	14.67	14.62	14.62	14.60	14.59	14.58	14.57	14.56
1988 Sep	$\log(\nu_o F_{\nu_0})$	12.27	12.25	12.29	12.28	12.26	12.28	12.28	12.27	12.25	12.21	12.20	12.16
		0.01	0.01	0.03	0.02	0.01	0.01	0.01	0.02	0.02	0.01	0.02	0.03
1988 Jun	$\log(\nu_o F_{\nu_0})$	12.19	12.19	12.24	12.24	12.24	-	-	-	-	-	-	-
		0.02	0.01	0.04	0.03	0.01	-	-	-	-	-	-	-
Q1613+658	$\log(\nu_o)$	14.69	14.68	14.66	14.65	14.63	14.59	14.58	14.57	14.56	14.54	14.53	14.52
1988 Sep	$\log(\nu_o F_{\nu_0})$	12.12	12.08	12.12	12.13	12.12	12.11	12.08	12.06	12.05	-	-	-
		0.02	0.01	0.03	0.01	0.01	0.01	0.01	0.02	0.02	-	-	-
1988 Jun	$\log(\nu_o F_{\nu_0})$	12.11	12.06	-	-	-	-	-	-	-	-	-	-
		0.02	0.03	-	-	-	-	-	-	-	-	-	-
Q1704+608	$\log(\nu_o)$	14.61	14.59	14.58	14.56	14.55	14.50	14.49	14.48	14.47	14.46	14.45	14.44
1988 Sep	$\log(\nu_o F_{\nu_0})$	11.95	11.90	11.86	11.85	11.83	-	-	-	-	-	-	-
		0.01	0.02	0.02	0.03	0.02	-	-	-	-	-	-	-
1988 Jun	$\log(\nu_o F_{\nu_0})$	-	-	-	-	-	-	-	-	-	-	-	-
		-	-	-	-	-	-	-	-	-	-	-	-
Q1803+676	$\log(\nu_o)$	14.69	14.67	14.66	14.64	14.63	14.58	14.58	14.56	14.55	14.54	14.53	14.52
1988 Sep	$\log(\nu_o F_{\nu_0})$	11.90	11.88	11.92	11.92	11.92	11.87	11.86	11.85	11.83	-	-	-
		0.01	0.01	0.02	0.01	0.01	0.02	0.02	0.02	0.03	-	-	-
1988 Jun	$\log(\nu_o F_{\nu_0})$	11.84	11.84	-	-	-	-	-	-	-	-	-	-
		0.02	0.05	-	-	-	-	-	-	-	-	-	-

TABLE 9(a)

NEAR INFRARED PHOTOMETRY: UV sample quasars

Object	1.2μm J	1.65μm H	2.2μm K	3.5μm L	3.8μm L′	Date	Telescope	Aper
Q0007+106	13.28±0.06	12.51±0.06	11.34±0.06	9.89±0.07		1985 Sep 27	MMT	5″
Q0026+129	13.77±0.05	13.30±0.05	12.47±0.05	10.87±0.22		1984 Sep 14	MMT	5″
	13.91±0.05	13.52±0.05	12.49±0.05	11.01±0.12		1985 Sep 26	MMT	5″
Q0049+171	14.63±0.05	13.98±0.06	13.07±0.04			1984 Sep 14	MMT	5″
	15.52±0.06	14.79±0.06	13.94±0.05	$12.45\pm^{0.46}_{0.32}$		1988 Jan 31	MMT	5″
Q0054+144	13.96±0.06	13.21±0.06	12.11±0.06	10.65±0.12		1984 Sep 14	MMT	5″
	13.95±0.06	13.24±0.06	12.01±0.06	10.43±0.10		1985 Sep 26	MMT	5″
Q0134+329	14.52±0.05	13.90±0.04	12.81±0.05			1984 Sep 14	MMT	5″
	14.55±0.05	13.97±0.06	12.80±0.06	$12.01\pm^{0.86}_{0.47}$		1985 Sep 26	MMT	5″
	14.50±0.06	13.85±0.06	12.74±0.06	11.24±0.11		1985 Sep 26	MMT	5″
Q0205+024	14.22±0.07	13.62±0.06	12.62±0.06			1984 Sep 14	MMT	5″
	14.29±0.06	13.70±0.06	12.61±0.06	11.20±0.11		1985 Sep 27	MMT	5″
Q0837−120	14.83±0.06	14.07±0.06	12.86±0.06	11.30±0.09		1988 Feb 1	MMT	5″
Q0844+349	13.28±0.0	12.63±0.0	11.89±0.04		10.30±0.04	1988 Apr 25	IRTF	6″
Q1028+313	14.48±0.05	13.85±0.04	12.92±0.05	11.33±0.15		1985 Jun 2	MMT	9″
		13.93±0.05		11.87±0.19		1985 Jun 3	MMT	5″
Q1100+772	14.66±0.05	13.93±0.06	12.92±0.06	11.36±0.11		1988 Feb 1	MMT	5″
Q1116+215	13.45±0.05	12.66±0.05	11.42±0.05			1986 Feb 27	MMT	9″
	13.70±0.01	12.73±0.02	11.61±0.02		10.01±0.03	1986 Feb 4	IRTF	6″
	13.45±0.0	12.44±0.0	11.35±0.04		9.51±0.05	1988 Apr 25	IRTF	6″
	13.48±0.06	12.51±0.06	11.30±0.05	9.70±0.05		1988 Apr 8	MMT	9/5″
Q1137+660	14.93±0.05	14.75±0.05	13.86±0.05		11.95±0.08	1986 Feb 4	IRTF	6″
Q1146−037	16.25±0.07	15.49±0.04	14.68±0.07			1986 Feb 23	MMT	9″
	16.42±0.0	15.77±0.0	14.78±0.06			1988 Apr 25	IRTF	6″
Q1202+281	14.74±0.06	14.05±0.06	12.77±0.06	11.11±0.15		1985 May 4	MMT	5″
	14.95±0.04	13.96±0.04	12.78±0.01		11.16±0.05	1986 Feb 4	IRTF	6″
Q1211+143	13.25±0.02	12.36±0.01	11.21±0.01		9.49±0.01	1986 Feb 4	IRTF	6″
	12.98±0.05	12.32±0.05	11.16±0.05	9.56±0.06		1986 Feb 23	MMT	9″
	13.27±0.0	12.47±0.0	11.35±0.04		9.27±0.05	1988 Apr 25	IRTF	6″
	13.56±0.05	12.56±0.06	11.36±0.06	9.73±0.07		1988 Apr 8	MMT	9/5″
Q1219+755	13.08±0.05	12.40±0.04	11.60±0.05	10.46±0.09		1985 Jun 1	MMT	9″
	13.14±0.05	12.40±0.05	11.58±0.05			1986 Feb 27	MMT	9″
Q1226+023	11.71±0.06	10.84±0.06	9.71±0.06	8.23±0.06		1988 Apr 7	MMT	5″
	11.78±0.0	10.87±0.0	9.78±0.04		7.91±0.04	1988 Apr 25	IRTF	6″

TABLE 9(a) (continued)

Object	1.2μm J	1.65μm H	2.2μm K	3.5μm L	3.8μm L′	Date	Telescope	Aperture
Q1307+085	14.12±0.0	13.56±0.0	12.63±0.04		10.81±0.06	1988 Apr 25	IRTF	6″
	14.09±0.06	13.51±0.06	12.55±0.05	11.19±0.09		1988 Apr 8	MMT	9/5″
Q1407+265	14.86±0.06	14.49±0.06	13.84±0.08	12.21±0.2		1988 Apr 7	MMT	5″
	14.85±0.0	14.39±0.0	13.88±0.05		11.74±0.07	1988 Apr 25	IRTF	6″
	14.88±0.05	14.48±0.06	13.82±0.05	11.86±0.26		1988 Apr 7	MMT	9/5″
Q1416−129	14.62±0.05	14.01±0.05	13.02±0.06		12.05±0.22	1983 Feb 6	IRTF	6″
	13.87±0.05	14.05±0.05	12.95±0.05		11.25±0.09	1986 Feb 5	IRTF	6″
	14.87±0.06	14.03±0.06	12.81±0.05			1988 Apr 8	MMT	9″
	14.88±0.0	13.97±0.0	12.83±0.05		11.01±0.05	1988 Apr 25	IRTF	6″
Q1426+015	13.30±0.05	12.50±0.03	11.54±0.04		10.24±0.09	1983 Feb 6	IRTF	6″
	13.01±0.06	12.27±0.06	11.21±0.06	9.76±0.08		1985 May 5	MMT	6″
	12.97±0.06	12.19±0.06	11.18±0.04			1986 Feb 27	MMT	9″
	13.43±0.0	12.59±0.0	11.59±0.05		9.73±0.04	1988 Apr 25	IRTF	6″
Q1501+106	12.96±0.07	12.12±0.08	11.19±0.05		9.84±0.07	1983 Feb 6	IRTF	6″
	12.82±0.05	12.17±0.05	11.23±0.04	9.82±0.04		1986 Feb 23	MMT	9″
		12.13±0.06				1986 Feb 27	MMT	9″
	13.38±0.0	12.65±0.0	11.82±0.05		10.05±0.04	1988 Apr 25	IRTF	6″
Q1545+210	14.68±0.06	14.03±0.06	12.98±0.06	>10.96		1985 May 5	MMT	5″
	14.74±0.0	14.00±0.0	13.11±0.04		11.16±0.04	1988 Apr 25	IRTF	6″
Q1613+658	13.90±0.05	12.77±0.06	11.86±0.06			1984 Sep 15	MMT	9″
				$11.50\pm^{0.55}_{0.37}$		1984 Sep 15	MMT	5″
	13.44±0.05	12.77±0.06	11.79±0.06	10.37±0.08		1985 May 5	MMT	5″
	13.55±0.06	12.73±0.06	11.72±0.05	10.30±0.10		1988 Apr 7	MMT	5″
	13.64±0.0	12.75±0.0	11.82±0.05		10.05±0.04	1988 Apr 25	IRTF	6″
Q1704+608	14.45±0.06	13.76±0.05	12.77±0.05	11.02±0.09		1988 Apr 7	MMT	5″
	14.44±0.0	13.73±0.0	12.84±0.05		10.62±0.06	1988 Apr 25	IRTF	6″
Q1721+343	14.27±0.08	13.82±0.04	12.77±0.07	11.60±0.25		1984 Sep 14	MMT	5″
	14.12±0.08	13.74±0.08	12.64±0.07	>10.74		1985 May 31	MMT	9″
	14.13±0.13	13.67:±0.13	12.82:±0.12	11.33:±0.18		1985 Sep 25	MMT	5″
	14.39±0.0	13.77±0.0	12.75±0.05		10.87±0.05	1988 Apr 25	IRTF	6″
Q1803+676	14.35±0.04	13.56±0.06	12.42±0.05	$11.18\pm^{0.52}_{0.35}$		1984 Sep 14	MMT	5″
	14.27±0.06	13.50±0.06	12.37±0.06	10.83±0.11		1985 Sep 27	MMT	5″
	14.52±0.0	13.56±0.0	12.45±0.05		10.73±0.06	1988 Apr 25	IRTF	6″
Q2130+099	12.81±0.06	11.83±0.06	10.72±0.06	9.3±0.06		1984 Sep 14	MMT	5″
	13.11±0.05	12.15±0.06	10.97±0.06	9.38±0.06		1985 Sep 26	MMT	5″
Q2135−147	14.11±0.06	13.50±0.01	12.35±0.05	10.85±0.11		1985 Sep 27	MMT	5″

TABLE 9(b)

NEAR INFRARED PHOTOMETRY: Other IPC quasars

Object	1.2μm J	1.65μm H	2.2μm K	3.5μm L	3.8μm L′	Date	Telescope	Aperture
Q0003+155	14.82±0.06	14.30±0.06	13.78±0.06			1984 Sep 14	MMT	5″
	14.76±0.05	14.20±0.05	13.68±0.05	12.42±0.19		1988 Jan 31	MMT	5″
Q0003+199	12.23±0.06	11.41±0.05	10.30±0.06	8.77±0.08		1984 Sep 14	MMT	5″
Q0050+124	12.03±0.06	11.13±0.06	9.90±0.06	8.35±0.06		1984 Sep 14	MMT	5″
Q0112−017	16.79±0.12	15.88±0.10	15.45±0.13			1984 Sep 14	MMT	5″
Q0133+20	15.83±0.08	14.88±0.05	13.75±0.06	12.04±0.13		1988 Jan 31	MMT	5″
Q0219+42	13.57±0.06	12.85±0.06	12.02±0.06	10.46±0.06		1984 Sep 14	MMT	5″
Q0323+022	14.69±0.06	14.07±0.05	13.37±0.08			1984 Sep 14	MMT(cloud)	5″
		14.04±0.35	13.44±0.09			1984 Sep 14	MMT	5″
Q0424−131	15.95±0.06	15.31±0.09	14.50±0.09			1988 Jan 31	MMT	5″
	15.98±0.06	15.41±0.05	14.62±0.05	>12.79		1988 Feb 1	MMT	5″
Q0804+76	13.27±0.06	12.49±0.06	11.18±0.06	9.36±0.18		1984 Sep 14	MMT	5″
	13.25±0.04	12.47±0.04	11.20±0.04	9.60±0.04		1986 Feb 23	MMT	5″
Q0923+129	12.78±0.05	12.02±0.06	11.32±0.06			1985 May 2	MMT	5″
	12.77±0.06	12.05±0.05	11.33±0.06	10.04±0.01		1985 May 4	MMT	5″
	12.77±0.01	11.92±0.01	11.29±0.01		10.07±0.05	1986 Feb 4	IRTF	6″
	12.48±0.06	11.72±0.06	11.06±0.02			1986 Feb 17	MMT	9″
Q0923+392	15.60±0.60	15.20±0.05	14.16±0.05			1985 Jun 2	MMT	9″
	15.55±0.09	15.11±0.11	14.07±0.10			1985 Sep 27	MMT	5″
Q1012+008	14.16±0.07	13.45±0.05	12.46±0.05	11.18±0.12		1986 Feb 22	MMT	9″
		13.60±0.04	12.57±0.04	11.17±0.08		1986 Feb 23	MMT	5″
	14.66±0.0	13.78±0.0	12.81±0.05		10.89±0.05	1988 Apr 25	IRTF	6″
Q1121+422	14.95±0.04	14.28±0.05	13.21±0.05	11.59±0.07		1986 Feb 26	MMT	9″
Q1217+023	14.95±0.04	14.28±0.05	13.16±0.06			1985 Jun 2	MMT	9″
		14.23±0.05		11.67±0.30		1985 Jun 3	MMT	5″
	15.28±0.05	14.47±0.03	13.41±0.03		11.94±0.06	1986 Feb 4	IRTF	6″
Q1244+026	14.69±0.06	13.86±0.04	13.09±0.03		11.74±0.08	1983 Feb 6	IRTF	6″
Q1253−055	14.71±0.06	13.84±0.06	12.87±0.06	11.33±0.10		1986 Feb 22	MMT	9″
Q1318+290	15.41±0.04	14.92±0.04	14.12±0.05			1986 Feb 26	MMT	5″
Q1346−036	15.51±0.06	15.04±0.06	14.22±0.05			1986 Feb 22	MMT	9″
Q1352+183	14.85±0.04	14.22±0.04	13.01±0.05	11.43±0.09		1986 Feb 23	MMT	5″
Q1517+23	16.81±0.12	16.17±0.10	15.46±0.13			1986 Feb 26	MMT	9″

TABLE 9(b) (continued)

Object	1.2μm J	1.65μm H	2.2μm K	3.5μm L	3.8μm L′	Date	Telescope	Aperture
Q1635+119	15.05±0.05	14.38±0.06	13.61±0.06	> 12.79		1986 Feb 22	MMT	9″
	15.51±0.0		14.10±0.07		12.71±0.28	1988 Apr 25	IRTF	6″
Q2112+059	14.34±0.04	13.71±0.05	12.59±0.04	10.94±0.12		1986 Sep 20	MMT	9″(L=5″)
Q2126−158	15.42±0.11	14.93±0.11	14.25±0.09			1984 Sep 14	MMT	5″
Q2233+134	15.48±0.07	14.86±0.05	13.59±0.07	12.19±0.24		1986 Sep 20	MMT	9″(L=5″)
Q2209+181	13.79±0.05	13.14±0.06	12.44±0.05	$11.55\pm^{0.59}_{0.38}$		1984 Sep 14	MMT	5″
Q2214+139	13.16±0.04	12.43±0.04	11.58±0.05	10.30±0.08		1986 Sep 20	MMT	9″(L=5″)
Q2251+113	14.15±0.04	13.42±0.05	12.34±0.05	10.75±0.09		1986 Sep 20	MMT	9″(L=5″)
Q2251−178	13.20±0.06	12.58±0.06	11.61±0.06	10.07±0.12		1984 Sep 14	MMT	5″
Q2254+023	16.28±0.05	15.75±0.05	14.89±0.08	>11.80		1986 Sep 20	MMT	9″(L=5″)

TABLE 10(a)

N AND Q BAND INFRARED PHOTOMETRY: UV sample quasars

Object	10.2μm N	20μm Q	Date	Telescope	Aperture
Q0003+199	5.52±0.08	>3.85	1984 Sep 23	IRTF	6″
	5.56±0.09	3.66±0.16	1985 Aug 28	IRTF	6″
Q0026+129	7.76±0.11		1985 Aug 29	IRTF	6″
Q0054+144	7.24±0.17		1985 Aug 28	IRTF	6″
Q0205+024	7.09±0.12		1985 Aug 28	IRTF	6″
Q1116+215	6.85±0.09	>5.02	1986 Feb 1,5	IRTF	6″
Q1202+281	7.37±0.15		1986 Feb 1	IRTF	6″
Q1211+143	6.1±0.11	3.75±0.12	1986 Feb 1	IRTF	6″
Q1426+015	6.80±0.18	$4.41\pm^{0.54}_{0.36}$	1984 Mar	UKIRT	5″
	6.72±0.13		1985 Apr 2	IRTF	4″
Q1501+106	6.06±0.08	3.60±0.24	1984 Mar 6	UKIRT	5″
Q1545+210	$8.31\pm^{0.76}_{0.44}$		1985 Apr 3	IRTF	6″
Q1613+658	6.86±0.15		1985 Apr 2	IRTF	4″
	6.27±0.24		1985 Aug 27	IRTF	6″
	6.65±0.10		1985 Aug 28	IRTF	6″
Q1721+343	7.84±0.17		1985 Aug 29	IRTF	6″
Q2130+099	6.10:±0.10		1984 Sep 23	IRTF	6″
	6.18±0.08	3.68±0.15	1985 Aug 28	IRTF	6″
Q2135-147	$7.80\pm^{0.48}_{0.33}$		1985 Aug 28	IRTF	6″
	7.93±0.18		1985 Aug 29	IRTF	6″

TABLE 10(b)

N AND Q BAND INFRARED PHOTOMETRY: Other IPC quasars

Object	10.2μm N	20μm Q	Date	Telescope	Aperture
Q0050+124	4.74±0.05		1984 Sep 23	IRTF	6″
Q0219+42	>6.8:		1984 Sep 23	IRTF	6″
Q0923+129	6.55±0.18		1985 Apr 4	IRTF	6″
	6.40±0.09	4.19±0.22	1986 Feb 1,2,5	IRTF	6″
Q1217+023	$8.62\pm^{0.87}_{0.48}$		1986 Feb 1	IRTF	6″
Q2251-178	6.61:±0.20		1984 Sep 23	IRTF	6″

TABLE 11(a)

IRAS FLUXES: UV sample quasars

Object	12μm	25μm	60μm	100μm	Obs
Q0007+106	0.10 ±0.01	0.15 ±0.01	0.22 ±0.01	1.40 ±0.04	AO
Q0026+129	<0.06	<0.04	<0.03	<0.11	AO
Q0049+171	< 0.15	< 0.12	< 0.14	< 0.46	LA
Q0052+251	0.06 ±0.01	0.09 ±0.02	0.10 ±0.02	0.45 ±0.07	AO
Q0054+144	0.06 ±0.01	0.09 ±0.01	0.30 ±0.01	0.77 ±0.03	AO
Q0121−590	0.369 ±0.005	0.54 ±0.01	0.62 ±0.02	0.89 ±0.06	AO
Q0134+329	0.048 ±0.006	0.15 ±0.01	0.78 ±0.01	1.14 ±0.03	AO
Q0205+024	0.05 ±0.01	0.12 ±0.02	0.10 ±0.02	<0.15	AO
Q0312−770	<0.04	<0.04	<0.07	< 0.49	AO
Q0637−752	< 0.07	0.13±0.02	0.20±0.03	< 0.39	LA
Q0837−120	<0.03	<0.05	0.071 ±0.016	<0.05	AO
Q0844+349	0.10±0.03	0.18±0.04	0.14±0.03	< 0.29	LA
Q1028+313	< 0.10	< 0.12	< 0.14	< 0.39	LA
Q1100+770	<0.02	0.040 ±0.006	0.07 ±0.01	<0.11	AO
Q1137+660	<0.04	<0.05	<0.07	<0.25	AO
Q1146−037	< 0.11	< 0.32	< 0.22	< 0.70	LA
Q1202+281	< 0.10	0.21±0.05	0.20±0.04	0.37±0.12	LA
Q1211+143	0.28±0.06	0.29±0.08	0.32±0.06	0.69±0.12	LA
Q1219+755	< 0.08	< 0.08	< 0.34	< 2.15	AO
Q1226+023	0.40 ±0.01	0.95 ±0.03	1.89 ±0.01	3.41 ±0.05	AO
Q1307+085	< 0.15	< 0.23	0.19±0.04	< 0.57	LA
Q1407+265	< 0.12	0.11±0.04	< 0.15	< 0.43	LA
Q1416−129	< 0.11	< 0.22	< 0.12	< 0.37	LA
Q1426+015	0.14±0.03	0.23±0.05	0.27±0.04	< 0.26	LA
Q1501+106	0.24 ±0.03	0.50±0.05	0.45 ±0.03	<0.37	LA
Q1545+210	<0.03	<0.04	0.08 ±0.02	<0.10	AO
Q1613+658	0.08 ±0.01	0.21 ±0.01	0.65 ±0.02	1.30 ±0.08	AO
Q1704+608	0.06 ±0.01	0.18 ±0.01	0.17 ±0.03	<0.17	LA
Q1721+343	0.08±0.02	0.12±0.02	0.14±0.03	< 0.92	LA
Q1803+676	<0.03	<0.03	<0.06	<0.21	AO
Q2130+099	0.17 ±0.01	0.31 ±0.01	0.47 ±0.02	0.25 ±0.05	AO
Q2135−147	< 0.11	0.14±0.03	0.17±0.05	< 0.52	LA

TABLE 11(b)

IRAS FLUXES: Other IPC quasars

Object	12μm	25μm	60μm	100μm	Obs
Q0003+199	0.30 ±0.01	0.41 ±0.02	0.43 ±0.02	<0.19	AO
Q0003+155	<0.04	<0.08	<0.07	<0.23	AO
Q0050+124	0.53 ±0.01	1.05 ±0.02	2.39 ±0.02	3.56 ±0.06	AO
Q0112-017	< 0.14	< 0.21	< 0.27	Cirrus	LA
Q0133+207	< 0.11	< 0.17	0.17±0.05	0.40±0.13	LA
Q0414-060	< 0.09	< 0.11	< 0.10	< 0.38	LA
Q0804+762	0.17±0.02	0.25±0.03	0.16±0.04	< 0.51	LA
Q0923+129	0.17±0.04	0.27±0.07	0.58±0.04	1.21±0.15	LA
Q0923+392	<0.02	<0.03	<0.03	<0.10	AO
Q1012+008	< 0.16	< 0.16	< 0.14	< 0.2	LA
Q1048-090	< 0.14	< 0.11	< 0.12	< 0.2	LA
Q1121+422	< 0.12	< 0.07	< 0.10	< 0.29	LA
Q1217+023	< 0.23	< 0.26	0.21±0.03	< 0.31	LA
Q1244+026	< 0.14	< 0.25	0.29±0.06	< 0.47	LA
Q1253-055	0.10±0.03	0.29±0.07	0.24±0.05	< 0.46	LA
Q1351+640	0.17±0.03	0.63±0.03	0.82±0.04	1.33±0.07	LA
Q1352+183	< 0.09	< 0.11	< 0.13	< 0.43	LA
Q1435-067	< 0.11	< 0.17	< 0.09	< 0.46	LA
Q1635+119	< 0.08	< 0.11	< 0.11	< 0.81	LA
Q2126-158	<0.04	<0.07	0.09 ±0.02	<0.23	AO
Q2128-123	<0.04	<0.09	0.08 ±0.02	0.95 ±0.08	AO
Q2209+184	0.04 ±L	<0.05	<0.07	0.34 ±0.07	AO
Q2251-178	0.09 ±0.01	0.15 ±0.02	0.32 ±0.02	<0.78	60μ AO
Q2304+042	< 0.12	< 0.26	0.15±0.04	< 0.6	LA

TABLE 12

RADIO CORE FLUXES

Object	ν(GHz)	S(mJy)	Date	Telescope	Resolution (")	Ref
Q0007+106	5	151±0.07	1983 Nov	VLA	0.5	1
	5	184±10	1983 Aug	VLA	0.3	4
	5	470±1	1982 Apr	VLA	0.5	3
	1.5	296±15	1983 Aug	VLA	1.0	4
	1.5	340±1	1982 Apr	VLA	1.0	3
Q0026+129	5	0.2±0.07	1983 Nov	VLA	0.5	1
Q0049+171	5	0.65±0.1	1983 Nov	VLA	0.5	1
Q0052+251	5	0.42±0.07	1983 Nov	VLA	0.5	1
Q0054+144	5	1.0±0.2	1986	VLA	5	2
Q0121-590	8.4	<10	1986 Jun	PKS		4
Q0134+329	2.3	210±50	1984?	VLBI		5
Q0205+024	5	0.8±0.15	1982 Mar	VLA	0.3	7
	1.4	1.2±0.2	1982 Mar	VLA	2.0	7
	15	< 0.8	1982 Oct	VLA		7
Q0312-770	0.4	<1500		PKS		22
	1.4	600		PKS		22
	2.7	500±20		PKS		23
	5.0	560±30		PKS		24
Q0637-752	5.0	5490	1970	PKS		20
	0.6	6610±320		PKS		21
	1.4	5530±160		PKS		21
	2.7	5900	1970	PKS		20
	8.9	5530±200		PKS		19
Q0837-120	5	160±10	1973/4	WSRT	6	8
	5	181	1987	VLA		17
	0.6	<700	19734	WSRT	49	8
	1.4	165±10	1971/4	WSRT	21	8
	15	221	1987	VLA		17
	22.5	199.2	1987	VLA		17
Q0844+349	5	<0.25	1983 Nov	VLA	0.5	1
Q1028+313	5	91±13	1982 Oct	VLA	4.0	6
	5	110±1	1982 Apr	VLA	0.5	3
	1.4	< 100	1982 Oct	VLA	13	6
	1.5	89±1	1982 Apr	VLA		3

TABLE 12 (continued)

Object	ν(GHz)	S(mJy)	Date	Telescope	Resolution (")	Ref
Q1100+772	5	76±0.07	1983 Nov	VLA	0.5	1
	5	75±20	1974	WSRT	6	8
	5	100	1981	VLA		13
	5	78±10	1987	VLA		17
	15	78	1987	VLA		17
	22.5	68.6	1987	VLA		17
Q1116+215	5	1.9±0.07	1983 Nov	VLA	0.5	1
Q1137+660	5	130	1973	OMT		10
	5	169	1981	VLA		13
	5	162±8	1974	WSRT		8
	2.7	94±32	1975	GB	0.2	15
	8.1	153±19	1975	GB	0.2	15
Q1146-037	1.4	115	1980/1	VLA	2	16
	2.7	180		NRAO	3.5	14
	8.1	190		NRAO		14
Q1202+281	5	0.65±0.07	1983 Nov	VLA	0.5	1
Q1211+143	5	1.2±0.07	1983 Nov	VLA	0.5	1
Q1219+755	5	1.2±0.1	1986	VLA	5	2
Q1226+023	5	26400	1983 Nov	VLA	0.5	1
	5	30500		VLA	0.4	11
	5	41500±2100	1974	WSRT	6	8
Q1307+085	5	<0.35	1983 Nov	VLA	0.5	1
Q1407+265	5	2.9±0.07	1983 Nov	VLA	0.5	1
Q1416-129	5	0.8±0.07	1983 Nov	VLA	0.5	1
Q1426+015	5	0.93±0.07	1983 Nov	VLA	0.5	1
Q1501+106	5	0.50±0.10	1983 Nov	VLA	0.5	1
Q1545+210	5	32±0.07	1983 Nov	VLA	0.5	1
	5	45	1981	VLA		13
	5	30±6	1974	WSRT	6	8
	1.5	35±1	1982 Apr	VLA		3
Q1613+658	5	0.78±0.07	1983 Nov	VLA	0.5	1
	5	2.19±0.11	1986	VLA	3	18
	1.5	4.26±0.42	1986	VLA	9	18
	14.9	1.51±0.23	1985	VLA	1	18
	40	<237	1985	FCRAO		18

TABLE 12 (continued)

Object	ν(GHz)	S(mJy)	Date	Telescope	Resolution (")	Ref
Q1704+608	5	8.0±0.07	1983 Nov	VLA	0.5	1
	5	17.7	1987	VLA		17
	5	18±2	1974	WSRT	6	8
	1.4	<700	1974	WSRT	21	8
	15	8.2	1987	VLA		17
	22.5	4.8±0.8		VLA		17
Q1721+343	5	370±1	1982 Apr	VLA	0.5	3
	1.5	450±1	1982 Apr	VLA		3
Q1803+676		< 0.4				18
Q2130+099	5	1.3±0.07	1983 Nov	VLA	0.5	1
	5	2.09±0.11	1986	VLA	3	18
	1.5	4.71±0.32	1986	VLA	9	18
	14.9	1.47±0.23	1985	VLA	1	18
	40	<258	1985	VLA		18
Q2135-147	5	97±10	1974	WSRT	6	8
	5	126±1	1982 Apr	VLA	0.5	3
	0.6	<600	1974	WSRT	49	8
	1.4	<75	1974	WSRT	21	8
	1.5	87±1	1982 Apr	VLA		3

(1) Kellerman et al (1989); (2) I. Gioia, private communication; (3) Gower and Hutchings (1984); (4) Unger et al (1987);
(5) Preston et al (1985); (6) Feigelson, Isobe and Kembhavi (1984); (7) Rudnick, Sitko, and Stein (1984);
(8) Miley and Hartsuijker (1978); (9) Price and Milne (1965); (10) Pooley and Henbest (1974); (11) Perley (1982);
(12) Spencer et al (1989); (13) Swarup, Sinha, and Hilldrup (1978); (14) Wills (1979); (15) Owen, Porcas and Neff (1978);
(16) Hintzen, Ulvestad and Owen (1983); (17) Antonucci and Barvainis (1988); (18) Hutchings and Gower (1985);
(19) Shimmins and Bolton (1981); (20) Bolton and Butler (1975); (21) Wills (1975); (22) Ekers (1969);
(23) Shimmins and Bolton (1972a); (24) Shimmins and Bolton (1972b)

TABLE 12(b)

EXTENDED RADIO SOURCE FLUXES

Object	ν(GHz)	S(mJy)	Date	Telescope	Ref
Q0007+106 ERS	5	170±0.07	1983	VLA	1
Q0026+129 ERS	5	4.9±0.07	1983	VLA	1
	5	2.9±0.4	1982 Oct	VLA	7
	1.4	4.6±0.7	1982 Oct	VLA	7
	15	1.2±0.2	1982 Oct	VLA	7
Q0049+171 ERS	5	<0.2	1983	VLA	1
Q0052+251 ERS	5	0.32±0.07	1983	VLA	1
Q0054+144 ERS	5	<1.0	1986	VLA	2
Q0121-590 ERS	8.4	<10	1986 Jun	PKS	4
Q0134+329 ERS	5	5510	1982 Oct	MERLIN	12
	1.5	1530	1982 Jun	VLA	12
Q0205+024 ERS	5	<0.3	1982 Oct	VLA	7
	1.4	3.3±0.5	1982 Oct	VLA	7
Q0312-770 ERS	0.4	1500		PKS	22
	1.4	<600		PKS	22
	2.7	<500		PKS	23
	5.0	<560		PKS	24
Q0637-752 ERS	5.0	<5490	1970	PKS	20
Q0837-120 ERS	5	672±50	1974	WSRT	8
	1.4	1374±45	1974	WSRT	8
	0.6	3510±200	1974	WSRT	8
Q0844+349 ERS	5	0.31±0.1	1983	VLA	1
Q1028+313 ERS	5	54±8	1982 Oct	VLA	6
	1.4	124±50	1982 Oct	VLA	6
Q1100+772 ERS	5	584±0.1	1983	VLA	1
	5	856	1981	VLA	13
	5	1398±30	1974	WSRT	8
	1.4	2350±75	1974	WSRT	8
Q1116+215 ERS	5	0.86±0.07	1983 Nov	VLA	1
Q1137+660 ERS	5	840	1981	VLA	13
	2.7	1610	1975	GB	15
	8.1	545	1975	GB	15
	5	913±40	1974	WSRT	8
	1.4	2915±58	1974	WSRT	8
Q1146-037 ERS	1.4	199	1980/1	VLA	16

TABLE 12(b) (continued)

Object	ν(GHz)	S(mJy)	Date	Telescope	Ref
Q1202+281 ERS	5	0.18±0.07	1983 Nov	VLA	1
Q1211+143 ERS	5	155.8±0.1	1983 Nov	VLA	1
Q1219+755 ERS	5	<1.2	1986	VLA	2
Q1226+023 ERS	5	10600	1983 Nov	VLA	1
Q1307+085 ERS	5	0.35±0.1	1983 Nov	VLA	1
Q1407+265 ERS	5	5.0±0.1	1983 Nov	VLA	1
Q1416-129 ERS	5	2.8±0.1	1983 Nov	VLA	1
Q1426+015 ERS	5	0.28±0.1	1983 Nov	VLA	1
Q1501+106 ERS	5	1.0±0.1	1983 Nov	VLA	1
Q1545+210 ERS	5	688	1983 Nov	VLA	1
	5	631	1981	VLA	13
	5	794±40	1974	WSRT	8
	1.4	2284±114	1974	WSRT	8
	0.6	4667±250	1974	WSRT	8
Q1613+658 ERS	5	2.25±0.1	1983 Nov	VLA	1
Q1704+608 ERS	5	1230	1983 Nov	VLA	1
	2.7	1502	1975	GB	15
	8.1	624	1975	GB	15
	5	1042±53	1974	WSRT	8
	1.4	3142±157	1974	WSRT	8
	0.6	6050±320	1974	WSRT	8
Q1721+343 ERS					
Q1803+676 ERS	5	< 0.4			
Q2130+099 ERS	5	0.75±0.1	1983 Nov	VLA	1
Q2135-147 ERS	5	1049±70	1974	WSRT	8
	1.4	3268±163	1974	WSRT	8
	0.6	6991±350	1974	WSRT	8

TABLE 13

MILLIMETRE FLUXES

Object	λ(mm)	S(mJy)	Date	Telescope	Ref
Q0007+106	3.3	1600±100	1979	NRAO	4
	3.3	2600±400	1978	NRAO	4
	1.0	800±200	1979	Hale	5
Q0026+129	1.0	<1600	1982	UKIRT	1
	1.0	<1000	19	Hale	5
	3.3	190±40	1980	NR	3
Q0054+144	3.3	<360	1980	NRAO	3
	1.3	<3.0	1988	IRAM	7
Q0134+329	1.0	<700	1979	Hale	5
Q0205+024	3.3	<60	1984	UKIRT	1
Q0844+349	1.3	<3.4	1988	IRAM	7
Q1028+313	3.3	140±30	1980	NRAO	3
Q1137+660	3.3	140±90	1980	NRAO	3
Q1202+281	3.3	<210	1980	NRAO	3
Q1211+143	1.3	<2.8	1988	IRAM	7
Q1219+755	3.3	<90	1980	NRAO	3
	1.0	<900	1978	Hale	5
Q1226+023	3.3	20280±1960	1977	\	2
	3.3	12900±1000	1978	NRAO	4
	3.3	14800±900	1979	NRAO	4
	3.3	16320±1640	1980	NRAO	3
	3.3	31300±400	1982	NRAO	6
	1.9	19000±2000	1982	NRAO	6
	1.1	11000±1000	1982	UKIRT	6
	1.0	10200±2100	1977	Hale	5
	0.8	8700±1500	1982	UKIRT	6
	0.4	4900±900	1982	UKIRT	6
Q1426+015	1.3	<4.3	1988	IRAM	7
Q1613+658	1.3	<3.1	1988	IRAM	7
Q1704+608	3.3	<180	1980	NRAO	3
	1.0	<1000	1979	Hale	5
Q2130+099	1.3	2.1±0.7	1988	IRAM	7
Q2135-147	3.3	230±50	1980	NRAO	3
	1.0	<800	1979	Hale	5

1) Robson, et al (1985); 2) Owen, etal (1978); 3) Owen and Puschell (1982);
4) Landau, Epstein and Rather (1980); 5) Ennis, Neguebauer and Werner (1982);
6) Clegg, et al (1983); 7) Chini, Kreysa and Biermann (1989).

TABLE 14

VARIABILITY ESTIMATES

Object	Var(2 μm)	Var(5000Å)	Var(2500Å)	Var(1350Å)
Q0007+106			<1.2 (6 yr)	4.1 (6 yr)
Q0026+129	<1.1 (1 yr)	<1.1 (1 yr)	<1.2 (6 yr)	
Q0049+171	2.2 (3.3 yr)			
Q0052+251				
Q0054+144	1.1 (1 yr)	1.1 (1 yr)		
Q0121-590	2.6 (9 yr)	2.8 (6 yr)	1.7 (4 yr)	1.8 (4 yr)
Q0205+024	<1.1 (1 yr)			
Q0312-770				2.3 (0.8 yr)
Q0637-752				1.2 (0.5yr)
Q0837-120	1.3 (2 yr)	1.6 (1 yr)		
Q0844+349			1.3 (1 yr)	1.3 (1 yr)
Q1028+313				
Q1100+772				4.8? (6 yr)
Q1116+215	1.3 (2 yr)			1.5 (2 yr)
Q1137+660				
Q1146-037	1.1 (2 yr)			
Q1202+281	<1.1 (1 yr)		1.5 (6 yr)	2.8 (6 yr)
Q1211+143	1.2 (2 yr)		<1.2 (1 yr)	1.6 (1 yr)
Q1219+755	<1.1 (0.8 yr)	1.2 (1 yr)	2.4 (5 yr)	1.5 (5 yr)
Q1226+023	1.2 (2 yr)	1.3 (2 yr)	1.6 (11 yr)	2.2 (11 yr)
Q1307+085				
Q1407+265				
Q1416-129	1.2 (5 yr)			<1.2 (8 yr)
Q1426+015	1.5 (5 yr)	1.1 (1 yr)	1.3 (2 yr)	1.8 (2 yr)
Q1501+106	1.8 (5 yr)			
Q1545+210	1.1 (2 yr)	1.3 (1 yr)		
Q1613+658	1.1 (4 yr)		<1.2 (1.6yr)	1.2 (1.6 yr)
Q1704+608			<1.2 (7 yr)	<1.2 (4 yr)
Q1721+343	<1.1 (4 yr)		<1.2 (3 yr)	<1.2 (3 yr)
Q1803+676	<1.1 (4 yr)			
Q2130+099	1.2 (1 yr)	1.1 (1 yr)	<1.2 (7 yr)	1.7 (7 yr)
Q2135-147	1.2 (2 yr)	1.1 (1 yr)	<1.2 (4 yr)	1.3 (4 yr)

TABLE 15

MAGNITUDE SCALE ZERO POINTS

Band	Effective λ (μm)	Zero pt (Jy) (Vega)	Zero pt (Jy) ($\alpha = 1$)
U	0.363	1375	1779
B	0.442	4476	4206
V	0.548	3693	3702
R	0.698	2867	2902
I	0.913	2262	2255
J	1.208	1695	1712
H	1.627	1083	1081
K	2.154	729	734
L	3.455	324	332
L'	3.765	269	272
M	4.664	176	176
N	10.49	36.3	43.1
Q	20.66	9.4	10.2

TABLE 16

EXTINCTION LAW

$\log \nu$	A_λ/A_V (RL85)	$\log \nu$	A_λ/A_V (SM79)
13.36	0.029	13.95	0.05
13.38	0.032	14.13	0.12
13.40	0.039	14.38	0.28
13.42	0.048	14.52	0.48
13.44	0.061	14.63	0.75
13.46	0.074	14.74	1.00
13.48	0.077	14.83	1.32
13.50	0.087	14.875	1.42
13.52	0.074	14.940	1.58
13.55	0.045	15.039	2.00
13.57	0.023	15.079	2.35
13.48	0.055	15.097	2.58
13.78	0.026	15.115	2.86
13.93	0.061	15.136	3.12
		15.155	3.01
		15.176	2.78
		15.198	2.58
		15.220	2.50
		15.246	2.54
		15.273	2.62
		15.304	2.63
		15.334	2.74
		15.380	3.11
		15.405	3.40
		15.432	3.73
		15.456	4.16
		15.477	4.65

TABLE 17

HOST GALAXIES ($H_0 = 50, \Omega_0 = 1$)

Object	M_B(host)	M_B(QSO)	Ref
Q0007+106	-21.5	-22.6	1
Q0026+129			
Q0049+171	-19.6	-22.3	3
Q0052+251	-21.8	-23.5	1
Q0054+144	-21.6	-23.6	2
Q0121−590			
Q0134+329	-24.0	- 25.7	4
Q0134+329	-23.3	- 24.8	1
Q0134+329	-23.5	- 24.8	5
Q0205+024	>-21.0	-24.7	3
Q0312−770			
Q0637−752			
Q0837−120			
Q0844+349			
Q1028+313			
Q1100+772	-22.3	-25.6	6
Q1116+215	-22.1	-24.9	6
Q1137+660			
Q1146−037			
Q1202+281	-21.8	-24.4	6
Q1211+143			
Q1219+755			
Q1226+023	-21.8	-27.1	6
Q1307+085			
Q1407+265			
Q1416−129			
Q1426+015			
Q1501+106	-21.2	-22.1	1
Q1545+210			
Q1613+658	-23.3	-22.8	1
Q1704+608	-19.0	-21.4	7
Q1721+343			
Q1803+676			
Q2130+099	-21.9	-23.2	3
Q2135−147	-23.0	-25.0	3

Refs

1 Boroson, T.A., Oke, J.B., and Green, R.F., 1982 263, 32
2 Gehren, T., Fried, J., Wehinger, P.A and Wyckoff,S. 1984 278,11
3 Smith EP Heckman TM Bothun GD Romanishin W and Balick B 1986 306,64

4 Boroson TA Oke JB 1984 281, 535
5 Malkan 1984 287 555
6 Boroson T A Persson S E and Oke JB 1985 293 120
7 Malkan MA Margon B and Chanan GA 1984 280 66

Table 18

BOLOMETRIC LUMINOSITIES

Name	UVOIR (0.1 – 100μm)	Bolometric (1 m-10 keV)
Q0007+106	$61.1^{+5.29}_{-4.81}$	$88.7^{+25.8}_{-9.89}$
Q0026+129	$90.2^{+16.2}_{-18.6}$	$137^{+31.5}_{-27.2}$
Q0049+171	$6.48^{+11.5}_{-1.50}$	$12.8^{+180}_{-2.63}$
Q0052+251	$126^{+18.4}_{-15.4}$	$232^{+516}_{-67.8}$
Q0054+144	$131^{+14.2}_{-16.8}$	$164^{+16.4}_{-24.4}$
Q0121-590	$53.7^{+16.1}_{-11.8}$	$78.1^{+25.4}_{-17.6}$
Q0134+329	$719^{+82.0}_{-124}$	945^{+125}_{-279}
Q0205+024	$102^{+15.0}_{-14.4}$	$169^{+22.7}_{-20.1}$
Q0312-770	$121^{+77.8}_{-49.7}$	$194^{+199}_{-79.5}$
Q0637-752	2398^{+322}_{-259}	3657^{+556}_{-827}
Q0837-120	$85.6^{+15.1}_{-36.8}$	$161^{+32.4}_{-56.0}$
Q0844+349	$30.4^{+3.71}_{-3.90}$	$34.3^{+8.69}_{-4.59}$
Q1028+313	$67.6^{+62.3}_{-19.7}$	$122^{+75.8}_{-25.6}$
Q1100+772	$214^{+17.5}_{-14.7}$	$296^{+74.0}_{-59.0}$
Q1116+215	$282^{+34.3}_{-45.2}$	$399^{+76.5}_{-60.5}$
Q1137+660	753^{+581}_{-269}	1352^{+912}_{-408}
Q1146-037	$61.0^{+413}_{-25.0}$	$106^{+531}_{-45.8}$
Q1202+281	$108^{+20.7}_{-19.2}$	$150^{+55.0}_{-39.8}$
Q1211+143	$98.0^{+13.7}_{-12.6}$	$184^{+420}_{-51.3}$
Q1219+755	$21.9^{+13.6}_{-5.16}$	$34.2^{+24.5}_{-6.81}$
Q1226+023	1220^{+169}_{-142}	1911^{+273}_{-234}
Q1307+085	$103^{+9.84}_{-13.0}$	$136^{+43.3}_{-11.2}$
Q1407+265	2518^{+960}_{-760}	3680^{+3775}_{-1119}
Q1416-129	$40.4^{+49.7}_{-13.4}$	$74.8^{+121}_{-26.3}$
Q1426+015	$77.2^{+15.4}_{-14.1}$	$126^{+43.9}_{-27.5}$
Q1501+106	$16.1^{+2.96}_{-2.44}$	$25.7^{+4.10}_{-3.39}$
Q1545+210	$200^{+44.7}_{-36.6}$	$313^{+122}_{-91.6}$
Q1613+658	$122^{+13.9}_{-14.6}$	$163^{+21.2}_{-25.9}$
Q1704+608	$588^{+53.9}_{-69.8}$	$699^{+151}_{-98.2}$
Q1721+343	$214^{+48.6}_{-29.1}$	$324^{+133}_{-68.9}$
Q1803+676	$74.2^{+0.00}_{-37.7}$	$52.4^{+33.3}_{-8.65}$
Q2130+099	$44.7^{+5.24}_{-4.44}$	$61.8^{+7.73}_{-6.80}$
Q2135-147	$152^{+27.1}_{-25.0}$	$219^{+58.3}_{-44.7}$

Table 19

DECADE LUMINOSITIES

Name	(10-100 μm)	(1-10 μm)	(0.1-1 4μm)	(0.1-1 keV)	(1-10 keV)
Q0007+106	$12.8^{+0.93}_{-0.94}$	$20.4^{+2.54}_{-2.24}$	$27.8^{+1.82}_{-1.64}$	$2.00^{+7.88}_{-0.79}$	$9.09^{+1.45}_{-0.93}$
Q0026+129	< 10.5	$26.9^{+4.28}_{-3.54}$	$55.8^{+8.85}_{-6.92}$	$6.26^{+0.08}_{-0.00}$	$8.34^{+0.97}_{-0.81}$
Q0049+171	< 6.72	$1.72^{+4.33}_{-0.00}$	$4.61^{+0.60}_{-0.38}$	$1.34^{+287}_{-0.19}$	$2.32^{+2.22}_{-0.66}$
Q0052+251	$25.0^{+4.81}_{-4.81}$	$29.0^{+3.90}_{-3.33}$	$72.4^{+9.71}_{-7.29}$	$10.7^{+552}_{-6.51}$	$7.70^{+2.51}_{-2.60}$
Q0054+144	$45.3^{+3.55}_{-7.32}$	$48.5^{+4.66}_{-4.54}$	$37.8^{+5.99}_{-4.99}$	$5.84^{+1.18}_{-0.25}$	–
Q0121-590	$11.1^{+0.27}_{-0.37}$	$15.3^{+4.70}_{-3.64}$	$27.2^{+11.2}_{-7.82}$	$4.09^{+1.20}_{-0.92}$	$2.38^{+0.19}_{-0.19}$
Q0134+329	$407^{+15.2}_{-73.7}$	$177^{+33.6}_{-27.9}$	$134^{+33.1}_{-22.3}$	$12.2^{+17.5}_{-5.25}$	–
Q0205+024	$22.2^{+5.15}_{-5.78}$	$28.6^{+2.82}_{-2.84}$	$51.5^{+7.07}_{-5.87}$	$20.5^{+4.66}_{-1.27}$	–
Q0312-770	< 36.3	$23.3^{+15.6}_{-17.1}$	$88.3^{+35.7}_{-22.6}$	$2.26^{+10.2}_{-0.83}$	–
Q0637-752	583^{+129}_{-244}	$673^{+47.9}_{-49.8}$	1141^{+145}_{-124}	$52.7^{+8.43}_{-7.47}$	$168^{+46.1}_{-42.5}$
Q0837-120	$16.2^{+4.06}_{-13.6}$	$28.4^{+4.20}_{-0.00}$	$40.8^{+6.89}_{-5.65}$	$12.7^{+6.54}_{-4.24}$	$16.6^{+2.98}_{-2.52}$
Q0844+349	$5.76^{+1.17}_{-1.71}$	$7.69^{+0.70}_{-0.63}$	$16.9^{+1.84}_{-1.56}$	$0.32^{+0.71}_{-0.13}$	–
Q1028+313	< 43.7	$18.5^{+19.4}_{-0.12}$	$43.1^{+5.22}_{-4.51}$	$9.26^{+1.33}_{-0.16}$	–
Q1100+772	$41.0^{+7.21}_{-12.7}$	$71.3^{+4.01}_{-4.01}$	$101^{+6.33}_{-5.75}$	$18.1^{+27.6}_{-10.2}$	–
Q1116+215	< 28.7	$89.0^{+8.16}_{-11.0}$	$174^{+16.9}_{-14.7}$	$5.51^{+7.68}_{-1.33}$	–
Q1137+660	< 290	165^{+170}_{-111}	540^{+168}_{-109}	$54.2^{+67.0}_{-14.2}$	$75.4^{+18.7}_{-19.7}$
Q1146-037	< 305	$12.6^{+95.5}_{-9.64}$	$43.8^{+17.0}_{-10.7}$	$7.25^{+14.3}_{-2.26}$	–
Q1202+281	$46.0^{+9.18}_{-10.5}$	$35.8^{+6.27}_{-4.71}$	$26.5^{+5.30}_{-4.03}$	$9.53^{+10.3}_{-4.72}$	–
Q1211+143	$25.0^{+4.66}_{-5.10}$	$27.8^{+1.79}_{-1.58}$	$45.1^{+7.34}_{-5.99}$	$41.9^{+916}_{-25.4}$	$4.91^{+1.63}_{-1.60}$
Q1219+755	< 10.1	$8.84^{+2.50}_{-0.81}$	$11.0^{+3.06}_{-2.22}$	$3.12^{+0.08}_{-0.02}$	$2.40^{+0.46}_{-0.35}$
Q1226+023	$277^{+38.3}_{-31.7}$	$316^{+35.4}_{-30.9}$	$625^{+95.6}_{-79.7}$	$50.8^{+0.48}_{-0.24}$	$122^{+13.5}_{-12.3}$
Q1307+085	$23.5^{+5.25}_{-8.83}$	$23.3^{+1.10}_{-1.06}$	$56.2^{+3.49}_{-3.16}$	$4.39^{+7.42}_{-1.01}$	–
Q1407+265	604^{+681}_{-499}	744^{+144}_{-152}	1169^{+134}_{-108}	$184^{+6610}_{-94.2}$	$100^{+86.1}_{-44.9}$
Q1416-129	< 29.6	$9.96^{+10.8}_{-0.00}$	$29.2^{+10.4}_{-7.30}$	$8.01^{+47.3}_{-4.42}$	$8.20^{+4.01}_{-1.78}$
Q1426+015	$15.3^{+4.02}_{-4.84}$	$18.6^{+2.99}_{-2.55}$	$43.2^{+8.39}_{-6.80}$	$7.73^{+9.37}_{-2.72}$	$5.10^{+0.87}_{-0.64}$
Q1501+106	$5.22^{+0.99}_{-0.88}$	$4.57^{+0.68}_{-0.57}$	$6.39^{+1.30}_{-0.99}$	$2.20^{+0.11}_{-0.02}$	$1.41^{+0.11}_{-0.11}$
Q1545+210	$32.2^{+5.83}_{-11.4}$	$50.5^{+8.51}_{-9.55}$	$118^{+30.4}_{-20.8}$	$15.9^{+22.3}_{-9.54}$	–
Q1613+658	$49.3^{+2.78}_{-5.56}$	$32.9^{+7.89}_{-6.20}$	$39.8^{+3.31}_{-2.91}$	$6.39^{+2.06}_{-1.50}$	–
Q1704+608	$188^{+28.0}_{-45.1}$	$187^{+13.3}_{-12.9}$	$213^{+12.5}_{-11.7}$	$1.58^{+3.80}_{-0.49}$	–
Q1721+343	$50.1^{+27.0}_{-10.1}$	$42.6^{+6.15}_{-5.74}$	$121^{+15.4}_{-13.2}$	$11.6^{+14.3}_{-3.50}$	–
Q1803+676	< 8.63	$20.4^{+0.00}_{-1.27}$	$32.2^{+7.54}_{-5.02}$	$0.45^{+0.49}_{-0.15}$	–
Q2130+099	$12.0^{+0.89}_{-0.90}$	$15.0^{+1.48}_{-1.32}$	$17.7^{+2.87}_{-2.22}$	$3.07^{+0.35}_{-0.11}$	$1.15^{+0.18}_{-0.15}$
Q2135-147	$46.9^{+17.7}_{-16.3}$	$47.4^{+4.90}_{-4.57}$	$57.9^{+4.58}_{-4.15}$	$7.95^{+1.36}_{-1.14}$	$22.0^{+3.94}_{-4.46}$

Table 20

OCTAVE LUMINOSITIES

Name	(1-2 μm)	(0.4-0.8 μm)	(0.2-0.4 μm)	(0.1-0.2 μm)	(0.1-0.2 keV)	(1-2 keV)
Q0007+106	$4.55^{+0.79}_{-0.67}$	$5.57^{+0.19}_{-0.18}$	$9.66^{+0.49}_{-0.46}$	$11.1\ ^{+0.99}_{-0.86}$	$0.35^{+2.85}_{-0.18}$	$1.38^{+1.15}_{-0.56}$
Q0026+129	$7.54^{+1.20}_{-1.03}$	$11.5\ ^{+0.30}_{-0.29}$	$17.6\ ^{+0.99}_{-0.92}$	$23.1\ ^{+7.35}_{-5.52}$	$1.72^{+0.27}_{-0.20}$	$2.24^{+0.06}_{-0.06}$
Q0049+171	$0.82^{+0.10}_{-0.09}$	$0.97^{+0.02}_{-0.02}$	$1.77^{+0.16}_{-0.15}$	$1.57^{+0.40}_{-0.20}$	$0.28^{+210}_{-0.04}$	$0.71^{+2.02}_{-0.44}$
Q0052+251	$7.89^{+0.47}_{-0.44}$	$10.5\ ^{+0.17}_{-0.17}$	$21.2\ ^{+1.71}_{-1.52}$	$37.9\ ^{+7.70}_{-5.48}$	$3.50^{+442}_{-2.56}$	$2.78^{+1.21}_{-1.42}$
Q0054+144	$11.6\ ^{+0.30}_{-0.29}$	$12.2\ ^{+1.37}_{-1.22}$	$13.0\ ^{+2.78}_{-2.27}$	$9.03^{+1.73}_{-1.38}$	$3.75^{+1.60}_{-0.74}$	$1.33^{+0.16}_{-0.15}$
Q0121-590	$4.12^{+1.80}_{-1.25}$	$4.03^{+2.30}_{-1.46}$	$8.91^{+3.75}_{-2.58}$	$13.4\ ^{+4.77}_{-3.52}$	$1.13^{+0.52}_{-0.35}$	$1.43^{+0.16}_{-0.16}$
Q0134+329	$34.1\ ^{+2.76}_{-2.53}$	$31.9\ ^{+1.52}_{-1.45}$	$40.7\ ^{+5.54}_{-4.27}$	$52.1\ ^{+25.5}_{-16.1}$	$2.86^{+7.20}_{-1.59}$	$5.70^{+1.99}_{-1.42}$
Q0205+024	$5.98^{+0.48}_{-0.44}$	$8.78^{+0.43}_{-0.41}$	$18.4\ ^{+2.83}_{-2.37}$	$22.1\ ^{+3.69}_{-2.98}$	$16.1\ ^{+5.82}_{-2.77}$	$1.03^{+0.18}_{-0.16}$
Q0312-770	$8.19^{+0.47}_{-2.00}$	$15.3\ ^{+1.42}_{-1.30}$	$19.4\ ^{+8.28}_{-4.91}$	$50.4\ ^{+25.8}_{-16.2}$	$0.28^{+3.22}_{-0.15}$	$2.24^{+2.57}_{-0.77}$
Q0637-752	$180\ ^{+5.36}_{-5.43}$	$217\ ^{+23.1}_{-20.6}$	$291\ ^{+68.8}_{-55.4}$	$575\ ^{+50.6}_{-45.7}$	$9.51^{+2.31}_{-1.67}$	$34.5\ ^{+2.22}_{-3.36}$
Q0837-120	$6.74^{+0.69}_{-0.63}$	$6.04^{+0.37}_{-0.34}$	$11.2\ ^{+2.10}_{-1.73}$	$21.5\ ^{+4.30}_{-3.46}$	$2.96^{+2.32}_{-1.29}$	$5.90^{+1.28}_{-1.10}$
Q0844+349	$2.50^{+0.09}_{-0.09}$	$3.94^{+0.14}_{-0.13}$	$6.26^{+0.72}_{-0.63}$	$5.78^{+0.94}_{-0.76}$	$0.07^{+0.31}_{-0.04}$	$0.17^{+0.10}_{-0.05}$
Q1028+313	$6.38^{+0.26}_{-0.28}$	$8.56^{+0.47}_{-0.45}$	$13.3\ ^{+1.75}_{-1.53}$	$18.7\ ^{+2.89}_{-2.42}$	$5.54^{+2.05}_{-0.98}$	$1.99^{+0.25}_{-0.24}$
Q1100+772	$20.8\ ^{+1.21}_{-1.15}$	$30.1\ ^{+1.22}_{-1.17}$	$43.5\ ^{+1.51}_{-1.44}$	$20.4\ ^{+2.90}_{-2.49}$	$5.47^{+13.5}_{-3.90}$	$5.47^{+2.07}_{-1.37}$
Q1116+215	$21.7\ ^{+2.63}_{-2.34}$	$26.8\ ^{+0.91}_{-0.87}$	$55.4\ ^{+2.40}_{-2.25}$	$86.1\ ^{+13.0}_{-11.0}$	$1.65^{+4.00}_{-0.53}$	$1.66^{+0.34}_{-0.30}$
Q1137+660	$52.4\ ^{+2.91}_{-2.81}$	$86.9\ ^{+3.78}_{-3.63}$	$163\ ^{+21.9}_{-17.5}$	$274\ ^{+142}_{-87.7}$	$12.6\ ^{+26.8}_{-4.49}$	$25.1\ ^{+6.67}_{-3.04}$
Q1146-037	$4.84^{+0.87}_{-1.87}$	$6.43^{+1.45}_{-1.01}$	$17.4\ ^{+6.33}_{-4.43}$	$18.3\ ^{+9.14}_{-5.19}$	$1.13^{+4.68}_{-0.52}$	$5.65^{+2.88}_{-1.18}$
Q1202+281	$6.09^{+1.40}_{-1.13}$	$5.23^{+0.27}_{-0.25}$	$8.52^{+1.38}_{-1.09}$	$11.0\ ^{+3.53}_{-2.59}$	$3.10^{+5.29}_{-1.94}$	$2.46^{+0.80}_{-0.65}$
Q1211+143	$5.79^{+0.99}_{-0.84}$	$10.1\ ^{+0.85}_{-0.74}$	$16.7\ ^{+2.88}_{-2.35}$	$16.1\ ^{+3.43}_{-2.74}$	$23.2\ ^{+780}_{-16.2}$	$2.33^{+0.64}_{-0.84}$
Q1219+755	$3.24^{+0.31}_{-0.28}$	$3.68^{+0.36}_{-0.33}$	$3.18^{+1.47}_{-0.98}$	$3.16^{+1.14}_{-0.83}$	$1.49^{+0.14}_{-0.09}$	$0.87^{+0.04}_{-0.04}$
Q1226+023	$84.4\ ^{+8.55}_{-7.77}$	$110\ ^{+5.57}_{-5.28}$	$212\ ^{+21.7}_{-19.2}$	$277\ ^{+66.8}_{-53.8}$	$21.4\ ^{+1.18}_{-1.01}$	$21.2\ ^{+0.55}_{-0.54}$
Q1307+085	$6.88^{+0.29}_{-0.27}$	$11.2\ ^{+0.67}_{-0.62}$	$17.2\ ^{+1.35}_{-1.24}$	$24.8\ ^{+1.31}_{-1.15}$	$1.22^{+3.89}_{-0.40}$	$1.53^{+0.28}_{-0.30}$
Q1407+265	$129\ ^{+14.5}_{-12.9}$	$180\ ^{+6.66}_{-6.42}$	$370\ ^{+11.6}_{-11.2}$	$582\ ^{+114}_{-89.2}$	$64.6\ ^{+4730}_{-40.2}$	$40.8\ ^{+55.5}_{-8.24}$
Q1416-129	$3.39^{+0.57}_{-0.46}$	$5.46^{+0.93}_{-0.70}$	$10.6\ ^{+4.27}_{-2.98}$	$11.7\ ^{+5.02}_{-3.42}$	$2.22^{+22.9}_{-1.50}$	$2.79^{+3.40}_{-1.21}$
Q1426+015	$5.03^{+0.98}_{-0.82}$	$5.22^{+0.29}_{-0.27}$	$12.7\ ^{+2.09}_{-1.74}$	$23.6\ ^{+5.85}_{-4.65}$	$2.73^{+5.18}_{-1.23}$	$1.68^{+0.45}_{-0.30}$
Q1501+106	$1.18^{+0.26}_{-0.21}$	$1.26^{+0.33}_{-0.23}$	$2.06^{+0.65}_{-0.47}$	$2.61^{+0.29}_{-0.26}$	$1.30^{+0.14}_{-0.08}$	$0.41^{+0.04}_{-0.04}$
Q1545+210	$13.5\ ^{+0.52}_{-0.50}$	$21.3\ ^{+0.50}_{-0.48}$	$39.5\ ^{+8.54}_{-5.69}$	$52.4\ ^{+21.2}_{-14.5}$	$4.05^{+9.34}_{-3.07}$	$6.42^{+3.30}_{-2.03}$
Q1613+658	$8.07^{+1.15}_{-1.01}$	$8.80^{+0.46}_{-0.42}$	$12.7\ ^{+1.67}_{-1.39}$	$15.7\ ^{+0.92}_{-0.86}$	$2.08^{+1.03}_{-0.69}$	$1.65^{+0.16}_{-0.15}$
Q1704+608	$38.2\ ^{+3.38}_{-3.14}$	$46.0\ ^{+1.91}_{-1.83}$	$66.3\ ^{+4.66}_{-4.32}$	$89.0\ ^{+5.10}_{-4.78}$	$0.20^{+0.99}_{-0.09}$	$1.57^{+1.24}_{-0.37}$
Q1721+343	$10.4\ ^{+0.80}_{-0.75}$	$18.1\ ^{+1.00}_{-0.95}$	$41.8\ ^{+3.22}_{-2.94}$	$57.2\ ^{+10.8}_{-9.04}$	$2.22^{+4.97}_{-1.00}$	$7.03^{+2.83}_{-1.35}$
Q1803+676	$5.18^{+0.25}_{-0.24}$	$5.81^{+0.28}_{-0.26}$	$11.4\ ^{+1.55}_{-1.25}$	$13.2\ ^{+5.57}_{-3.37}$	$0.04^{+0.08}_{-0.02}$	$0.63^{+0.39}_{-0.17}$
Q2130+099	$3.31^{+0.62}_{-0.52}$	$3.33^{+0.10}_{-0.09}$	$5.77^{+0.27}_{-0.25}$	$7.81^{+2.44}_{-1.82}$	$2.47^{+0.49}_{-0.28}$	$0.27^{+0.04}_{-0.03}$
Q2135-147	$12.1\ ^{+1.41}_{-1.24}$	$16.0\ ^{+0.80}_{-0.75}$	$19.7\ ^{+1.31}_{-1.22}$	$18.0\ ^{+1.99}_{-1.75}$	$1.86^{+0.51}_{-0.40}$	$3.63^{+0.22}_{-0.21}$

Table 21

The '1 μm' Inflection

Quasar	Band	$\lambda(\mu)$	L_{44},Err
Q0007+106	J	1.11	5.65+/- 0.07
Q0026+129	H	1.42	9.77+/- 0.07
Q0049+171	H	1.53	1.11+/- 0.06
Q0052+251	H	1.41	9.79+/- 0.03
Q0054+144	H	1.39	14.35+/- 0.01
Q0121-590	I	0.87	3.74+/- 0.16
Q0134+329	H	1.19	36.45+/- 0.03
Q0205+024	H	1.41	7.55+/- 0.04
Q0312-770	H	1.33	10.05+/- 0.02
Q0637-752	H	0.98	235.68+/- 0.02
Q0837-120	H	1.36	8.35+/- 0.03
Q0844+349	H	1.53	3.35+/- 0.01
Q1028+313	H	1.38	8.14+/- 0.02
Q1100+772	H	1.24	27.07+/- 0.02
Q1116+215	J	1.03	25.09+/- 0.05
Q1137+660	H	0.98	57.66+/- 0.02
Q1146-037	H	1.21	6.53+/- 0.06
Q1202+281	J	1.04	6.63+/- 0.05
Q1211+143	J	1.11	7.58+/- 0.09
Q1219+755	I	0.85	4.30+/- 0.03
Q1226+023	J	1.04	107.14+/- 0.05
Q1307+085	H	1.41	8.82+/- 0.01
Q1407+265	K	1.11	146.40+/- 0.03
Q1416-129	H	1.44	4.09+/- 0.02
Q1426+015	J	1.11	6.79+/- 0.10
Q1501+106	H	1.57	1.62+/- 0.09
Q1545+210	H	1.28	17.37+/- 0.01
Q1613+658	J	1.07	10.91+/- 0.07
Q1704+608	H	1.19	46.86+/- 0.03
Q1721+343	H	1.35	12.85+/- 0.02
Q1803+676	J	1.06	6.67+/- 0.04
Q2130+099	I	0.86	3.56+/- 0.03
Q2135-147	H	1.35	14.62+/- 0.06

TABLE 22

MEAN ENERGY DISTRIBUTION

Range λ (μm)	Relative Flux ($\nu F_\nu = \lambda F_\lambda$)
>100	
80–100	$0.68\,(\lambda/100)^{-0.8}$
15–80	$0.81\,(\lambda/100)^{-0.4}$
2–15	$1.6\,(\lambda/10)^{0.12}$
1.4–2	$1.0\,(\lambda/1.4)^{0.8}$
0.5–1.4	$1.0\,(\lambda/1.4)^{-0.4}$
0.32–0.5	$2.5\,(\lambda/0.32)^{-1.1}$
0.27–0.32	$2.5\,(\lambda/0.32)^{-0.6}$
0.22–0.27	$2.5\,(\lambda/0.22)^{0.6}$
0.15-0.22	$2.5\,(\lambda/0.22)^{0.75}$
0.10-0.15	$3.0\,(\lambda/0.1)^{0.2}$
0.01-0.1	$3.0\,(\lambda/0.1)^{0.8}$

Range E (keV)	Relative Flux ($\nu F_\nu = \lambda F_\lambda$) R-Quiet	R-Loud
0.1-0.6	$0.19\,(E)^{-0.5}$	$0.16\,(E)^{-0.4}$
0.6-2	$0.27\,(E)^{0.05}$	$0.30\,(E)^{0.5}$
2-10	$0.28\,(E)^{0.0}$	$0.41\,(E)^{0.25}$

TABLE 23

BOLOMETRIC CORRECTIONS

Ratio	Mean	Sigma
L_V/L_{Base}	1.4	0.3
L_{UVOIR}/L_{Base}	11.5	3.1
L_{Bol}/L_{Base}	17.3	5.0
L_{UVOIR}/L_V	8.5	2.9
L_{Bol}/L_V	12.7	4.2
$L(0.1-0.2\mu)/L(1-2\mu)$	3.05	1.33

Fig. 1

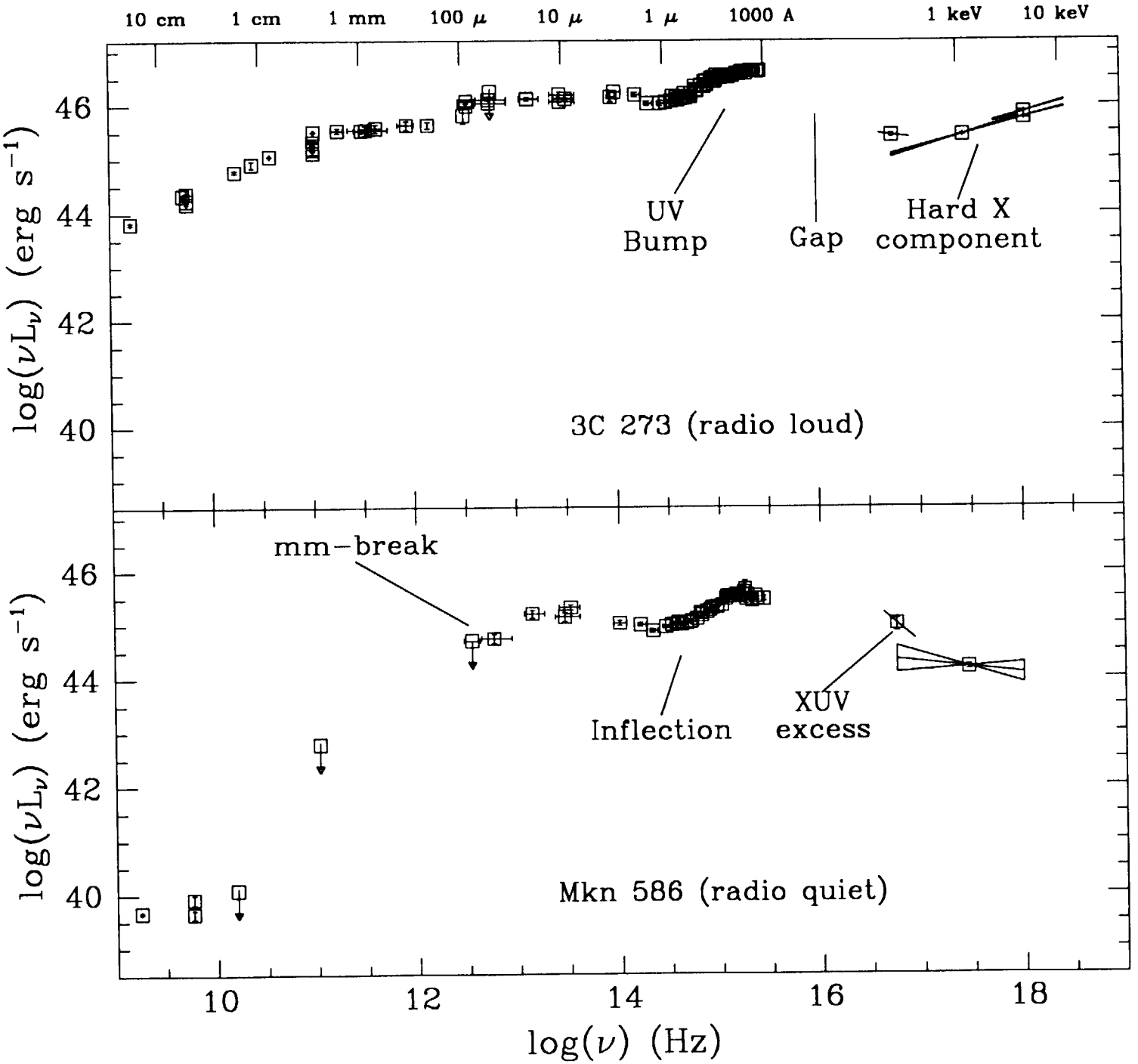
10 cm
1 cm
1 mm
100 μ
10 μ
1 μ
1000 A
1 keV
10 keV
log(νL_ν) (erg s^-1)
46
44
42
40
UV
Bump
Gap
Hard X
component
3C 273 (radio loud)
mm−break
Inflection
XUV
excess
Mkn 586 (radio quiet)
10
12
14
16
18
log(ν) (Hz)

Fig. 2

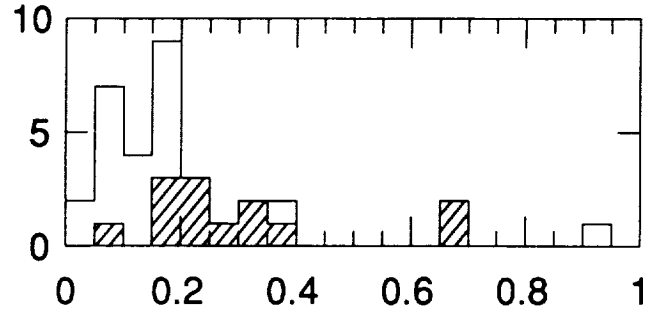

Redshift z

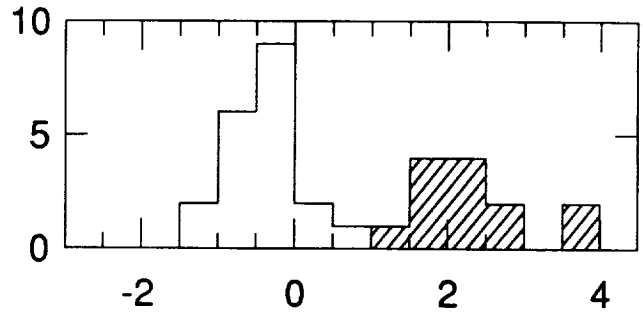

Radio Loudness R_L

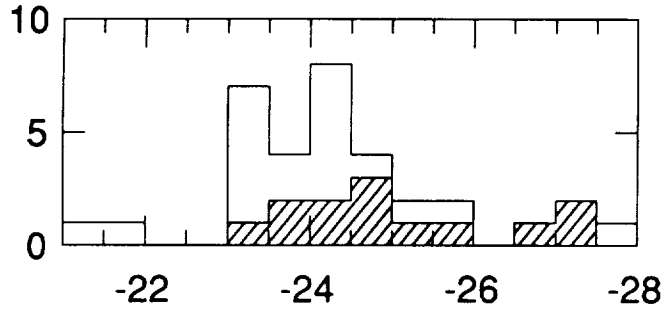

Absolute Mag M_V

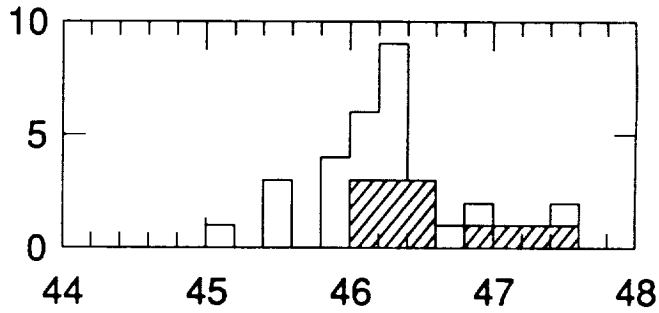

Bolometric Luminosity L_{Bol}

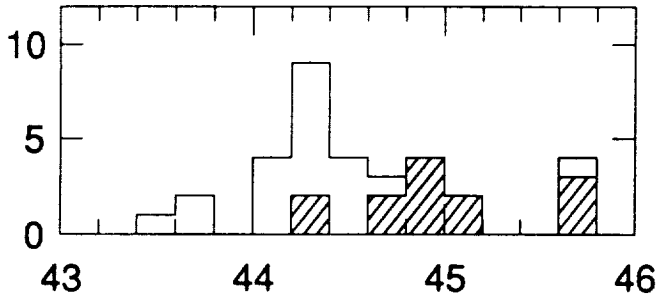

2 keV luminosity log(L_x, erg/s)

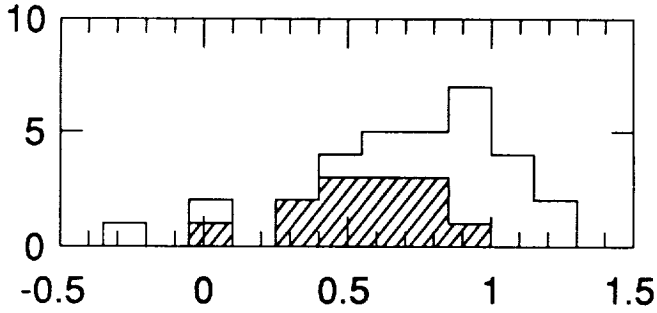

X−ray slope α_x

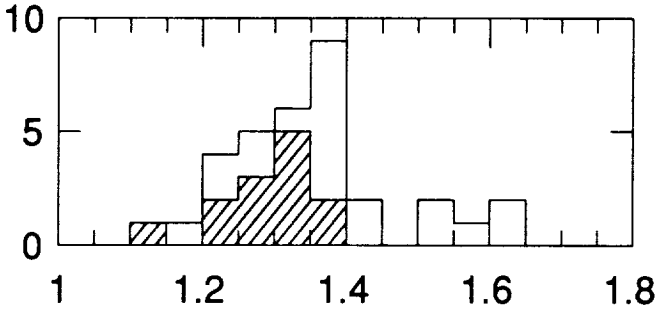

UV to x−ray slope α_{ox}

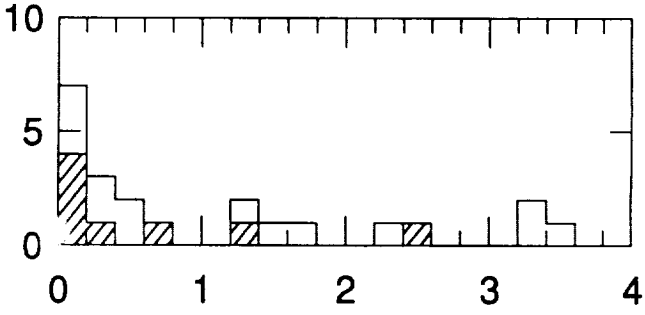

Browne parameter R_B

Fig. 3

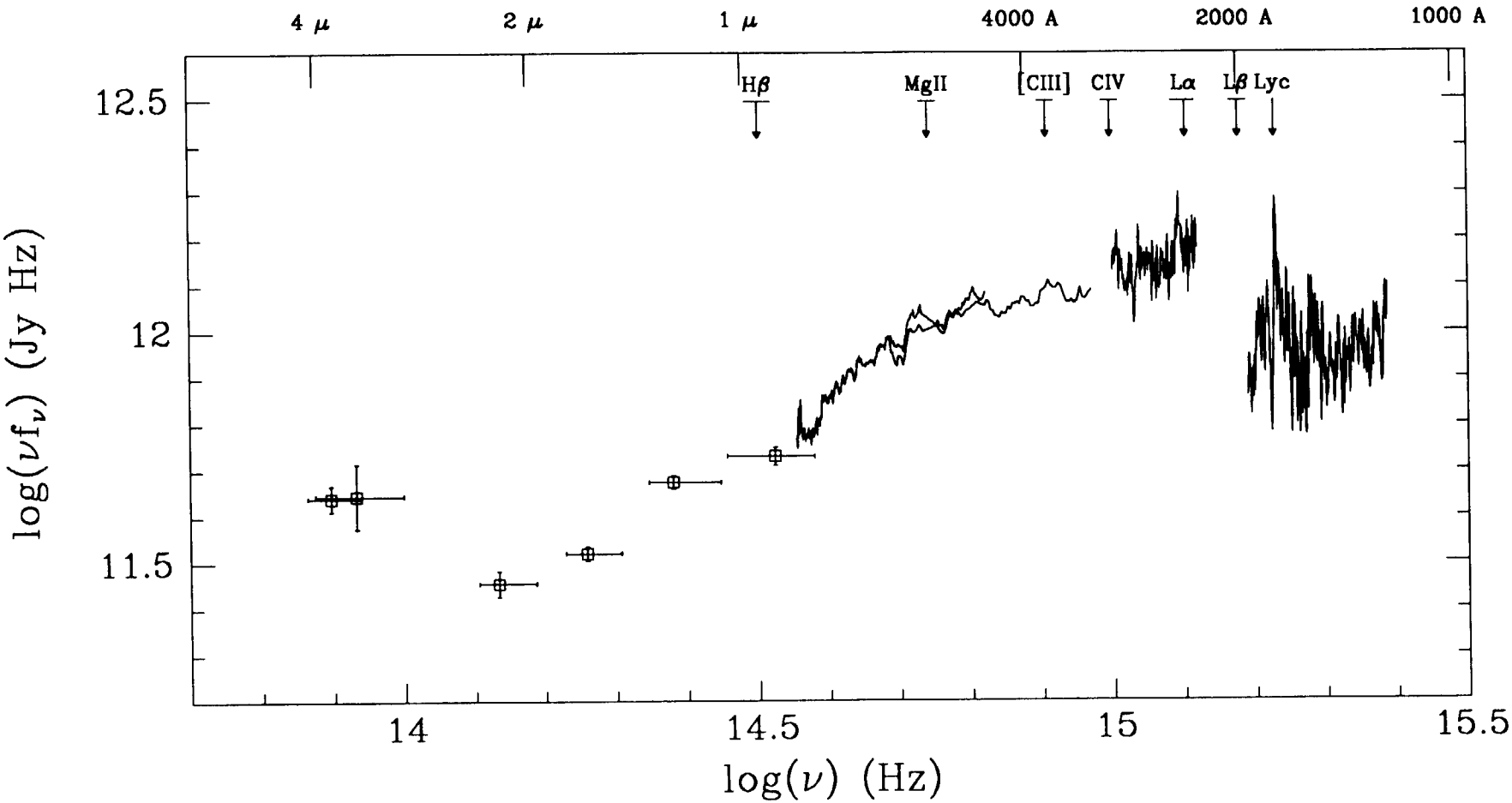
4 μ
2 μ
1 μ
4000 A
2000 A
1000 A
Hβ
MgII
[CIII]
CIV
Lα
Lβ
Lyc
12.5
12
11.5
log(νf_ν) (Jy Hz)
14
14.5
15
15.5
log(ν) (Hz)

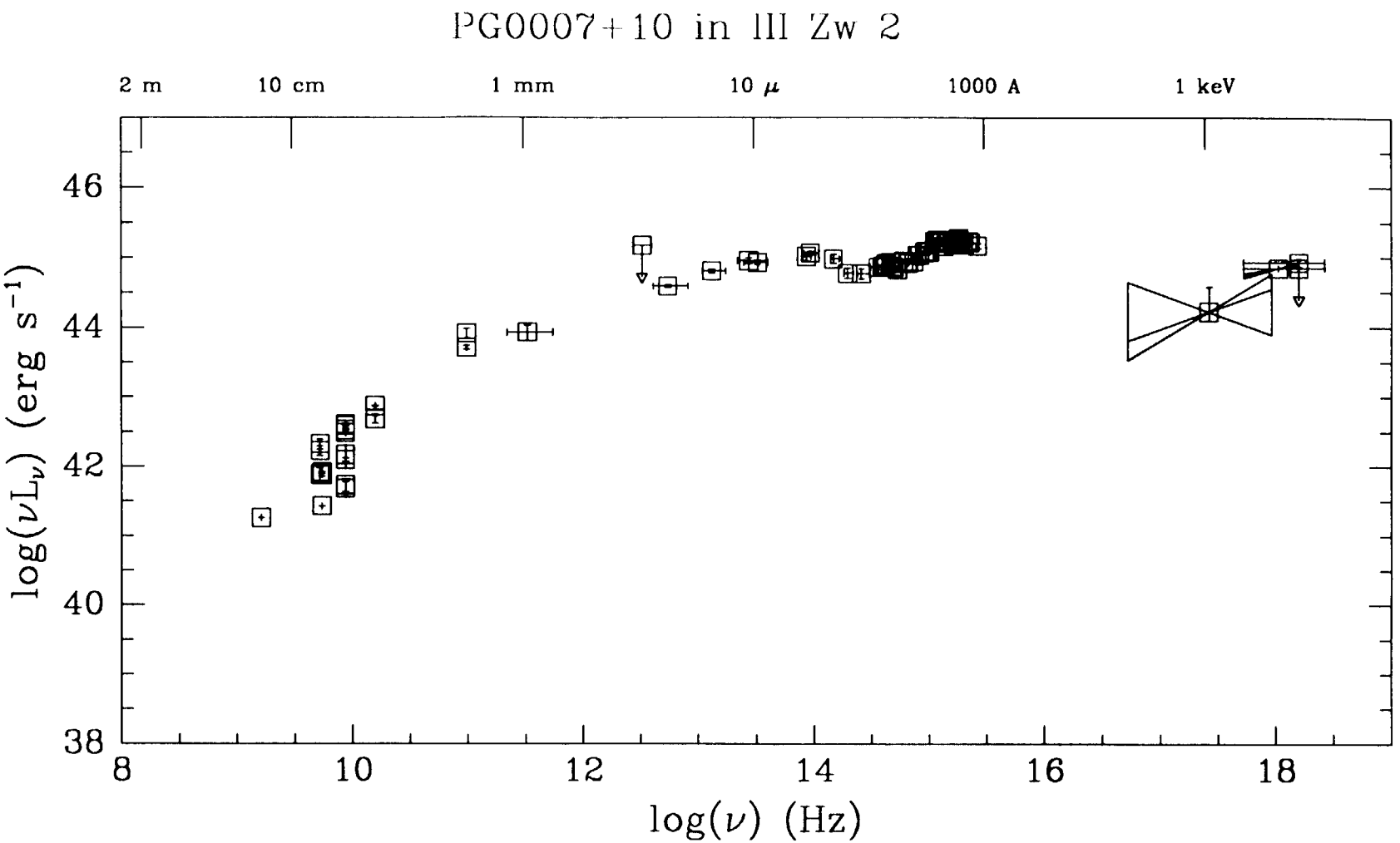
PG0007+10 in III Zw 2
2 m
10 cm
1 mm
10 μ
1000 A
1 keV
46
44
42
40
38
8
10
12
14
16
18
log(νL_ν) (erg s^-1)
log(ν) (Hz)

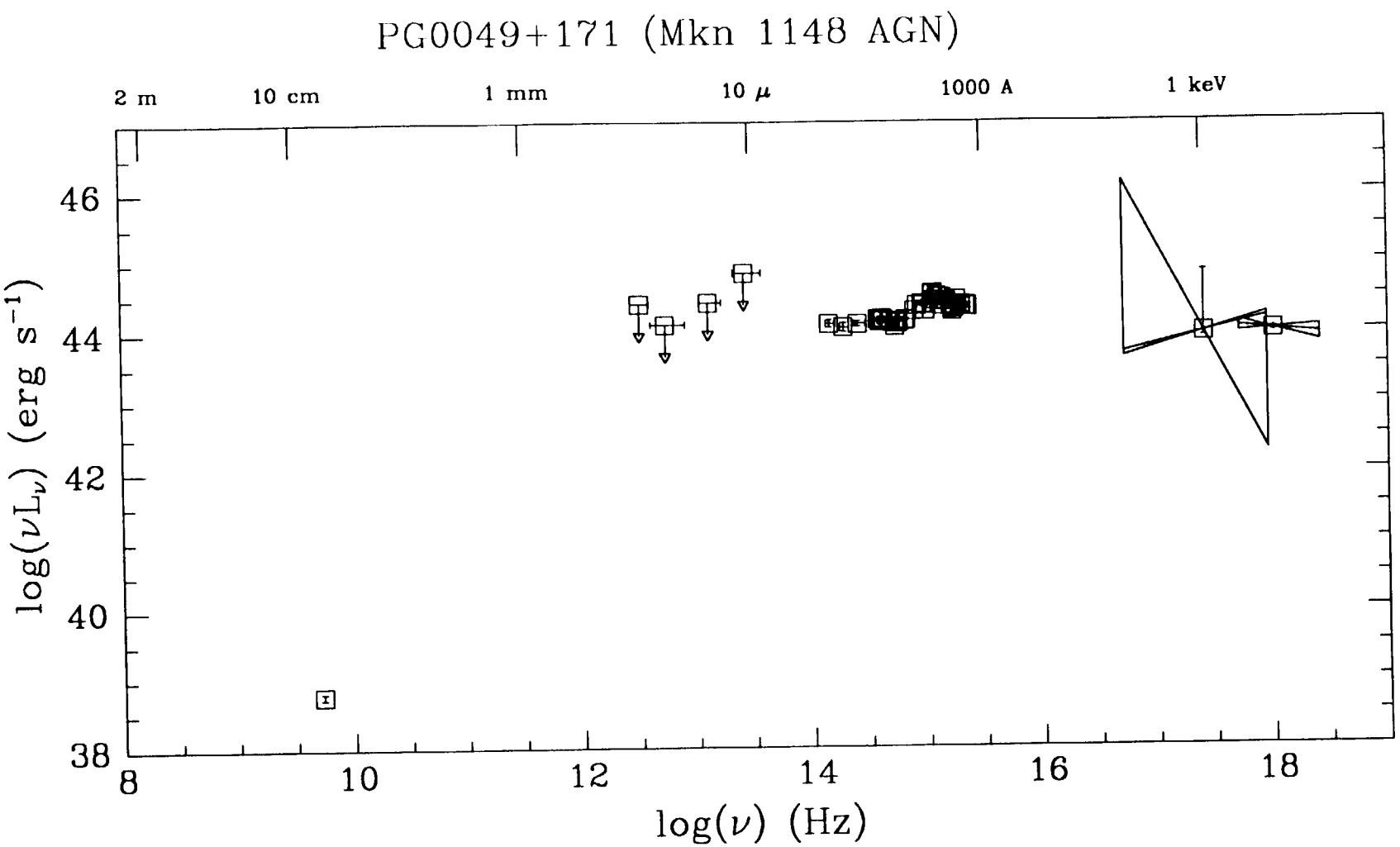
PG0049+171 (Mkn 1148 AGN)
2 m
10 cm
1 mm
10 μ
1000 A
1 keV
log(νL_ν) (erg s^-1)
46
44
42
40
38
8
10
12
14
16
18
log(ν) (Hz)

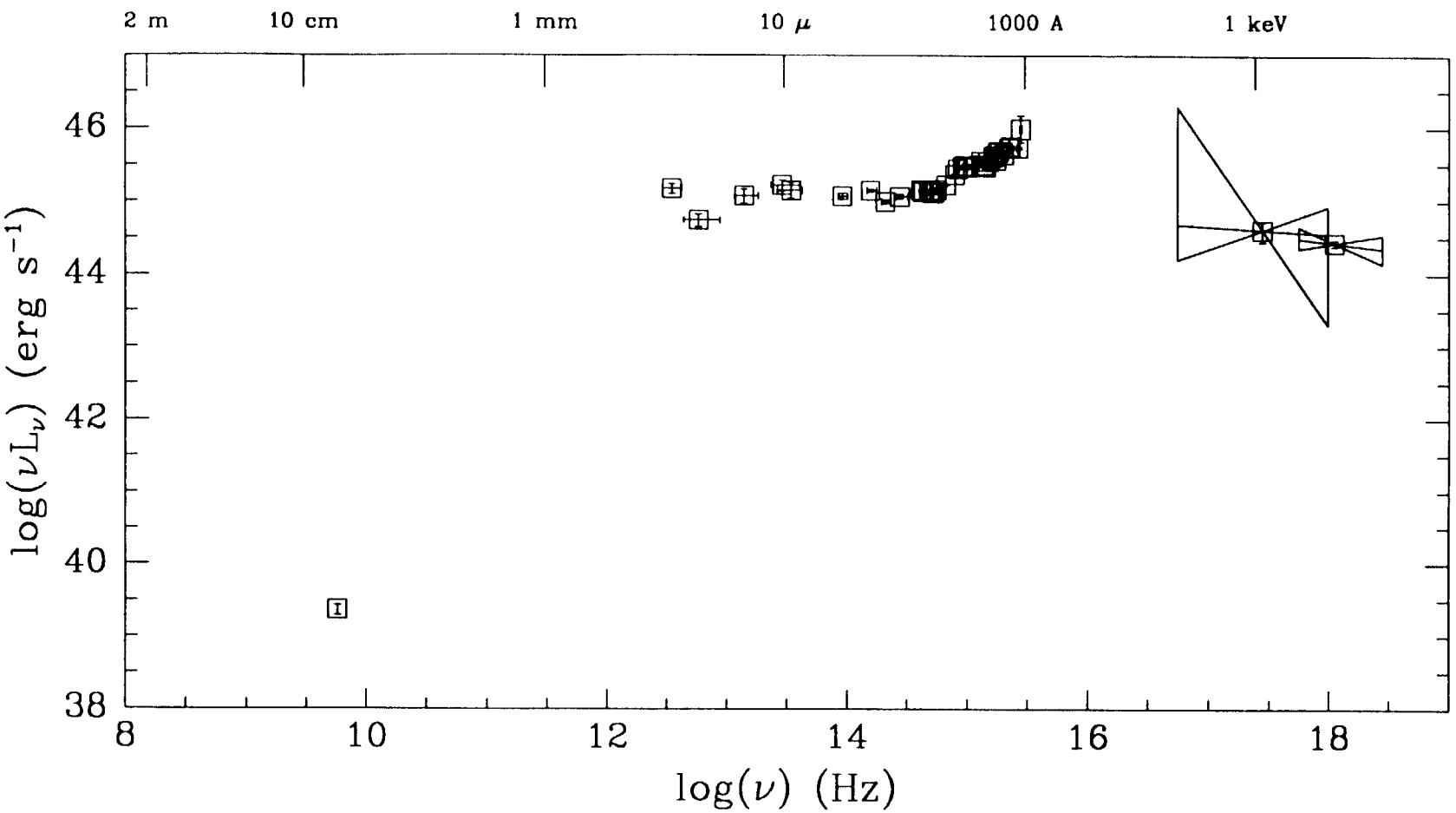
PG0052+251
2 m
10 cm
1 mm
10 μ
1000 A
1 keV
46
44
42
40
38
log(νL_ν) (erg s^-1)
8
10
12
14
16
18
log(ν) (Hz)

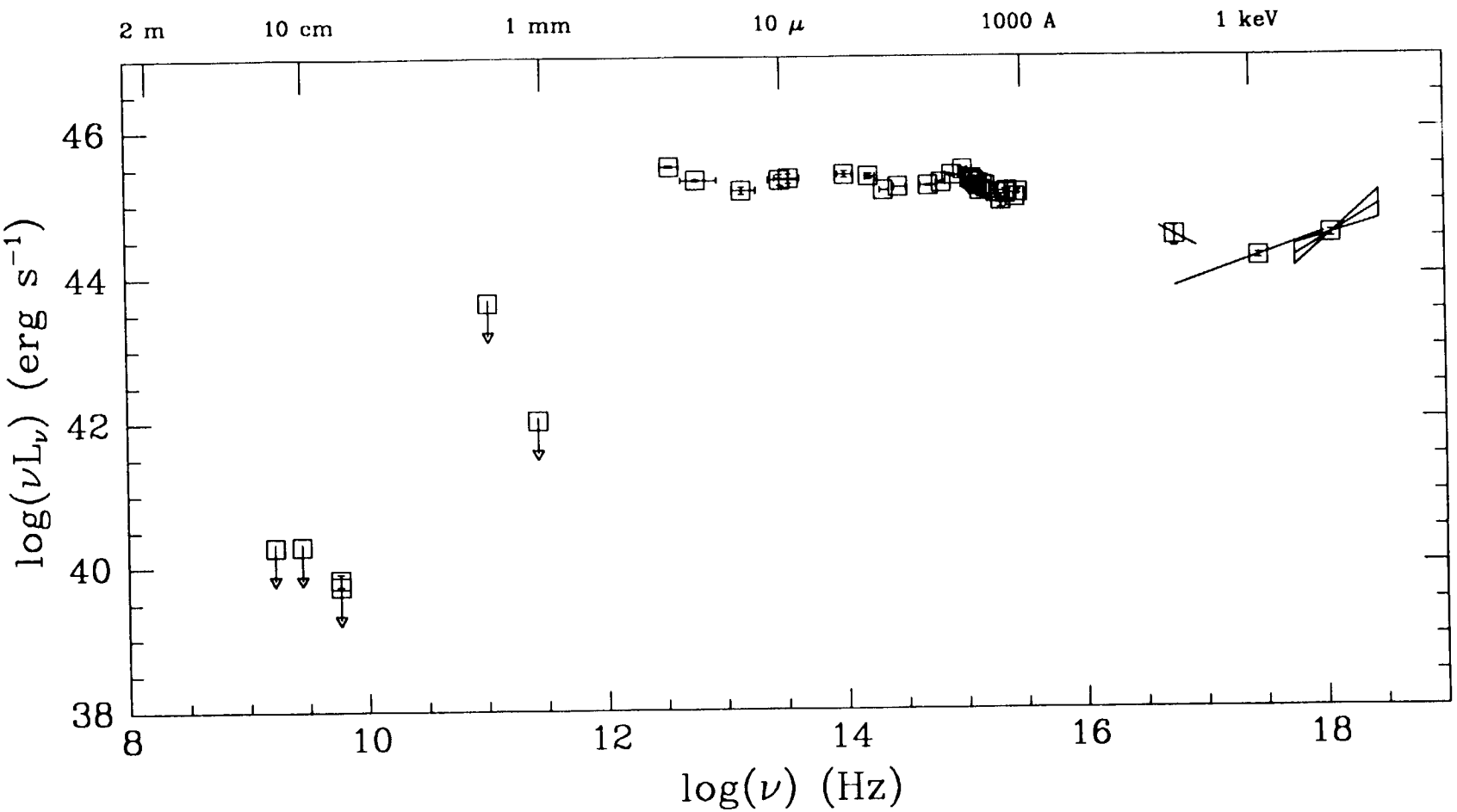
PHL 909 (Q0054+144)
2 m
10 cm
1 mm
10 μ
1000 A
1 keV
46
44
42
40
38
8
10
12
14
16
18
log(νL_ν) (erg s^-1)
log(ν) (Hz)

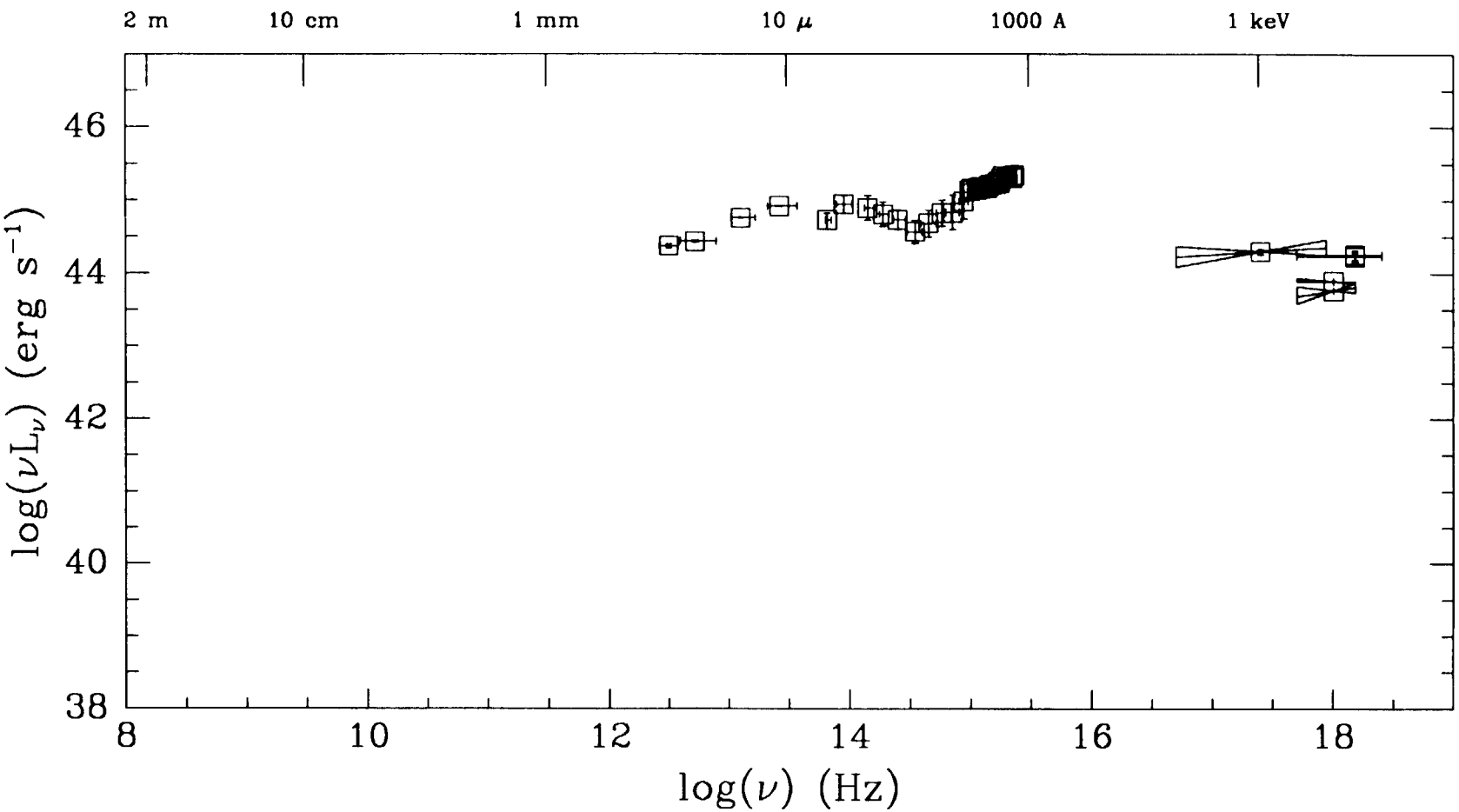
Q0121−590 in Fairall 9 (ES0113−G55)
2 m
10 cm
1 mm
10 μ
1000 A
1 keV
log(νL_ν) (erg s^-1)
46
44
42
40
38
8
10
12
14
16
18
log(ν) (Hz)

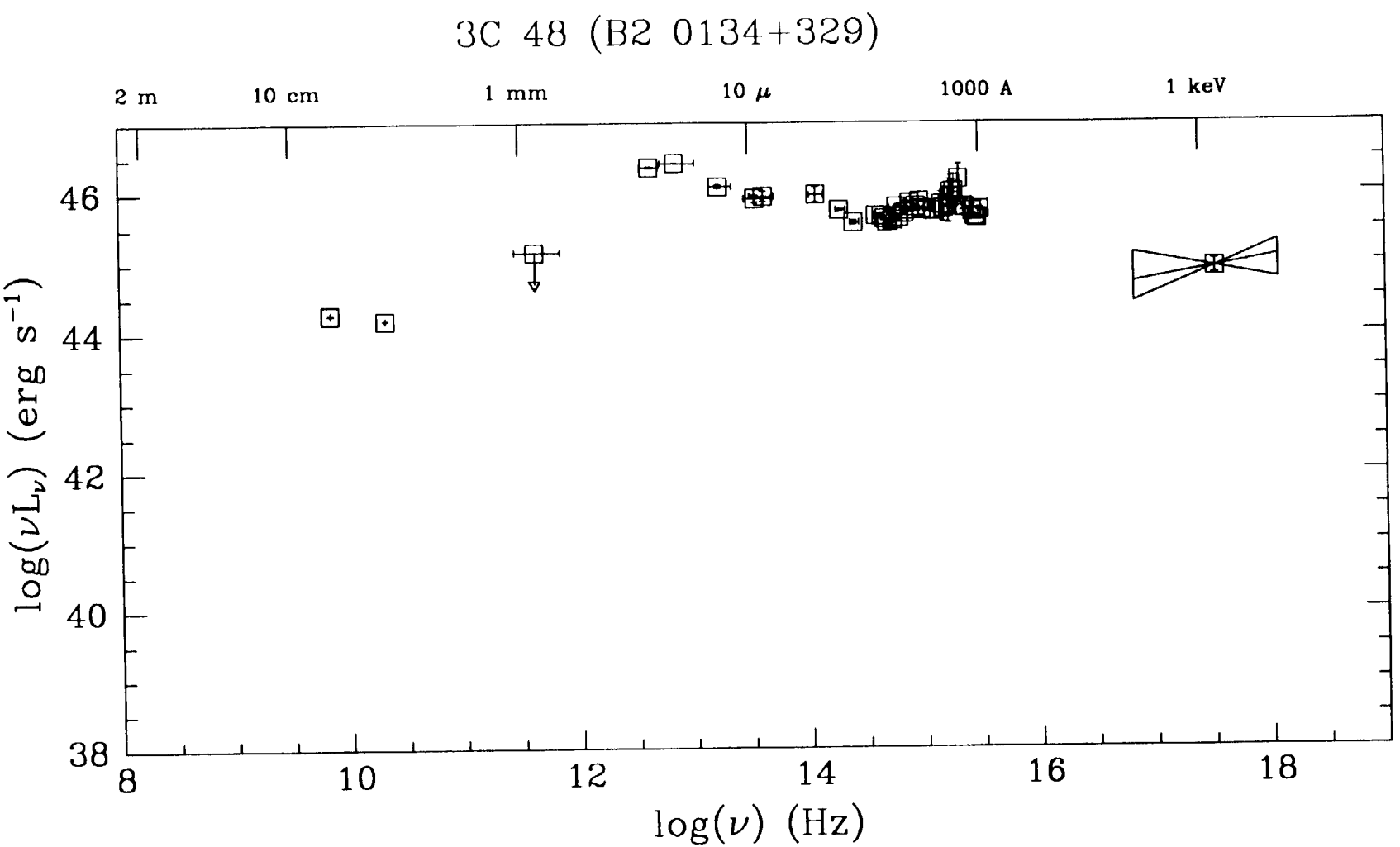
3C 48 (B2 0134+329)
2 m
10 cm
1 mm
10 μ
1000 A
1 keV
46
44
42
40
38
log(νL_ν) (erg s^-1)
8
10
12
14
16
18
log(ν) (Hz)

C-2

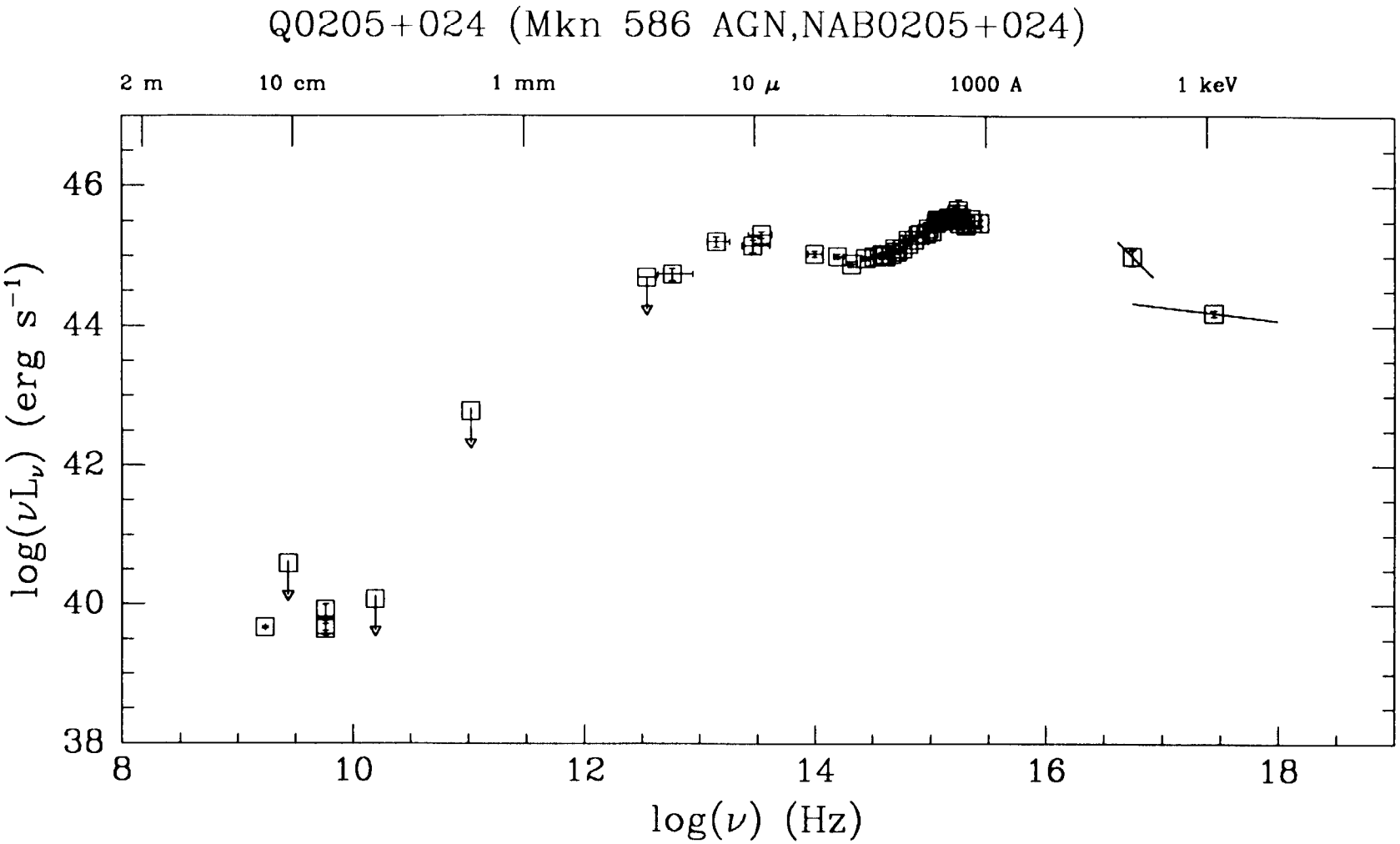
Q0205+024 (Mkn 586 AGN,NAB0205+024)
2 m
10 cm
1 mm
10 μ
1000 A
1 keV
46
44
42
40
38
log(νL_ν) (erg s^-1)
8
10
12
14
16
18
log(ν) (Hz)

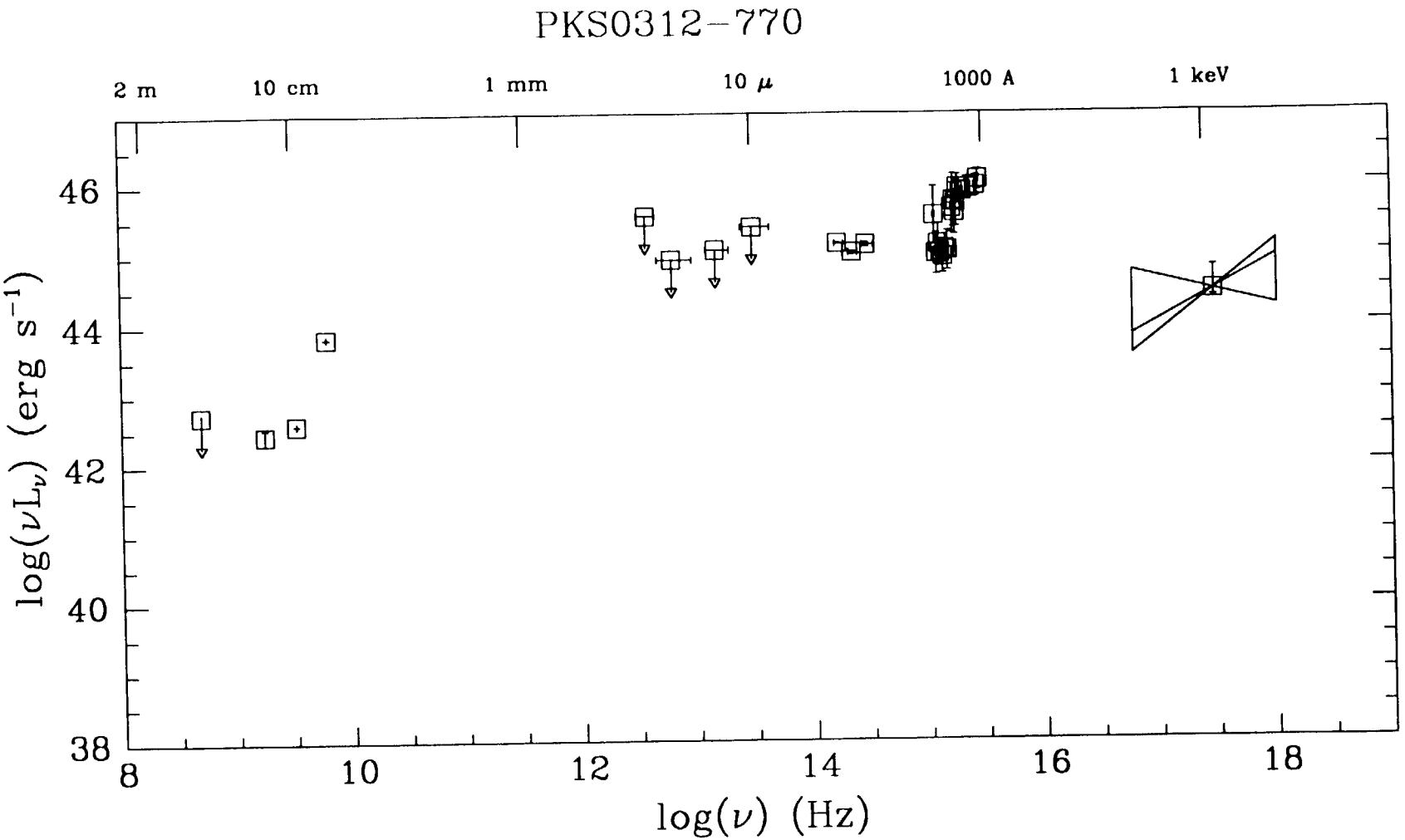
PKS0312−770
2 m
10 cm
1 mm
10 μ
1000 A
1 keV
46
44
42
40
38
8
10
12
14
16
18
log(νL_ν) (erg s^-1)
log(ν) (Hz)

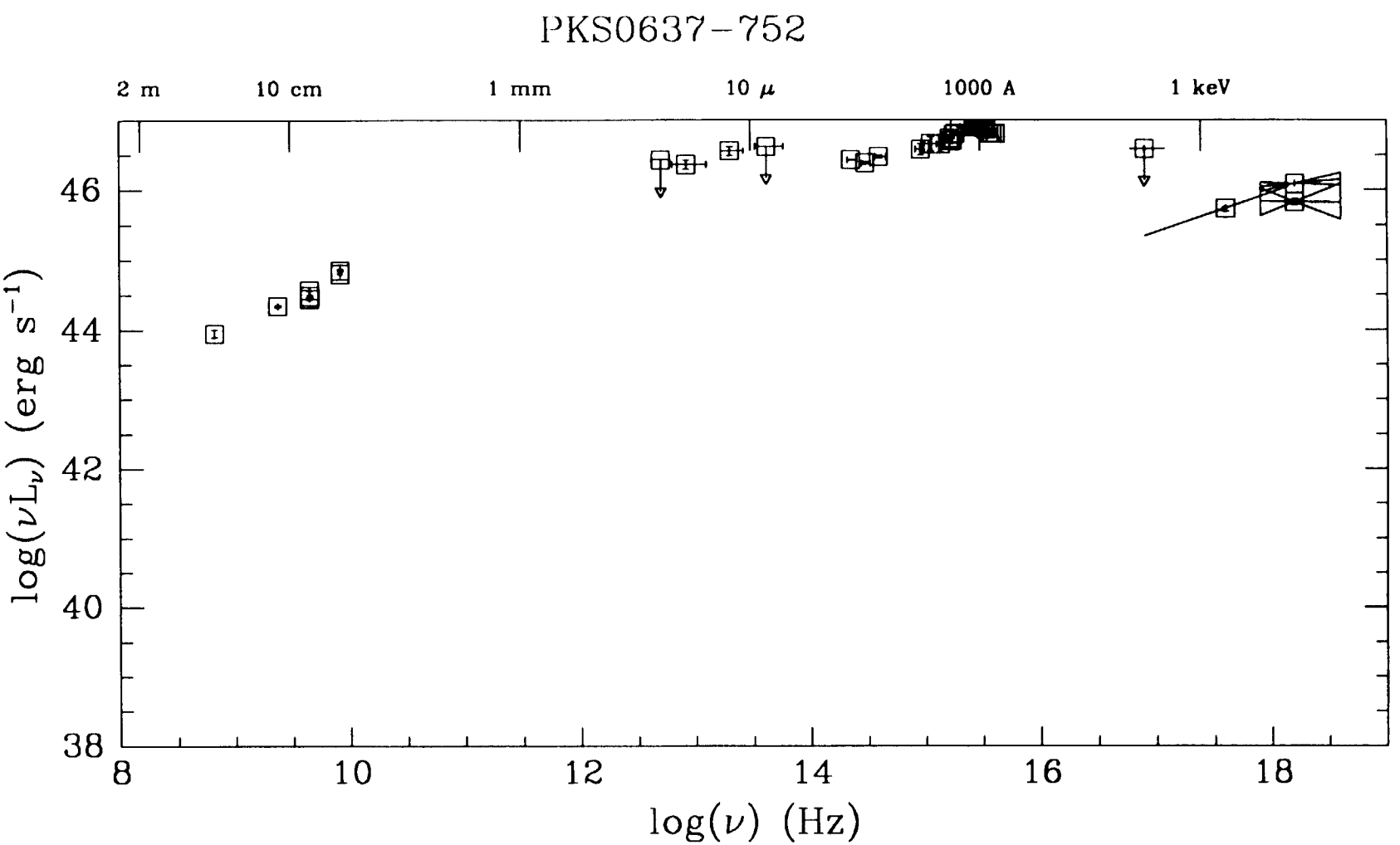
PKS0637−752
2 m
10 cm
1 mm
10 μ
1000 A
1 keV
46
44
42
40
38
8
10
12
14
16
18
log(νL_ν) (erg s^-1)
log(ν) (Hz)

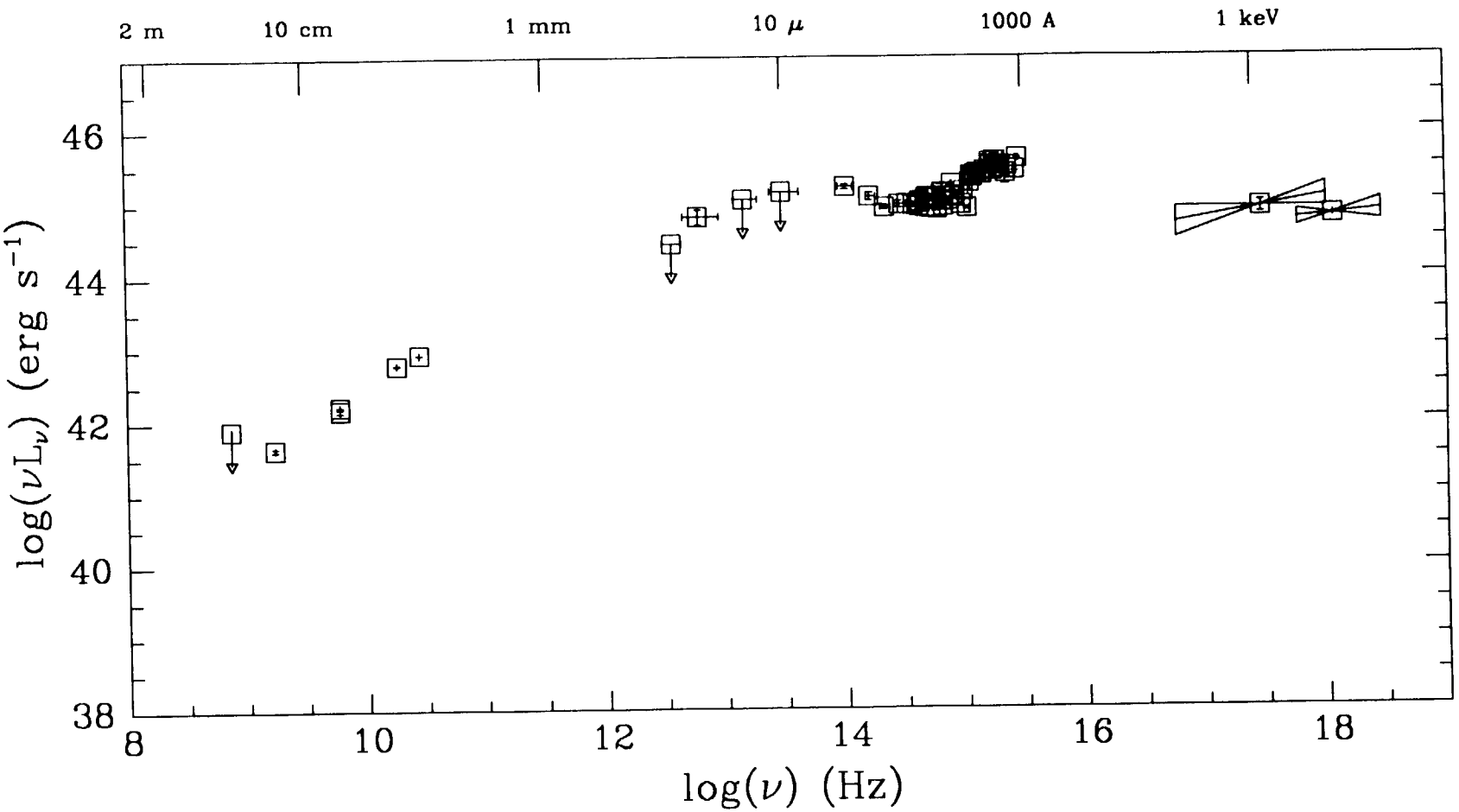
3C 206 (PKS0837−120)
2 m
10 cm
1 mm
10 μ
1000 A
1 keV
46
44
42
40
38
log(νL_ν) (erg s^-1)
8
10
12
14
16
18
log(ν) (Hz)

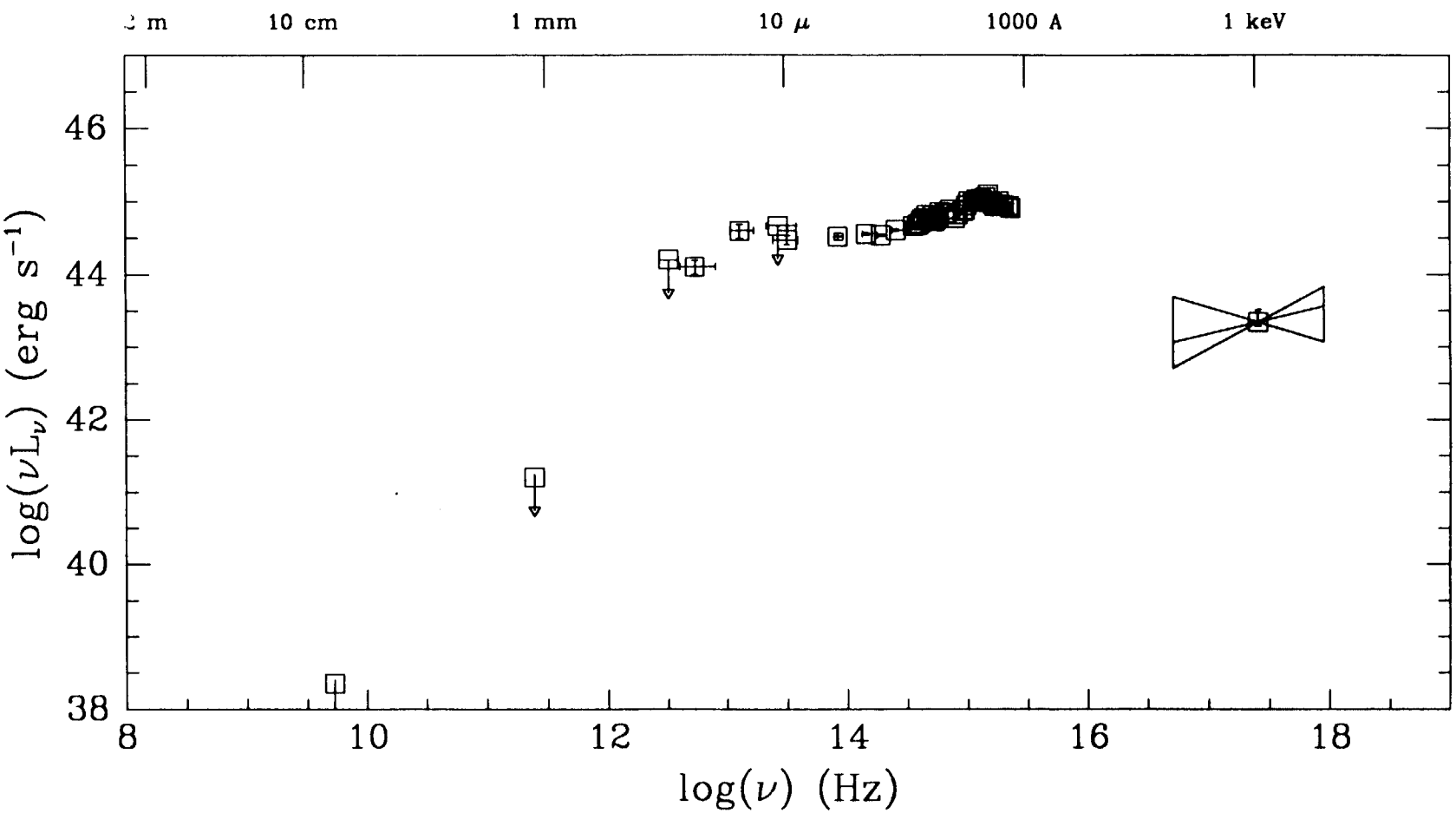
PG0844+349 (Ton 951)
3 m
10 cm
1 mm
10 μ
1000 A
1 keV
46
44
42
40
38
log(νL_ν) (erg s^-1)
8
10
12
14
16
18
log(ν) (Hz)

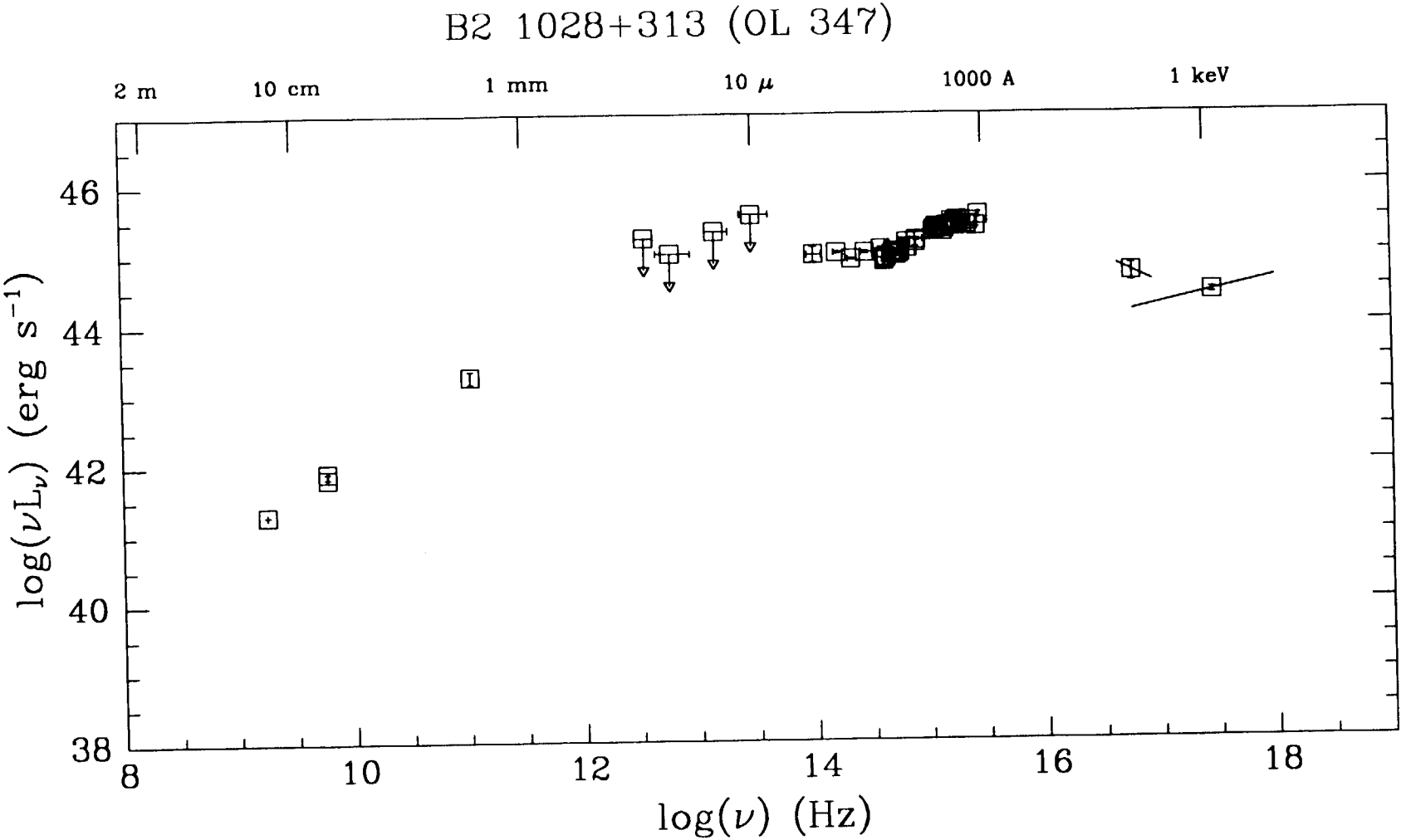
B2 1028+313 (OL 347)
2 m
10 cm
1 mm
10 μ
1000 A
1 keV
46
44
42
40
38
8
10
12
14
16
18
log(νL_ν) (erg s^-1)
log(ν) (Hz)

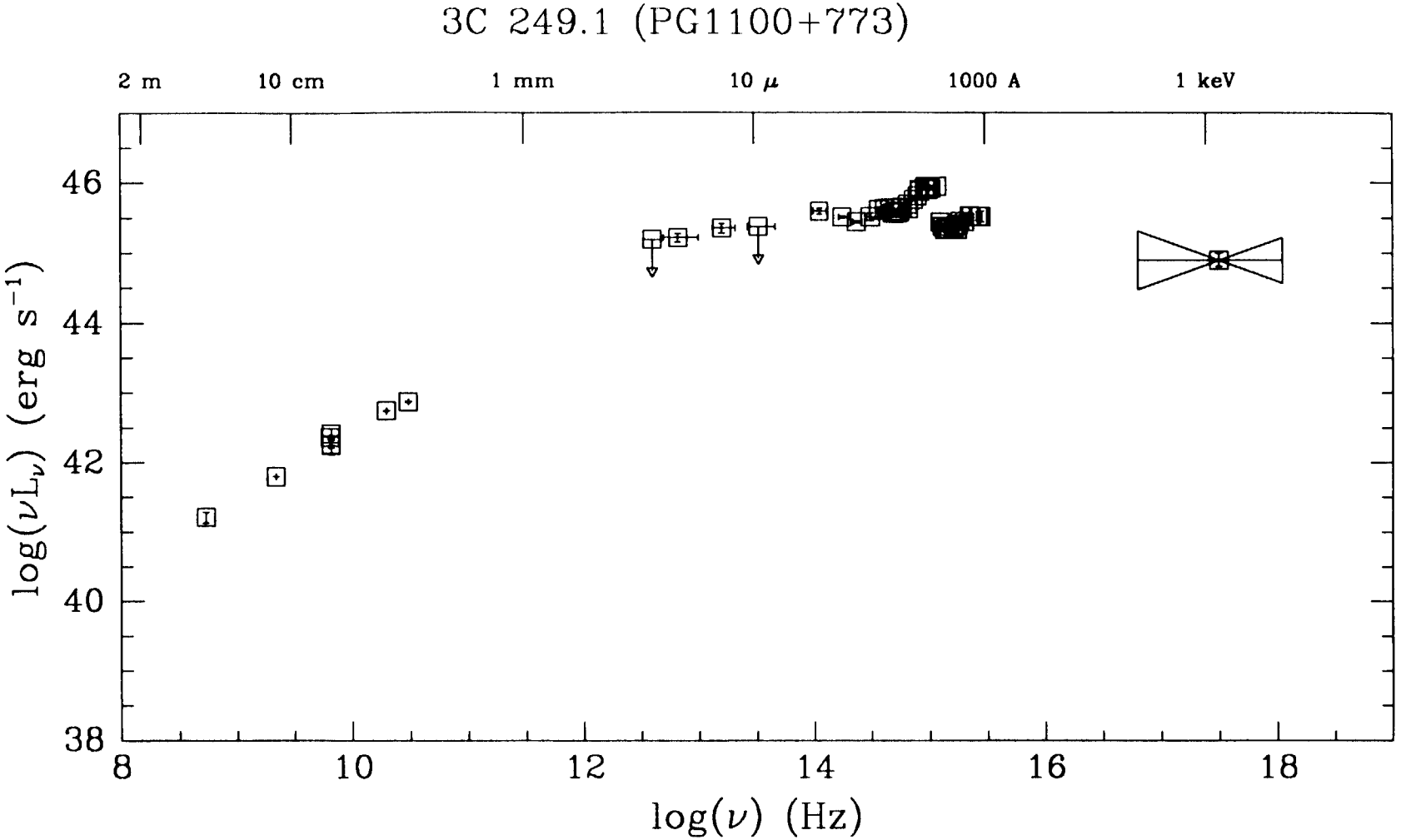
3C 249.1 (PG1100+773)
2 m
10 cm
1 mm
10 μ
1000 A
1 keV
log(νL_ν) (erg s^-1)
46
44
42
40
38
8
10
12
14
16
18
log(ν) (Hz)

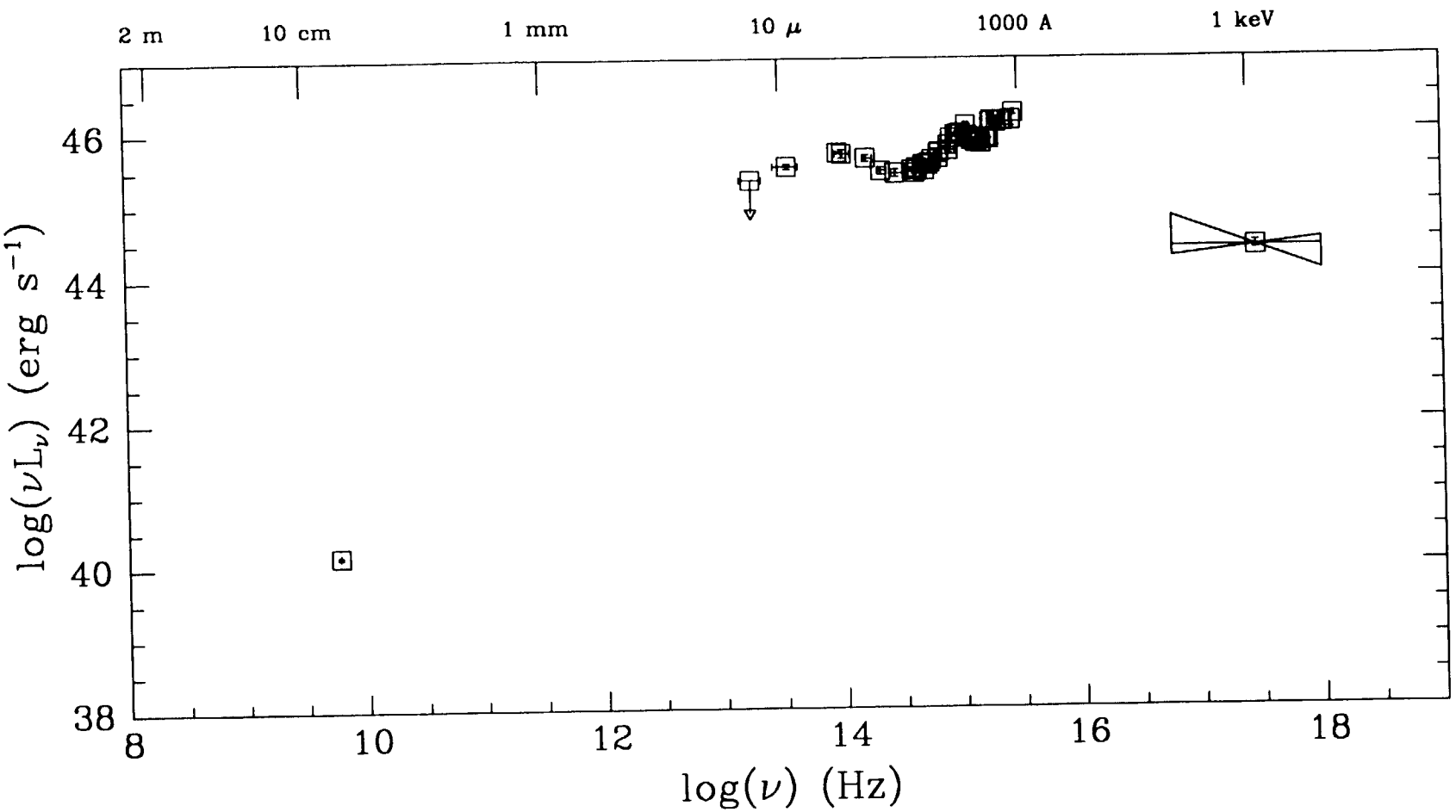
PG1116+215 (Ton 1388)
2 m
10 cm
1 mm
10 μ
1000 A
1 keV
log(νL_ν) (erg s^-1)
46
44
42
40
38
8
10
12
14
16
18
log(ν) (Hz)

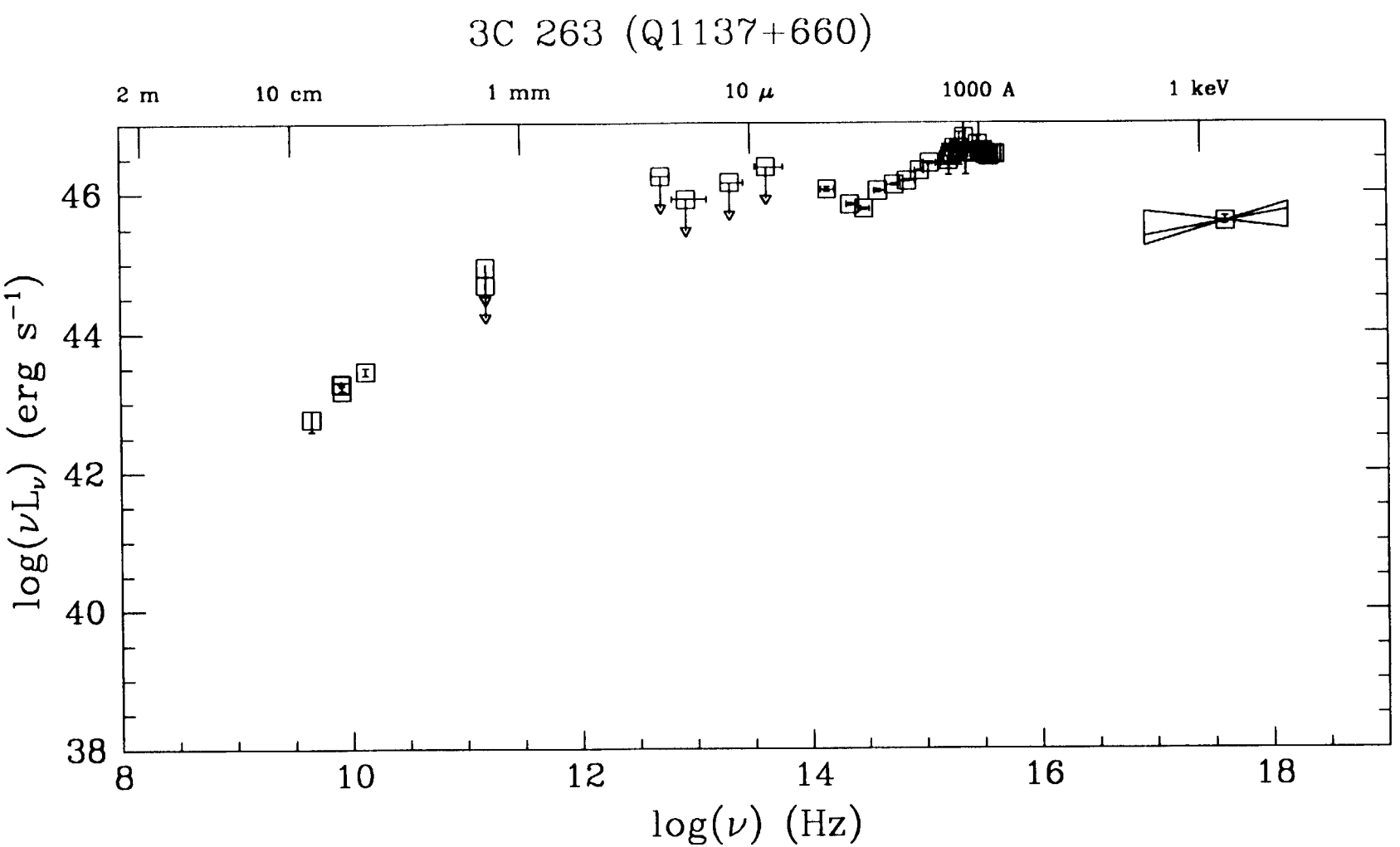
3C 263 (Q1137+660)
2 m
10 cm
1 mm
10 μ
1000 A
1 keV
log(νL_ν) (erg s^-1)
46
44
42
40
38
8
10
12
14
16
18
log(ν) (Hz)

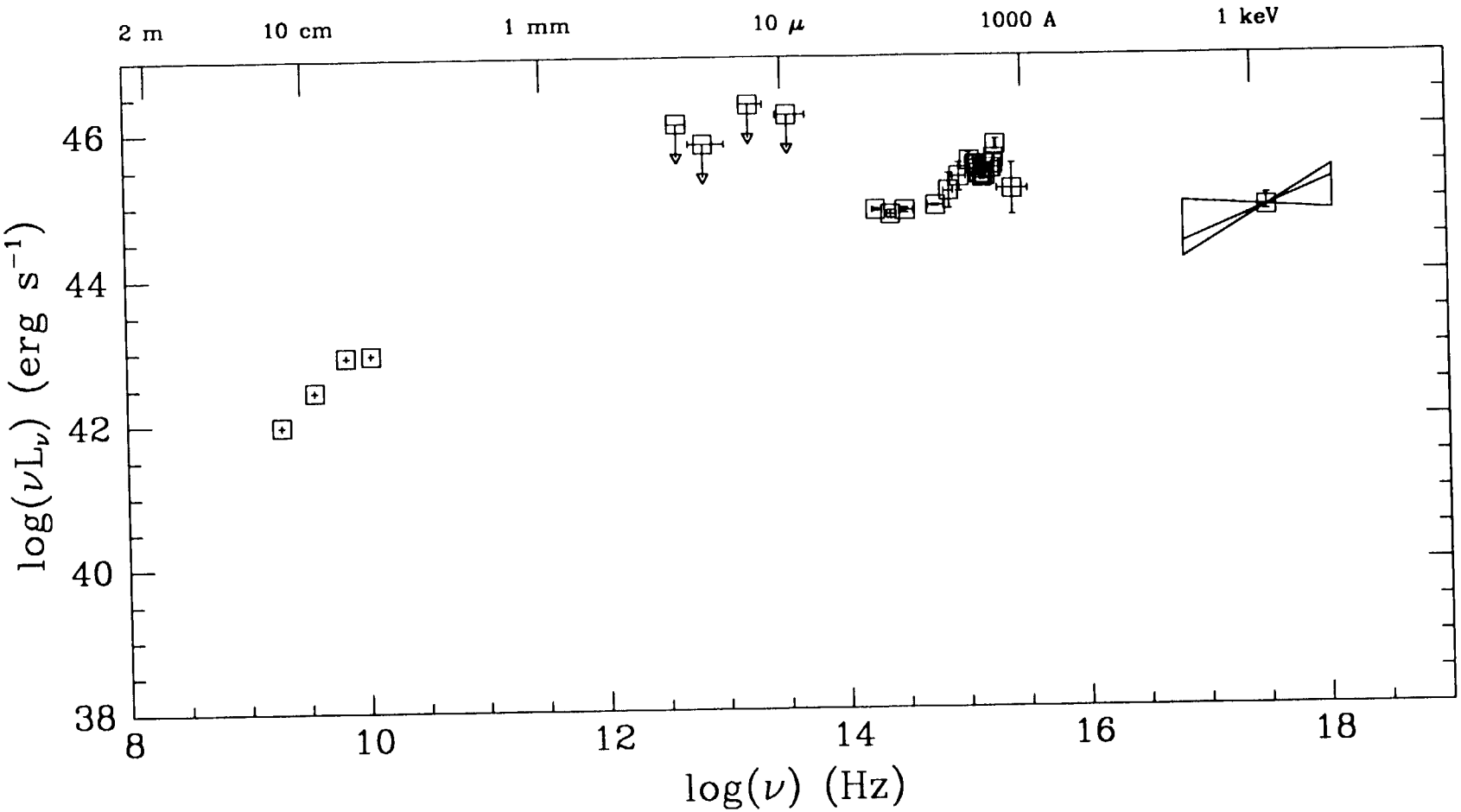
PKS1146−037
2 m
10 cm
1 mm
10 μ
1000 A
1 keV
46
44
42
40
38
8
10
12
14
16
18
log(νL_ν) (erg s^-1)
log(ν) (Hz)

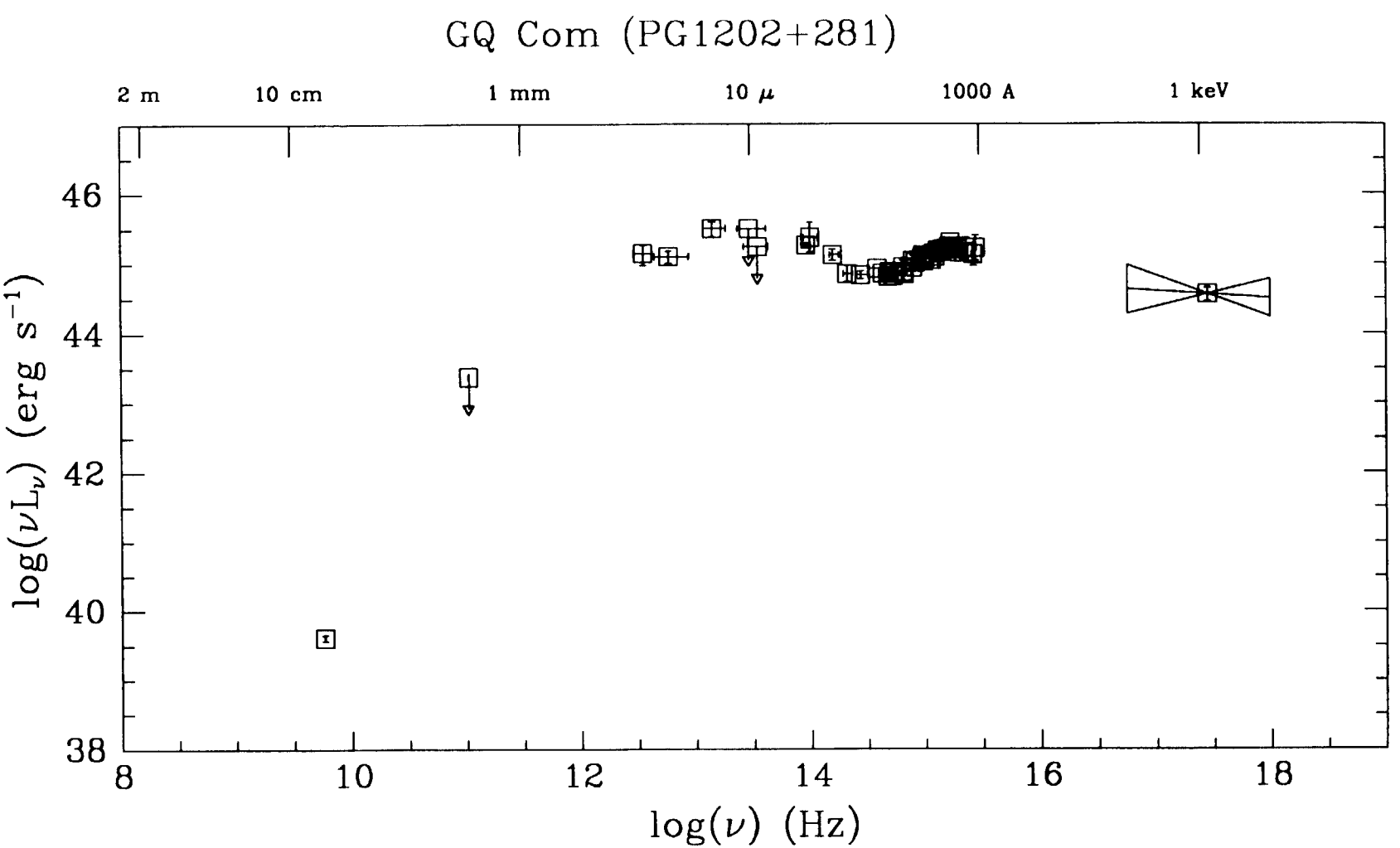
GQ Com (PG1202+281)
2 m
10 cm
1 mm
10 μ
1000 A
1 keV
log(νL_ν) (erg s^-1)
46
44
42
40
38
8
10
12
14
16
18
log(ν) (Hz)

PG1211+143

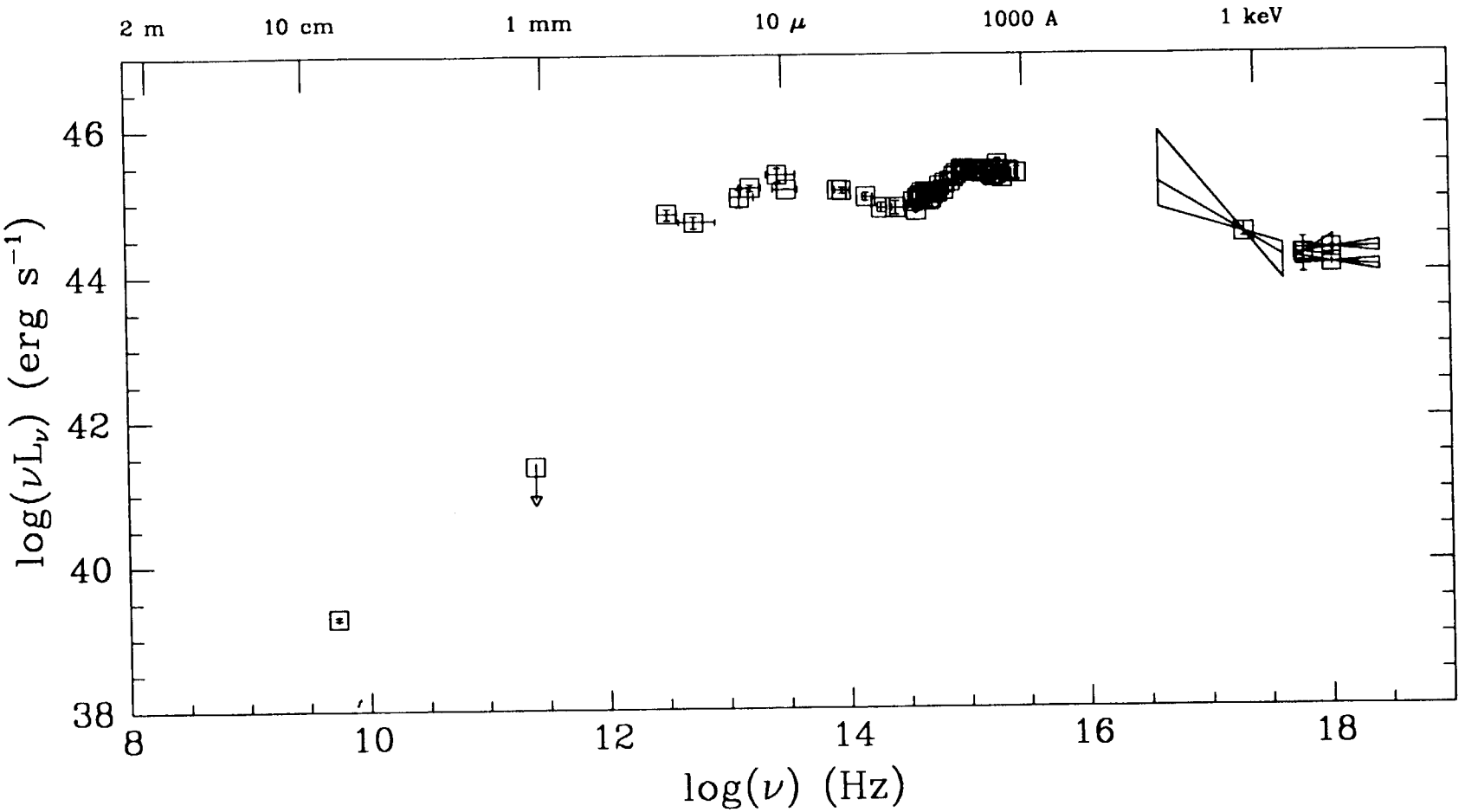
2 m
10 cm
1 mm
10 μ
1000 A
1 keV
46
44
42
40
38
8
10
12
14
16
18
log(νL_ν) (erg s^-1)
log(ν) (Hz)

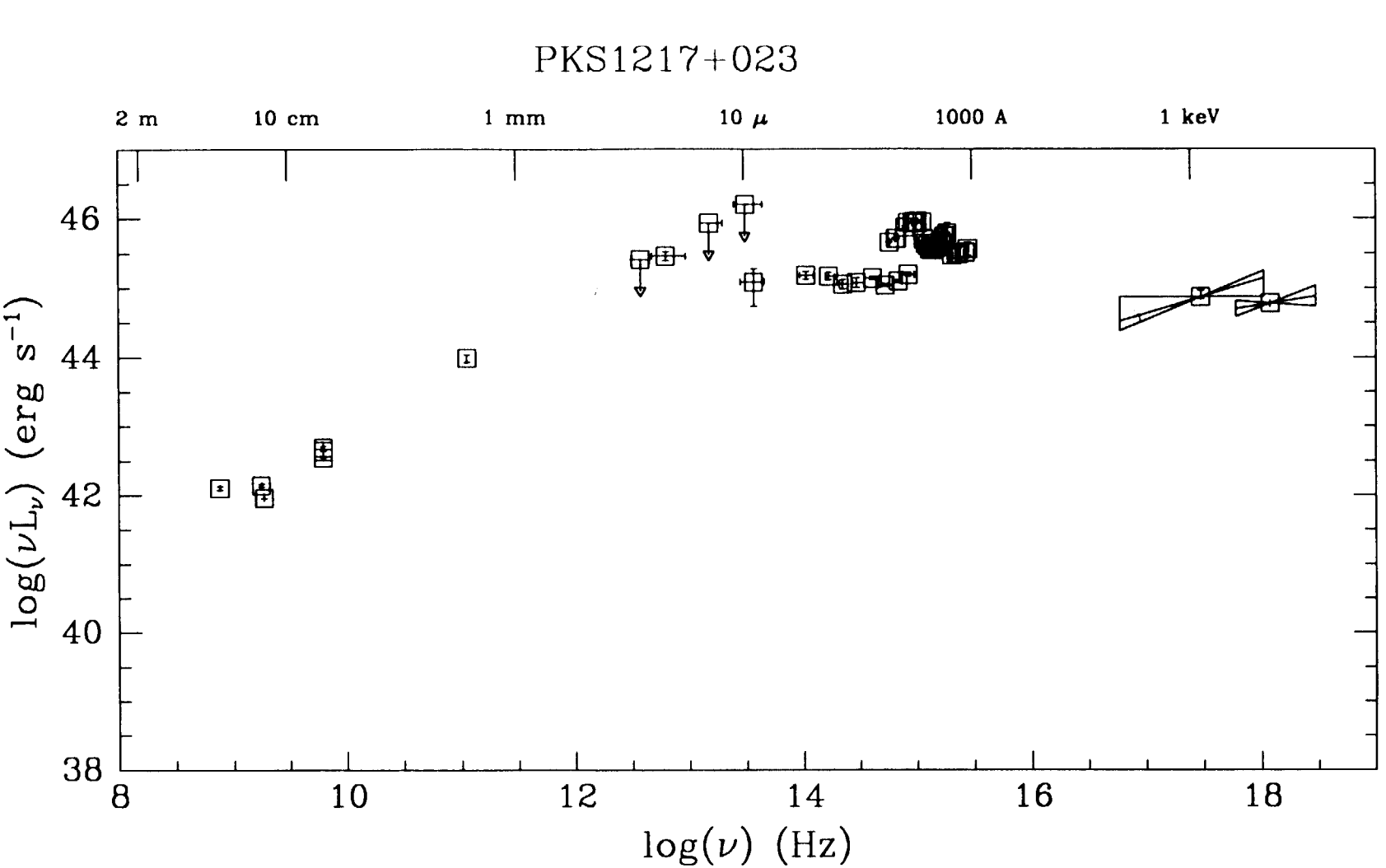
PKS1217+023
2 m
10 cm
1 mm
10 μ
1000 A
1 keV
46
44
42
40
38
8
10
12
14
16
18
log(νL_ν) (erg s^-1)
log(ν) (Hz)

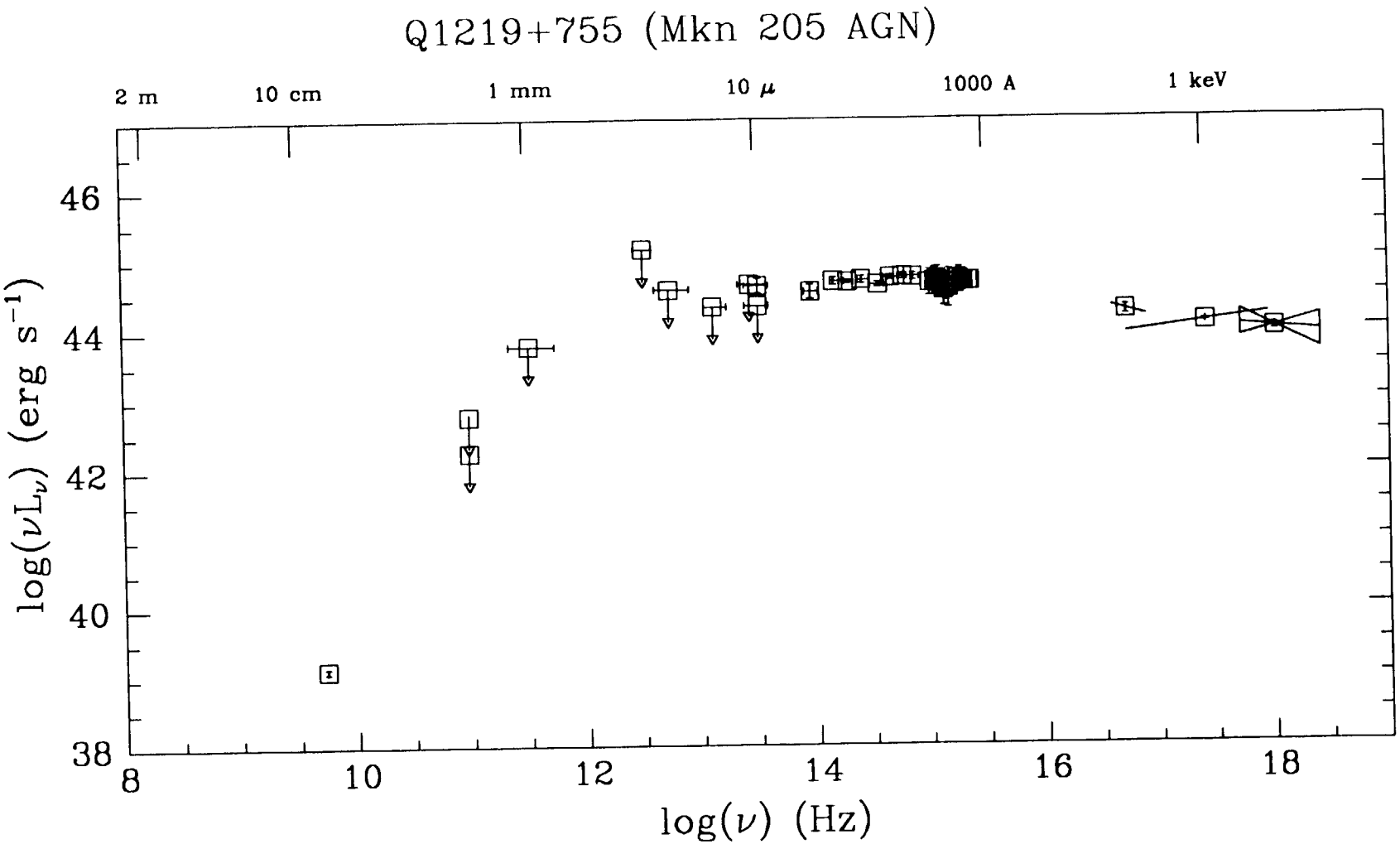
Q1219+755 (Mkn 205 AGN)
2 m
10 cm
1 mm
10 μ
1000 A
1 keV
log(νL_ν) (erg s^-1)
log(ν) (Hz)
38
40
42
44
46
8
10
12
14
16
18

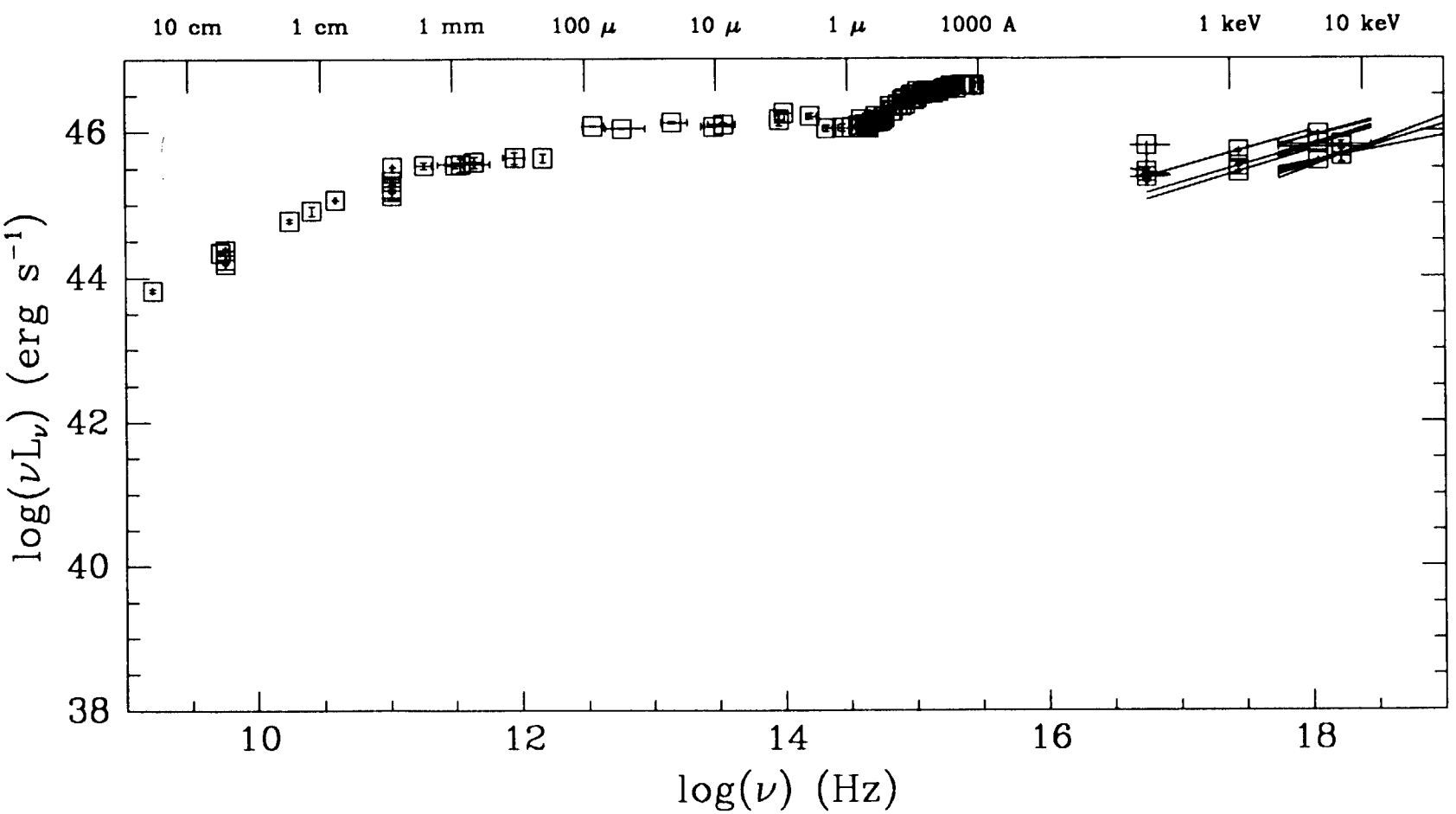
3C 273 (PKS1226+023)
10 cm
1 cm
1 mm
100 μ
10 μ
1 μ
1000 A
1 keV
10 keV
46
44
42
40
38
log(νL_ν) (erg s^-1)
10
12
14
16
18
log(ν) (Hz)

PG1307+085

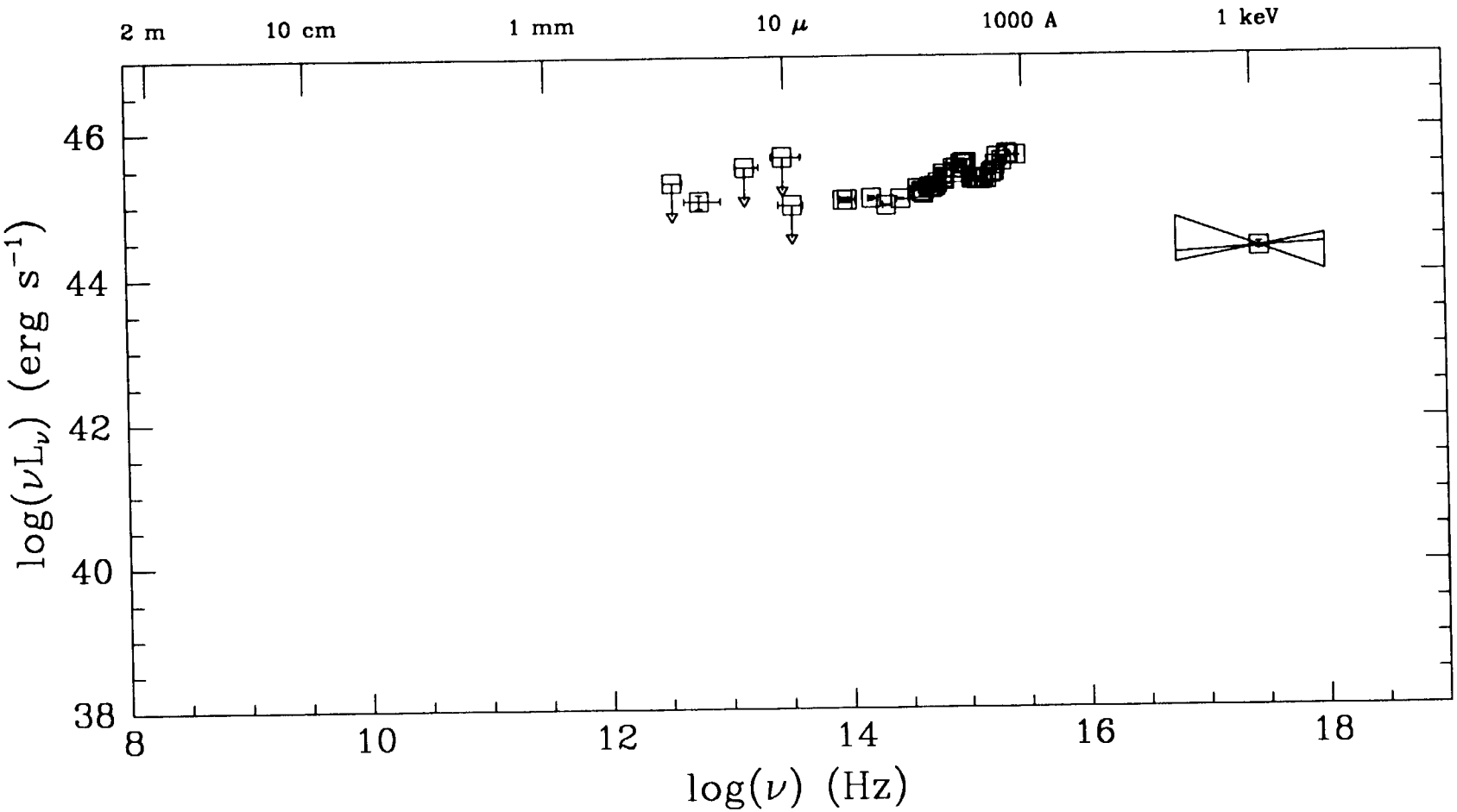
2 m
10 cm
1 mm
10 μ
1000 A
1 keV
46
44
42
40
38
8
10
12
14
16
18
log(νL_ν) (erg s^-1)
log(ν) (Hz)

PG1407+265

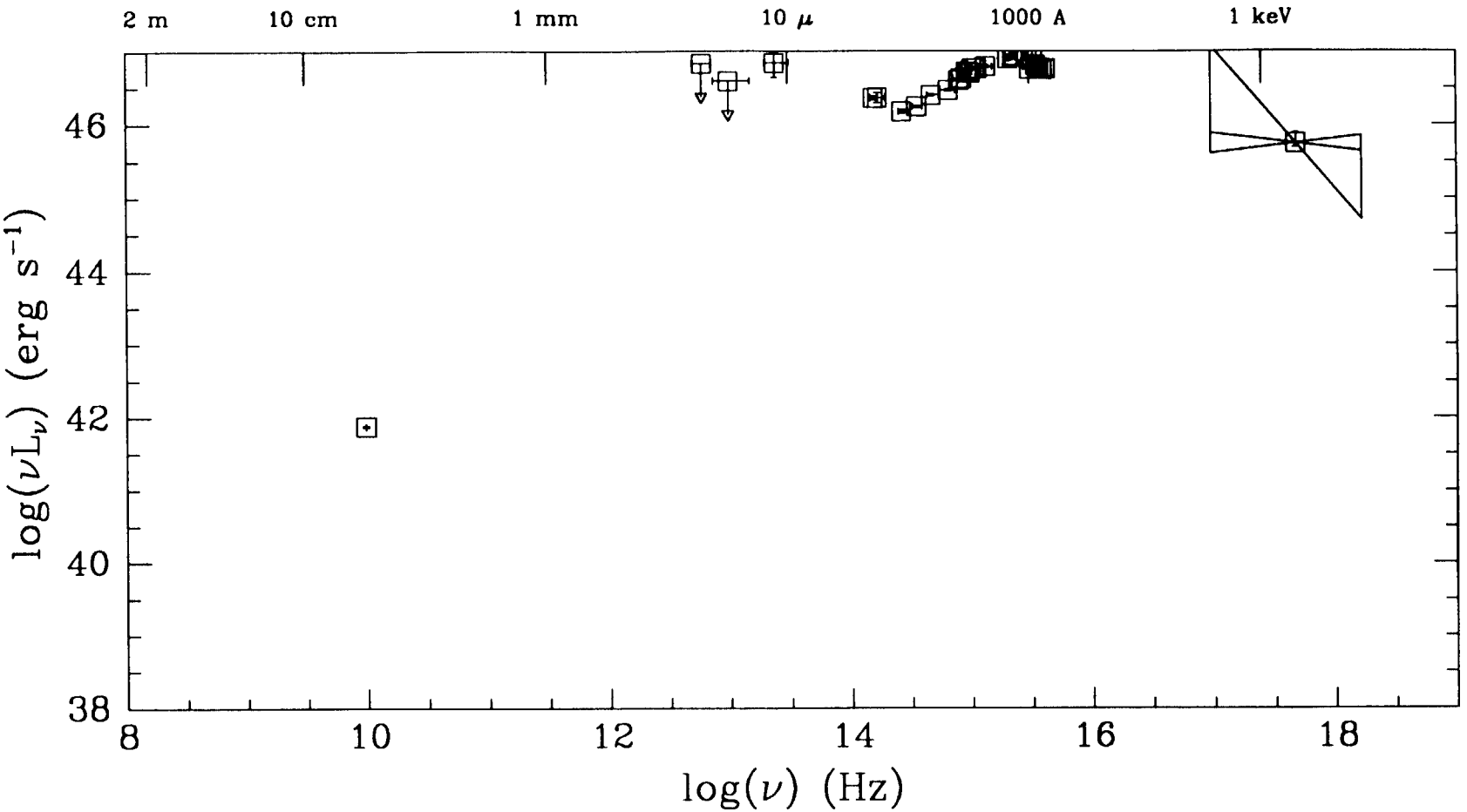
2 m
10 cm
1 mm
10 μ
1000 A
1 keV
46
44
42
40
38
8
10
12
14
16
18
log(νL_ν) (erg s^-1)
log(ν) (Hz)

PG1416−129

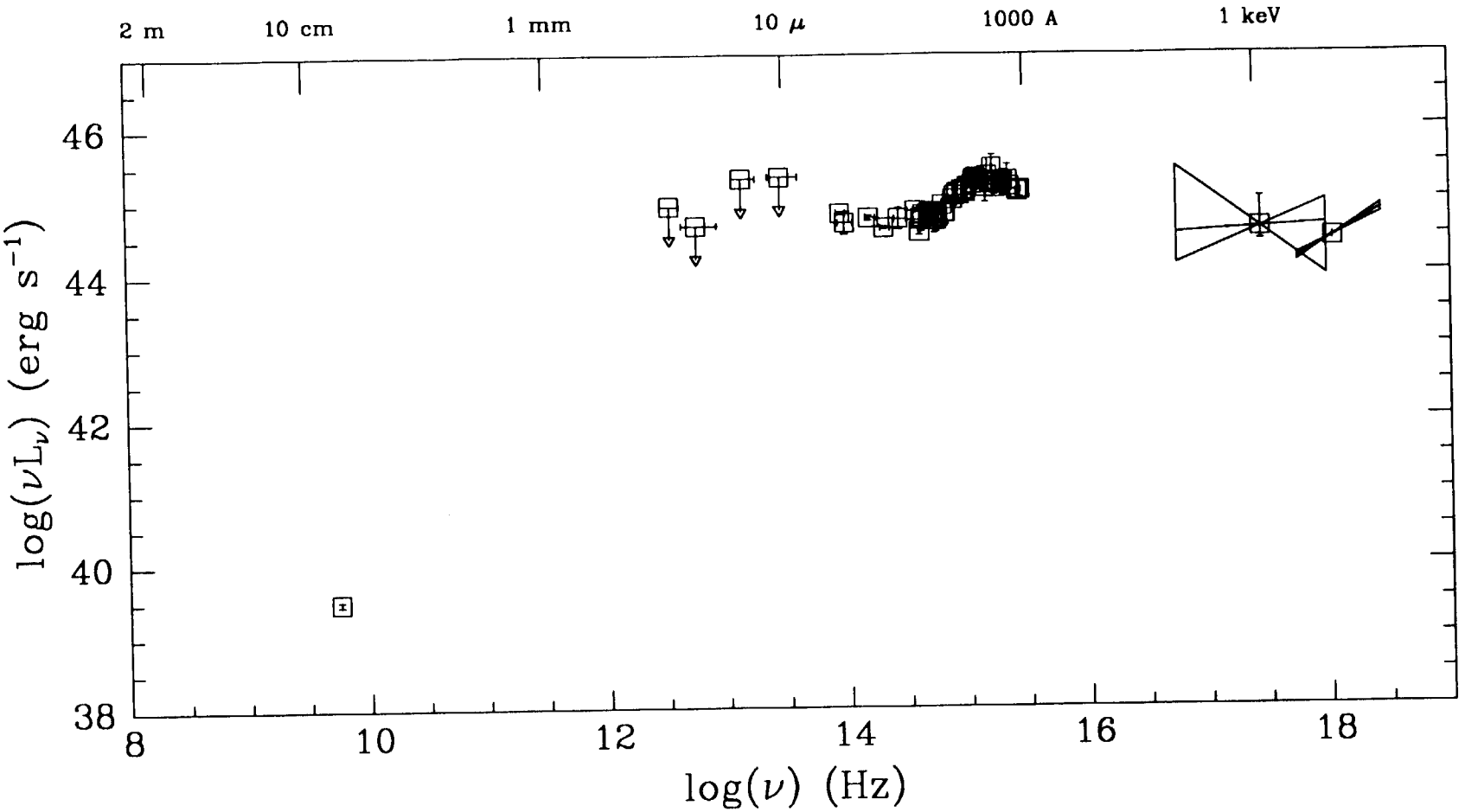
2 m
10 cm
1 mm
10 μ
1000 A
1 keV
46
44
42
40
38
8
10
12
14
16
18
log(νL_ν) (erg s^-1)
log(ν) (Hz)

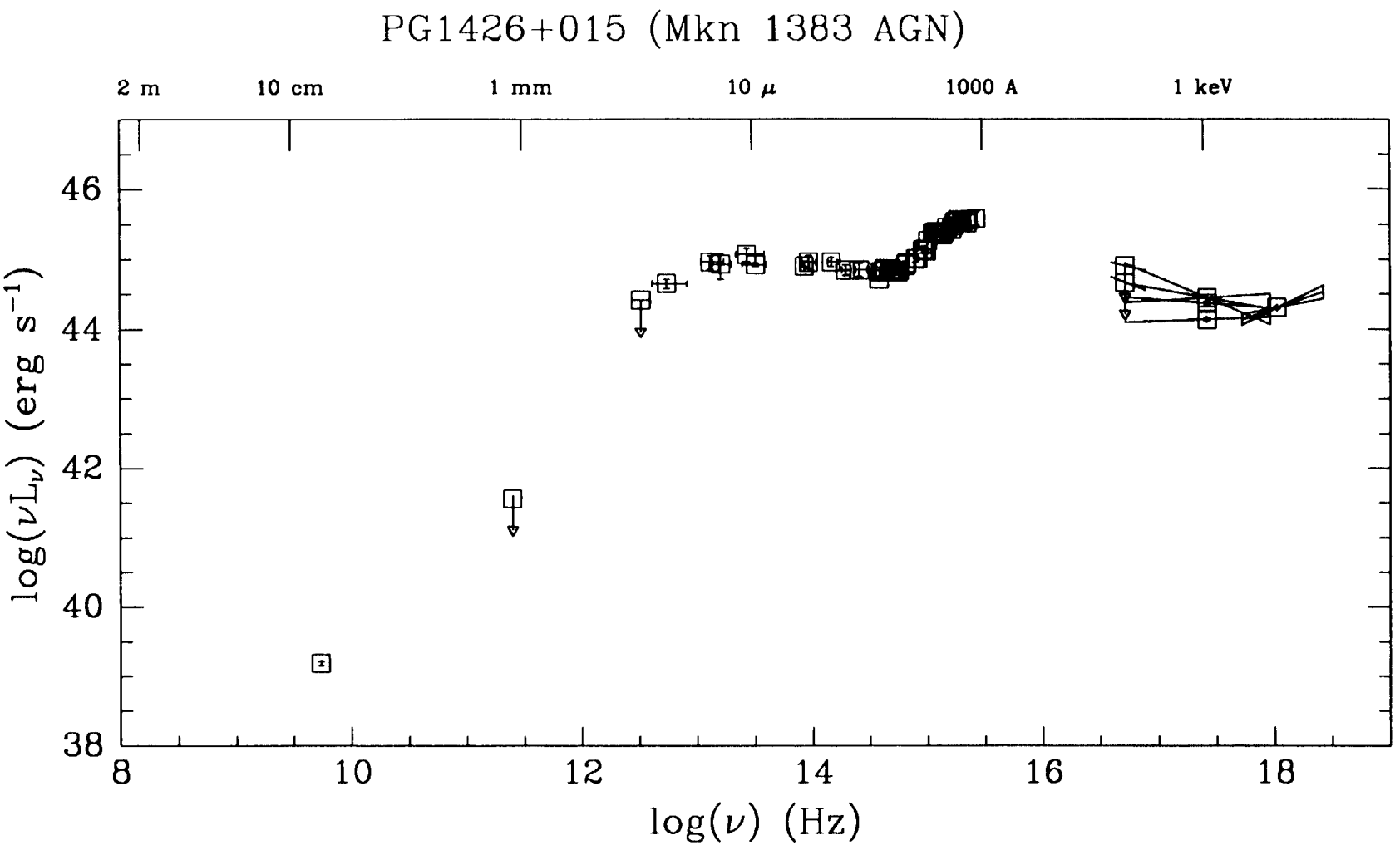
PG1426+015 (Mkn 1383 AGN)
2 m
10 cm
1 mm
10 μ
1000 A
1 keV
log(νL_ν) (erg s^-1)
46
44
42
40
38
8
10
12
14
16
18
log(ν) (Hz)

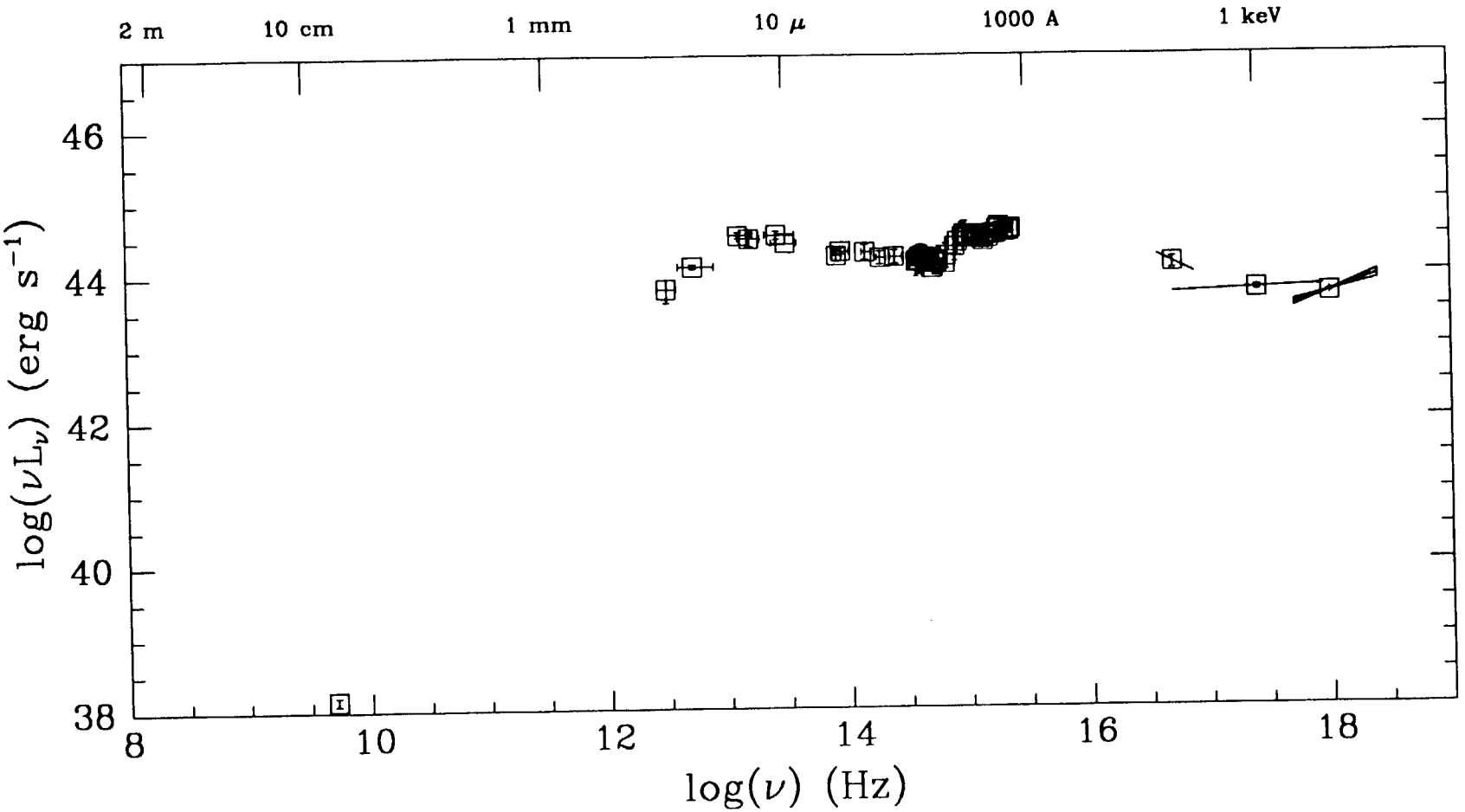
Q1501+106 (Mkn 841 AGN)
2 m
10 cm
1 mm
10 μ
1000 A
1 keV
46
44
42
40
38
log(νL_ν) (erg s^-1)
8
10
12
14
16
18
log(ν) (Hz)

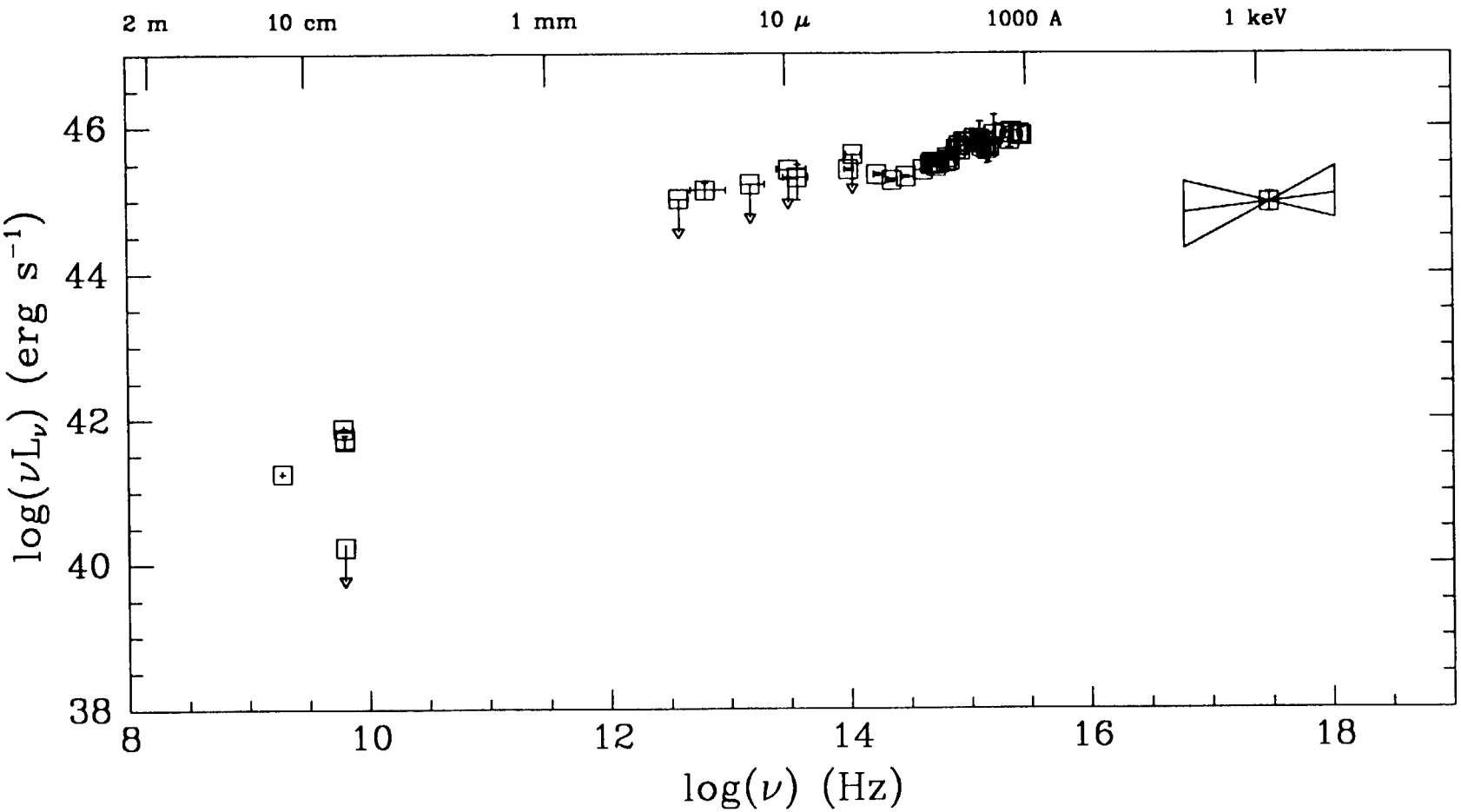
3C 323.1 (PKS1545+210,PG1545+210)
2 m
10 cm
1 mm
10 μ
1000 A
1 keV
log(νL_ν) (erg s^-1)
46
44
42
40
38
8
10
12
14
16
18
log(ν) (Hz)

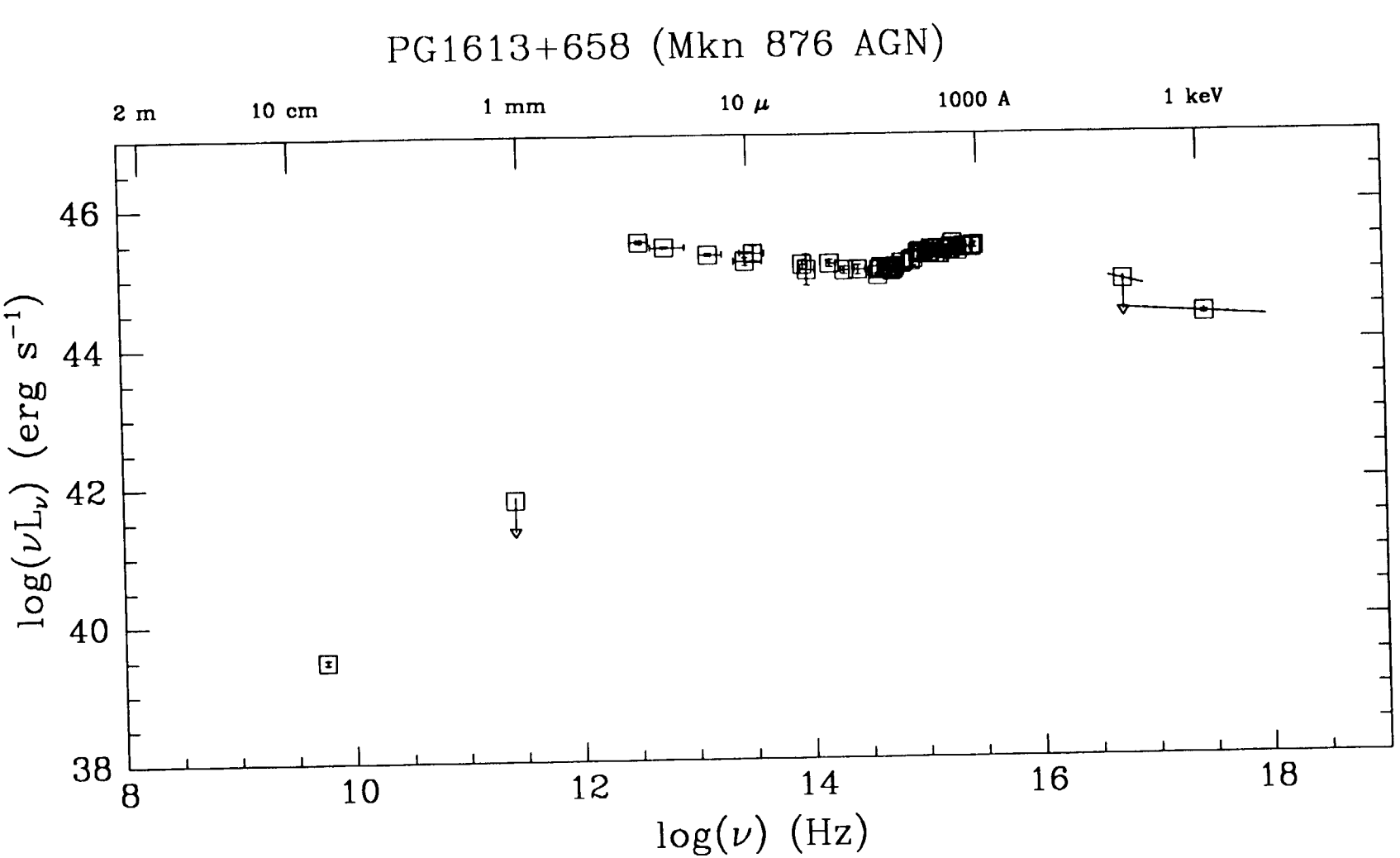
PG1613+658 (Mkn 876 AGN)
2 m
10 cm
1 mm
10 μ
1000 A
1 keV
46
44
42
40
38
log(νL_ν) (erg s^-1)
8
10
12
14
16
18
log(ν) (Hz)

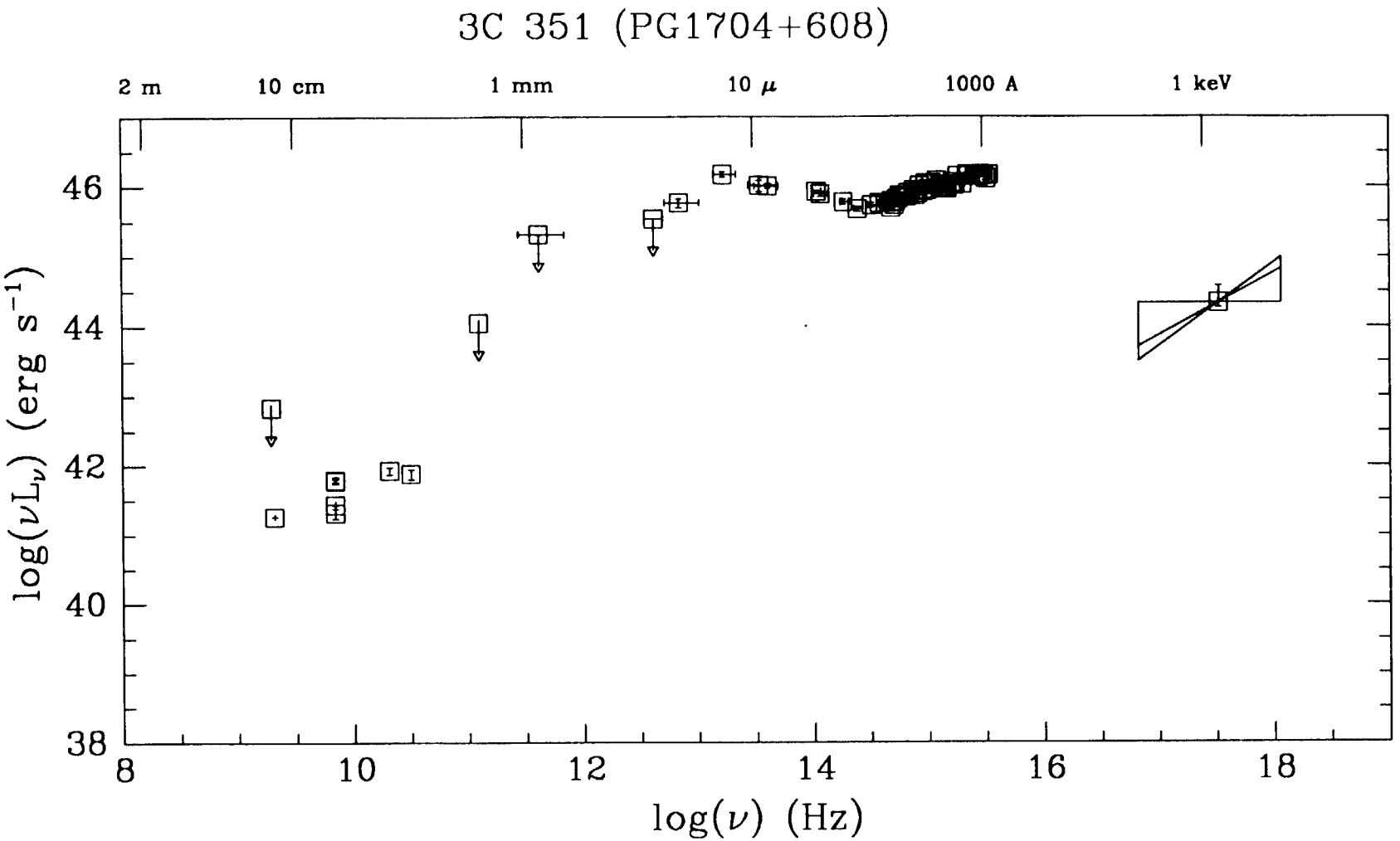
3C 351 (PG1704+608)
2 m
10 cm
1 mm
10 μ
1000 A
1 keV
log(νL_ν) (erg s^-1)
46
44
42
40
38
8
10
12
14
16
18
log(ν) (Hz)

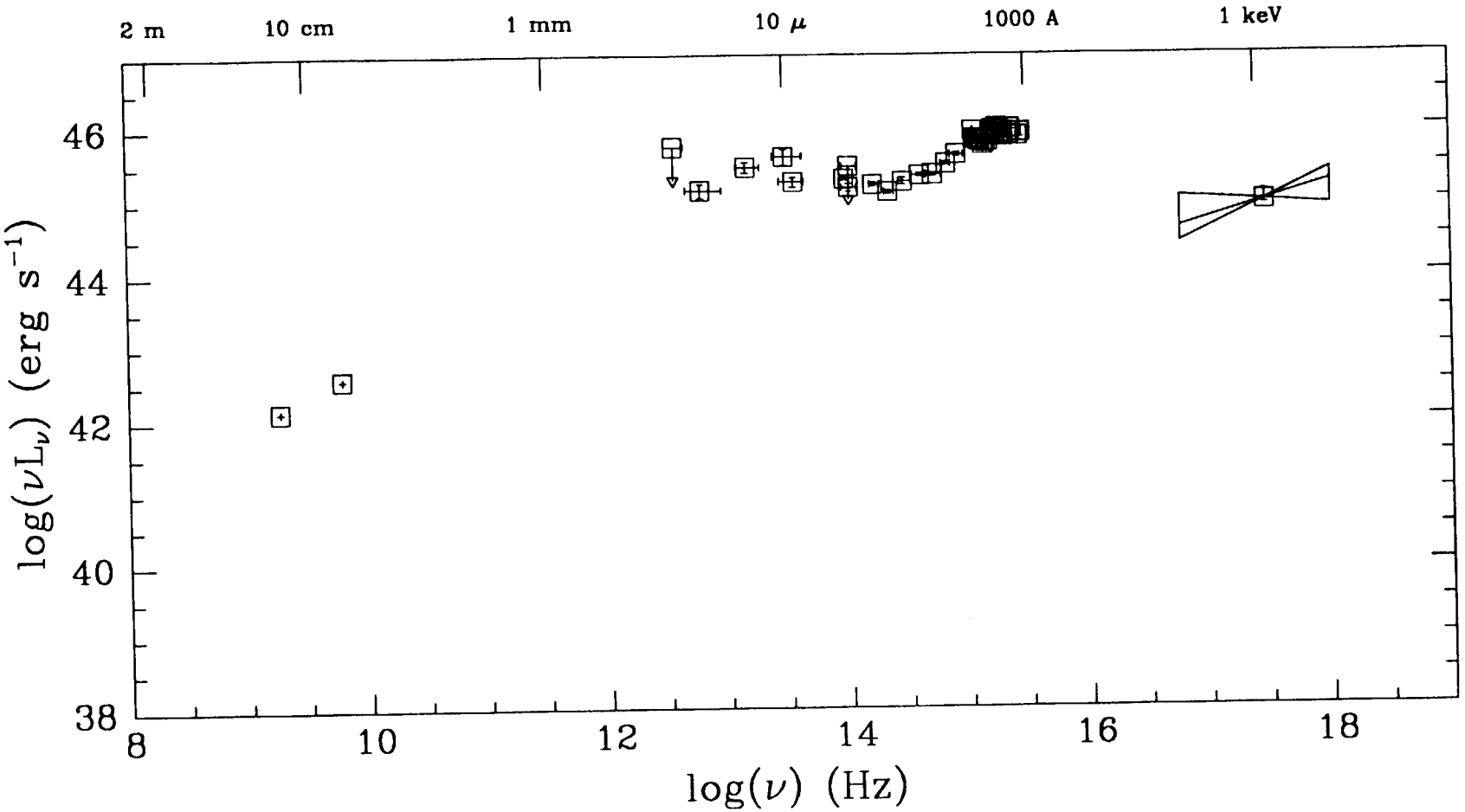
4C 34.47 (B2 1721+343)
2 m
10 cm
1 mm
10 μ
1000 A
1 keV
46
44
42
40
38
log(νL_ν) (erg s^-1)
8
10
12
14
16
18
log(ν) (Hz)

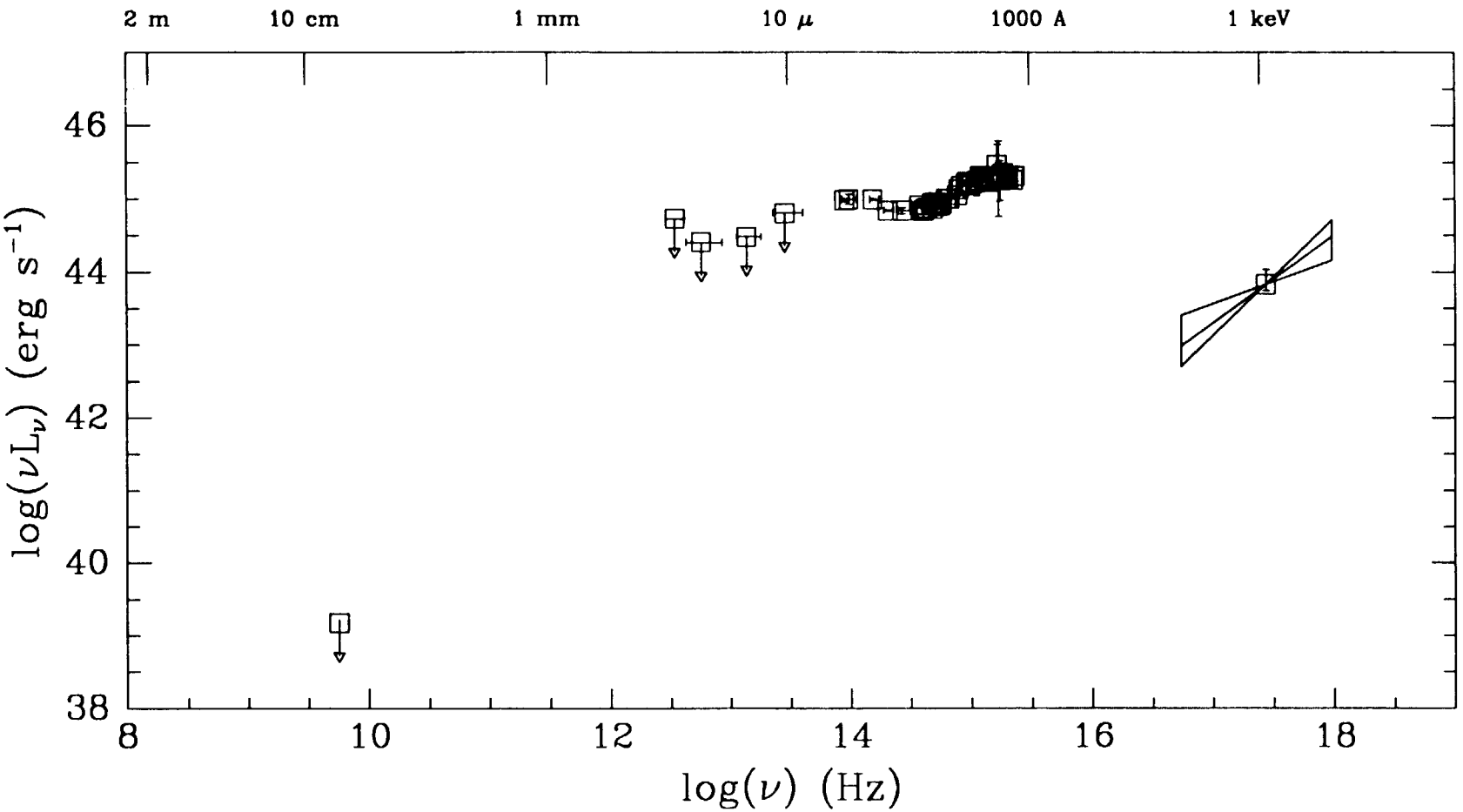
Q1803+676 in Kazaryan 102
2 m
10 cm
1 mm
10 μ
1000 A
1 keV
46
44
42
40
38
log(νL_ν) (erg s^-1)
8
10
12
14
16
18
log(ν) (Hz)

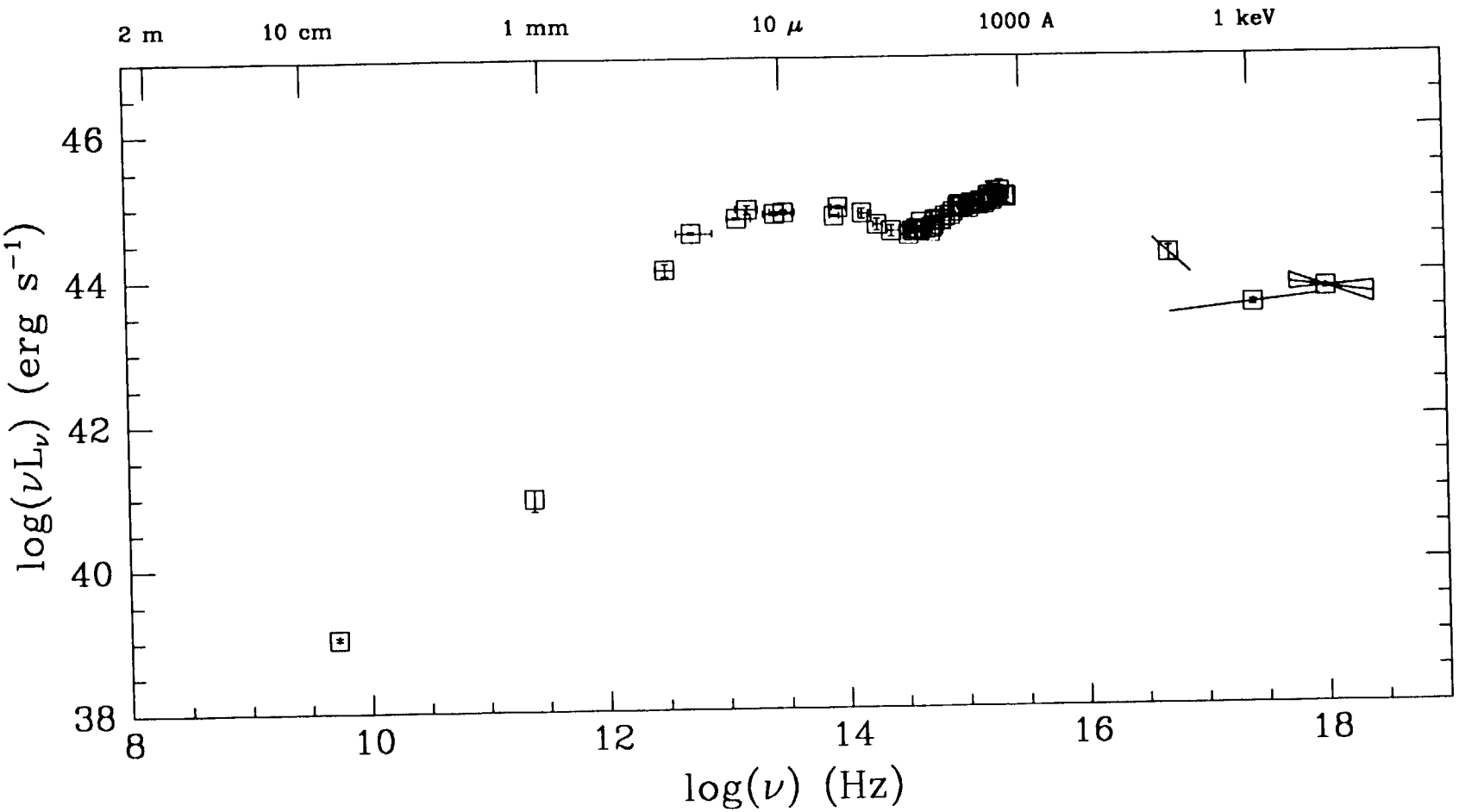
PG2130+099 in II Zw 136
2 m
10 cm
1 mm
10 μ
1000 A
1 keV
46
44
42
40
38
8
10
12
14
16
18
log(νL_ν) (erg s^-1)
log(ν) (Hz)

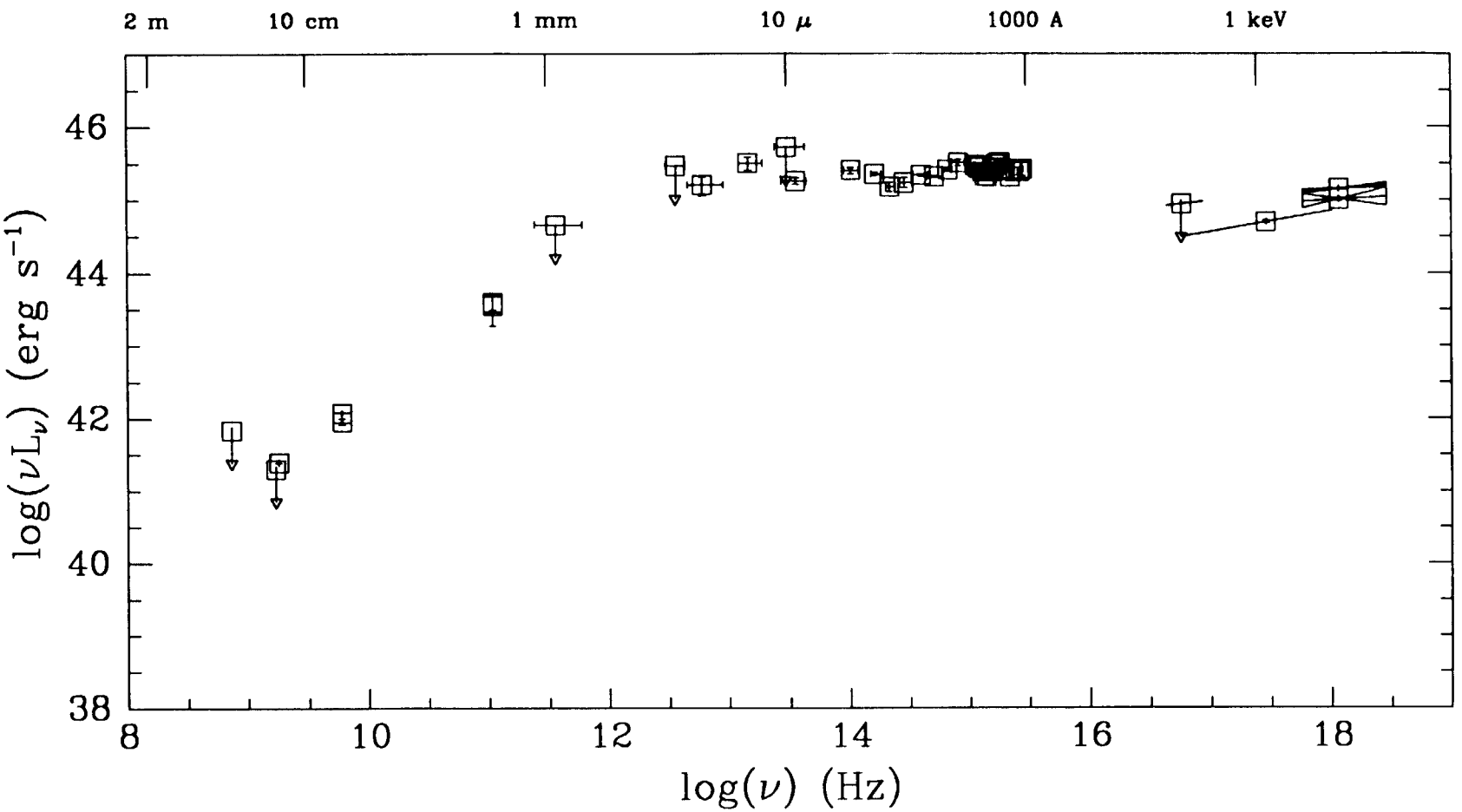
PHL 1657 (PKS2135−147)
2 m
10 cm
1 mm
10 μ
1000 A
1 keV
46
44
42
40
38
8
10
12
14
16
18
log(νL_ν) (erg s^-1)
log(ν) (Hz)

Fig. 5

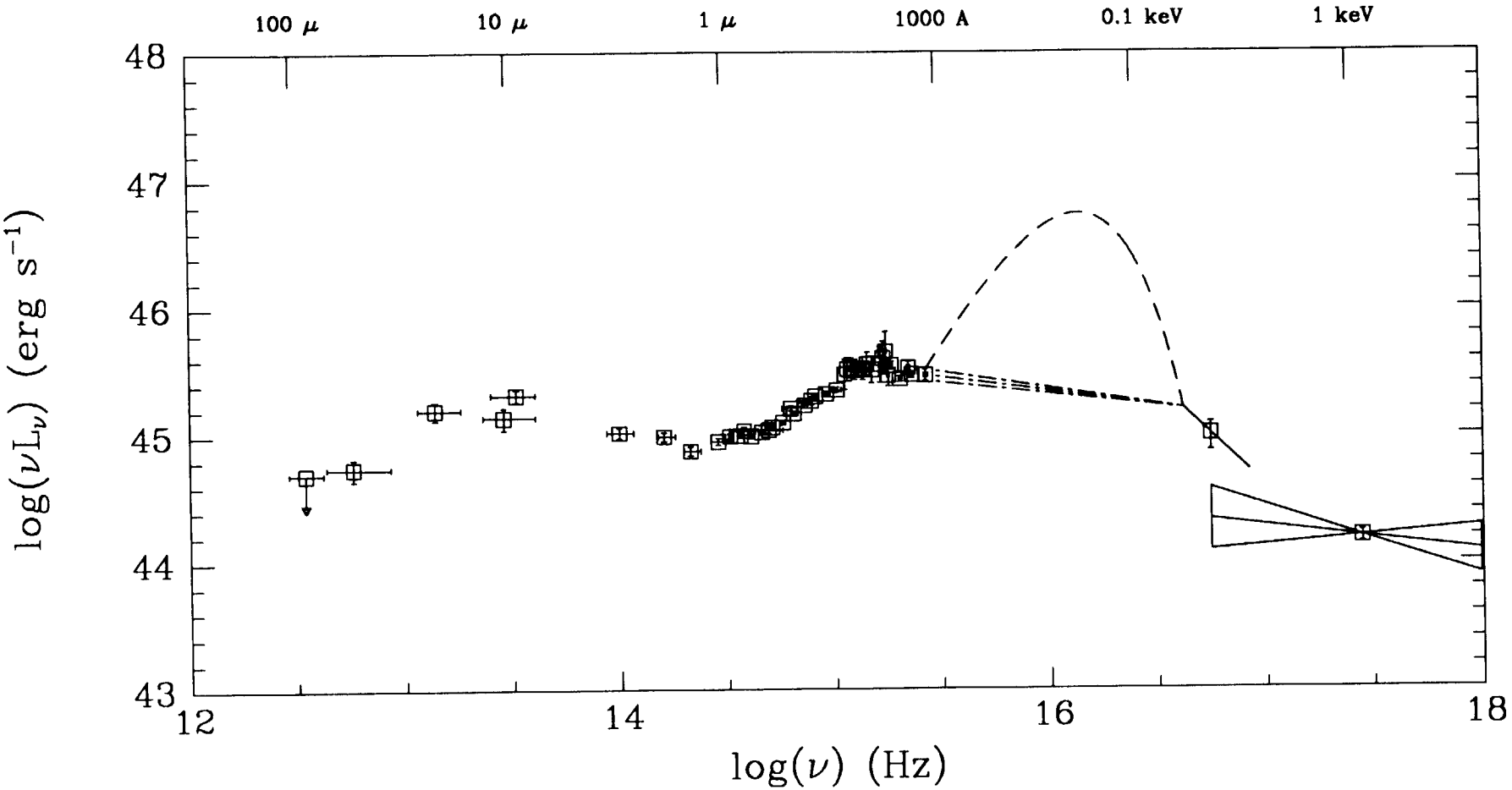
100 μ
10 μ
1 μ
1000 A
0.1 keV
1 keV
48
47
46
45
44
43
12
14
16
18
log(νL_ν) (erg s^-1)
log(ν) (Hz)

Fig. 6

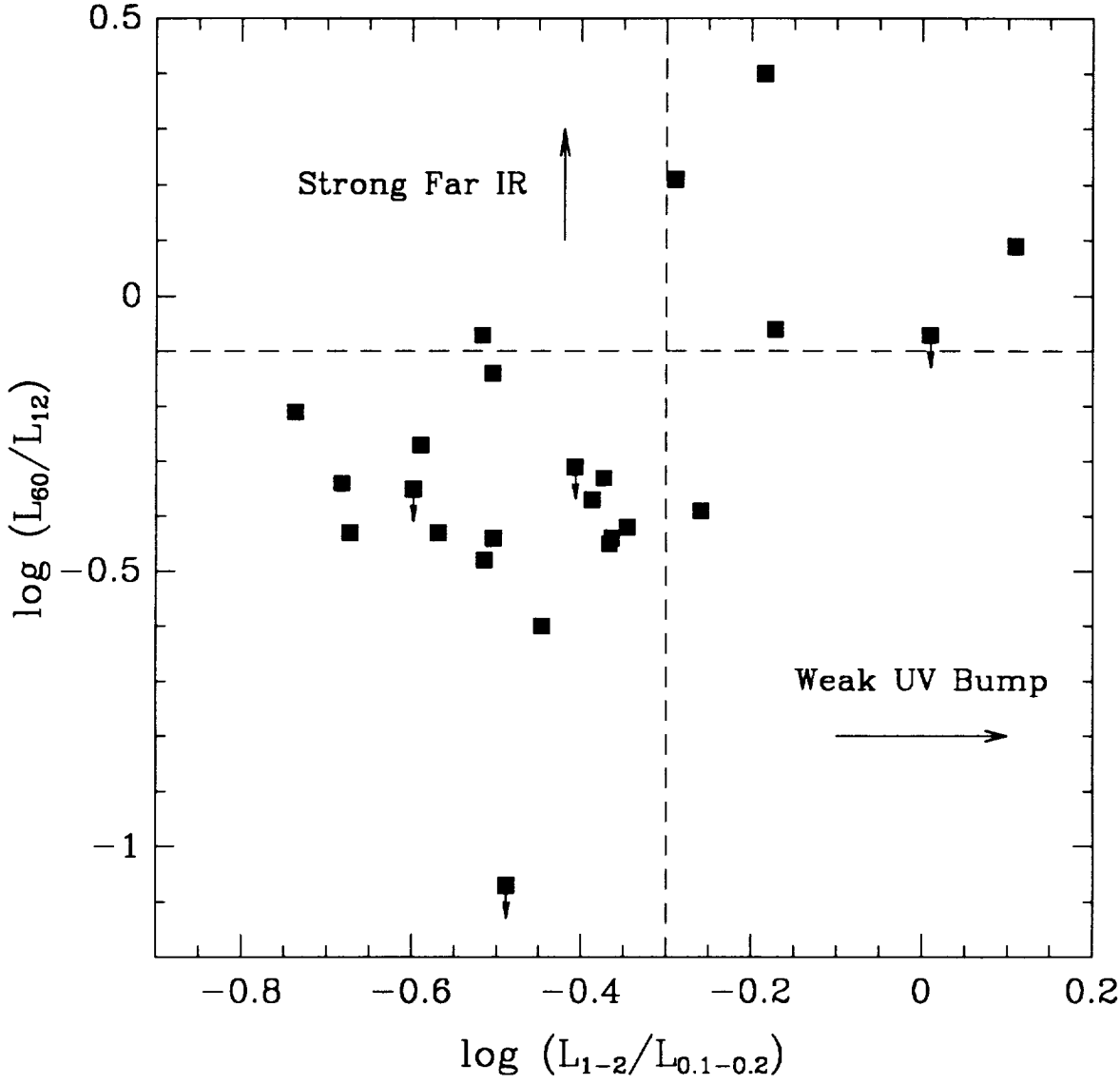
0.5
0
−0.5
−1
log (L60/L12)
Strong Far IR
Weak UV Bump
−0.8
−0.6
−0.4
−0.2
0
0.2
log (L1−2/L0.1−0.2)

Fig. 7

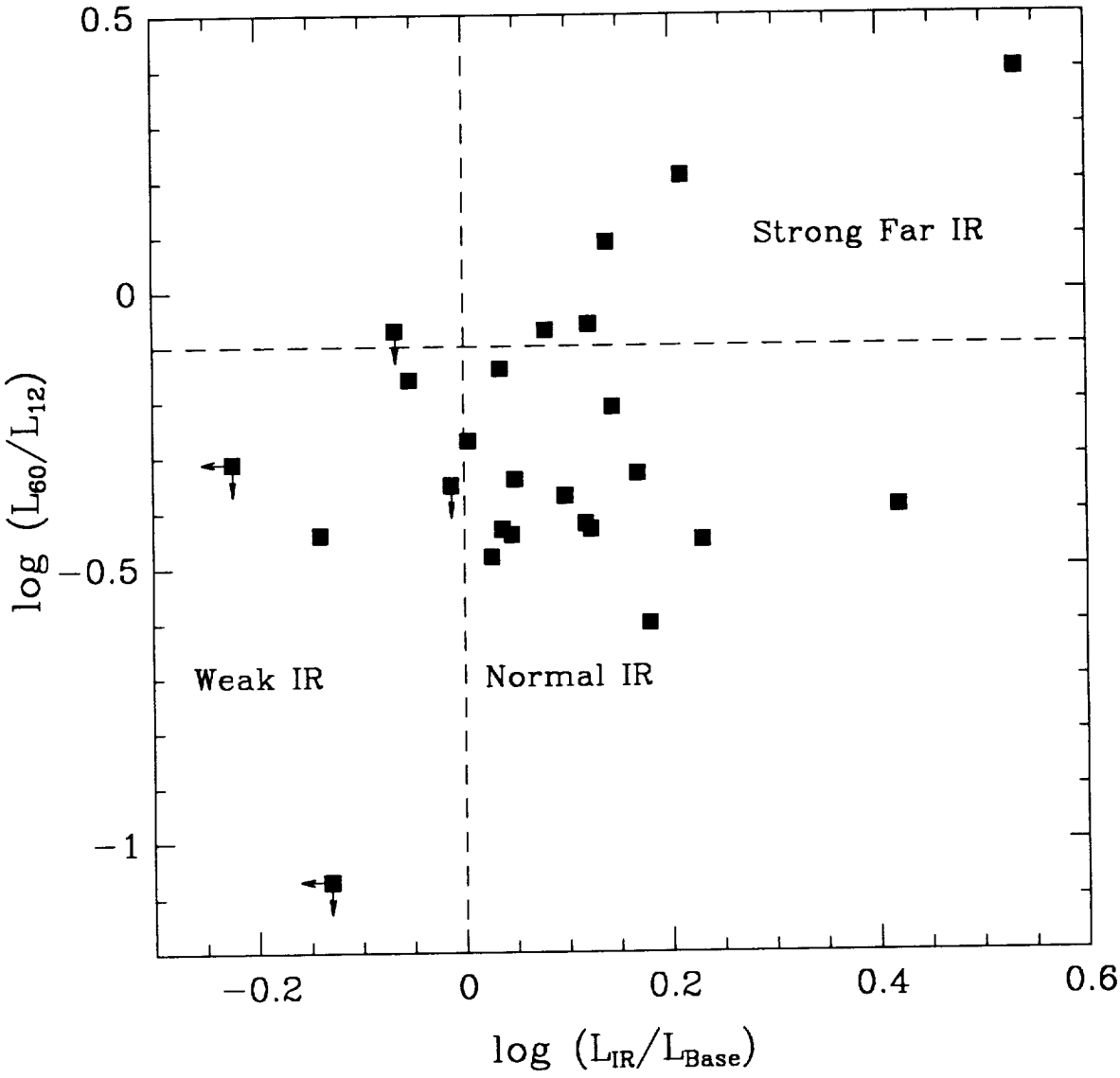
0.5
0
−0.5
−1
log (L60/L12)
Strong Far IR
Weak IR
Normal IR
−0.2
0
0.2
0.4
0.6
log (LIR/LBase)

Fig. 7

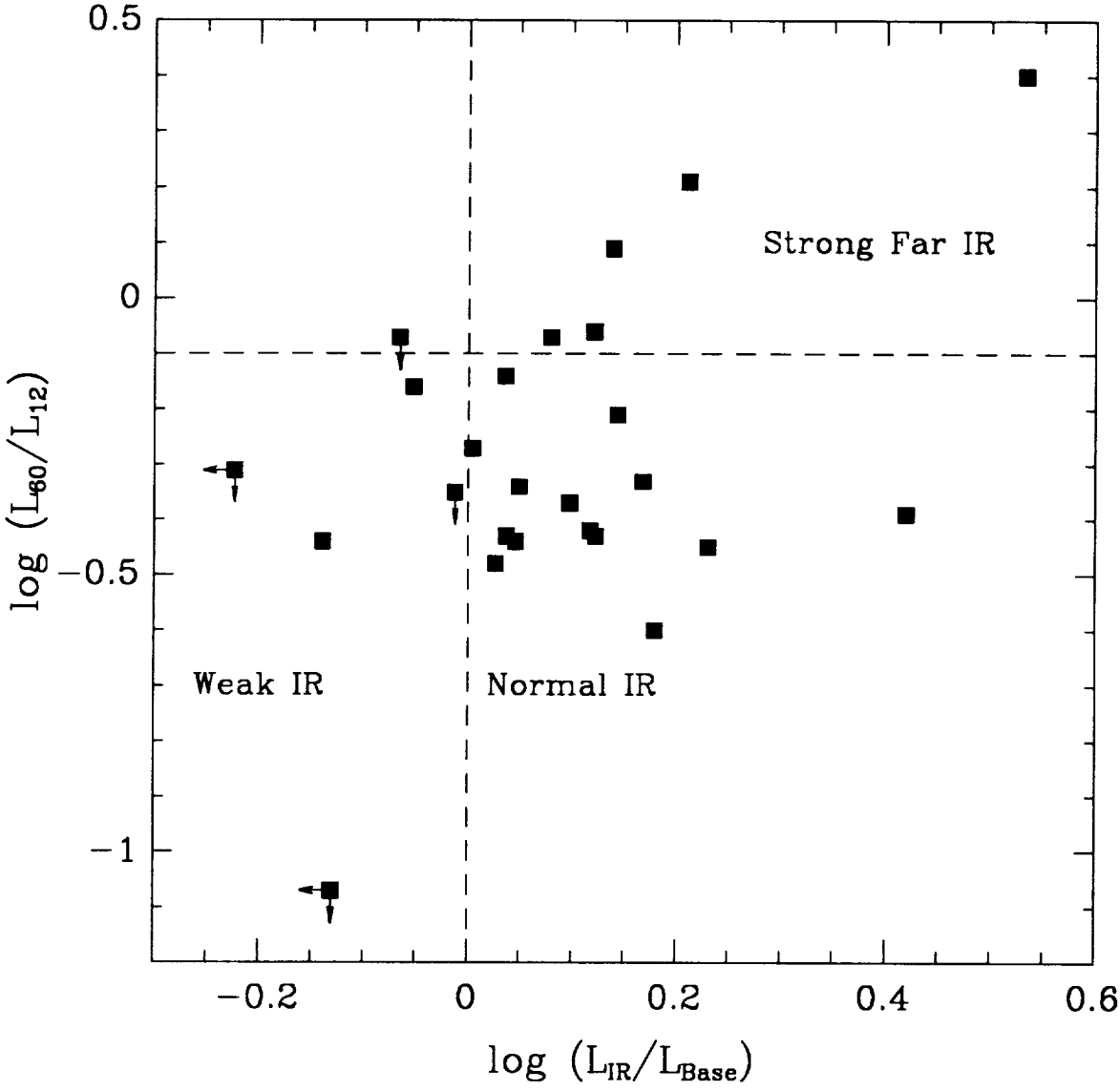
0.5
0
−0.5
−1
log (L60/L12)
Strong Far IR
Weak IR
Normal IR
−0.2
0
0.2
0.4
0.6
log (LIR/LBase)

Fig. 8(b)

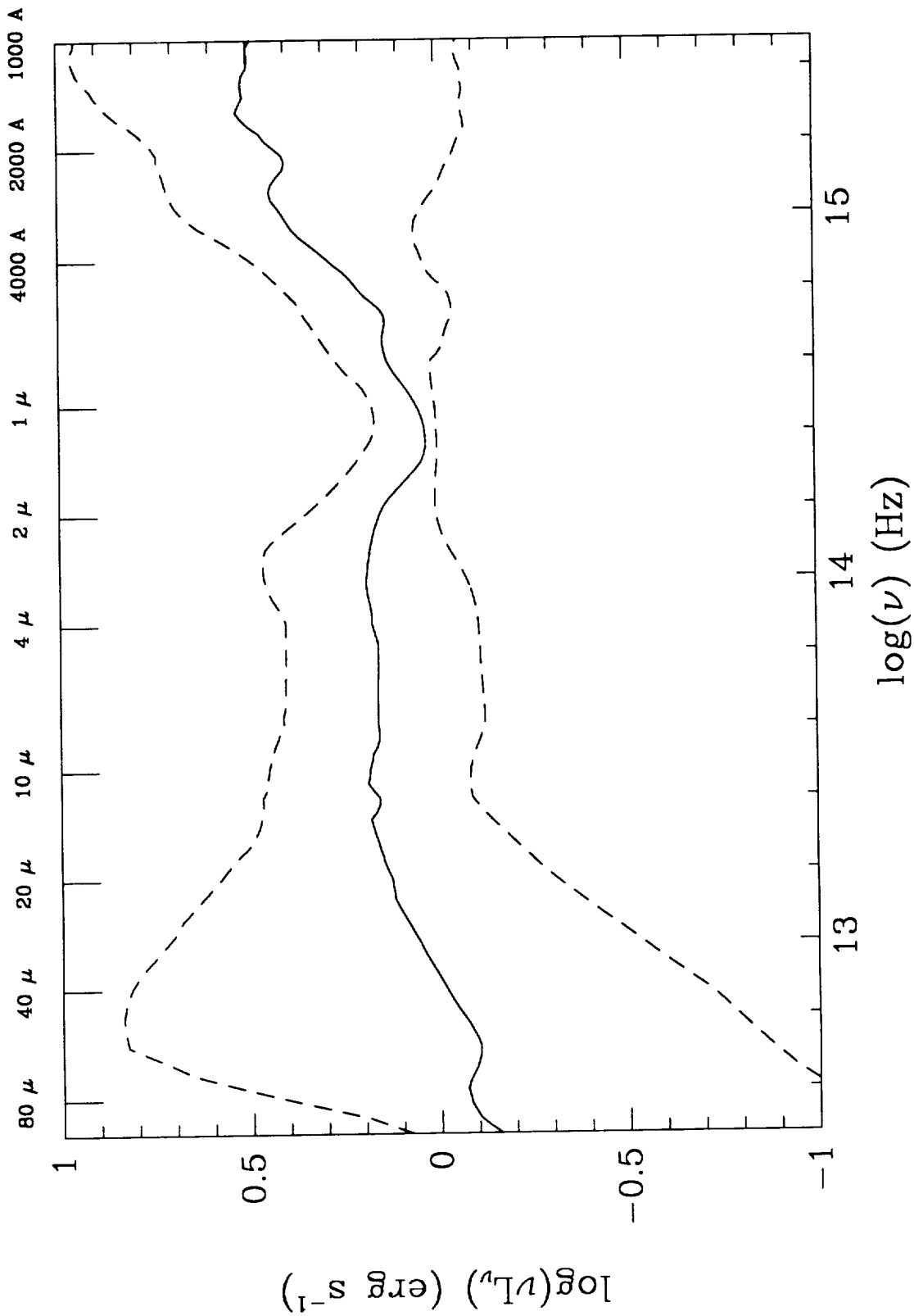

PRECEDING PAGE [redacted] NOT FILMED

SAME
Fig. 7

Fig. 9

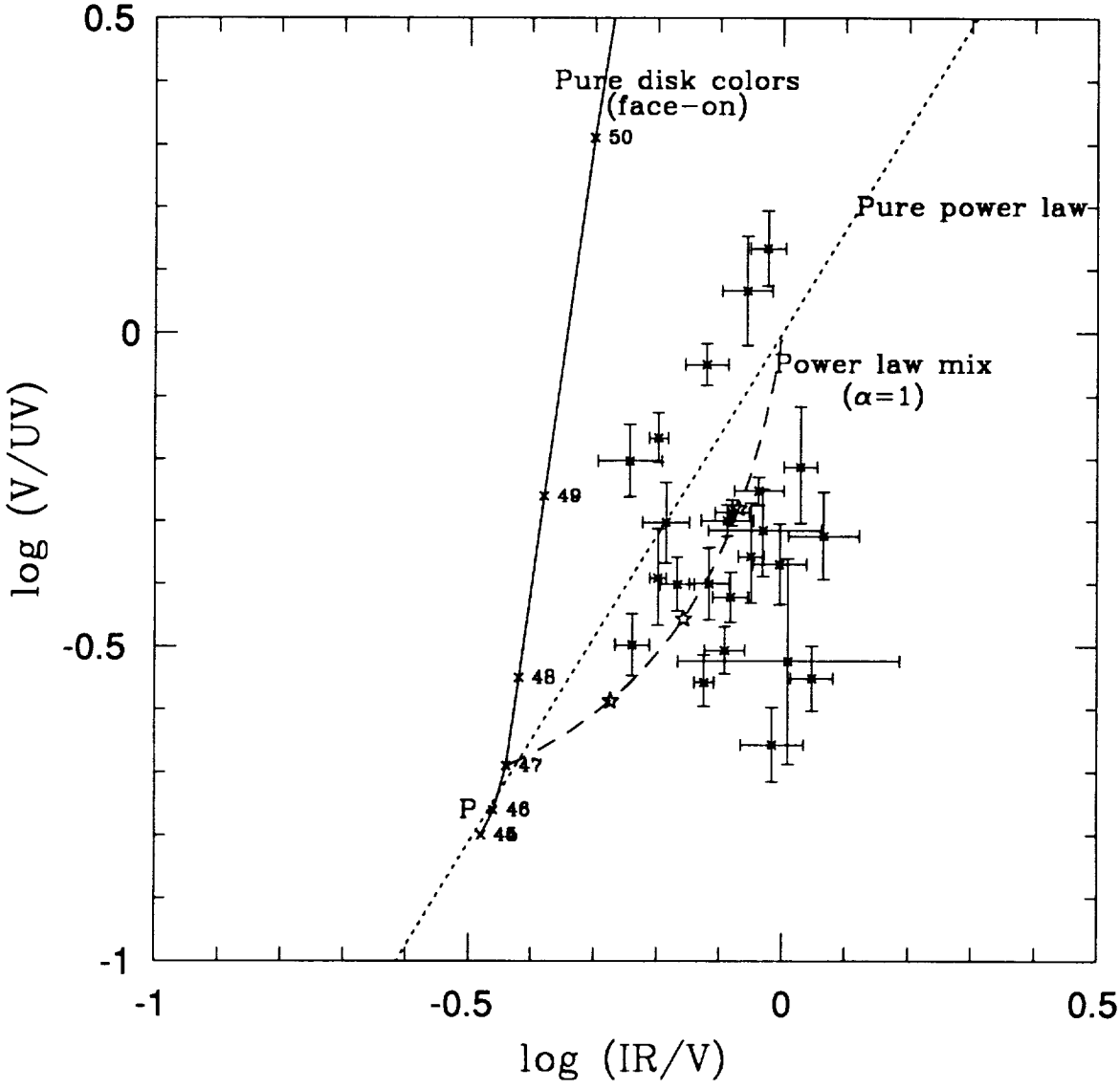
Pure disk colors
(face-on)
Pure power law
Power law mix
(α=1)
50
49
48
47
46
45
P
0.5
0
-0.5
-1
log (V/UV)
log (IR/V)

Appendix B

cfa248.harvard.edu:elvis

stdin

Thu Sep 5 10:01:17 1991

lpm / LaserWriter II NTX

lpm cfa248.harvard.edu:elvis Job: stdin Date: Thu Sep 5 10:01:17 1991

lpm cfa248.harvard.edu:elvis Job: stdin Date: Thu Sep 5 10:01:17 1991

lpm cfa248.harvard.edu:elvis Job: stdin Date: Thu Sep 5 10:01:17 1991

lpm cfa248.harvard.edu:elvis Job: stdin Date: Thu Sep 5 10:01:17 1991

Center for Astrophysics
Preprint Series No. 2779

Accurate Galactic N_H Values Toward Quasars and AGN

Martin Elvis [1], Felix J. Lockman [2] and Belinda J. Wilkes [1]

Astronomical Journal, in press (March 1989)

October 4, 1988

[1]Harvard-Smithsonian Center for Astrophysics

[2]NRAO[3], Charlottesville

[3]The National Radio Astronomy Observatory is operated by Associated Universities, Inc., under contract with the National Science Foundation.

Abstract

We have measured integrated Galactic 21cm column densities toward ~200 quasars and active galactic nuclei using the NRAO 140 ft telescope at Green Bank. These data have been corrected for stray radiation with the technique of Lockman *et al.*(1986). The 21 arcmin beam size of the 140 ft is small enough to minimize the uncertainty in N_H due to angular variations in the HI of the Galaxy at high latitudes. The resulting column densities are accurate to $\sim 1 \times 10^{19}$ atoms cm^{-2} or $\sim$ 5%, whichever error is larger. Opacity uncertainties dominate the errors above $N_H \sim 4 \times 10^{20}$ atoms cm^{-2}.

I. The Need for Accurate N_H Values

The extension of sensitive extragalactic x-ray measurements into the band below the 0.28 keV Carbon edge (the 'C-band', McCammon *et al.*1983) has made it important to determine accurately the opacity of the interstellar medium of our own Galaxy at these energies. Interpretation of spectral results from the ***Einstein*** IPC (Imaging Proportional Counter, Gorenstein *et al.*1981) and the EXOSAT CMA (Channel Multiplier Array, Taylor *et al.*1981) depend critically on a knowledge of the Galactic N_H. The inferred properties of the recently discovered 'ultra-soft excesses' in the x-ray spectra of quasars and active galactic nuclei (AGN) are particularly sensitive to this value (Wilkes and Elvis 1987, Branduardi *et al.* 1987, Giommi and Tagliaferri 1987).

Most x-ray astronomers currently use the unpublished but widely circulated 'Bell Labs' survey (Stark *et al.*, 1984) of 21cm HI emission to determine the column densities of interstellar material toward extragalactic sources. This survey is superior to previous all-sky HI surveys because the telescope's unblocked aperture makes it almost free of 'stray radiation' entering the signal from distant sidelobes. The small size of the antenna, however, has the disadvantage that its angular resolution is poor, typically $\sim 2^\circ \times 3^\circ$. Small scale structure in the HI distribution on the sky is thus liable to introduce errors in the column toward any particular line of sight. Elvis *et al.*(1986, Appendix B) estimated that the 90% errors introduced by small scale structure were $\pm 1 \times 10^{20}$ atoms cm^{-2} . For a typical high Galactic latitude position with $N_H \sim 3 \times 10^{20}$ atoms cm^{-2} this uncertainty of 1×10^{20} atoms cm^{-2} in N_H leads to an uncertainty in the intrinsic x-ray flux density of a source at 0.2 keV of a factor 2.4. More accurate column densities than the Bell Labs survey provides are thus clearly needed.

A method for achieving high angular resolution HI measurements free from stray radiation has recently been developed for the Green Bank 140 ft telescope (Lockman, Jahoda and McCammon 1986, Appendix A). We have used this technique to produce accurate HI column densities toward a large number of quasars and AGN that are bright and well-observed x-ray sources. We present these column densities here. We also analyze the results to provide an assessment of the remaining errors and to determine more carefully the uncertainties involved in using the Bell survey values when no more accurate measurement is available.

II. Observations

The sample of objects includes a wide selection of x-ray observed AGN and quasars. It includes, so far as they were observable from Green Bank (*i.e.*declination $\gtrsim -40^\circ$): all the quasars with ***Einstein*** IPC spectra in Wilkes and Elvis (1987); all the BL Lac objects with ***Einstein*** IPC spectra in Madejski (1985) ; a substantial

number of other ***Einstein*** observed quasars for which IPC x-ray 'colors' are available (Brunner ***et al.***, in preparation); all of the members of the complete hard (2–10 keV) x-ray selected 'Piccinotti' sample of AGN (Piccinotti ***et al.***1982); and a selection of the AGN detected by the Medium Energy instrument on EXOSAT (Sternberg ***et al.***1986). In addition we mapped the accessible ***Einstein*** Deep Survey regions (Giacconi ***et al.***1979), the 'Braccesi' survey region covered by Marshall ***et al.***(1984), and SA57 and the North Ecliptic Pole regions that will be observed in depth by ROSAT. The maps for these extended regions will be presented separately.

The observing technique was as detailed by Lockman ***et al.***(1986, Appendix A). Briefly, the 140ft telescope is used to map out the beam covered by the Bell Labs observation that was centered closest to the position of each AGN. The 140ft data are then convolved with the beam profile of the Bell antenna to give the 21cm spectrum that the 140ft would observe if it had the same beam shape as the Bell antenna, ***i.e.***including the stray radiation seen by the 140ft at this position. This spectrum is dependent on the altitude and azimuth of the telescope as well as on the celestial position. The difference between the Bell spectrum and the convolved 140ft spectrum is then the stray radiation seen by the 140ft at that position. This is then be subtracted from the 140ft spectrum taken at the precise position of the active galactic nucleus.

In practice two independent spectra were taken at each AGN position. Total integration times were 2 – 6 minutes. Because of the low system temperature (18 K at zenith), these integration times are sufficient to make the uncertainty in N_H due to noise negligible. An observation of particularly low signal-to-noise is shown in figure 1. Each AGN position was observed both immediately before and after the Bell beam was mapped and the results averaged, to minimize time dependent effects. Remaining errors in the observation are primarily due to uncertainties in the baseline (Lockman ***et al.***1986) and amount to $\sim 2 \times 10^{18}$ atoms cm^{-2}. The amount of the stray radiation removed was equivalent to HI columns of a few$\times 10^{19}$ atoms cm^{-2}, or $\sim$ 15% for typical values of N_H . Figure 2 shows an example of a particularly large stray radiation spectrum compared with the observed 140ft spectrum. There is uncertainty in the stray radiation correction at a level of a few times 10^{18} atoms cm^{-2} and the form of the uncertainty is not well determined.

To derive an integral N_H measurement from the observed spectrum requires a correction for the opacity, τ, of the gas. Although at high galactic latitudes this correction is generally small it is sometimes dominant. The correction is intrinsically uncertain. The observed spectrum is made up of contributions from different clouds in the interstellar medium which generally have a wide range of temperatures and optical depths and many possible geometric arrangements (see discussions in Dickey and Benson 1982 and Lockman and Dickey 1989). The distribution of these clouds cannot be derived from a 21cm spectrum. The size of the uncertainty can be

estimated using the peak observed brightness temperature in the spectrum, T_{peak}, since

$$T_{peak} = T_{spin}(1 - e^{-\tau})$$

if we assume that the emission arises from gas of a fixed kinetic temperature (called the spin temperature, T_{spin}, for historical reasons). If T_{peak} is small then τ is always small for reasonable values of T_{spin}, but for larger T_{peak} τ is more likely to be significant and one must make an opacity correction. Figure 3 shows the uncertainty in N_H due to opacity corrections, $\Delta N_H(T_{spin})$, plotted against T_{peak}. $\Delta N_H(T_{spin})$ was calculated using T_{spin} values of 10^4 K and 125 K as extreme cases. A best fit to figure 3 gives

$$\Delta N_H(T_{spin}) = (0.073 \pm 0.005)T_{peak} - (0.063 \pm 0.007) \quad (10^{20} \text{ atoms cm}^{-2})$$

This expression, or figure 3, can be used to estimate the opacity correction uncertainty in our N_H measurements.

The best estimate column densities are given in Table 1. Values of N_H are given for an assumed effective spin temperature of 250 K which is a good approximation to that of the interstellar HI (Dickey 1988, private communication. see also Dickey 1988). When the HI signal is brighter than several tens of Kelvins the Bell Labs survey data, and hence our techniques for removing stray radiation, become unreliable. But the brightness of the HI means also that stray radiation will be a relatively unimportant component of the total N_H and the "uncorrected" 140 ft spectra are thus fairly accurate. Sources so affected are flagged in table 1; the uncertainty in their N_H is dominated by the uncertain opacity correction. We also tabulate the peak brightness temperature (T_{peak}). The dominant error in the tabulated column densities may be due to either the baseline noise referred to above or to the uncertainty due to the opacity correction. Figure 4 shows how the uncertainty in N_H due to T_{spin},$\Delta N_H(T_{spin})$ dominates above the measurement errors of 1×10^{19} atoms cm^{-2} (dashed line) for $N_H \gtrsim 4 \times 10^{20}$ atoms cm^{-2}. If the area under Galactic HI profiles could always be measured to $\sim$2%, then opacity correction uncertainties would dominate at all values of N_H.

Figures 5 a,b compare the optically thin 140ft and Bell values of N_H as both a ratio and a difference as a function of N_H (140ft). The ratio of 140ft/Bell stays constant with N_H while the difference seems to grow slightly. This suggests that small scale structure is a constant fraction of the total. That is, at high latitudes the galactic N_H in a 21' field is equal to that in the $3^\circ \times 2^\circ$ Bell fields with a 1σ uncertainty of 11% on average.

IV. Conclusions

The values of N_H tabulated here have typical uncertainties of $\sim 10^{19}$ atoms cm^{-2} and so are about ten times more accurate than column densities derived from the Bell Labs survey alone. It is worth noting here that for the purposes of investigating small amounts of x-ray absorption it is the column density due to hydrogen and helium alone that contributes to the photoelectric cross-section in the 'C-band' below 0.28 keV (Morrison and McCammon 1983). Hydrogen in any form other than atomic appears to be uncommon at high Galactic latitudes (Blitz, Magnani and Mundy 1984) so that the 21cm data give an unusually direct and clean means of determining the column that must absorb x-rays.

The extreme x-ray–ultraviolet telescopes on ROSAT (Pye 1984) and EUVE (Bowyer 1987) can only detect extragalactic sources if they lie in directions of unusually small Galactic column density. There are two AGN in table 1 with N_H below 0.9×10^{20} atoms cm^{-2} and seven with N_H below 1.1×10^{20} atoms cm^{-2}. These low N_H AGN will make good targets for the extreme x-ray–ultraviolet telescopes. Our nearly 200 AGN form an essentially random sample of the high latitude sky. We can estimate then that roughly 1% of the sky has column densities of 0.9×10^{20} atoms cm^{-2} or less.

The need for more accurate column densities will rise rapidly with the many soft x-ray sources that are expected to be discovered with the soft x-ray sky survey satellite ROSAT (Trümper 1984, due for launch in February 1990). The effects of uncertain Galactic N_H can be important to *logN–logS* studies and hence to questions of quasar evolution and the origin of the x-ray background (Zamorani *et al.* 1988). An all-sky survey of Galactic N_H with a similar beam size to that used here and free of stray radiation would substantially reduce these problems and would be of great utility for x-ray astronomy.

ACKNOWLEDGMENTS This work was supported in part by NASA contract NAS8-30751, and by NASA Astrophysics Data Program grant NAG8-689.

REFERENCES

Blitz L., Magnani L., and Mundy L., 1984, *Ap. J. Letters*, **282**,L9.

Bowyer S.,1986, Adv. Space Res., **6**, 153.

Branduardi-Raymont G., *et al.*, 1987, in *The Physics of Accretion onto Compact Objects*, p407, Lecture Notes in Physics, **266**,[Berlin:Springer-Verlag].

Brunner H.,*et al.*,1988, in preparation.

Dickey J.M., 1988, in "QSO Absorption Lines: probing the Universe", eds. J.C. Blades, D. Turnshek, C.A. Norman [Cambridge:CUP], p.254.

Dickey J.M., and Benson J.M., 1982, *A. J.*, **87**, 278.
Elvis M., Green R.F., Bechtold J., Schmidt M., Neugebauer G., Soifer B.T., Matthews K., and Fabbiano G., 1986, *Ap. J.*, **310**,291.
Giacconi R., 1979, *Ap. J.*, **230**,540.
Giommi P., and Tagliaferri G., 1987, IAU Symposium no. 124, "Observational Cosmology", eds. A. Hewitt *et al.*, [Dordrecht:Reidel],p.601.
Gorenstein P., Harnden R.F., and Fabricant D., 1981, IEEE Trans. Nucl. Sci., **NS-28**,869.
Lockman F.J., Jahoda K., and McCammon D., 1986, *Ap. J.*, **302**,432.
Lockman F.J., and Dickey J., 1989, *Ann. Rev. Astr. Ap.*, in press.
Madejski G., 1985, PhD. Thesis, Harvard University.
Marshall H.L., *et al.*1984, *Ap. J.*, **283**,50.
McCammon D., Burrows D.N., Sanders W.T., and Kraushaar W.L., 1983, *Ap. J.*, **269**,107.
Morrison R., and McCammon D., 1983, *Ap. J.*, **270**, 119.
Piccinotti G., Mushotzky R.F., Boldt E.A., Holt S.S., Marshall E.E., Serlemitsos P.J., and Shafer R.A., 1982, *Ap. J.*, **253**,485.
Pye J.P., 1984, in *"X-ray and UV emission from Active Galactic Nuclei"*, eds. Brinkmann and Trümper,[Garching:MPE],p.261.
Stark A.A., Heiles C., Bally J., and Linke R., 1984, Bell Labs, privately distributed magnetic tape.
Sternberg J.R., White N.E., Barr P., and Osborne L., 1986, *The EXOSAT Observing Log*, [Noordwijk:ESTEC].
Trümper J., 1984, in *"X-ray and UV emission from Active Galactic Nuclei"*,ed. Brinkmann and Trümper,[Garching:MPE],p.254.
Taylor B.G., Anderson R.D., Peacock A. and Zobl R., 1981, Space Sci. Rev., **30**,479.
Wilkes B.J. and Elvis M.,1987, *Ap. J.*, **323**,243.
Zamorani G., Gioia I.M., Maccacaro T., and Wolter A., 1988, *Astr. Ap.*, **196**, 39.

Table 1: Galactic Column Densities Toward AGN
From Green Bank 140ft Data

Object	R.A.	decl.	N_{HI}^{a}	T_{peak}	Notes
MCS 18	00 02 46.2	05 07 30	3.87	9.6	
PHL658	00 03 25.0	15 53 08	3.94	14.7	
IIIZW2	00 07 56.7	10 41 47	6.09	24.5	
3C 9	00 17 50.0	15 24 17	4.02	18.7	
PG0026+129	00 26 38.1	12 59 29	4.93	18.6	
0038-020	00 38 23.7	−02 02 51	2.57	5.9	
UM 275	00 43 39.5	00 48 04	2.03	5.6	
PKS0044+030	00 44 31.3	03 03 34	3.00	9.0	
PG0049+171	00 49 16.5	17 09 40	4.26	16.5	
I ZW I	00 50 57.7	12 25 20	5.07	20.3	
0052+251	00 52 11.1	25 09 24	4.50	13.9	
PHL909	00 54 31.9	14 29 59	4.20	14.0	
0106+013	01 06 04.3	01 19 01	2.63	6.9	
MKN1152	01 11 21.7	−15 06 36	1.67	4.3	
0112-017	01 12 43.4	−01 42 59	5.37	15.3	
PG0117+213	01 17 34.6	21 18 05	4.85	18.6	
PG0119+229	01 19 56.9	22 54 36	5.65	20.1	
NGC 526A	01 21 37.2	−34 19 33	2.33	6.3	
3CR48	01 34 49.8	32 54 20	4.35	9.5	
0205+024	02 05 14.5	02 28 41	2.99	8.3	
MKN590	02 12 00.4	−00 59 58	3.07	8.7	
NGC931	02 25 14.4	31 05 22	7.07	21.7	
0226-038	02 26 22.2	−03 50 55	2.37	6.5	
PHL 1377	02 32 36.5	−04 15 09	2.29	6.0	
0235+164	02 35 53.0	16 24 05	7.60	20.6	
PKS0237-233	02 37 52.5	−23 22 06	2.23	6.6	
0241+622	02 41 01.2	62 15 29	73.30	73.8	1
H0323+022	03 23 38.0	02 14 47	8.68	24.8	
NRAO 140	03 32 22.0	32 08 38	14.22	59.0	1
H0414+009	04 14 18.0	00 58 03	9.15	26.9	
3C 111	04 15 00.6	37 54 19	32.61	63.0	1
0420-388	04 20 29.6	−38 51 42	1.91	5.8	
0420-014	04 20 43.3	−01 27 24	9.43	39.2	
3C120	04 30 31.6	05 14 58	12.32	56.0	1
3C 138	05 18 16.9	16 35 27	23.28	60.5	1

PKS0521-365	05 21 12.8	−36 30 15	3.37	13.4	
0537-286	05 37 56.7	−28 41 26	1.95	3.6	
3C 147	05 38 43.0	49 49 45	21.64	45.1	1
H0548-322	05 48 48.9	−32 16 60	2.49	3.9	
NGC2110	05 49 46.3	−07 28 01	18.60	53.4	1
MCG8-11-11	05 51 09.7	46 25 51	20.27	39.7	1
H0557-385(A)	05 56 21.0	−38 20 15	3.35	6.6	
0642+449	06 42 52.9	44 54 31	11.61	26.2	
3C 175	07 10 15.9	11 51 26	11.51	26.7	
MKN376	07 10 35.7	45 47 09	9.32	16.3	
PKS0735+17	07 35 14.0	17 49 09	4.35	9.2	
0736+017	07 36 42.3	01 44 00	8.91	26.5	
MKN 79	07 38 46.8	49 55 46	5.89	22.3	
3C 186	07 40 56.9	38 00 32	4.87	9.7	
3C 191	08 02 03.9	10 23 56	2.54	4.7	
PG0804+76	08 04 35.4	76 11 31	3.12	12.2	
3C 196	08 09 58.9	48 22 09	4.93	14.3	
0830+112	08 30 35.5	11 15 30	3.43	7.7	
3C 204	08 33 17.9	65 24 04	4.85	18.3	
3C 205	08 35 09.9	58 04 53	4.34	20.8	
3C 206	08 37 27.9	−12 03 53	5.85	11.9	
3C 207	08 38 01.9	13 23 05	5.40	14.1	
PG0844+34	08 44 33.9	34 56 08	3.39	9.7	
3C 208	08 50 23.0	14 03 58	3.60	10.2	
OJ 287	08 51 57.2	20 17 58	2.75	5.4	
3CR215	09 03 44.1	16 58 16	3.75	7.8	
0906+015	09 06 34.9	01 33 46	3.38	8.9	
MKN 704	09 15 39.4	16 30 59	3.15	6.3	
H0917-074	09 17 03.0	−07 22 57	3.30	7.8	
0923+201	09 23 05.6	20 07 06	4.16	11.2	
PG0923+129	09 23 20.1	12 57 07	4.03	12.0	
4C39.25	09 23 55.3	39 15 23	1.69	1.8	
PG0934+013	09 34 26.4	01 19 12	4.69	12.4	
NGC 2992	09 43 17.4	−14 05 44	5.56	16.2	

PG1001+054	10 01 43.3	05 27 35	1.88	6.2
1011+25	10 11 05.6	25 04 09	3.10	16.3
1012+008	10 12 20.7	00 48 33	3.22	8.9
1020-103	10 20 04.0	−10 22 32	4.89	12.5
B2 1028+313	10 28 09.8	31 18 20	1.98	2.7
3C245	10 40 05.9	12 19 16	2.70	8.1
3CR249.1	11 00 27.3	77 15 08	2.92	6.9
MKN 421	11 01 40.5	38 28 42	1.45	1.5
3C254	11 11 53.3	40 53 41	1.75	1.7
1115+080	11 15 41.4	08 02 25	3.61	10.4
PG1116+215	11 16 30.0	21 35 42	1.44	2.2
MKN734/PG	11 19 10.9	12 00 48	2.74	5.1
1121+422	11 21 52.0	42 16 52	2.33	5.2
MKN180	11 33 29.9	70 24 60	1.27	1.5
3C263	11 37 09.3	66 04 26	.82	1.3
PG1138+040	11 38 42.4	04 03 39	1.87	3.5
1146-037	11 46 23.8	−03 47 29	2.77	4.9
NGC 4051	12 00 36.3	44 48 34	1.31	1.6
GQ COMAE	12 02 08.9	28 10 54	1.72	2.6
PG1211+143	12 11 44.8	14 19 53	2.83	5.9
ON235	12 15 21.1	30 23 41	1.60	2.3
1217+023	12 17 38.3	02 20 20	1.97	4.5
1219+305	12 18 51.6	30 27 15	1.78	2.9
MKN 205	12 19 33.7	75 35 17	2.74	5.0
1225+317	12 25 55.8	31 47 12	1.23	1.1
PG1229+204	12 29 32.9	20 26 03	2.58	6.7
NGC 4593	12 37 04.6	−05 04 15	1.97	4.4
PG1241+176	12 41 40.8	17 37 26	1.93	7.5
PG1244+026	12 44 02.0	02 38 30	1.93	4.6
3C277.1	12 50 14.9	56 50 38	1.03	1.1
1252+119	12 52 07.5	11 57 19	2.63	9.3
3C279	12 53 35.7	−05 31 06	2.22	5.8
MKN 231	12 54 04.9	57 08 36	1.03	1.3
PG1307+085	13 07 16.1	08 35 48	2.20	6.3
NGC 5033	13 11 09.1	36 51 29	1.00	1.9

3C287	13 28 15.9	25 24 38	1.06	1.8
3C286	13 28 49.9	30 45 58	1.14	2.2
1331+170	13 31 09.9	17 04 23	1.76	4.6
MCG-6-30-15	13 33 01.8	−34 02 26	4.06	9.4
PG1333+176	13 33 36.5	17 40 31	1.76	4.7
3C288.1	13 40 29.8	60 36 49	2.09	2.8
IC4329A	13 46 27.8	−30 03 41	4.55	10.4
MKN 279	13 51 51.8	69 33 13	1.64	1.4
PG1352+183	13 52 12.5	18 20 01	1.84	4.6
PG1352+011	13 52 25.7	01 06 51	2.10	6.1
PG1402+266	14 02 58.7	26 10 01	1.42	4.0
PG1404+226	14 04 02.7	22 37 59	2.00	6.4
PG1407+265	14 07 07.6	26 32 29	1.38	3.3
NGC 5506	14 10 39.1	−02 58 24	4.22	16.2
PG1416-129	14 16 21.3	−12 56 59	7.20	21.1
3C298	14 16 38.9	06 42 21	2.06	7.3
PG1425+267	14 25 21.7	26 45 38	1.54	5.1
PG1426+015	14 26 33.7	01 30 27	2.64	8.1
3C309.1	14 58 58.0	71 52 13	2.41	1.8
PG1501+106	15 01 36.3	10 37 57	2.23	6.3
PG1519+226	15 19 02.0	22 38 22	3.88	19.1
MKN290	15 34 45.3	58 04 00	2.32	3.4
3CR323.1	15 45 31.0	21 01 28	4.04	11.5
1546+027	15 46 58.2	02 46 07	6.78	28.9
PG1552+085	15 52 19.0	08 31 08	3.47	11.2
1611+343	16 11 47.8	34 20 21	1.44	3.4
TON256	16 12 08.5	26 11 47	3.77	12.6
MKN 876	16 13 36.2	65 50 37	2.66	3.3
MKN 877	16 17 56.7	17 31 34	4.35	14.0
3C334	16 18 06.9	17 43 31	4.22	13.4
3C336	16 22 31.8	23 52 03	4.52	17.4
PG1630+377	16 30 15.1	37 44 11	.90	1.8
1634+706	16 34 51.8	70 37 37	5.74	11.7
1635+119	16 35 26.0	11 55 40	4.29	11.7
3C345	16 41 17.6	39 54 10	.74	1.8

MKN501	16 52 11.6	39 50 24	1.73	3.8	
3C351	17 04 03.4	60 48 32	2.26	3.2	
1721+343	17 21 31.9	34 20 41	3.06	7.8	
1725+044	17 25 56.0	04 29 29	7.03	29.2	
I ZW 186	17 27 04.2	50 15 31	2.58	10.2	
PKS1739+17	17 39 26.7	17 21 59	5.44	20.8	
1803+676	18 03 37.3	67 37 53	5.00	6.7	
3C380	18 28 12.8	48 42 40	6.60	14.0	
NGC6814	19 39 55.5	−10 26 33	9.80	33.9	
PKS2121+053	21 21 14.7	05 22 28	6.27	33.5	
3C433	21 21 30.5	24 51 18	8.75	29.9	
2126-158	21 26 26.7	−15 51 48	4.85	22.0	
2128-123	21 28 52.5	−12 20 20	4.83	10.2	
IIZW136	21 30 01.1	09 54 59	4.20	8.5	
PKS2134+004	21 34 05.2	00 28 26	5.12	19.1	
PHL1657	21 35 01.1	−14 46 26	4.45	11.9	
NGC 7172	21 59 07.2	−32 06 36	1.65	5.0	
BL LAC	22 00 39.2	42 02 08	20.15	58.0	1
2201+315	22 01 01.2	31 31 06	9.91	20.6	
PG2209+184	22 09 30.1	18 27 01	4.82	10.8	
MKN304	22 14 45.2	13 59 26	5.23	14.7	
2216-038	22 16 15.9	−03 50 33	6.18	24.8	
3C446	22 23 11.0	−05 12 16	5.26	18.9	
CTA102	22 30 07.7	11 28 24	5.05	13.1	
NGC7314	22 33 00.1	−26 18 31	1.45	5.3	
MR2251-179	22 51 25.7	−17 50 54	2.84	6.0	
3C354.3	22 51 29.4	15 52 55	7.13	14.4	
PKS2251+113	22 51 40.5	11 20 40	5.53	21.6	
PKS2254+023	22 54 44.4	02 27 15	5.88	22.2	
NGC7469	23 00 44.2	08 36 15	4.82	15.4	
2304+042	23 04 30.0	04 16 40	5.52	16.1	2
NGC7582	23 15 38.3	−42 38 31	1.48	4.3	
PKS2344+092	23 44 03.4	09 1- 06	5.05	19.9	
2345+184	23 45 56.7	18 27 29	4.25	15.8	
MKN 541	23 53 28.0	07 14 36	5.02	17.7	

a. For an assumed T_{spin} of 250 K (see text).
1.Bright HI spectrum. Was not corrected for stray radiation (see text). Opacity correction dominates over stray radiation correction in most cases.
2. Bell Labs survey was extrapolated to correct this spectrum. Error may be larger than normal.

figure 1: A low signal to noise 21cm spectrum from the NRAO 140ft. The integral cleaned N_H of this spectrum corrected for stray radiation is 1.23×10^{20} atoms cm^{-2} (1225+317).

figure 2: A sample of the stray radiation spectrum (lower line) removed from the observed data (upper line).

figure 3: Percentage error in N_H due to opacity uncertainties (T_{spin}) as a function of N_H(140ft).

figure 4: Uncertainty due to opacity uncertainties (N_H(10000 K)- N_H(125 K)) as a function of peak brightness temperature (T_{peak}) in the 140ft spectrum. The horizontal line is the uncertainty due to other effects. Opacity uncertainties dominate above about 4×10^{20} atoms cm^{-2}.

figure 5: (a) Ratio, and (b) difference, between N_H(140ft) and N_H(Bell) as a function of N_H (140ft) in units of 10^{20} atoms cm^{-2}.

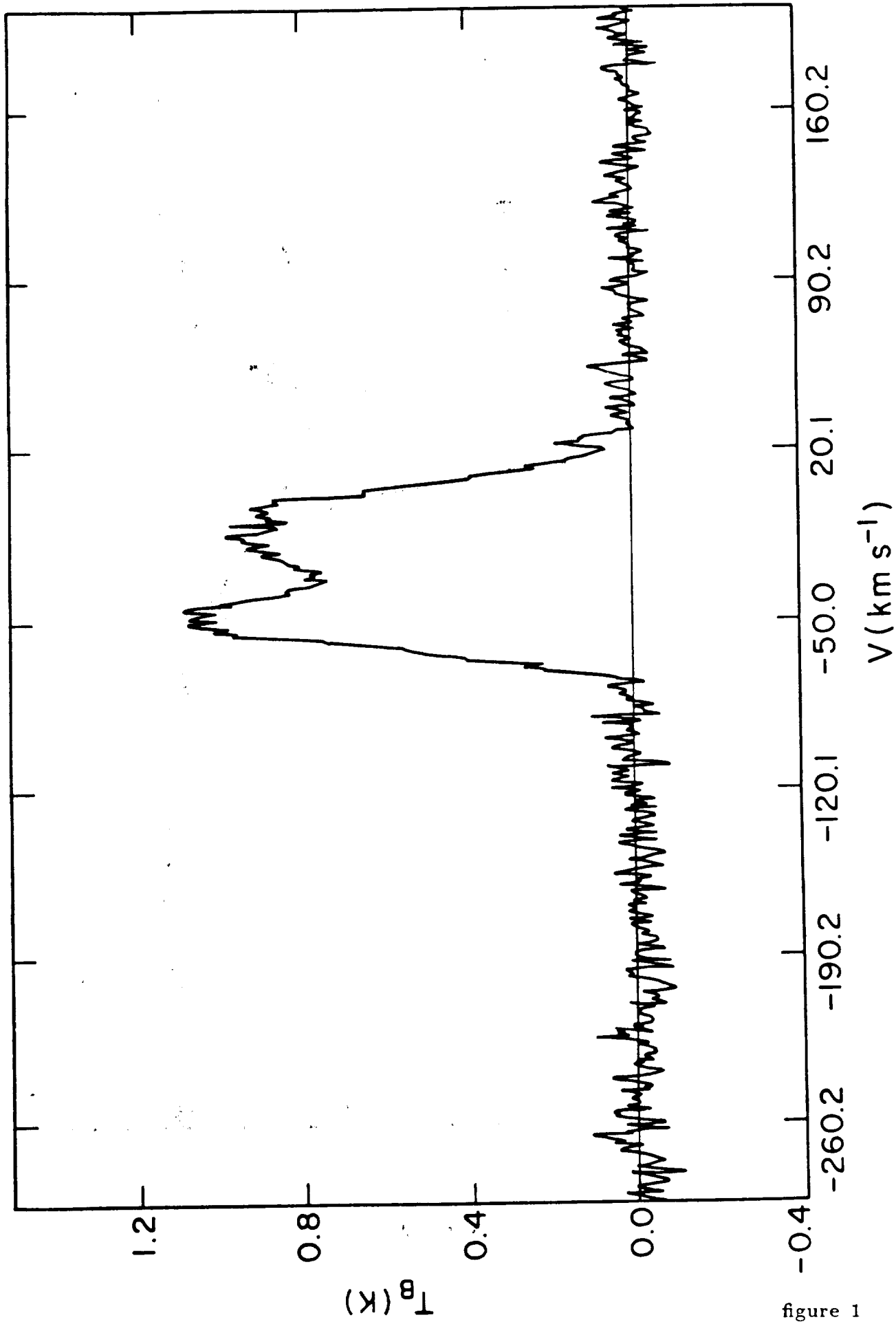

figure 1

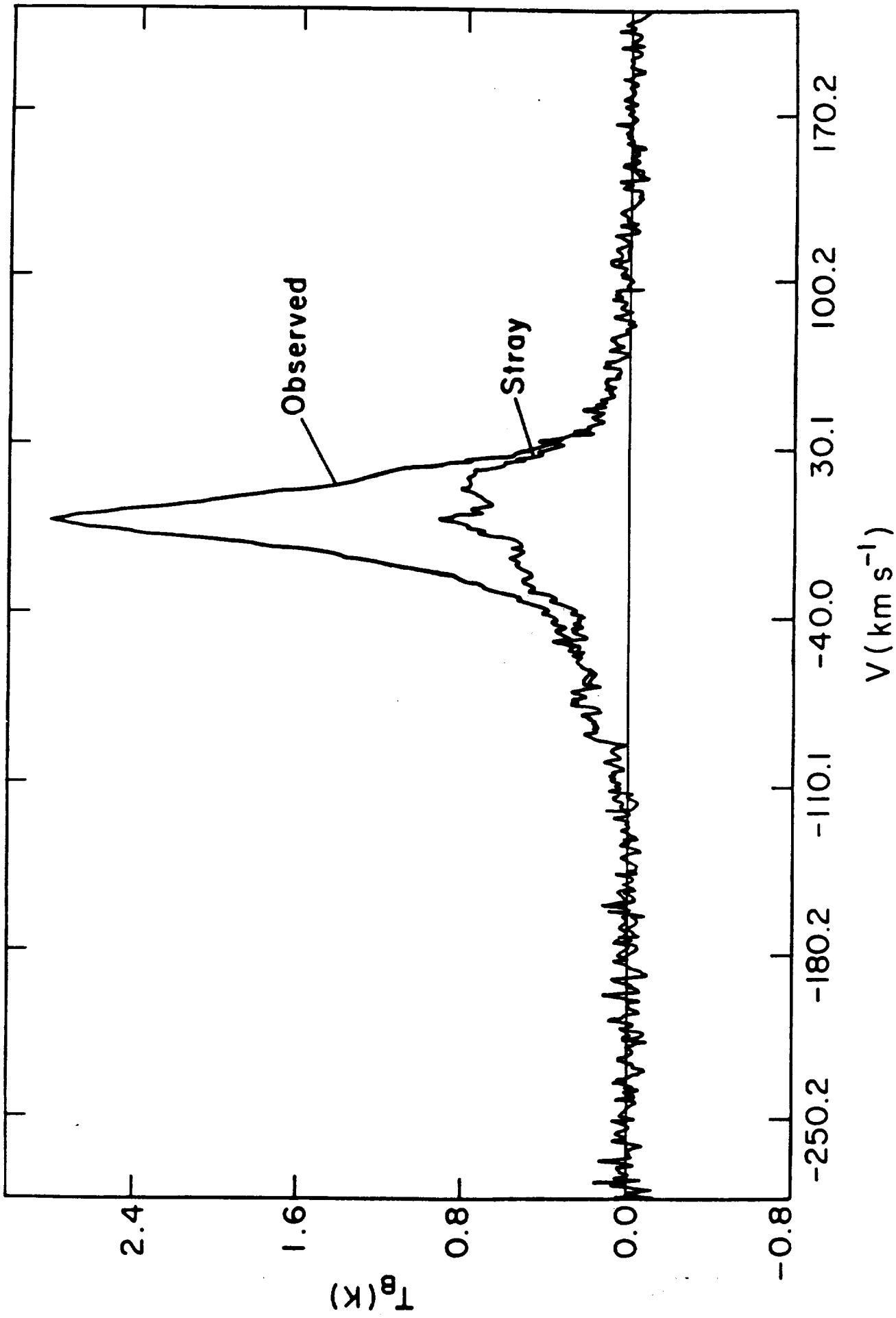
Observed
Stray
2.4
1.6
0.8
0.0
-0.8
$T_B(K)$
-250.2
-180.2
-110.1
-40.0
30.1
100.2
170.2
V (km s^{-1})

figure 2

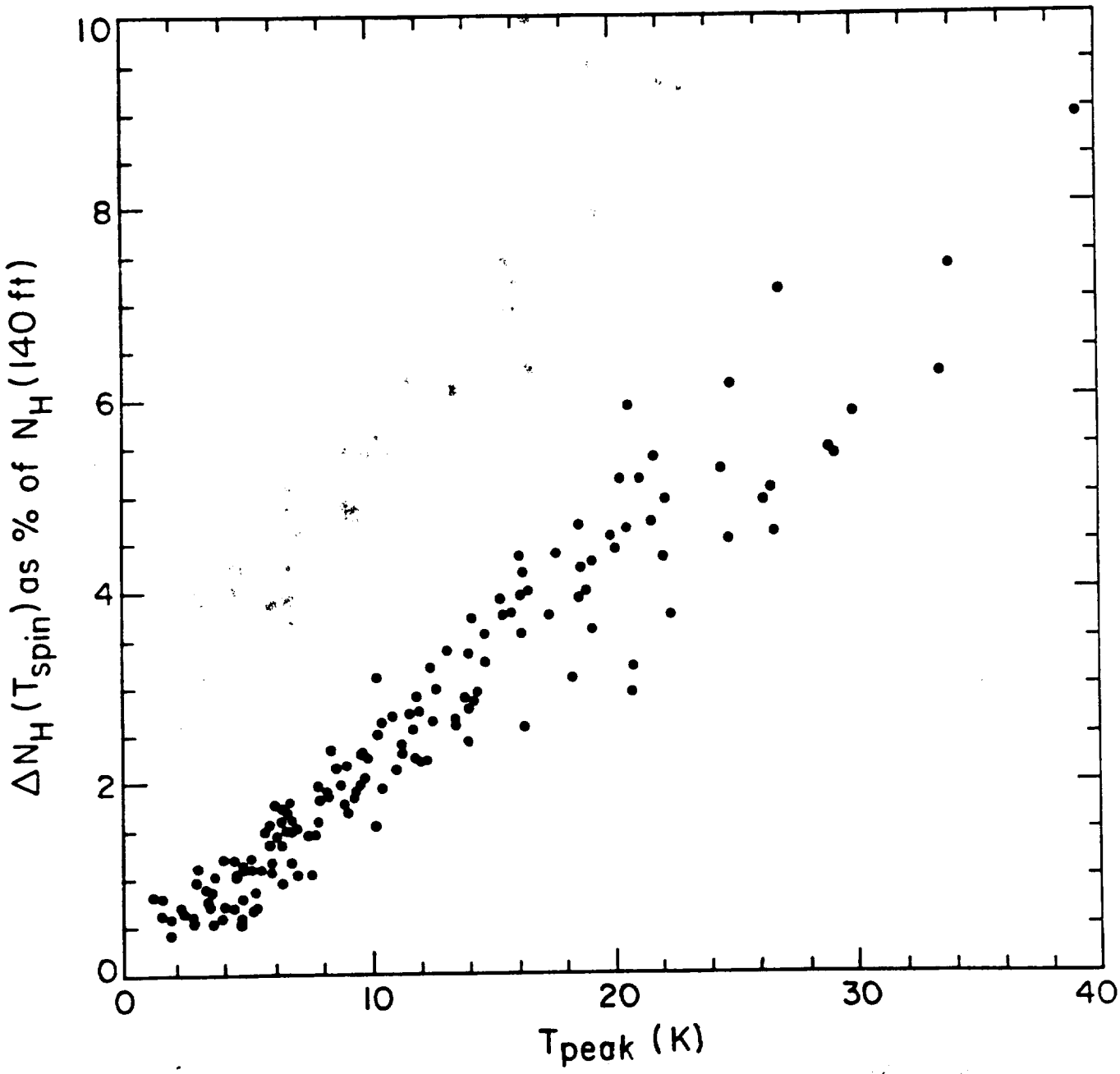

figure 3

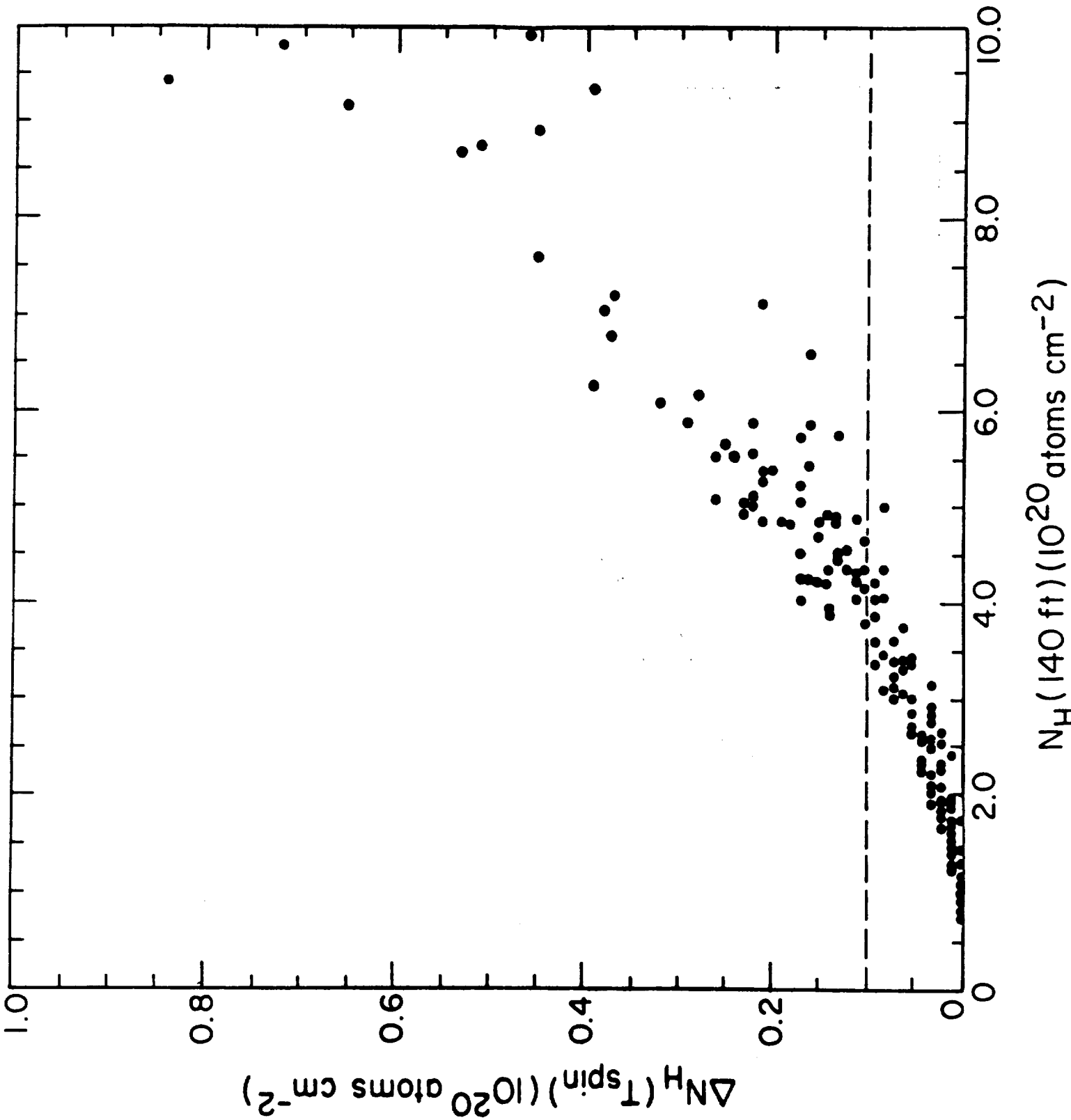
ΔN_H (T_{spin}) (10^{20} atoms cm^{-2})
1.0
0.8
0.6
0.4
0.2
0
N_H (140 ft) (10^{20} atoms cm^{-2})
0
2.0
4.0
6.0
8.0
10.0

figure 4

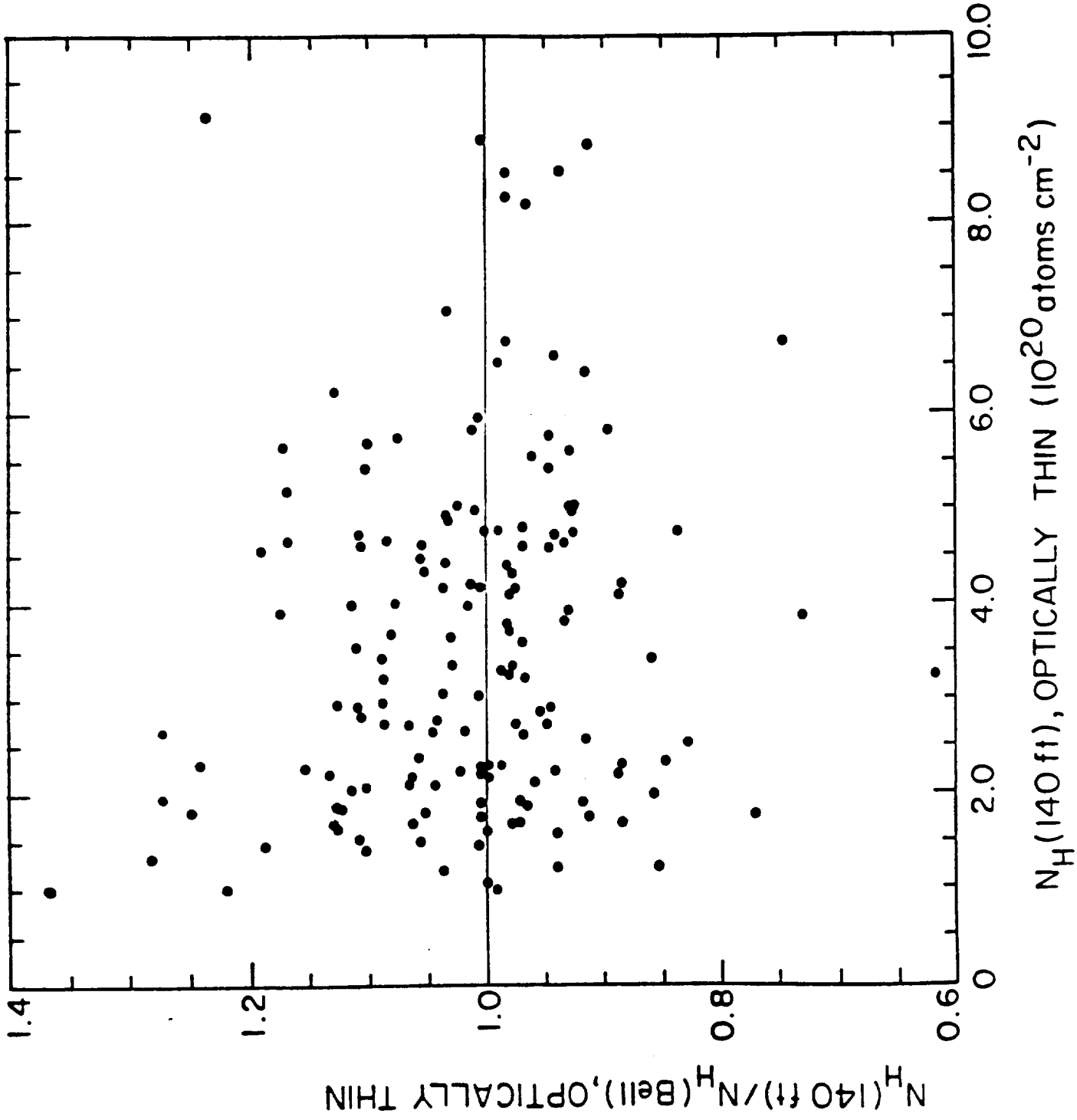
1.4
1.2
1.0
0.8
0.6
0
2.0
4.0
6.0
8.0
10.0
N_H(140 ft), OPTICALLY THIN (10^{20} atoms cm^{-2})
N_H(140 ft)/N_H(BeII), OPTICALLY THIN

figure 5a

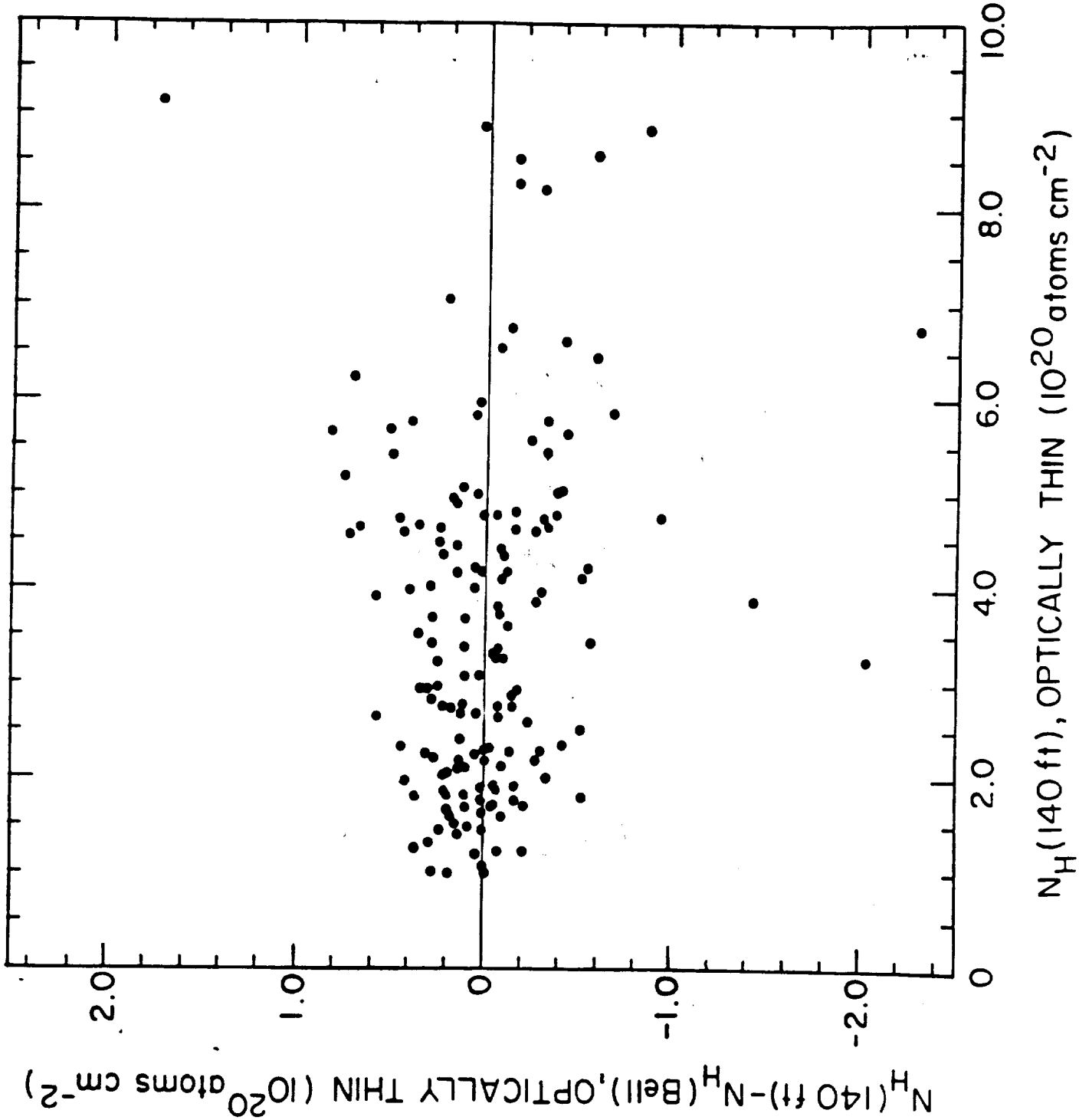
$N_H(140\,ft)-N_H(BeII)$, OPTICALLY THIN (10^{20} atoms cm^{-2})
2.0
1.0
0
-1.0
-2.0
$N_H(140\,ft)$, OPTICALLY THIN (10^{20} atoms cm^{-2})
0
2.0
4.0
6.0
8.0
10.0

figure 5b

Center for Astrophysics
Preprint Series No. 2923

WEAK BUMP QUASARS

JONATHAN C. MCDOWELL, MARTIN ELVIS, BELINDA J. WILKES
STEVEN P. WILLNER, M.S. OEY[1], ELISHA POLOMSKI[2]
Harvard-Smithsonian Center for Astrophysics

JILL BECHTOLD
Steward Observatory,University of Arizona

AND

RICHARD F. GREEN
Kitt Peak National Observatory, NOAO[3]

To appear in *Astrophysical Journal Letters*

[1]Current address: Steward Observatory

[2]Current address: Boston University

[3]Operated by the Association of Universities for Research in Astronomy, Inc., under contract with the NSF

ABSTRACT

The recent emphasis on 'Big Bumps' dominating the ultraviolet continuum of quasars has obscured the fact that bump properties vary widely, and that there are objects in which no such component is evident. As part of a survey of quasar continuum spectra, we have identified a class of quasars in which the optical-ultraviolet continuum 'Big Bump' feature appears to be weak or absent, relative to both infrared and x-ray. These 'Weak Bump' quasars are otherwise normal objects, and constitute a few percent of the quasar population.

Subject headings: Quasars - spectrophometry - ultraviolet: spectra

I. INTRODUCTION

The ultraviolet 'Big Bump ' is the most striking feature in the continuum energy distributions of quasars (Malkan 1983). This bump is part of a larger feature that extends through the optical and, probably, soft x-ray bands (Arnaud *et al.* 1985,Czerny and Elvis 1987). The feature is thought to be a signature of thermal radiation from the accretion flow (which is often modelled as a disk) at a few tens of Schwarzschild radii from the central compact object (Malkan 1983, Bechtold *et al.* 1987, and others). During a study of Big Bump properties in a sample of quasars with fully observed energy distributions (100μm-4 keV), we found that in a minority of quasars (5 of the 31) the bump appears unusually weak or possibly absent.

II. WEAK BUMP QUASARS

The range of bump strengths in our sample is illustrated in Fig. 1 by three quasar energy distributions. The ***Einstein*** x-ray observations are plotted as a 'bow-tie' illustrating the best fit power law slope and 90% errors (see Wilkes and Elvis 1987, hereafter QED1, for details). Spectrophotometric and photmetric observations are plotted as solid lines and individual points respectively. Optical spectrophotometry is from Neugebauer *et al.* (1979,1987). IRAS AO photometry, near IR and optical photometry, and IUE spectrophotometry are from our QED Atlas, Elvis *et al.* (in preparation).

The data have been corrected for Galactic reddening and converted to the emitted frame assuming $H_0 = 50$km s^{-1} Mpc^{-1} and $q_0 = 0.5$; Emission lines have been removed and a reddening correction has been made using a standard Galactic extinction law (Savage and Mathis 1979) normalized using small beam N_H values obtained in the direction of the quasars (Elvis, Lockman and Wilkes 1989). In cases where substantial variability is evident in the data, an attempt has been made to keep only observations of similar dates. In most of our objects only mild variability is evident.

3C 263 (Fig. 1a) has one of the most prominent bumps in our sample, while PG1116+215 (Fig. 1b) is a more typical object; its ultraviolet bump is less pronounced (It does have a large 3000Å bump caused by Balmer continuum and unresolved Fe II line emission, Wills, Netzer and Wills 1985). In contrast, Mkn 876 (Fig. 1c) clearly has a much flatter spectrum than the other two objects; it is a 'weak bump' quasar. Our sample contains four more 'weak bump' quasars, shown in Fig. 2, that have no significant rise in their continuum flux toward the far ultraviolet other than the 3000Åfeature.

While the objects noted as lacking strong ultraviolet bumps by Edelson and Malkan (1986) and Ward *et al.*(1987) were clearly reddened, we will argue that the five objects discussed here are intrinsically weak in the ultraviolet. Properties of the five weak bump quasars are listed in Table 1(a). For comparison we list the other quasars from Fig. 1, and seven quasars whose energy distributions were published in Elvis *et al.* (1986) and Bechtold *et al.* (1986), in Table 1(b). The luminosities of the weak bump quasars are typical of the others in the sample, a few times 10^{45} erg s^{-1} in the near infrared, bright enough that contamination due to host galaxy starlight can be ignored. (Mkn 205 is less luminous, at a few times 10^{44}.) Most of our sample objects, and our five weak bump objects in particular, vary by at most 0.1-0.2 dex (i.e. $\Delta \log L_\nu \sim 0.1 - 0.2$) based on our observations and those from the literature (Table 1). Variability closer to 0.5 dex would be needed to simulate the weak bump energy distributions.

To define ultraviolet bump strength objectively we use a far-ultraviolet to near-infrared color,

$$C_{UV/IR} = \log(\frac{L(0.1 - 0.2\mu\mathrm{m})}{L(1 - 2\mu\mathrm{m})}).$$

Fig. 3 shows the histogram of bump strengths for all quasars in our sample analysed so far. Despite the near-constant location of the $1\mu m$ inflection (Elvis *et al.*1986), there is a large range in the bump amplitudes. Most of our QED sample objects have strong ultraviolet bumps, with colors bluer than $C_{UV/IR} = 0.4$ (Table 1b). However there is a tail in the distribution to redder $C_{UV/IR}$, and those objects picked out visually as having weak bumps are exactly those with $C < 0.15$ (Table 1a). Could it be that the infrared is enhanced rather than that the ultraviolet is weakened? It seems not. Three-way comparisons between the infrared (1-2μm), ultraviolet bump, and x-rays show that the weak bump quasars differ from other quasars by being weak in the ultraviolet rather than abnormally strong in the infrared. Also the (far-IR to far-UV) luminosities of the quasars range from 10^{45} to 10^{47} erg s^{-1} and there is no evidence within this sample for a correlation of bump strength with luminosity.

III. LIMITS ON INTERNAL REDDENING

An obvious possibility is that the range in bump strengths is due to differing amounts of internal reddening in the sources. To test this, we construct color-color diagrams using ratios between the estimated luminosities in various frequency octaves. Fig. 4 is an (IR/visible, visible/UV) color-color plot. As noted earlier, the bump occurs at $\lambda < 1\mu$m, so that the ratio of visual ($4000 - 8000\AA$) and far ultraviolet ($1000 - 2000\AA$) luminosities largely measures its shape, while the near

infrared ($1-2\mu$m) to visual luminosity ratio measures their 'power law continuum' relative to the bump component. (We avoid the $2000-4000\AA$ region where the 3000Å bump is important, Wills, Netzer and Wills 1985). The reddening lines illustrate that the colors of the weak bump objects could be explained by reddening the 'normal' objects by a plausible E(B-V) of 0.1 to 0.2 magnitudes.

The x-ray data make it unlikely, however, that such strong internal reddening is present. The IPC x-ray spectra for our objects are no different from those of strong bump quasars at the same level of radio loudness (QED1), and are inconsistent with the large hydrogen columns ($> 10^{21}\mathrm{cm}^{-2}$) that would be associated with the internal reddening (0.2 mag) discussed above. For all the weak bump objects no single power-law x-ray fit with this column is acceptable at the 90% level (see Fig. 2 in QED1). The presence of E(B-V) = 0.2 of reddening would imply that the intrinsic spectrum must be curved and extremely steep in the soft x-rays. For instance, for PG1613+658 the extra intrinsic column density would imply an energy index in the 0.1–4 keV range of $\alpha_E > 2.5$, and neither a single power law nor a two power law model gives a good fit to the data if both are absorbed by $10^{21}\mathrm{cm}^{-2}$. The x-ray column density is unlikely to be smaller than the ultraviolet column since the x-rays are believed to come from a smaller region on energetic grounds. Indeed there is some evidence that the column to the x-ray emitting plasma may be greater than toward that emitting at other frequencies (Reichert *et al.* 1985). We therefore conclude that reddening is not likely to be the cause of the bump weakness, unless an extra unabsorbed x-ray component is present (e.g. NGC 4151, Elvis, Briel and Henry 1983, Pounds *et al.* 1986).

IV. DISCUSSION

If reddening is not the dominant effect, there are a number of alternate explanations for the diversity in bump strengths. There does not seem to be any correlation of bump strength with the other main continuum feature, the level of radio loudness, since two of the five weak bump quasars are radio-loud objects. It is possible that the bump may be highly variable in a given object; in this case all quasars may spend some time in the weak bump state, rather than there being a separate class of objects. This would provide strong constraints on parameters for accretion disk models of the bump . While some quasars do vary violently in the ultraviolet, (e.g. GQ Comae, Sitko 1986) in the five cases where we have multiple IUE observations, the variation is small compared to the range in bump strengths in the sample. Nevertheless this is a possibility and would be checked by repeated simultaneous optical and ultraviolet observation of the objects in Table 1.

The remaining possibilities require intrinsic differences between the bumps in these objects and those in most quasars. For example, the bump may be present but peak at an abnormally high frequency, in which case its strength would anticorrelate with excesses in the soft x-rays. At present no quantitative measure of soft excess strength is available, and qualitative comparisons are inconclusive; several weak bump quasars seem to have no soft x-ray excess, but PHL909, the weakest of all, does show an excess (Masnou *et al.* 1989). Alternatively, the bump may peak at the same frequency but be intrinsically weaker relative to the power law continuum in these objects, compared to the objects in Table 1(b). This could be due either to a true luminosity change or to an inclination effect (c.f. Netzer 1985). The range of bump strengths relative to the total luminosity is a factor of 20-50, reasonable for an inclination effect. We note that the expected x-ray behaviour with inclination is uncertain, as the central region may become occulted at large inclinations. Finally, the slope of the bump component may be flatter in the weak bump objects. This could occur in accretion disk models if the disks in weak bump quasars were accreting using a different mechanism (with a different geometry?) from those with strong bumps and had a wider range of contributing temperatures.

If the bump is really absent in some of our objects, what is causing the optical and ultraviolet flux that we do see (especially in the well observed $0.1 - 0.5\mu$m range)? It has been argued (e.g. Sanders *et al.*1989) that the infrared continuum is entirely due to dust, but dust could not contribute in the optical since the most refractory grains evaporate at around 2000K. A fairly weak bump and a thermal infrared continuum could conspire to give a continuous infrared to ultraviolet power law, but such a coincidence seems contrived. We suggest that the most probable explanation is still that the radiation is nonthermal in origin. The weak bump objects offer new possibilities for studying quasars and may allow us to examine the 'bare' non-thermal component in the optical and ultraviolet.

ACKNOWLEDGEMENTS

This work was supported by NASA Astrophysics Data Program grant NAG 8-689, NASA IUE grant NAG 5-87, and NASA contract NAG 8-30751.

REFERENCES

Arnaud, K.A., *et al.* 1985, *M.N.R.A.S.* **217**,105.

Bechtold J., *et al.* 1987, *Ap. J.*, **314**, 699.

Carleton N.P., *et al.* , 1987, *Ap. J.*, **318**, 595.

Czerny B. and Elvis M., 1987, *Ap. J.*, **321**, 305.

Edelson, R., and Malkan, M.A., 1986 *Ap. J.* **308**, 59.

Elvis M. *et al.* 1989, 'QED Atlas', in preparation.

Elvis, M., Briel, U. G., and Henry, J. P., 1983, *Ap. J.*, **268**, 105.

Elvis M., Lockman F.J., and Wilkes B.J., 1989, *A. J.*, **97**,777.

Elvis M., *et al.* 1986, *Ap. J.*, **310**, 291.

Malkan M.A., 1983. *Ap. J.*, **268**, 582.

Masnou, J-L., *et al.* , 1989, in preparation.

Neugebauer, G., Oke, J.B., Becklin, E.E., and Matthews, K., 1979. *Ap. J.*, **230**. 79.

Neugebauer, G., Green, R.F., Matthews, K, Schmidt, M., Soifer, B.T., and Bennett, J., 1987. *Ap. J. Suppl.*, **63**. 615.

Netzer, H., 1985, *M.N.R.A.S.* **216**,63.

Pounds K.A., Warwick R.S., Culhane J.L., and de Korte P.A.J., 1986, *M.N.R.A.S.*, **218**, 685.

Reichert, G. *et al.*, 1985, *Ap. J.* **296**, 69.

Richstone and Schmidt, M., 1980, *Ap. J.*, **235**, 361.

Sanders, D.B., Phinney, E.S, Neugebauer, G., Soifer, B.T., Matthews, K., and Green, R.F., 1989, preprint.

Savage B.D., and Mathis, J.S., 1979, *Ann. Rev. Astr. Ap.*, **17**, 73.

Sitko M. ,1986, in *"Continuum Emission in AGN"*, ed. M. Sitko, [Tucson:NOAO] p.29.

Ward M.J., *et al.* 1987, *Ap. J.*, **315**, 74.

Wilkes, B.J., and Elvis, M., 1987, *Ap. J.* **323**, 243. (QED1)

Wills B.J., Netzer H., and Wills D., 1985, *Ap. J.*, **288**, 94.

Table 1

Object	Coord name	z	Bump Strength $C_{UV/IR}$	Observation date			Optical Var. (dex)
				Near IR	Optical	IUE	
(a) Weak Bump Quasars							
PHL 909	Q0054+144	0.17	-0.20	1985	1978	1987	
3C 48	Q0134+329	0.37	-0.01	1975	1978,1985	1982	0.1
Mkn 205	Q1219+755	0.05	0.15	1986	1972,1986	1983	0.1
Mkn 876	Q1613+658	0.13	0.14	1985	1980,1985	1981/3	0.1
PHL 1657	Q2135-147	0.20	0.09	1985	1969,1985	1982	0.2
(b) Other Quasars							
PG1116+215	Q1116+215	0.18	0.50	1986	1980,1986	1982	0.2
3C 263	Q1137+660	0.65	0.66	1986	1986	1982	
PG1211+143	Q1211+143	0.09	0.56	1986	1980,1985	1982	0.2
3C 273	Q1226+023	0.16	0.64	Many	1980, 1986	1982	0.3
PG1307+085	Q1307+085	0.16	0.62	1988	1980,1986	1980	0.1
PG 1416-129	Q1416-129	0.13	0.59	1988	1980,1985	1980	0.2
Mkn 1383	Q1426+015	0.09	0.82	1983	1980,1986	1983	0.2
Mkn 841	Q1501+106	0.04	0.21	1986	1980,1986	1983	0.2
3C 323.1	Q1545+210	0.27	0.46	1985	1980,1986	1983	0.1

References: Elvis et al (1986,1989), Bechtold et al (1987), Neugebauer et al (1979,1987)

FIGURE CAPTIONS

Figure 1: Sample rest frame energy distributions for three quasars, illustrating the range of ultraviolet bump strengths. The energy distributions are plotted as $\log(\nu L_\nu)$ against $\log \nu$; (a) 3C 263 has one of the strongest bumps of any of our sample quasars, while (b) PG1116+215 is typical. (c) Markarian 205 is a weak bump quasar.

Figure 2: Rest frame energy distributions of weak bump quasars: (a) PHL 909; (b) 3C 48; (c) Mkn 205; and (d) PHL 1657. Note the presence of the 3000Å bump at $\log \nu = 14.5 - 15$; it is especially prominent in (a) and (d).

Figure 3: Histogram of bump strength colors $C_{IR/UV} = \log L(0.1 - 0.2\mu m)/L(1 - 2\mu m)$ for a sample of 30 quasars, including those described in the text. Weak bump quasars are shaded.

Figure 4: Near infrared/optical/ultraviolet color-color diagram comparing the locus of sample objects with the direction of the reddening line. The lines shows the effect of reddening PG1211+143 (center left) and 3C 273 (lower right) by E(B-V)=0.1 and 0.2. Quasars are identified by their right ascensions; weak bump quasars are denoted by crosses, while quasars from Table 1(b) are represented by filled squares.

Figure 1

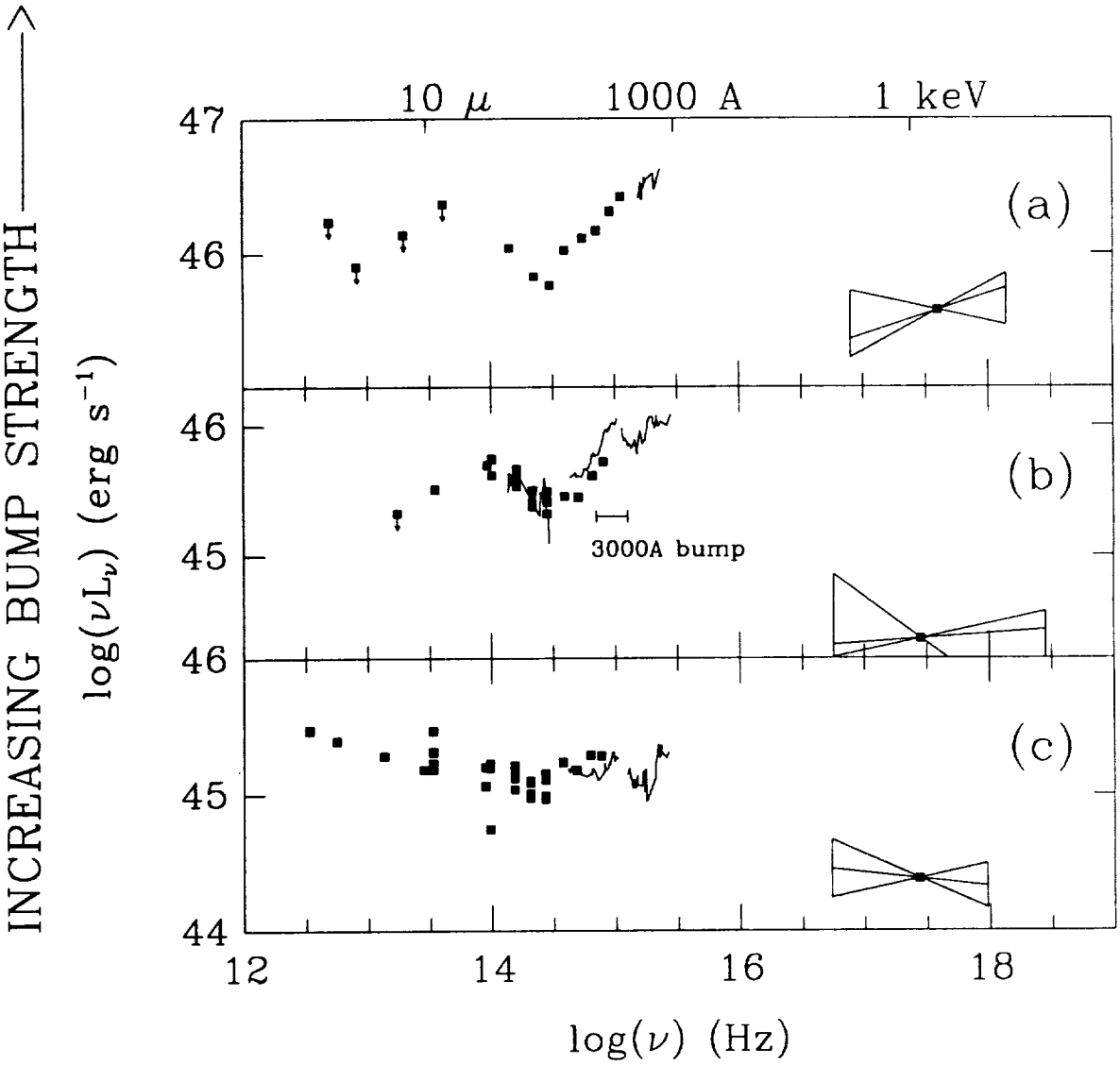
INCREASING BUMP STRENGTH
10 μ
1000 A
1 keV
47
46
46
45
46
45
44
(a)
(b)
(c)
3000A bump
12
14
16
18
log(νL_ν) (erg s^-1)
log(ν) (Hz)

Figure 2

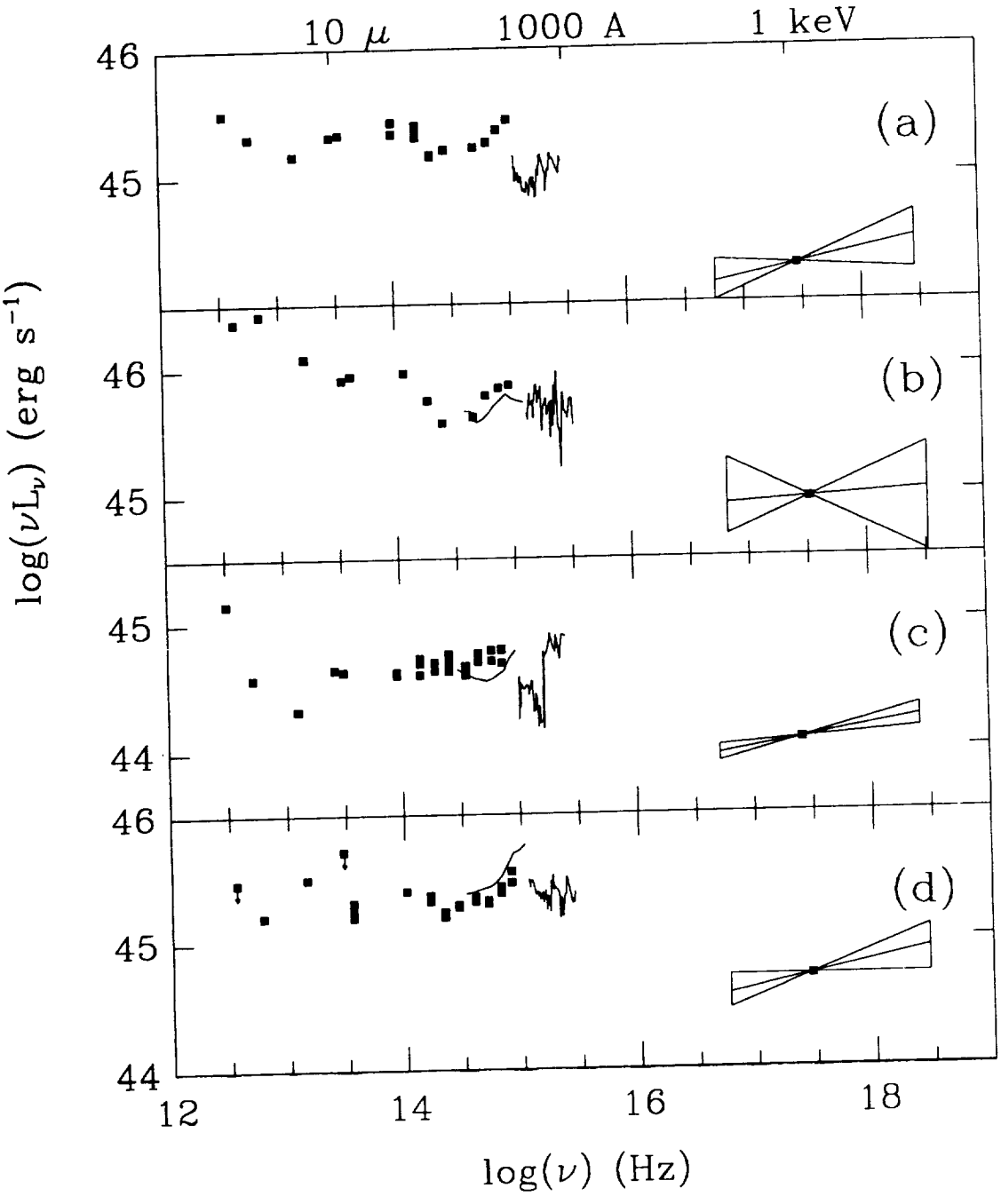
10 μ
1000 A
1 keV
(a)
(b)
(c)
(d)
46
45
46
45
45
44
46
45
44
12
14
16
18
log(νL_ν) (erg s^-1)
log(ν) (Hz)

Figure 3

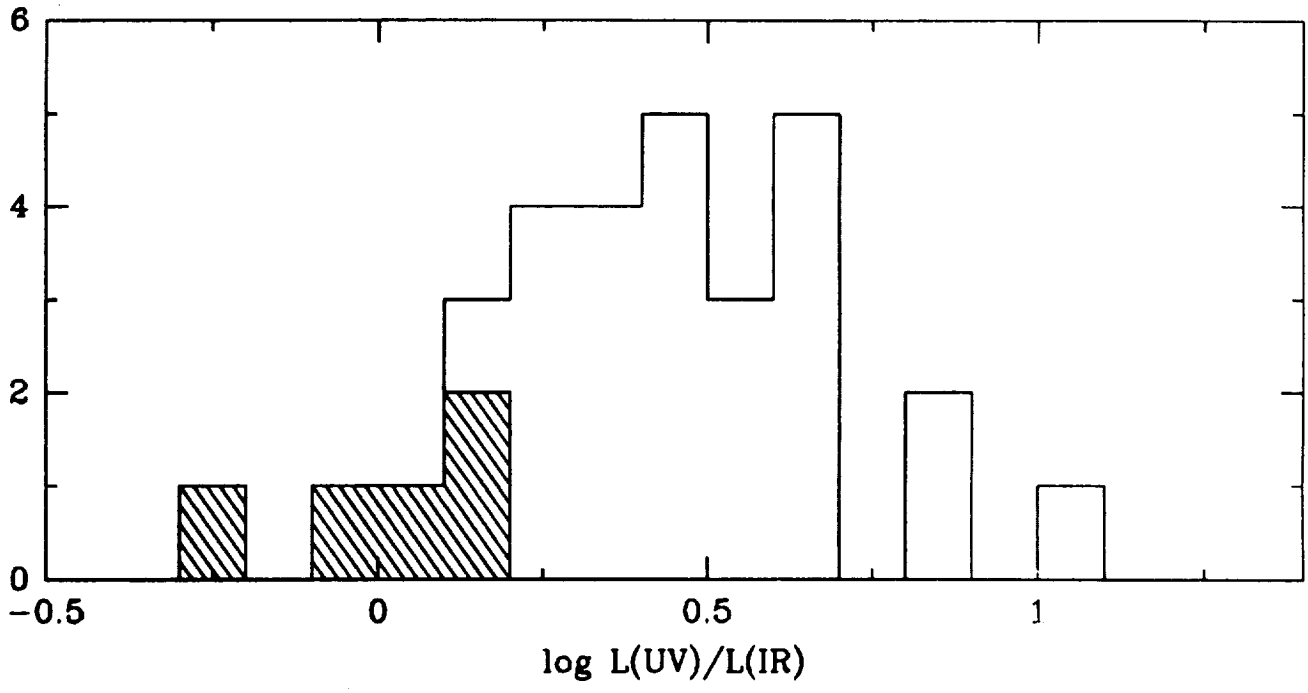

Figure 4

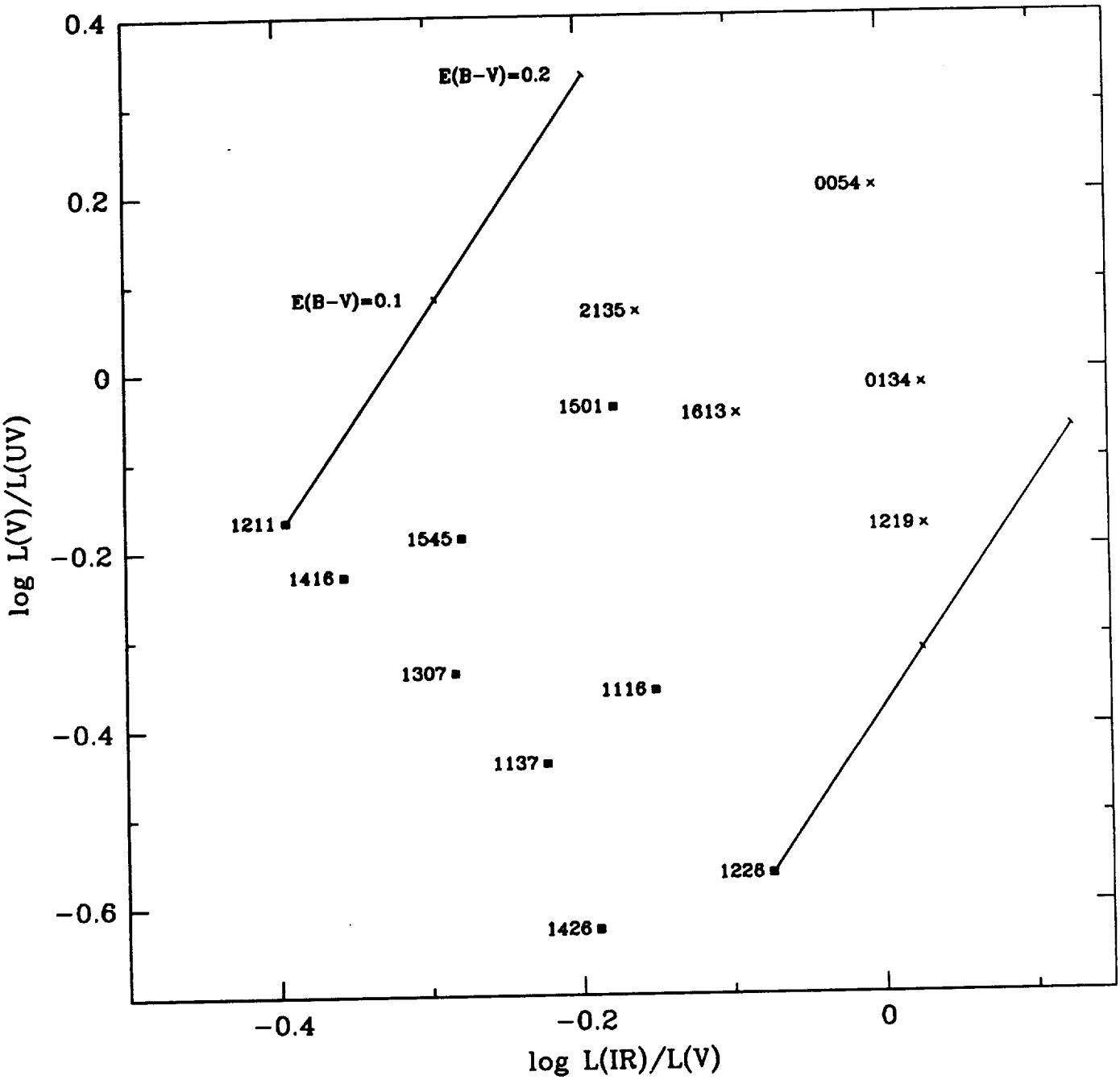
0.4
0.2
0
−0.2
−0.4
−0.6
−0.4
−0.2
0
log L(V)/L(UV)
log L(IR)/L(V)
E(B−V)=0.2
E(B−V)=0.1
0054
2135
0134
1501
1613
1211
1219
1545
1416
1307
1116
1137
1226
1426

JONATHAN MCDOWELL, MARTIN ELVIS, BELINDA WILKES AND STEVEN WILLNER: Harvard-Smithsonian Center for Astrophysics, 60 Garden St, Cambridge, MA 02138

JILL BECHTOLD AND M.S. OEY: Steward Observatory, the University of Arizona, Tucson, AZ 85721

RICHARD GREEN: Kitt Peak National Observatory, NOAO, 950 N. Cherry, PO Pox 26732, Tuscon, AZ 85726

ELISHA POLOMSKI: Department of Astronomy, Boston University, 725 Commonwealth Ave., Boston, MA 02215

Mon. Not. R. astr. Soc. (1991) **248**, 91-100

Millimetre measurements of hard X-ray selected active galaxies: implications for the nature of the continuous spectrum

A. Lawrence,[1] M. Rowan-Robinson,[1] A. Efstathiou,[1] M. J. Ward,[2] M. Elvis,[3] M. G. Smith,[4] W. D. Duncan[4] and E. I. Robson[5]

[1] *Astronomy Unit, School of Mathematical Sciences, Queen Mary and Westfield College, Mile End Road, London E1 4NS*
[2] *Royal Greenwich Observatory, Madingley Road, Cambridge CB3 0HA*
[3] *Center for Astrophysics, 60 Garden Street, Cambridge, MA 02138, USA*
[4] *Joint Astronomy Centre, 665 Komohana Street, Hilo, Hawaii 96720, USA*
[5] *School of Physics and Astronomy, Lancashire Polytechnic, Preston PR1 2TQ*

Accepted 1990 August 10. Received 1990 August 10; in original form 1990 January 22

SUMMARY

We report measurements of 11 hard X-ray selected active galaxies at 800 and 1100 μm made with the James Clerk Maxwell Telescope, and discuss these in the context of the continuum energy distribution from radio to X-ray wavelengths. Four other radio-loud AGN were also measured. Radio-loud objects show a spectrum which decreases smoothly in flux to higher frequencies, and supporting evidence strongly suggests a non-thermal origin. For radio-quiet objects we report only upper limits, but in all cases the fall from 100 μm to 1 mm is steep, strongly suggesting that thermal emission dominates the far-IR emission. Any underlying synchrotron components must become self-absorbed by a few tens of μm, implying that such non-thermal sources would have sizes of the order light hours (in conflict with the lack of far-IR variability) and should be heavily dominated by Compton scattering. We examine the alternative possibility that IR emission is entirely due to thermal dust re-emission of the observed UV continuum. Using a physical model in which we solve the radiative transfer through a spherical dust cloud, we find that to explain both the continuum shape over 5 μm to 1 mm, and the lack of silicate absorption, we require a region with $\tau_{uv} \sim 10$, and with density following r^{-1}. To explain the continuum near 1 μm seems to need a strong stellar component, even in the unresolved nucleus, but we argue that such a nuclear star cluster may in fact be present. The strongest objections to such thermal models are the unexplained fine-tuning required, and a possible energy balance problem.

1 INTRODUCTION

Our picture of the spectral distribution of the continuous radiation from active galactic nuclei (AGN) has improved dramatically in the last few years, especially following the availability of far-infrared (far-IR) data from the *IRAS* satellite (Miley, Neugebauer & Soifer 1985; Neugebauer *et al.* 1986; Edelson & Malkan 1986; Ward *et al.* 1987). The authors of the present paper, along with other collaborators, have been involved in collecting multi-wavelength data for AGN seen in hard X-ray all-sky surveys, and in particular for a complete flux limited sample taken from the *HEAO-A2* survey (Piccinotti *et al.* 1982). Broad-band data from 100 (*IRAS*) to 0.3 μm (*U*-band) have been discussed by Ward *et al.* (1987) and Carleton *et al.* (1987). VLA radio maps at 6 and 20 cm have been discussed by Unger *et al.* (1987). X-ray spectra from 0.1 to 20 keV, measured with *EXOSAT*, are discussed by Turner & Pounds (1989). Ultraviolet (UV) spectra, measured with *IUE*, will be discussed in Boisson *et al.* (in preparation).

Comparison of far-IR and radio data shows that the millimetre-wavelength region is of key importance, in the most general sense for delimiting the overall continuum shape, and specifically for critical tests of emission mechanisms. This is especially true for radio-quiet AGN, where there is a drop of several decades in νF_ν between available far-IR and radio data (see the discussion by Lawrence 1987). Millimetre facilities have recently improved to the extent that observations of extragalactic radio-quiet objects are now feasible: at wavelengths of 1 mm and shorter on the James Clerk Maxwell Telescope (e.g. this paper and Edelson *et al.* 1988), and wavelengths of 1.3 mm and longer on the IRAM facility

(Chini, Kreysa & Salter 1987; Chini *et al.* 1988; Chini, Kreysa & Biermann 1989). In this paper we present 1.1- and 0.8-mm measurements of three radio-loud and eight radio-quiet hard X-ray selected AGN (which together constitute roughly one-third of the complete Picinotti sample), and four other radio-loud AGN.

We then proceed to discuss the overall radio to optical energy distributions, in the light of the new measurements. The most contentious issue remains whether the continua of radio-quiet objects are dominated by thermal or non-thermal emission mechanisms. It seems likely that varying combinations of both are required (Carleton *et al.* 1987), but for the purposes of this paper we examine critically the consequences of extreme assumptions in either direction.

It should be noted that throughout this paper, we present plots of log νF_ν versus log ν. There are two reasons why νF_ν is preferred to F_ν for diagrammatic purposes: (i) νF_ν is energy per unit $\log_e \nu$, and so is easier for the eye to mentally integrate when plotted against log ν; and (ii) over a large range in frequency, AGN energy distributions show νF_ν constant to within an order of magnitude. Plotting νF_ν then enables one to reduce the vertical plot range, and so emphasize details in the shape. We shall, however, preserve the traditional notation for spectral index in the positive form, i.e α is defined by $F_\nu = \nu^\alpha$. Where applicable we assume a Hubble constant of $H_0 = 50$ km s^{-1} Mpc^{-1}.

2 OBSERVATIONS

The observations were made during 1988 January 30 to February 1, on the UK–Netherlands–Canada submillimetre facility, the James Clerk Maxwell Telescope (JCMT), on the island of Hawaii. The JCMT is a 15-m segmented parabolic dish with chopping secondary. The secondary mirror distance is continuously adjusted as a function of telescope altitude and azimuth to keep focus during the homologous deformations of the dish. The photometer used was the common-user millimetre/submillimetre bolometer system, UKT14 (Duncan *et al.* 1990). To reduce background noise and sky fluctuations, standard techniques of chopping and nodding were employed, with a beam separation of 60 arcsec in azimuth at a chopping frequency of about 7 Hz.

The UKT14 system is equipped with filters that are relatively narrow and well matched to the atmospheric bands. This both reduces sky-noise, and minimizes colour effects in calibration. The effective frequencies of the observations are given by the expression

$$\tilde{\nu} = \frac{\int_0^\infty \nu F(\nu) D(\nu) d\nu}{\int_0^\infty F(\nu) D(\nu) d\nu},$$

where $F(\nu)$ is the source spectrum, and $D(\nu)$ is the responsivity curve, including telescope, detector, filters and atmosphere. For reasonably good conditions, with Precipitable Water Vapour (PWV) = 1 mm, and assuming a source spectrum $F_\nu = \text{constant} \times \nu^\alpha$ with $\alpha = +2$, the effective frequencies (wavelengths) of the '1100', '800' and '450' broad-band filters are 277 GHz (1082 μm), 385 GHz (779 μm) and 672 GHz (446 μm), respectively. Changing the assumed source spectral index from $\alpha = +2$ to $\alpha = -1$ changes these values by less than 10 per cent in all cases. Most of our calibrators and targets have spectra rising steeply towards short wavelengths, so we choose the effective frequencies appropriate to PWV = 1 and $\alpha = +2$ to be the frequencies at which we estimate a monochromatic calibration. The uncertainty caused by colour effects will almost certainly be smaller than our main uncertainties due to (i) determination of atmospheric optical depth, and (ii) pointing errors.

The primary calibrators used were the planets Jupiter and Mars. The quasar 3C 273, bright enough on the JCMT to be visible in real time on the strip chart, was also used to check the estimation of optical depth, on the assumption that it did not vary significantly in the course of a night. Planet fluxes and angular sizes for the dates in question were obtained from the JCMT FLUXES program, as discussed by Duncan *et al.* (1990). To perform the calibration at our chosen frequencies, we assume that both planets have spectral index $\alpha = +2$. We also assumed that all of our targets were point sources. (This may not be quite true, as for some of the radio-quiet AGN, dust emission from the parent galaxies may be comparable with the nuclear emission). The fluxes from extended planetary sources therefore require beam correction. To perform this correction, we assumed that the planets were discs of uniform surface brightness, and that the telescope beam was of Gaussian shape, with Half Power Beam Width (HPBW) = 19 arcsec at both 1100 and 800 μm. As the observed ratio of signals from Mars and Jupiter agreed with prediction within a few per cent, we have reasonable confidence in both the beam correction and the overall calibration.

At the time of our observations, the system zero-point was not very well known, so we determined both zero-point and atmospheric optical depth from observations of Jupiter and Mars at a range of airmasses. We assumed a plane parallel atmosphere, and so determined calibrations between instrumental units and F_ν of the form $\log_e(\text{Jy/mV}) = A + B \times$ airmass. The optical depths B on the two good nights of the run were found to be ~ 0.05 and 0.15 for 1100 μm and ~ 0.3 and 0.65 for 800 μm. From the scatter in these calibrations, we believe that changes in optical depth may lead to errors in the derived fluxes of typically 10 per cent up to 20 per cent.

The other major uncertainty arises from pointing errors. The brighter objects allowed 'peaking-up' before a photometric measurement. (In subsequent data reduction we discarded a few objects measured in this way, where we felt that the peaking-up measurements were not of high enough signal-to-noise ratio.) The procedure for blank fields was to peak-up on the nearest mm-bright object and then to offset to the target. Planets were peaked-up by hand. Other bright objects were measured at five positions – nominal pointing position, and north, south, east and west by half a beam-width. Local pointing offsets were then derived from the fitted profile. To ensure greater accuracy, this procedure was repeated until a good centred fit was obtained. However, there remain systematic errors in the telescope pointing model, and secular drifts over periods of time. Since our observing run in 1988 January/February, both kinds of problem have been substantially reduced. Given the beamsize of ~ 19 arcsec HPBW, it is necessary to maintain pointing to within ~ 3–4 arcsec to keep flux calibration errors within 10 per cent. Experimentation on the nights in question showed that this required re-pointing roughly every fifteen minutes, which was done. Even so, we cannot, of course, completely

dismiss occasional larger errors. The upper limits quoted in this paper are derived from many observations over extended periods at a variety of telescope altitudes and azimuths, so that completely missing a detectable source is very unlikely. Nonetheless, occasional pointing problems for blank-field sources may have led to substantial net errors.

The primary targets were AGN selected by hard X-ray emission. Eleven of these were measured. We also examined four other radio-loud AGN. The results are summarized in Table 1(a) and (b). The signal-to-noise and formal error are based only on the *statistical* noise, estimated from the scatter within individual integrations; it should be remembered that the real uncertainties are of the order ~ 30 per cent for bright objects, and possibly substantially larger for blank fields. Where the formal significance of the measurement is below 5 σ, we have also quoted an upper limit. Because of the possible pointing problems, we quote a conservative 3-σ limit, rather than the more usual 1- or 2-σ limit.

2.1 Comparison with other measurements

Observations of the radio-quiet members of our X-ray selected sample represent the first ~1-mm wavelength measurements of these objects deep enough to allow detailed discussions of their emission mechanisms. [Note, however, that Edelson *et al.* (1988) have measured NGC 4151 at 438 μm using the same system.] Three radio-loud objects in the sample have been measured previously by other workers. The quasar 3C 273 has been measured many times and is clearly variable at mm wavelengths (Elias *et al.* 1978; Ennis, Neugebauer & Werner 1982; Clegg *et al.* 1983; Robson *et al.* 1983; Landau *et al.* 1986; Robson *et al.* 1986; Courvoisier *et al.* 1988; Robson *et al.*, in preparation). We found it at a fairly typical flux level. It seems likely that the 1-mm measurement by Landau *et al.* (1986), at 69.9. Jy, is in error, especially as their 1-mm measurement is higher than both their 3-mm and their 350-μm measurements. Our measurement of IIIZW2 is lower than, but statistically consistent with, the 4-σ measurement of Ennis *et al.* (1982). Our measurement of MKN 501 is also lower than that of the latter authors, but in good agreement with Joyce & Simon (1976), assuming a spectral index of ~ 0, as is typical for blazars.

For our other targets, PKS1413 and OJ287 are in good agreement. Our measurement of 3C 446 is somewhat lower than the UKIRT measurement made by Gear *et al.* (1985) but again the difference is statistically marginal, as the older measurement is of low significance. This object is known to be variable, as shown by the results of the monitoring campaign by the Preston group (Gear *et al.* 1985; Brown *et al.* 1986; Brown *et al.* 1989a,b).

3 RADIO TO OPTICAL CONTINUA

We now combine our new millimetre wavelength measurements with the radio core data (from Unger *et al.* 1987, and references therein), with *IRAS* data, with Kuiper Airborne Observatory (KAO) data, and with ground-based near-mid-IR and optical broad-band data (all from Ward *et al.* 1987, and references therein). We also add some data from pointed *IRAS* observations (Elvis *et al.*, in preparation). For NGC 4151 we also include far-IR and submillimetre data from Engargiola *et al.* (1989), and Edelson *et al.* (1988). Except where noted in the text, optical–near-IR data are nuclear point-source measurements, having been corrected for extended parent galaxy starlight by the methods described in Ward *et al.* (1987). Whether this correction actually removes all the starlight will be discussed in Section 4.3. The broad-band measurements will be contaminated to some extent by emission lines, but as we are here considering the gross shape of the continuum over many decades in frequency, this problem should not be too important. It should also be remembered that the measurements at various wavelengths are not in general simultaneous, so there may be some distortion of the continuum shape. This is much more likely to be a problem for the radio-loud objects in the sample, which all have 'blazar'-like cores.

The continuum energy distributions are shown in Fig. 1(a)–(c) corresponding to groups classified as explained in the subsections below. In this paper we are concentrating on the radio to optical continua but, for reference, we also indicate the νF_ν level at 6 keV.

Table 1. (a) Hard X-ray selected AGN. (b) Other AGN.

(a)	RESULTS FROM THIS PAPER					Previous measurements		
(1) NAME	(2) $\lambda(\mu m)$	(3) date	(4) F_ν(mJy)	(5) 3σ limit	(6) α_{IR-mm}	(7) $\lambda(\mu m)$	(8) F_ν(mJy)	(9) ref.
N2992	779	30/1/88	80±24	<152	+2.63			
	1082	30/1/88	47±34	<149				
N3227	1082	31/1/88	22±42	<148	> +2.03			
N4151	779	30/1/88	5±17	<55	> +2.47	438	<200	(6)
						3000	<270	(7)
N4593	1082	31/1/88	31±22	<97	> +1.76			
N5506	1082	31/1/88	11±17	<62	> +2.15			
N7314	1082	31/1/88	-20±29	<87	> +2.13			
IC4329A	1082	31/1/88	3±14	<45	> +1.56			
3C 273	1082	30/1/88	15150		−0.6	1000	see text	
	1082	31/1/88	15996					
	779	30/1/88	11666					
MKN 501	1082	30/1/88	411±34		−0.6	1000	800±200	(1)
	779	30/1/88	375±21			3200	370±60	(8)
MKN590	1082	31/1/88	-34±21	<63	> +1.34			
IIIZW2	1082	31/1/88	207±22		−0.16	1000	800±200	(1)

(b)	RESULTS FROM THIS PAPER				Previous measurements		
(1) NAME	(2) $\lambda(\mu m)$	(3) date	(4) F_ν(mJy)	(5) 3σ limit	(6) $\lambda(\mu m)$	(7) F_ν(mJy)	(8) ref.
3C446	1082	31/1/88	2783±68		800	3900±1000	(4)
					1100	6800±1700	(4)
					2000	5800±400	(4)
PKS1413	1082	31/1/88	1734±14		1100	1700±400	(4)
OJ287	1082	31/1/88	3531±63		1100	4000±1000	(4)
					1000	4900±500	(1)
					1000	8090	(5)
					1000	3500 - 6000	(2)
					3300	2640±290	(3)
NRA0530	1082	30/1/88	1563±41				
		30/1/88	1251±31				

Notes to columns: (2) effective wavelength as explained in text; (3) local calendar date at start of night; (4) error quoted is statistical error only. Systematic uncertainty in fluxes is of the order 30 per cent; (5) limit is formal estimate or 0 (whichever is greater) + 3σ; (6) spectral index between 100 μm and 779 or 1082 μm as appropriate. For MKN 501, have used 60-μm flux, as 100-μm measurement is an upper limit. (8) References: (1) Ennis *et al.* (1982); (2) Roellig *et al.* (1986); (3) O'Dell *et al.* (1978); (4) Gear *et al.* (1985); (5) Landau *et al.* (1986); (6) Edelson *et al.* (1988); (7) Blitz, Mathieu & Bally (1986); (8) Joyce & Simon (1976).

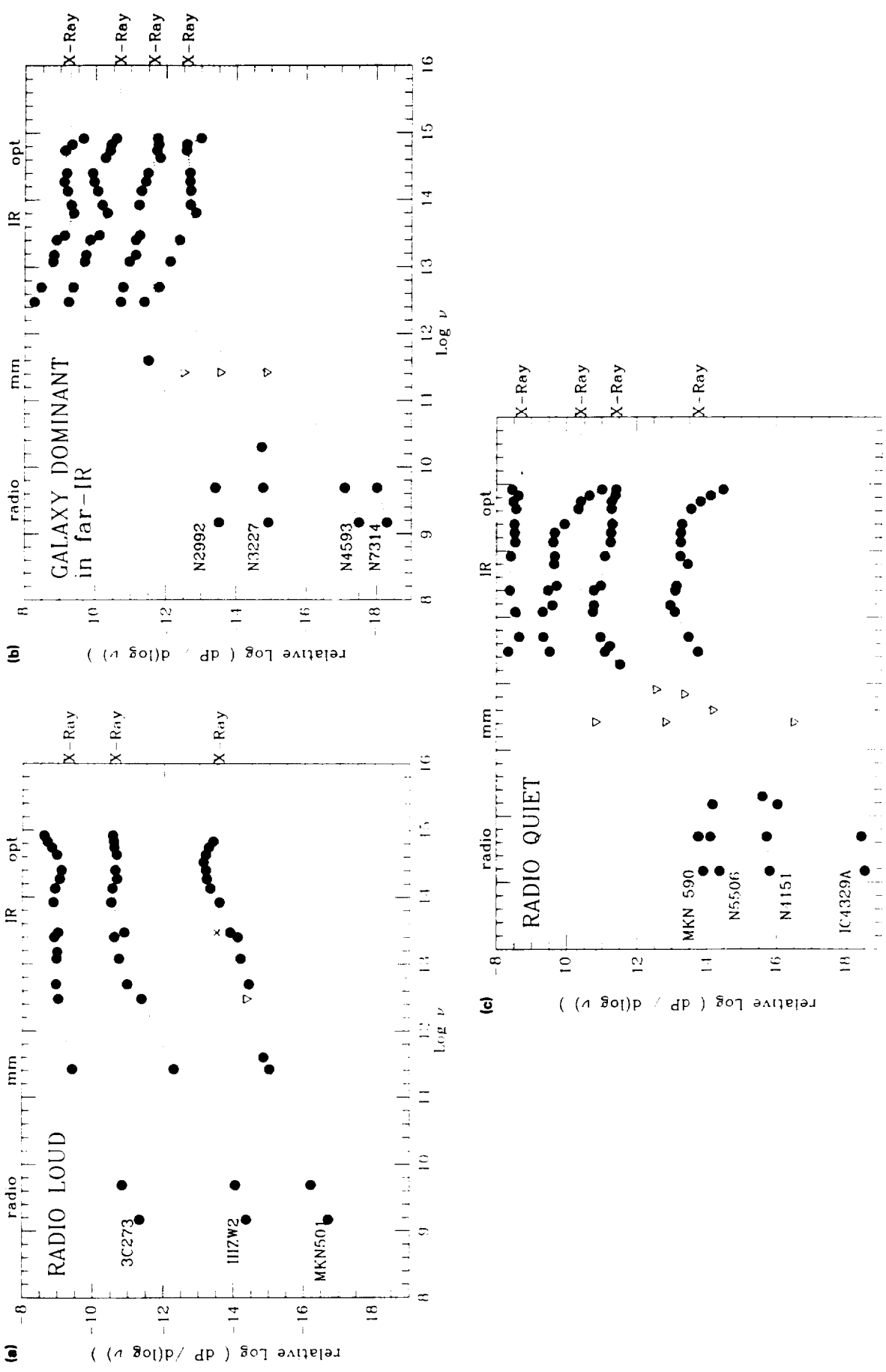

Figure 1. Radio through optical energy distributions for the 11 target galaxies. Data points at 1.1 and 0.8 mm are from this paper, other data as discussed in text. The vertical axis has been arbitrarily scaled in each case to accommodate several objects on one graph. Triangles indicate upper limits. The dotted lines are present only to connect points referring to the same object, and should not be taken as an indication of the intervening continuum. Horizontal dotted lines indicate the νF_ν level of 6-keV X-rays. The targets are divided into three groups as discussed in the text.

3.1 Radio-loud objects

Three of the 11 objects show energy distributions which are continuous throughout the optical–radio region (see Fig. 1a). These, of course, are all objects which have traditionally been classified as 'radio-loud'. The overall shape could be described either by a continuously curving spectrum (Landau *et al.* 1986), or by a series of power laws with self-absorbed synchrotron components in the mm to cm regime (Brown *et al.* 1989a). To second order, there are clear complications to the simple picture. The quasars 3C 273 and IIIZW2, show UV turn-ups, as is typical for quasars in general. The BL Lac object MKN501 shows a peak in the near-IR, presumably due to residual starlight – note that in this case the near-IR data are from uncorrected 5-arcsec aperture measurements. 3C 273 shows another peak at ~ 4 μm, which could well be due to hot dust in or near the broad emission-line region (Courvoisier *et al.* 1988).

So we see that, although the overall smoothness of the energy distribution over many decades of frequency is consistent with the idea that the continua of these objects are dominated by non-thermal radiation of some kind, in detail the explanation of these energy distributions may not be altogether simple. However, for these objects there is strong independent evidence for relativistic effects and generally non-thermal nature: superluminal motions, high polarization and large-scale variability. What we will stress below is that such supporting evidence is noticeably absent in radio-quiet objects.

3.2 Radio-quiet objects

The energy distributions of the remaining eight objects in the sample all show a dramatic fall from 100 μm to 1 mm (see Fig. 1b and c; Table 1a). Where the spectral index is greater than 2.5, this does not strictly rule out synchrotron emission as is commonly assumed, as steeper slopes are possible (de Kool, Begelman & Sikora 1989; de Kool & Begelman 1989). A break of some kind between the far-IR and radio data was, of course, previously required, but our new data refine the position of this break by two decades in frequency. Regardless of the nature of the IR continuum, these objects may all be called radio-quiet in the objective sense that the νF_ν level at 6 cm is typically 2–3 decades below that at 6 keV, compared to the objects in Fig. 1(a), where the difference is typically 1 decade. We caution, however, that 'radio-loudness' may be a continuous variable, rather than a bi-modal quantity (Unger *et al.* 1987; Lawrence 1987). These objects, in contrast to the radio-loud objects, are not known to show high polarization, dramatic variability, or superluminal motions, so any postulated non-thermal nature of the optical-IR continuum is on rather weaker ground. In particular, of course, given the steep fall from 100 μm to 1 mm, it is likely (though not certain) that the far-IR emission is dominated by thermal emission from dust. Similar conclusions have been arrived at recently for optically selected radio-quiet quasars, following measurements at 1.3 mm (Chini *et al.* 1989).

For the objects in Fig. 1(b), the case for thermal emission in the far-IR is fairly strong. In all these cases, νF_ν is rising to long wavelengths through the far-IR, with a slope typical of normal spiral galaxy disc 'cirrus' emission (Rowan-Robinson & Crawford 1989). These are all relatively nearby, low-luminosity Seyfert galaxies, so the large *IRAS* apertures are dominated by normal galaxy emission rather than the relatively weak nuclear emission, as discussed by Ward *et al.* (1987). The level of any underlying non-thermal continuum emission may be indicated either by the X-ray νF_ν level (assuming the spectral index to be roughly -1), or by the low points in the 1–100-μm continuum, as argued by Carleton *et al.* (1987). Such a power-law component would still need to become self-absorbed by ~ 1–200 μm, if it is not to exceed our millimetre upper limits. We also note that there is a tendency for these objects to show peaks around 1–2 μm, despite the 'starlight subtraction' performed by Ward *et al.* (1987).

The objects in Fig. 1(c), unlike those in Fig. 1(b), are not obviously dominated by parent-galaxy interstellar cirrus emission. The steep fall from the far-IR to our mm upper limits requires that a power-law component dominating in this region must certainly cut-off by 100 μm. (More stringent limits, of a few tens of μm, will be discussed in Section 4.1) However, it is not at all clear that such a power-law component is dominant. Both N4151 and IC4329A show clear peaks around 25 μm, and curve slowly down thereafter, strongly suggestive of a thermal component. Both N5506 and IC4329A show downturns in the optical. This is almost certainly due to reddening of a few magnitudes, consistent with the observation of large Hα/Hβ ratios, and small Hα/X-ray ratios (Ward *et al.* 1987).

For N4151, N5506, and IC4329A, the mid-IR νF_ν level is a factor of several above the 6-keV level, whereas for radio-loud objects it is level or below, apparently indicating an 'IR excess' in radio-quiet objects. Alternatively, this could be interpreted as an 'X-ray excess' in radio-loud objects. Indeed, it seems that radio-loud quasars are more X-ray luminous for a given optical luminosity, than are radio quiet quasars (Zamorani *et al.* 1981; Kembhavi, Feigelson & Singh 1986), possibly due to an extra flat X-ray component in radio-loud objects (Wilkes & Elvis 1987). At first glance, MKN 590 seems to be a flat power law, but in detail it has a turn-up from 60 to 100 μm (suggesting a galaxy disc component) and also shows a weak maximum at 25 μm.

4 DISCUSSION

The importance of dust is clear in objects with reddened optical continua or steep IR continua. However, even in radio-quiet objects with flat energy distributions (MKN 590, NGC 4151), the presence of local peaks and curvature rules out pure power-law models. Contributions due to dust heated by the UV excess source, and by interstellar cirrus and star-formation regions in the parent galaxy, must at least be taken into account. However, non-thermal emission could still be the dominating component in many wavelength regions. In Section 4.1 we fit maximal power-law models to MKN 590 and NGC 4151, and discuss briefly whether the physical characteristics of such synchrotron sources are reasonable. Given the lack of direct evidence (polarization, variability) for non-thermal emission, we might conservatively assume that all emission is thermal. The immediate problem for such a position is that around 1 μm neither dust emission nor the UV excess will contribute significantly. In Section 4.2 we discuss the possibility that the required extra component is starlight from a nuclear star cluster. In Section

4.3 we then proceed to compare the energy distributions of NGC 4151 and MKN 590 with multi-component thermal models. A reasonable match requires rather fine tuning of model parameters.

4.1 Maximal power-law model fits

Examples of maximal power-law fits are shown in Fig. 2(a) and (b). There is, of course, no unique solution unless models for the obvious excess components are also included, but the range of models shown gives us an indication of constraints on the self-absorption frequency, which in either case must be $\lambda_A < 75$ μm, and probably much less if we wish to minimize the mid-IR excesses. We can then derive physical characteristics of the synchrotron source: diameter d, brightness temperature T_b, equipartition magnetic field B, and ratio R of photon to magnetic field energy densities. In the discussion below we assume that the synchrotron source has a filling factor of unity, and that the ratio of proton to electron energy content is 100.

For NGC 4151, $\lambda_A = 75$ μm implies $d = 10$ light-hours, $B = 148$ G, $T_b = 4.8 \times 10^{10}$ and $R = 10$. If we do not assume equipartition but instead that $T_b = 10^{12}$, as usually seems to be the case for compact radio sources (Kellerman & Pauliny-Toth 1981), then $d = 2$ light-hours, $B = 543$ G and $R = 10^5$. In either case, most energy should emerge via Compton scat-

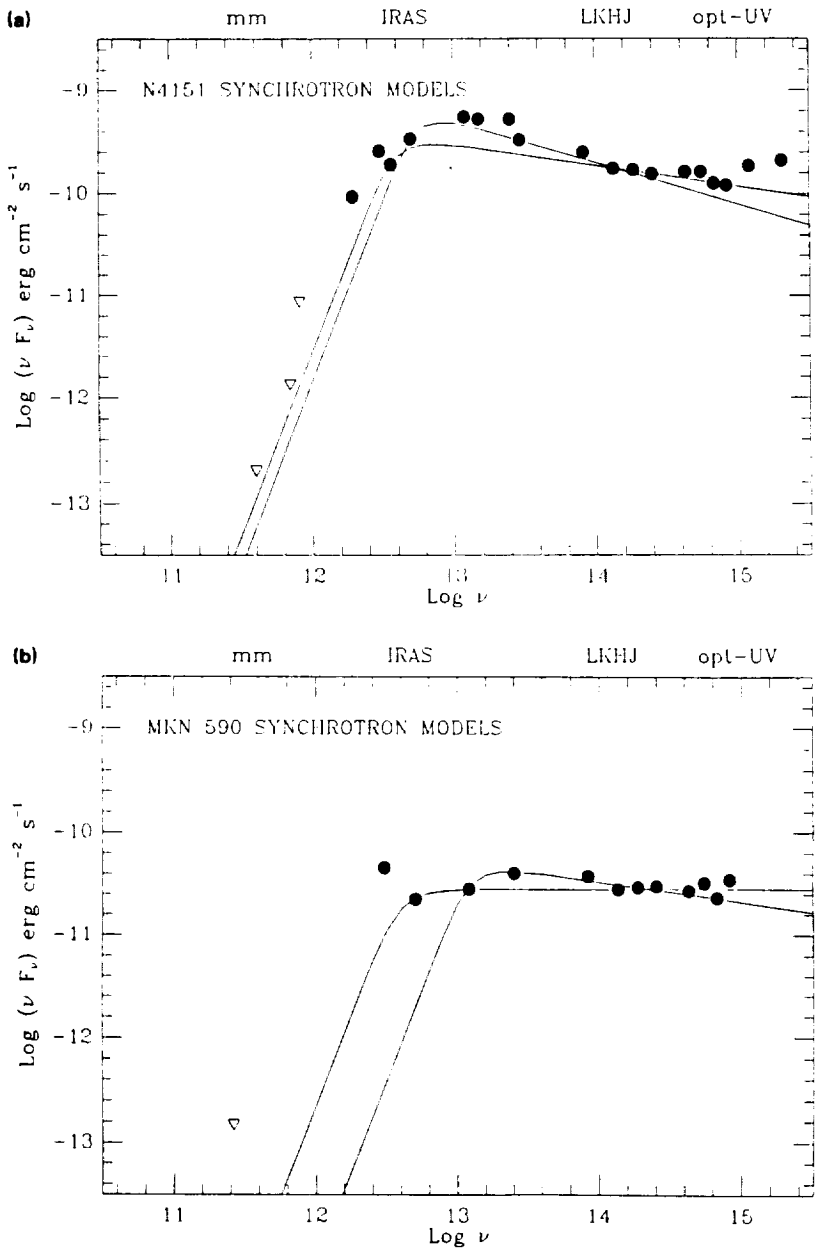

Figure 2. Self-absorbed homogeneous synchrotron models compared to the observed energy distributions. The turnover region is modelled as $F_\nu = \text{constant}(\nu/\nu_A)^{5/2}(1 - e^{-\tau_\nu})$, where the optical depth to self-absorption follows $\tau_\nu = (\nu/\nu_A)^{\alpha - 5/2}$. (a) NGC 4151. Models shown have spectral index and self-absorption wavelengths of $\alpha = -1.2$, $\lambda_A = 75$ μm and $\alpha = -1.4$, $\lambda_A = 54$ μm. (b) MKN 590. Models shown have $\alpha = -1.2$, $\lambda_A = 24$ μm and $\alpha = -1.0$, $\lambda_A = 75$ μm.

tering rather than synchrotron radiation. The observed X-ray luminosity of NGC 4151 is similar to the observed synchrotron luminosity, but as the spectral index of the X-ray emission is ~ 0.55 (Yaqoob, Warwick & Pounds 1989), it is patently not the corresponding Inverse Compton component. For MKN 590, $\lambda_A = 75$ μm implies $d = 2$ light-hours, $B = 1.2 \times 10^3$ G, $T_b = 6.2 \times 10^{11}$ and $R = 100$.

With $H_0 = 100$, T_b would be a factor of 4 lower, and d a factor of 2 lower. The large uncertainties in proton/electron ratio and filling factor result in uncertainties in d and B of factors of several, but not orders of magnitude. The very small sizes derived here therefore constitute a problem for synchrotron models, as an extensive study shows no variability in the *IRAS* bands for radio-quiet AGN (including NGC 4151), to a level of 15 per cent over one year (Edelson & Malkan 1987). In contrast, the same study demonstrates strong variability in several radio-loud objects.

4.2 A nuclear starlight component?

The data for NGC 4151 and MKN 590 that we use have in principle been corrected for parent galaxy starlight (Ward *et al.* 1987). This involved modelling CCD photometry with a point source of arbitrary colours, and an exponential disc and $r^{1/4}$ bulge with fixed colours representative of a late-type stellar population. However, if a nuclear star cluster is present, this will have been included in the point-source component. Even in quasars, an inflection point in the continuum consistently occurs around 1 μm and noticeably, the minimum is deepest for the most luminous quasars (Kriss 1988). It seems possible therefore that a point-source stellar component is common in AGN. Note that even at the relatively small redshift of NGC 4151 ($z = 0.0033$), requiring that such a starlight component be unresolved (~ 1 arcsec) only requires it to be ~ 100 pc across. [Ebstein, Carleton & Papaliolis (1989) find from speckle observations that NGC 4151 has an unresolved component of size 0.3 arcsec, but this is at 5000 Å.] The luminosity in such a stellar component for NGC 4151 is roughly equivalent to 10^7 K0 giants. Such a nuclear star cluster may provide the material for the broad-line clouds, and the fuel for accretion (Hills 1975; Penston 1988).

The obvious stellar feature to look for is the Ca II triplet at ~ 8542 Å. Unfortunately Ca II often appears in emission in broad-line objects (Persson 1988). It certainly appears in absorption in NGC 4151, but there is some controversy over the strength. Malkan & Fillipenko (1983) give a value of 1.1 Å for the equivalent width of one component of the triplet, Ca II 8542 Å, in the unresolved nuclear seeing disc, compared to an average value for spiral galaxies of 3.2 Å. Recent higher resolution work by Terlevich, Diaz & Terlevich (1990), however, indicates an equivalent width of 2.9 Å. These authors quote an equivalent width for the whole triplet of 6 Å – not very different from the average value they find in normal early-type spirals (7.7 Å). Similar results are found by Terlevich *et al.* for two other Type 1 Seyfert galaxies, NGC 3227 and 3516. This suggests a more or less undiluted normal old stellar population of red giants, in contrast to the substantial dilutions of the *G*-band and Mgb features seen at shorter wavelengths (Malkan & Fillipenko 1983; Terlevich *et al.* 1990). Alternatively the large Ca II equivalent width could represent a ~ 50 per cent dilution of young stars, i.e. red supergiants (Terlevich *et al.* 1990).

The continuum at ~ 1 μm cannot be entirely due to stars, as there is some variability, but it is consistently smaller than the blue-light variability, even for quasars (Cutri *et al.* 1985). For example, in the case of NGC 4151, Lebofsky & Rieke (1980) describe observations in an 8.6-arcsec aperture where the *U*-band varied by a factor of 2.5, but the *R*-, *I*-, *J*-bands by only 25 per cent. (In this example, variability increased again at longer wavelengths.) If the wavelength dependence of variability amplitude seen in NGC 4151 is due to dilution, we can conclude that the variable component contributes only 14 per cent of the light in the low-state, or 35 per cent in the high-state.

4.3 Purely thermal model fits

Here we consider all components that may be present to some degree – the UV excess, interstellar cirrus, star-formation regions, starlight, and dust heated by the UV excess. The latter is, of course, the most controversial and interesting part, so we develop a physical model for this region, whereas for the other components we use templates of fixed shape. (i) The UV excess is modelled as a single blackbody at 30 000 K. (ii) Following Rowan-Robinson & Crawford (1989), we model the interstellar cirrus as the sum of two greybodies, at 210 and 30 K, which provides a good fit to the spectrum of the interstellar medium in our own Galaxy (Boulanger, Baud & van Albada 1985; Hauser *et al.* 1984). We should note, however, that the 12-μm excess may be due to very small grains, so that in a galaxy with a powerful Seyfert nucleus, the hotter component may be absent. (iii) For the *star-formation* component, we use the model derived by Rowan-Robinson & Crawford (1989), which fits the IR–mm spectra of both hot-centred clouds in our own Galaxy, and the starburst ring in NGC 1068. (iv) The *nuclear starlight* component is modelled by the sum of blackbodies at 3000 and 5000 K, which we find adequately fits the bulge starlight colours quoted by Ward *et al.* (1987).

Finally, we consider a more detailed model of the dust intimately connected with the AGN itself. We assume that a dust shell surrounds and is heated by the UV excess source, with a density that falls off with radius as a power law. We then numerically solve the radiative transfer through this region (using the same software as Rowan-Robinson & Crawford 1989) in order to predict the detailed emergent IR–mm spectrum. The grain properties assumed are as in Rowan-Robinson (1982). The variable parameters are then the grain condensation temperature, the density-law slope, the UV optical depth, and the ratio of inner to outer radii. To first approximation, the overall spectral slope is fixed by the density law and optical depth. The melting temperature fixes the high-frequency cut-off, the outer radius fixes the low-frequency cut-off, and the optical depth also fixes the silicate feature strength. As well as matching the overall energy distribution, we aim to minimize the strength of the 9.7-μm silicate feature, as this is normally weak in Seyfert galaxies (Aitken & Roche 1985).

A fit to NGC 4151 is shown in Fig. 3(a). We assume that the far-IR is dominated by a strong starburst, and that most of the light in the *J*-band is due to starlight. What remains is

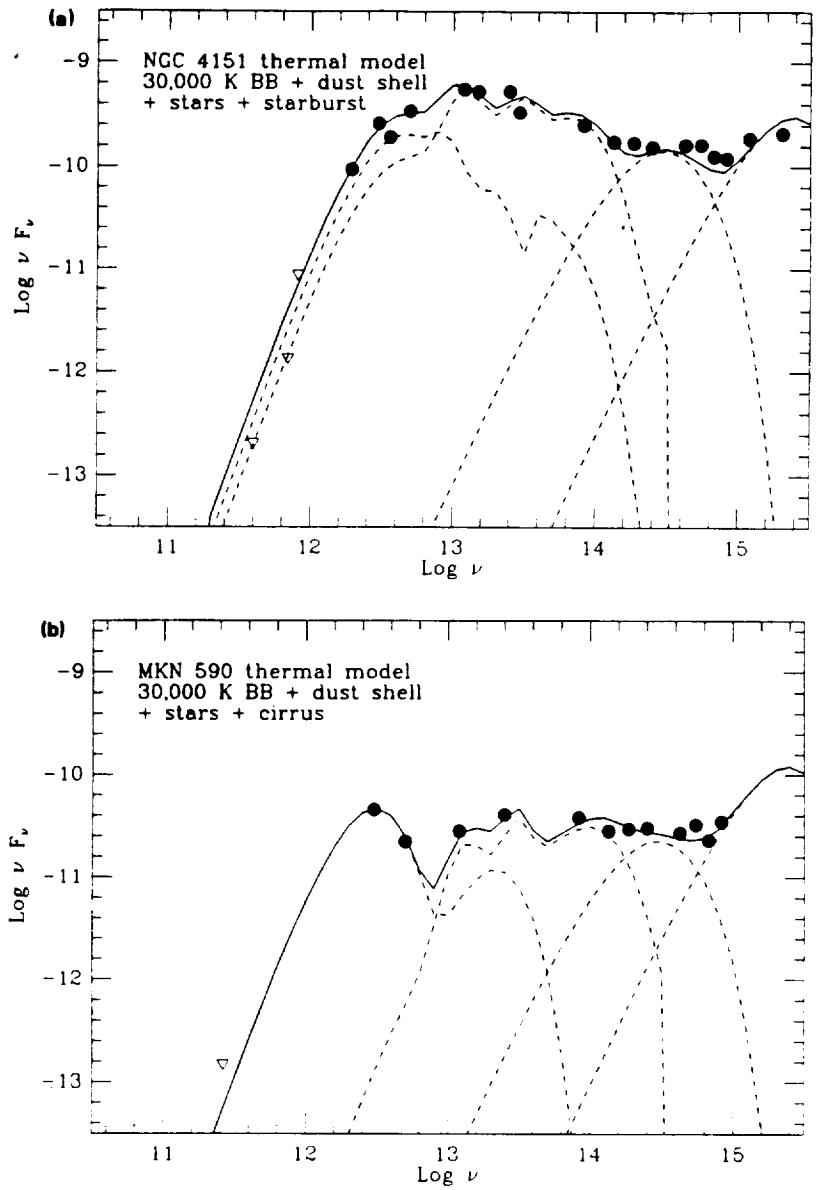

Figure 3. Thermal models compared to the observed energy distributions. (b) NGC 4151. The components used (discussed in more detail in the text) are the 30000-K blackbody, starlight, a star-formation region, and a dust shell with density law following r^{-1} and UV optical depth ~ 12. (b) MKN 590. The components used are the 30000-K blackbody, starlight, interstellar cirrus, and a dust shell with r^{-1} density law and UV optical depth ~ 6.

reasonably well-fitted by a dust-shell model with melting temperature 940 K, density following r^{-1}, $R_1/R_2 = 0.001$, and $\tau_{uv} = 12$. The optical depth needed to explain the continuum shape is close to that needed to minimize the size of the 9.7-μm silicate feature, but it is difficult to get these both perfect simultaneously. A fit to MKN 590 is shown in Fig. 3(b). Here we assume that the far-IR is dominated by cirrus, and that starlight dominates at *J*. What remains is well fitted by a dust-shell model that in some respects is very similar to that required for NGC 4151. Once again the density must follow r^{-1}, and the optical depth is of a similar order (6). However, the melting temperature required is slightly higher, 1380 K, and $R_1/R_2 = 0.01$ differs from NGC 4151 by a factor of 10.

With present broad-band data quality then, we can fit purely thermal models, but the physical properties of the dust shell need fine tuning. With future higher resolution data, the confrontation between model and data should become critical, as is obvious from the small-scale curvature of the model spectra. In particular, it is impossible to get the silicate features in both the 10- and 20-μm windows simultaneously minimized. From our model fits we expect to see the 20-μm feature weakly in emission. We therefore strongly encourage 20-μm spectroscopy of Seyfert galaxies. The most obvious contradiction in the modelling is that a spherical dust shell of such high optical depth would completely extinguish the UV source. One solution would be a patchy dust shell, and another would be a thick disc of dust, as

postulated to exist in the Seyfert 2 galaxy NGC 1068 to explain the optical spectropolarimetry (Antonucci & Miller 1985). Two of us (AE and MRR) have recently developed a two-dimensional numerical code for solving the problem of radiative transfer through dust in the axisymmetric situation (Efstathiou & Rowan-Robinson 1990). This will be applied to the Seyfert galaxy problem in future work.

The deduced luminosities in the heated dust component, and the observed UV component (up to 1500 Å) in NGC 4151 are $\sim 5\times10^{43}$ and 1×10^{43} erg s^{-1}, respectively. The XUV continuation of the UV component is extremely uncertain, and could result in several times more energy being available for heating, but a large covering factor would still be required to achieve consistency. However, if an optically thick disc model, such as envisaged for NGC 1068, turns out to be feasible, the energy available for heating could be very much larger, as hard X-rays will also be absorbed (via Compton scattering). The (2–10 keV) luminosity of NGC 4151 is variable, but of the order $\sim 5\times10^{42}$ erg s^{-1}. However, the γ-ray continuation suggests a total luminosity possibly as large as $\sim 10^{45}$ (Lawrence 1980).

5 CONCLUSIONS

New millimetre measurements have enabled us to examine the shape of the continuum from optical to radio wavelengths for hard X-ray selected AGN. Objects with strong radio cores are almost certainly dominated by non-thermal emission throughout the IR, mm and radio regions, but also show evidence for several secondary components and effects – the UV excess, reddening, residual starlight and some thermal dust emission. Objects with weak radio cores show a steep fall from the far-IR to mm wavelengths, as has also been recently found for optically selected quasars (Chini *et al.* 1989). Part of the emission from these objects is very likely to be thermal, but it is empirically possible to model the continuum shapes with and without a synchrotron power-law component. Such a synchrotron power-law component must, however, become self-absorbed by a few tens of μm. This implies a size of a few light-hours for the synchrotron source, in conflict with the lack of far-IR variability. Furthermore, such a synchrotron source should be heavily Compton-dominated. Confronted with these problems, and the fact that there is no supporting evidence for non-thermal phenomena, one might take the conservative stance that for such radio-quiet objects all the emission is thermal. The continuum shape longward of 2 μm can be duplicated by a combination of interstellar cirrus, star-formation regions, and a dust region heated by the observed UV source, if the dust shell has a density law following r^{-1}. An extra component is then needed, peaking around 1 μm. We suggest the existence of a nuclear star cluster, and argue that this idea is supported by the presence of Ca II absorption at 8542 Å, and by the fact that variability is a minimum at 1 μm.

The strongest arguments in favour of a power-law component underlying the continua of radio quiet objects are (i) the smoothness of the 8–13-μm spectrum, and (ii) the relative constancy of the overall continuum shape from object to object (reflected in the good correlation between near-IR and X-rays, and in the consistency of spectral indices defined by 'baseline' techniques). Both of these facts can be explained in purely thermal empirical models, but only by 'fine tuning', i.e. respectively by requiring a particular optical depth, and by requiring a fairly constant covering factor. In considering thermal versus non-thermal phenomenological models, we are then left then with the choice of (i) arbitrarily introducing an extra component not suggested by independent evidence, i.e. the synchrotron component, or (ii) keeping only to components definitely present, but having to fine-tune the properties of those components, with no good physical reasoning.

ACKNOWLEDGMENTS

We would like to thank the JCMT staff for help and advice. The James Clerk Maxwell Telescope is operated by the Royal Observatory Edinburgh on behalf of the Science and Engineering Research Council of the United Kingdom, the Netherlands Organisation for Scientific Research and the National Research Council of Canada. AL would also like to thank the SERC for the provision of an Advanced Fellowship.

REFERENCES

Aitken, D. K. & Roche, P. F., 1985. *Mon. Not. R. astr. Soc.*, **213**, 777.
Antonucci, R. R. & Miller, J. S., 1985. *Astrophys. J.*, **297**, 621.
Blitz, L., Mathieu, R. D. & Bally, J., 1986. *Astrophys. J.*, **311**, 142.
Boulanger, F., Baud, H. & van Albada, G. D., 1985. *Astr. Astrophys.*, **144**, L9.
Brown, L. M. J., Robson, E. I., Gear, W. K., Crosthwaite, R. P., McHardy, I. M., Hanson, C. G., Geldzahler, B. J. & Webb, J. R., 1986. *Mon. Not. R. astr. Soc.*, **219**, 671.
Brown, L. M. J. *et al.*, 1989a. *Astrophys. J.*, **340**, 129.
Brown, L. M. J., Robson, E. I., Gear, W. K. & Smith, M. G., 1989b. *Astrophys. J.*, **340**, 151.
Carleton, N. P., Elvis, M., Fabbiano, G., Willner, S. P., Lawrence, A. & Ward, M., 1987. *Astrophys. J.*, **318**, 595.
Chini, R., Kreysa, E. & Salter, C. J., 1987. *Astr. Astrophys.*, **182**, L63.
Chini, R., Kreysa, E. & Biermann, P. L., 1989. *Astr. Astrophys.*, **219**, 87.
Chini, R., Steppe, H., Kreysa, E., Krichbaum, Th., Quirrenbach, A., Schalinski, C. & Witzel, A., 1988. *Astr. Astrophys.*, **192**, L1.
Clegg, P. E., Gear, W. K., Ade, P. A. R., Robson, E. I., Smith, M. G., Nolt, I. G., Radostitz, I. G., Glaccum, W., Harper, D. A. & Low, F. J., 1983. *Astrophys. J.*, **273**, 258.
Courvoisier, T. L.-J., Robson, E. I., Blecha, A., Bouchet, P., Hughes, D. H., Krisciunas, K. & Schwarz, H., 1988. *Nature*, **335**, 330.
Cutri, R. M., Wisniewski, W. Z., Rieke, G. H. & Lebofsky, M. J., 1985. *Astrophys. J.*, **296**, 423.
de Kool, M. & Begelman, M. C., 1989. *Nature*, **338**, 474.
de Kool, M., Begelman, M. C. & Sikora, M., 1989. *Astrophys. J.*, **337**, 66.
Duncan, W. D., Robson, E. I., Ade, P. A. R., Griffin, M. G. & Sandell, G., 1990. *Mon. Not. R. astr. Soc.*, **243**, 126.
Ebstein, S. M., Carleton, N. P. & Papaliolis, C. P., 1989. *Astrophys. J.*, **336**, 103.
Edelson, R. A. & Malkan, M. A., 1986. *Astrophys. J.*, **308**, 59.
Edelson, R. A. & Malkan, M. A., 1987. *Astrophys. J.*, **323**, 516.
Edelson, R. A., Gear, W. K. P., Malkan, M. A. & Robson, E. I., 1988. *Nature*, **336**, 749.
Efstathiou, A. & Rowan-Robinson, M., 1990. *Mon. Not. R. astr. Soc.*, submitted.
Elias, J. H. *et al.*, 1978. *Astrophys. J.*, **220**, 25.

Ennis, D. J., Neugebauer, G. & Werner, M., 19[illegible]. *Astrophys. J.*, **262**, 460.
Engargiola, G., Harper, D. A., Elvis, M. & Willner, S. P., 1989. *Astrophys. J.*, **332**, L19.
Gear, W. K., Robson, E. I., Ade, P. A. R., Griffin, M. J., Brown, L. M. J., Smith, M. J., Nolt, I. G., Radostitz, I. G., Veeder, G. & Lebofsky, L., 1985. *Astrophys. J.*, **291**, 511.
Hauser, M. G., Silverberg, R. F., Steir, M. T., Kelsall, T., Gezari, D. Y., Dwelz, E., Walser, D. & Mather, J. C., 1984. *Astrophys. J.*, **285**, 74.
Hill, H. G., 1975. *Nature*, **254**, 295.
Joyce, R. R. & Simon, M., 1976. *Publs astr. Soc. Pacif.*, **88**, 870.
Kellerman, K. I. & Pauliny-Toth, I. I. K., 1981. *Ann. Rev. Astr. Astrophys.*, **19**, 373.
Khembhavi, A., Feigelson, E. D. & Singh, K. P., 1986. *Mon. Not. R. astr. Soc.*, **220**, 51.
Kriss, G. A., 1988. *Astrophys. J.*, **324**, 809.
Landau, R. *et al.*, 1986. *Astrophys. J.*, **308**, 78.
Lawrence, A., 1987. *Publs astr. Soc. Pacif.*, **99**, 309.
Lawrence, A., 1980. *Mon. Not. R. astr. Soc.*, **192**, 83.
Lebofsky, M. J. & Rieke, G. H., 1980. *Nature*, **284**, 410.
Malkan, M. A., 1984. In: *X-ray and UV emission from Active Galactic Nuclei*, p. 121, eds Brinkmann, W. & Trumper, S., Max-Planck-Institut fur extraterrestriche Physik, Garching.
Malkan, M. A. & Fillipenko, A. V., 1983. *Astrophys. J.*, **275**, 477.
Miley, G. K., Neugebauer, G. & Soifer, B. T., 1985. *Astrophys. J.*, **296**, L11.
Neugebauer, G., Miley, G. K., Soifer, B. T. & Clegg, P. E., 1986. *Astrophys. J.*, **308**, 815.
O'Dell, S. L., Puschell, J. J., Stein, W. A., Owen, F., Porcas, R. W., Mufson, S., Moffett, T. J. & Ulrich, M. H., 1978. *Astrophys. J.*, **224**, 22.
Penston, M. V., 1988. *Mon. Not. R. astr. Soc.*, **233**, 601.
Persson, S. E., 1988. *Astrophys. J.*, **330**, 751.
Piccinotti, G., Mushotzky, R. F., Boldt, E. A., Holt, S. S., Marshall, F. E., Serlemitsos, P. J. & Shafer, R. A., 1982. *Astrophys. J.*, **253**, 485.
Robson, E. I., Gear, W. K., Clegg, P. E., Ade, P. A. R., Smith, M. G., Griffin, M. J., Nolt, I. G., Radostitz, J. V. & Howard, R. J., 1983. *Nature*, **305**, 194.
Robson, E. I., Gear, W. K., Brown, L. M. J., Courvoisier, T. L.-J., Smith, M. G., Griffin, M. J. & Blecha, A., 1986. *Nature*, **323**, 134.
Roellig, T. L., Becklin, E. E., Impey, C. D. & Werner, M. W., 1986. *Astrophys. J.*, **303**, 646.
Rowan-Robinson, M., 1982. *Mon. Not. R. astr. Soc.*, **201**, 289.
Rowan-Robinson, M. & Crawford, J., 1989. *Mon. Not. R. astr. Soc.*, **238**, 523.
Terlevich, E., Diaz, A. I. & Terlevich, R., 1990. *Mon. Not. R. astr. Soc.*, **242**, 271.
Turner, T. J. & Pounds, K. A., 1989. *Mon. Not. R. astr. Soc.*, submitted.
Unger, S. W., Lawrence, A., Wilson, A. S., Elvis, M. & Wright, A. E., 1987. *Mon. Not. R. astr. Soc.*, **228**, 521.
Ward, M., Elvis, M., Fabbiano, G., Carleton, N. P., Willner, S. P. & Lawrence, A., 1987. *Astrophys. J.*, **315**, 74.
Wilkes, B. J. & Elvis, M., 1987. *Astrophys. J.*, **323**, 243.
Yaqoob, T., Warwick, R. S. & Pounds, K. A., 1989. *Mon. Not. R. astr. Soc.*, **236**, 153.
Zamorani, G. *et al.*, 1981. *Astrophys. J.*, **245**, 357.

Center for Astrophysics
Preprint Series No. 3224

Persistence and Change in the Soft X-ray Spectrum of the Quasar PG1211+143

Martin Elvis
Harvard-Smithsonian Center for Astrophysics
60, Garden St.
Cambridge, MA 02138 USA

P. Giommi
ESTEC
EXOSAT Observatory
Keplerlaan 1
2200 AG Noordwijk
The Netherlands

Belinda J. Wilkes and Jonathan McDowell
Harvard-Smithsonian Center for Astrophysics
60, Garden St.
Cambridge, MA 02138 USA

March 11 1991

Abstract

Two *Einstein* and three *EXOSAT* observations of PG1211+143 over a six year baseline show that strong steep-spectrum low energy x-ray emission is a persistent feature of this quasar. *EXOSAT* observations of PG1211+143 detected a factor 2.3 increase in its steep soft x-ray (C-band) flux in 18 days. The bulk of the soft x-ray emission of PG1211+143 therefore comes from a region $< 5 \times 10^{16} cm$ across. In another (quasar rest frame) interval of 193 days the soft x-rays decreased by a factor 3.7. Either an intrinsic emission variation or an increase of N_H from 3.4 to 7.6×10^{20} atoms cm^{-2} could produce the same change. In the same time interval the hard (2 - 10 keV) x-rays decreased by a factor 1.6 ± 0.05. This suggests a connection between the two energy regimes, and argues against variable absorption causing the soft X-ray variations. In order to decrease in luminosity so rapidly a thermal source in PG1211+143 would have to be optically thick to both electron scattering and free-bound absorption. The same argument applies to 6 of the 7 other rapidly variable soft excesses reported in the literature, suggesting that optically thin thermal models are ruled out in general.

1. INTRODUCTION

'Soft X-ray excesses' are a new component of the quasar continuum. At energies below the Carbon edge at 0.28 keV ($\geq$44Å, the 'C-band') half of all studied quasars and AGN are dominated by large excess flux over an extrapolation of their higher energy power-laws (Arnaud *et al.* 1985, Wilkes and Elvis 1987, Turner and Pounds 1989, Turner *et al.* 1990, Masnou *et al.* 1991, Comastri *et al.* 1991)[1]. It has been suggested that these soft x-ray/extreme-ultraviolet excesses are emitted from the inner edges of accretion disks (Arnaud *et al.* 1985, Bechtold *et al.* 1987, Czerny and Elvis 1987). In this case their radiation comes to us from the innermost identifiable region of a quasar. The spectral shapes of the soft X-ray excesses might then give us information on the peak temperatures in disks and hence determine the allowed values of the central masses and accretion rates.

Whatever their origin this new component deserves careful investigation. Existing constraints on their spectra are poor because the X-ray measurements cover a small energy range ($\sim$0.1 - 0.3 keV) and have almost no energy resolution. Also very few objects were observed more than once so that variability information is scarce. Clearly more studies of these ultra-soft excesses are needed. Variability data in particular will be most important to distinguish between extended and compact emission regions, and to limit the properties of accretion disk models (Siemiginowska and Czerny 1989).

PG1211+143 is an extreme case of a quasar with an soft x-ray excess. It has an excess extending to higher energies than in other cases ($\sim$2 keV, Bechtold *et al.* 1987), and is the only one of the 33 quasars with soft x-ray spectra in the *Einstein* IPC survey to be dominated by an extremely steep, soft x-ray spectrum (Wilkes and Elvis 1987). We therefore undertook a program of x-ray observations of PG1211+143 with the EXOSAT Observatory. This paper reports this series of observations.

The value of the absorbing Galactic column density is crucial to studies of soft X-ray excesses (see *e.g.* Elvis, Wilkes and McDowell 1990). We use the accurate Galactic column density of 2.8 $\pm$0.1 $\times 10^{20}$ atoms cm^{-2} from the study by Elvis, Lockman and Wilkes (1989). Values of the Hubble constant H_0 =50 km s^{-1} Mpc^{-1} and of $q_0 = 0$ are used throughout. The redshift of PG1211+143 is 0.085 (Schmidt and Green 1983).

---

[1] In fact their very soft spectra suggest that they would be more accurately named 'XUV excesses' to denote the energy band below the Carbon edge, however common usage has settled on the less precise 'Soft X-ray excess' which could apply to any energy from $\sim$0.2 to 2 keV

2. OBSERVATIONS

PG1211+143 was observed on three separate occasions by ***EXOSAT*** with intervals of 209 and 19 days between the observations. (For details of the ***EXOSAT*** instrumentation see de Korte ***et al.*** 1981 and Turner, Smith and Zimmerman 1981). Table 1 gives details of the observations, including the derived count rates.

The quasar was seen in all of the three energy bands defined by the 'thin lexan' (3LX), 'aluminum/parylene' (ALP) and 'Boron' (BOR) filters, which each cover the ~0.1 to 2 keV band with somewhat differently weighted responses, in front of the LE (Low Energy Channel Multiplier Array) during the first observation. In the later observations the source was fainter so the filters giving smaller effective areas (BOR, ALP) could not always be used. There were no serendipitous ***EXOSAT*** observations of PG1211+143.

The position of the source in all the LE detections are consistent with one another and with the optical (Schmidt and Green 1983) position of PG1211+143 to within the 6 arcsec uncertainties of the EXOSAT aspect (Osborne and Angelini 1986). The LE source appears point-like in all the exposures. The mean LE position for the source is: $\alpha = 12^h\ 11^m 44.9^s \pm 6''$; $\delta = 14°\ 19'\ 53'' \pm 0.''4$ (1950.0).

The LE count rates (Table 1) were estimated using a square box centered on the source centroid and of a size which maximizes the signal-to-noise. The background was measured from a nearby source-free area of the image and rescaled to the source position to take into account spatial non-uniformities in the LE (Giommi 1985). The count rates were corrected for the fraction of counts outside the box (Davelaar and Giommi 1985), for vignetting effects, and for telemetry and instrumental dead times (Osborne 1985).

On the first two occasions the source was clearly detected in the ME (Medium Energy) Argon detectors. Poor background subtraction in the third observation makes detection by the ME uncertain. The data from the 'inner' detectors of the ME were much noisier than the 'outer' detectors since they are less well shielded against particle background (Arnaud ***et al.*** 1985). We therefore used only the 'outer' detectors in our analysis. Background subtraction for the ME was performed according to the method of Smith (1984). The background in each case was taken from the same detectors during times when they were pointed away from the source during an 'array swap'. Periods of high count rate due to solar flares were excluded by visually inspecting the light curves of each detector 'half'. The source is detected over the PHA range 7 – 40 which corresponds to 2 – 10 keV.

A serendipitous observation of PG1211+143 (seq no. 6982) was made by the ***Einstein*** IPC (Imaging Proportional Counter, ~0.2–3.5 keV, Giacconi ***et al.*** 1979, Gorenstein, Harnden and Fabricant 1981). This IPC observation was made

in 1979, a year earlier than the targeted observation. This significantly extends our temporal baseline. In this observation the quasar was 21.8 arcminutes off-axis. At such positions the gain ('BAL', which measures the conversion from recorded pulse height to incoming photon energy) must be estimated using the spatial gain map ('DGNI', Harnden *et al.* 1984). The 'BAL' was 13.6 for this position (on a scale from $\sim$12 - $\sim$19). The IPC count rate has been corrected for vignetting and the loss of counts due to the degraded off-axis point response function. The targeted ***Einstein*** IPC observation of PG1211+143, reported by Elvis,Wilkes and Tananbaum (1985), Bechtold *et al.* (1987) and Wilkes and Elvis (1987), had a 20% higher count rate.

3. PERSISTENCE: A 6-YEAR SOFT EXCESS

The unusual feature of PG1211+143 is its steep soft X-ray spectrum. It is important to understanding this emission to know whether it is persistent or transient. The five EXOSAT LE and ***Einstein*** observations allow us to test this.

We have fitted a simple power-law plus absorption model [2] to each of the data sets. Table 2 gives the results of these fits. (The spectrum from the first observation is reported by Comastri *et al.* 1991). The errors on each fit are quite large but the error regions overlap in both spectral parameters. It is notable that the well-constrained fits (*i.e.* excluding the 79/339 and 86/008 data) give steeper values for the power law index than are typical of either low energy quasar spectra (Wilkes and Elvis 1987), or of higher energy AGN spectra (Mushotzky 1984, Turner and Pounds 1989). When the Galactic column density is imposed as a minimum value then slopes of around α_E $\sim$2.0 are required, even for the 79/339 (off-axis IPC) data. However the χ^2 values even for the best fit values (Table 2) are not good suggesting that the spectrum has curvature, steepening toward lower energies.

The LE data for 1985/164, having three data points, allow a fit to be made. This fit suggests an even steeper slope, $\sim$3.0. A black body fit to the same 1985/164 LE data gives a best fit temperature of 75$\pm$5 eV.

The unusually steep spectrum of PG1211+143 is thus not a transitory feature but is seen in observations spanning six years.

---

[2] $f_\nu \propto \nu^{-\alpha_E} e^{-N_H \sigma}$, cross-sections (σ), were taken from Morrison and McCammon (1983).

4. CHANGE: OPTICALLY THICK THERMAL EMISSION

On timescales of days to months significant variability is seen between each of the EXOSAT observations. In particular, in the quasar's frame, the LE 3LX data show a factor 3.7 $\pm$0.3 decrease in 193 days and a factor 2.3 $\pm$0.1 increase in 18 days (table 1). In the 193 day interval the hard (2 – 10 keV) x-rays also decreased, though only by a factor 1.6$\pm$0.05. This may indicate some physical link between the emission in the two energy regimes.

The variations may be due either to intrinsic emission variability or to changing intervening absorption. At these low energies quite small column densities can produce such changes. To produce the decrease by a factor 3.7 in the 3LX filter seen between the first (Jun 1985) and second (Jan 1986) EXOSAT observations needs an increase in N_H from 3.4×10^{20} atoms cm^{-2} (the best fit value for the first observation) to 7.6×10^{20} atoms cm^{-2}. This is a minimum value. Material with a larger column density could obscure up to half the source to produce the same effect.

The contemporaneous decrease in the higher energy ME count rate by a factor 1.6 argues against absorption as the only variable since 2–10 keV X-rays are negligibly affected by column densities less than 10^{21} atoms cm^{-2}.

If the XUV excess were due to an optically thin thermal plasma then its spectrum would be rich in diagnostic emission lines for the inner regions of quasars (Marshall 1990). However the variability information rules out an optically thin plasma quite strongly, assuming an intrinsic change in the emission, since it requires large optical depths to both bound-free and electron scattering in the emitting plasma, as shown below.

If we take the decrease in 3LX count rate between the first and second EXOSAT observations to define a minimum cooling time, we can derive an optical depth for the emission region, taking into account electron scattering within the source, which smears out variations and increases the observed timescales by a factor $(1+\tau_{es})$. Of course more rapid variations may have taken place between our observations, but the shorter implied cooling times only increase the required optical depth derived below. For simplicity we consider a uniform density sphere of constant temperature plasma.

A spherical optically thin source of radius r with electron density $n = \tau_{es}/r\sigma_T$ and temperature T has luminosity in the 0.1-0.3 keV range of

$$L = \frac{4}{3}\pi r^3 F_0 f n^2 T^{1/2} B(T)$$

$$= \left(\frac{4}{3}\pi\tau_{es}^2\sigma_T^{-2}F_0 f T^{1/2}\exp\left[-\frac{0.1\mathrm{keV}}{kT}\right]\right) r$$

where

$$F_0 = 2.4\times10^{-27}\mathrm{erg\ cm^3\ K^{-1/2}\ s^{-1}},$$

the bandpass factor

$$B(T) = \exp\left[-\frac{0.1\mathrm{keV}}{kT}\right],$$

which is sensitive to the uncertain effective lower frequency limit of the soft excess observation, and f is a factor giving the additional contribution of line emission to bremsstrahlung cooling, $1 < f < 10$ (Raymond and Smith 1977, Raymond 1990). The radius in this equation can be related to the minimum cooling time set by the variability, t_{var} by

$$r \leq \frac{ct_{var}}{(1+\tau_{es})}$$

(Optically thick sources vary slowly for their size, so the inferred size is smaller for high depth) and so, combining the above equations

$$\frac{\tau_{es}^2}{1+\tau_{es}} \geq g$$

where,

$$\begin{aligned} g &= \frac{3L\sigma_T^2}{4\pi c t_{var} F_0 f T^{1/2} B(T)} \\ &= 1.4\times10^{-33}\left(\frac{L}{1\mathrm{erg\ s^{-1}}}\right) f^{-1}\left(\frac{t_{var}}{1\mathrm{s}}\right)^{-1}(T/1\ \mathrm{K})^{-1/2}\exp\left[-1.2\left(\frac{T}{1\ \mathrm{K}}\right)^{-1}\right] \\ &= 7.1\times10^{2}\left(\frac{L}{10^{44}\mathrm{erg\ s^{-1}}}\right) f^{-1}\left(\frac{t_{var}}{1\mathrm{day}}\right)^{-1}\left(\frac{T}{5\times10^6\ \mathrm{K}}\right)^{-1/2}\exp\left[-0.24\left(\frac{T}{5\times10^6\ \mathrm{K}}\right)^{-1}\right]. \end{aligned}$$

If $g < 1$, it is the square of the electron scattering depth. If $g > 1$, the assumption of optical thinness leads to a contradiction and we may deduce that the source must be optically thick; g is then equal to the electron scattering depth as long as the formula for L remains valid.

Even if the source is optically thick to electron scattering, it will retain its optically thin spectral shape unless absorptive opacity is also present. Bound-free interactions are dominant in modifying the spectrum toward a black body. The

bound-free optical depth τ_{bf} is just $\tau_{es}.\frac{\sigma_{bf}}{\sigma_{es}}$ (where the σ are the corresponding cross-sections). The bound-free cross-section at these sub-kilovolt energies depends only weakly on temperature in the range above 1 million degrees; σ_{bf}/σ_{es} at 0.1–0.2 keV is in the range 1 – 5 with T between 1 and 10 million degrees (Krolik and Kallman 1984, Kallman private communication) and so the spectrum will indeed be modified towards thermal form if the source is optically thick. The upper limit to the optical depth obtainable from comparing the blackbody radius to the variability timescale is not interesting.

The decrease in 3LX count rate between the first and second EXOSAT observations of PG1211+143 gives a value g of ~14, implying that it is optically thick. If instead the flux decrease is due to changing absorption in front of the source then electron scattering delays do not apply. The variability gives the physical size directly if we assume an absorber local to the quasar which moves to occult at least the fraction of the source whose luminosity disappears. For a transverse velocity of the absorber, v, the optical depth to electron scattering is then $\sim 180(\frac{v}{c})^{-\frac{1}{2}}$, which is considerable even for a relativistically moving intervening absorber.

Variability of soft x-ray excesses is now known to be common in quasars and AGN (see summary in Elvis, Wilkes and McDowell 1990). In some cases the variations are far more rapid than in PG1211+143 (*e.g.* Mkn 335, Turner and Pounds 1988, Lee and Balick, 1988). Table 3 lists the seven cases in the literature for which luminosities and timescales for luminosity decreases are given. (Only decreases in luminosity were used since only these define cooling times.) These variations imply the values of g listed in Table 3 and are shown in Figure 1 against lines showing the g=0.5 (τ=1) and g=10 loci for electron scattering.

PG1211+143 is seen from Figure 1 (and Table 3) to be one of the least extreme of these soft X-ray excesses. Most are factors of 10 to 100 times more optically thick, to the extent that large values of g imply a large optical depth. (E1615+061 is the only exception but here the excess may not be real, Buckley *et al.* 1987). We conclude that optically thin emission rarely dominates the production of quasar soft X-ray excesses, so that strong line emission from this component is unlikely. Optically thick emission would tend to support an origin in the central regions of an accretion disk, although we note that the physics of the inner edge are not well understood (Shakura and Sunyaev 1973), and that other processes (*e.g.* Comptonization, Czerny and Elvis 1987) could well modify the emitted disk spectrum.

The changes in the LE/3LX flux of PG1211+143 between the EXOSAT observations trivially rule out a source for the soft excess x-rays in extended regions on the scale of the optical/ultraviolet narrow emission line cloud zones (~100 pc–1 kpc), such as suggested by Halpern and Filippenko (1984). They would also

have ruled out emission from the broad emission line regions (Krolik, McKee and Tarter 1981) under earlier assumptions about their size, however recent observations (Peterson *et al.* 1990) suggest that sizes of 5-30 light days are quite plausible for these regions, comparable to the light travel time size limits derived for the soft excess emission regions.

5. CONCLUSIONS

Over five observations covering six years the steep low energy x-ray spectrum of PG1211+143 was always present. In this quasar the 'XUV excess' is a persistent feature.

EXOSAT observations of the quasar PG1211+143 have detected large amplitude (factor >2) short timescale changes in its low energy X-ray emission: an increase in 18 days and a decrease in 193 days. The small size implied for the bulk of the soft x-ray emission from PG1211+143 implies large optical depths in the emitting plasma and so makes the presence of strong emission lines unlikely. This conclusion is true of most known variable XUV excesses in AGN and quasars. Optically thick emission is instead likely from the inner regions of an accretion disk, although modifications (due to *e.g.* Comptonization) can occur, and the detailed physics is not well understood.

Observations of variability and spectra of the XUV excess component of AGN continuum emission are proving valuable. ROSAT observations are likely to extend this work substantially.

ACKNOWLEDGMENTS

We thank K. Arnaud, R. Shafer and A. Tennant for their work on the XANADU data analysis system and J. Lockman for advice on the Galactic column density. The IPC data came from the ***Einstein*** data bank. ME thanks the ESTEC ***EXOSAT*** staff for their hospitality and support during a visit for data analysis. This work was supported in part by NASA grant NAG8-568 (***EXOSAT***), NASA contract NAS8-30751 (***HEAO-2***) and by NASA Astrophysics Data Program grant NAG8-689.

REFERENCES

Arnaud K.A. *et al.*, 1985, MNRAS, **217**, 105.

Avni Y., 1976, ApJ, **210**, 642.

Barr P., Giommi P., Wamsteker W., Gilmozzi R., and Mushotzky R.F., 1985, BAAS, **17**, no. 2, 608.

Barr P., and Mushotzky R.F., 1986, ***Nature***, **320**, 421.

Bechtold J., Czerny B., Elvis M., Fabbiano G., and Green R.F., 1987, ApJ, **314**, 699.

Buckley D.A.H., Tuohy I.R., Remillard R.A., Bradt H.V., and Schwartz D.A., 1987, ApJ, **315**, 273.

Comastri A., Setti G., Zamorani G., Elvis M., Giommi P., *et al.*, 1991, ApJ submitted

Czerny B., and Elvis M., 1987, ApJ, **321**, 694.

Davelaar J., and Giommi P., 1985, ***EXOSAT Express***, no.10, 45.

de Korte *et al.*, 1981, ***Space Science Reviews***, **30**, 495.

Elvis M., Lockman F.J. and Wilkes B.J., 1989, AJ, **97**, 777.

Elvis M., Wilkes B.J., and McDowell J.C., 1990, in ***"EUV Astronomy"***, eds. R. Malina, S. Bowyer [New York: Pergamon], p. 238.

Elvis M., Wilkes B.J., and Tananbaum H., 1985, ApJ, **292**, 357.

ESA (European Space Agency), 1984, ***EXOSAT Observers Guide, Part III: The Final Observation Tape Handbook***, Rev.2. [Noordwijk:ESA].

Giacconi R.,*et al.*, 1979, ApJ, **230**, 540.

Giommi P., 1985, ***EXOSAT Express***, no. 12, p. 33.

Gorenstein P., Harnden R.F.Jr., and Fabricant D., 1981, IEEE Trans. Nucl. Sci., NS-**28**, 869.

Halpern J.P., 1984, ApJ, **281**, 90.

Halpern J.P. and Filippenko A.V. , 1984, ApJ, **285**, 475.

Harnden R.F.Jr., Fabricant D.G., Harris D.E., and Schwarz J., 1984, ***SAO Special Report No. 393***.

Kaastra J.S., and Barr P., 1989, A&A, **226**, 59.

Krolik J.H., and Kallman T., 1984, ApJ, **286**, 366.

Krolik J.H., McKee C.F., and Tarter C.B., 1981, ApJ, **249**, 422.

Lawrence A., Watson M.G., Pounds K.A., and Elvis M., 1985, MNRAS, **217**, 685.

Lawrence A., Watson M.G., Pounds K.A., and Elvis M., 1987, ***Nature***, **253**, 694.

Lee M.G. and Balick B., ,1988, ApJ, **331**, 154.

Marshall H.L., 1990, in ***"EUV Astronomy"***, eds. R. Malina, S. Bowyer [New York: Pergamon], p.228.

Masnou J.-L., Wilkes B.J., Elvis M., McDowell J.C., and Arnaud K.A., 1991, A&A, submitted.

Morini M., *et al.*, ApJ, **307**, 366.

Morrison R., and McCammon D., 1983, ApJ, **270**, 119.
Mushotzky R.F., 1984, ***Advances in Space Research***, **3**, no.10-12, 157.
Osborne J., 1985, ***EXOSAT Express***, no.13, 42.
Osborne J., and Angelini L., 1986, ***EXOSAT Express***, no.17, 3.
Peterson B.M., *et al.*, ApJ, 1991, ApJ, **368**, 119.
Pravdo S.H., Nugent J.J., Nousek J.A., Wilson A.S., and Becker R.H., 1981, ApJ, **251**, 501.
Raymond J., 1980, private communication.
Raymond J., and Smith B.W., 1977, ApJS, **35**, 419.
Schmidt M., and Green R.F., 1983, ApJ, **232**, 463.
Siemiginowska A., and Czerny B., 1989, MNRAS, **239**, 289.
Shakura N.I., and Sunyaev R.A., 1973, A&A, **24**, 337.
Smith A., 1984, ***EXOSAT Express***, no.5, 48.
Turner M.J., Smith A. and Zimmerman 1981, ***Space Science Reviews***, **30**, 495.
Turner T.J., and Pounds K.A., 1988, MNRAS, **232**, 463.
Turner T.J., and Pounds K.A., 1989, MNRAS, **240**, 833.
Turner M.J., *et al.*, 1990, MNRAS, **244**, 310.
Urry C.M., Arnaud K., Edelson R.A., Kruper J.S. and Mushotzky R.F., 1989, ***Proceedings of the 23rd ESLAB Symposium: X-ray Astronomy***, p. 789, ESA SP-296.
Wilkes B.J., and Elvis M.,1987, ApJ, **323**, 243.

figure 1: Luminosity in the 'soft X-ray excess' component *vs.* observed timescale for a decrease in the soft X-ray component for the AGN from table 3. The lines show values of $g = 1$ (marginally optically thick) and $g = 10$ for thermal emission with electron scattering. Larger optical depths lie to the bottom right, implying that most soft excesses are optically thick.

Table 1: *Einstein* and *EXOSAT* Observations of PG1211+143

year/day	instrument/filter	exposure (s)	count s^{-1}
1979/339	IPC	6306	0.89± 0.02
1980/347	IPC	1795	1.28± 0.03
1985/164	ME[a]	22370	0.84±.02
	LE/3LX	1257	0.206±.012
	LE/ALP	3539	0.0867±.006
	LE/BOR	16560	0.0087±.0012
1986/008	ME[a]	17030	0.52±.02
	LE/3LX	15753	0.055±.0025
1986/028	LE/3LX	10065	0.13±.004
	LE/ALP	15753	0.05±.009

b. PHA 7–40, 2–10 keV

Table 2: Power-law fits to X-ray data for PG1211+143

year/day	instrument(s)	α_E^a	$N_H^{a,b}$	norm[a,c]	χ^2,d.o.f.[d]	P(χ^2 [e])
1979/339	IPC[f,g]	$1.3^{+0.9}_{-0.5}$	$0.9^{+1.5}_{-0.9}$	$4\ ^{+46}_{-1}$	12, 5	0.04
1980/346	IPC[g]	$2.0^{+1.7}_{-0.6}$	$2.3^{+4.8}_{-0.6}$	$5.5^{+0.8}_{-0.7}$	12, 5	0.04
1985/164	ME[h]	$1.7^{+0.6}_{-0.4}$	$0\ ^{+85}_{-0}$	$4.4^{+4.8}_{-1.3}$	43, 31	0.08
1985/164	ME[h]+LE	$1.8^{+0.3}_{-0.2}$	$2.2^{+1.5}_{-0.9}$	$4.8^{+1.3}_{-1.0}$	56, 34	0.01
1985/164	LE	$2.9^{+2.4}_{-0.9}$	$3.4^{+6.5}_{-1.5}$	$2.4^{+2.7}_{-2.1}$	0, 0	–
1986/008	ME[h]	$0.9^{+1.2}_{-0.6}$	$0.0^{+3.0}_{-0.0}$	$1.1^{+5.5}_{-0.6}$	47, 31	0.04
1986/008	ME[h]+LE	$0.9^{+0.7}_{-0.4}$	$0.3^{+2.5}_{-0.3}$	$1.1^{+1.3}_{-0.4}$	47, 32	0.04

a. 90% confidence ranges for 3 interesting parameters (χ^2_{min} + 6.25, Avni 1976).
b. 10^{20} atom cm^{-2}.
c. μJy at 1 keV.
d. degrees of freedom.
e. probability of obtaining the observed χ^2.
f. PHA 2–9.
g. errors include IPC gain uncertainties at this off-axis position.
h. PHA 7–40

Table 3: Optical Depths for Variable Soft Excesses in AGN

Name	log L_{xs}^{a} ($erg\ s^{-1}$)	log Δt s	variability factor	g^{b}	reference
Mkn 335	43.6	4.3	2.0	1000	Turner,Pounds 1988, Lee *et al.* 1988
Fairall 9	44.9	5.7	1.9	450	Morini *et al.* 1986
M81	40.5	2.7	2.0	30	Barr *et al.* 1985[c]
3C273	45.2	7.2	1.7	65	Turner *et al.* 1990, Masnou *et al.* 1991
NGC 4051[d]	41.5	3.0	2.0	300	Lawrence *et al.* 1985
PG 1211+143	44.7	7.2	3.7	14	*this paper*
NGC 5548	44.6	4.4	1.3	8100	Kaastra and Barr 1989
Mkn 841	44.4	4.6	1.5	3200	Arnaud *et al.* 1985
E1615+061[e]	44.0	8.0	1.5	0.5	Pravdo *et al.* 1981

a. luminosity in the soft excess, ~0.1 – 0.3 keV.

b. for $T = 5 \times 10^6$K. Values are ~5 times smaller for $T = 1 \times 10^6$K, while τ_{bf} is ~85 times larger.

c. quoted in Barr and Mushotzky 1986.

d. note the warnings of Lawrence *et al.* (1987) about picking timescales from 1/f variations.

e. but see Buckley *et al.* (1987) who note a nearby x-ray bright RSCVn system. This may be the cause of the apparent soft excess in this AGN.

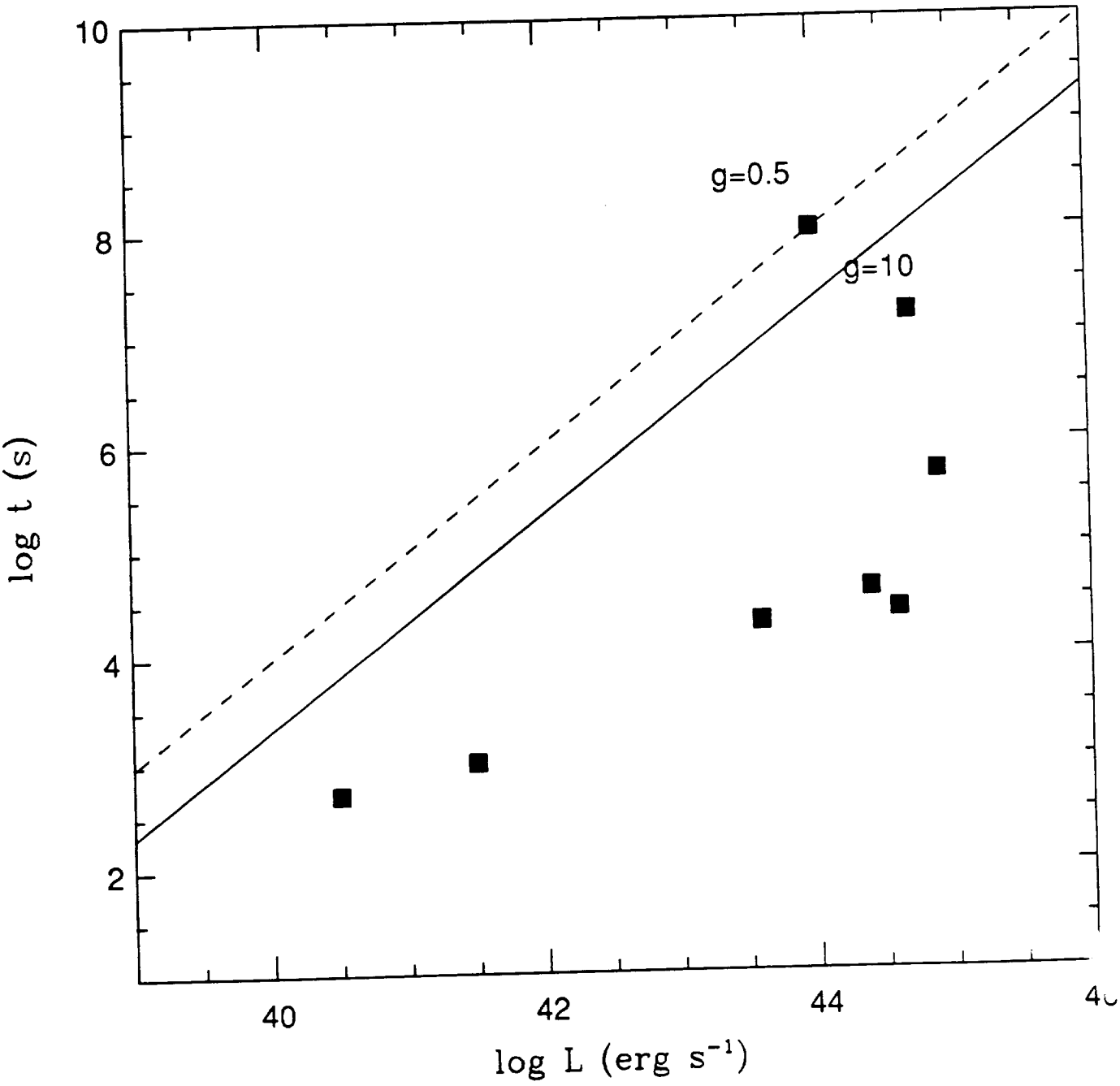

figure 1

Abstract.

We study the low energy excess above a high energy power-law in the X-ray spectra for a signal-to-noise limited, sub-sample of 14 quasars from the Wilkes & Elvis (1987) sample. Detailed analysis of the ***Einstein*** Imaging Proportional Counter (IPC) data, combined with Monitor Proportional Counter (MPC) data where possible, and the use of accurate Galactic N_H values allow us to estimate the flux of any detected excess and improve constraints on the spectral parameters at higher X-ray (> 0.6 keV) energies. We find a significant excess in 8 of the 14 objects, confined in all but one case to below 0.6 keV. The excess is typically strong, dominating the $\lesssim 0.3$ keV X-ray flux and being 1−6 times as strong as the high energy component at 0.2 keV. In 3C273, multiple observations show that the excess is variable. The lack of spectral information, uncertainty in the intrinsic line-of-sight absorption and the possibility of variation prevents the detection of any relation with the optical/ultra-violet blue bump. Comparison with an existing accretion disk model for the blue bump suggests that, for this model to explain both the blue bump and the soft X-ray excess, a range of disk parameters are required to explain the whole sample.

Key words : Quasars – X-Rays:spectroscopy – X-Rays:general

Center for Astrophysics
Preprint Series No. 3261

The Soft X-ray Excess in Einstein Quasar Spectra.

Jean–Louis Masnou[1*]
Belinda J. Wilkes[2], Martin Elvis[2], Jonathan C. McDowell[2***]**
and
Keith A. Arnaud[3**]**

[1]UPR176, DARC
Observatoire de Paris, Section de Meudon
5, Place Jules Janssen, 92195 Meudon France

[2]Harvard-Smithsonian Center for Astrophysics
60, Garden St., Cambridge, MA 02138 USA

[3]NASA/Goddard Space Flight Center
Greenbelt, MD 20771 USA

Send proofs to : J.–L. Masnou[1]

Offprint requests : J.–L. Masnou

Thesaurus : 17.01.1,24.04.1,24.03.1

Section : Extragalactic Astronomy

Accepted by : Astronomy and Astrophysics, Main Journal

April 17 1991

0* Visiting Scientist, Harvard–Smithsonian Center for Astrophysics, Cambridge, Mass., USA
0** Visiting Scientist, UPR176,DARC, Observatoire de Paris, Section de Meudon, France
0*** Now at Marshall Space Flight Center, Huntsville, USA
0**** Also Astronomy Program, University of Maryland, USA

1 Introduction.

Recent soft X-ray observations have shown that Active Galactic Nuclei (AGN) and quasars commonly show strong excess emission above the extrapolation of their higher energy slopes (Singh, Garmire & Nousek 1985, Arnaud *et al.* 1985, Branduardi-Raymont *et al.* 1985, Wilkes & Elvis 1987, Turner & Pounds 1989, Elvis, Wilkes & McDowell 1989). These excesses occur primarily in the C−band, *i.e.* below the 0.28 keV Carbon edge, and rise steeply to lower energies. Information is generally limited to a single discrepant point at low energies when compared with the slope at higher energies (1−10 keV) (*e.g.* Turner & Pounds 1989). In this paper we use the highest signal-to-noise Imaging Proportional Counter (IPC) observations from the Wilkes & Elvis (1987) quasar sample, combined with higher energy (2−10 keV) Monitor Proportional Counter (MPC) data where it is useful, to give data extending from 0.1−10 keV. These data combined with accurate Galactic N_H values (Elvis, Lockman & Wilkes 1989), allow two-component spectral fits and thus a well-constrained estimate of the observed flux in the soft excess.

Although there are viable alternatives, such as free-free emission (Barvainis 1990, Ferland, Korista and Peterson 1990), the optical/ultra-violet (UV) blue bump is generally modeled as thermal emission from an accretion disk possessing a range of temperatures (Shields 1978, Malkan & Sargent 1982), an interpretation which is enticing both observationally and theoretically. An obvious identification of the soft X-ray excess is then the high-energy tail of the thermal emission (Arnaud *et al.* 1985, Bechtold *et al.* 1986, Pounds *et al.* 1986, Czerny & Elvis 1987). In this case it would originate in the hottest material, at the innermost edge of the accretion disk at $\sim$ 10 Schwarzschild radii. Should this be confirmed, the excess will provide far stronger constraints on the physical conditions of this part of the disk than have been possible so far. Quantitative measurement of the soft excess is thus of considerable importance.

2 Analysis.

2.1 The Data.

We have selected the highest signal-to-noise observations in the Wilkes & Elvis (1987) sample of quasars observed with the *Einstein* IPC, those with $\gtrsim$1200 net counts. This yielded a subset of 14 quasars, 5 of which are radio-loud (radio-loudness, $R_L > 1.0$, Wilkes & Elvis 1987). Details of the X-ray observations along with redshift and Galactic column density of neutral hydrogen are given in Table 1. PG 1211+143, which is a member of the sample, is included for completeness in the discussion although it is not re-analyzed here. We include two additional

observations of 3C273 not reported by Wilkes & Elvis (1987). For completeness and comparison with the earlier results, the results of single power-law fits with free N_H to the IPC data alone for these two observations, using Brown & Gould (1970) absorption coefficients, are given in Table 2a and Figure 1. Throughout the remainder of our analysis, absorption coefficients are taken from Morrison & McCammon (1983).

The IPC X-ray data were analyzed following the standard procedure described in Elvis *et al.* (1986) and Wilkes & Elvis (1987). Briefly, counts in the energy range ~0.15−3.5 keV were obtained from a 3′ circle centered on the position of the source. A correction was applied for counts falling outside this circle and background counts were estimated from a 5′−6′ annulus centered upon the source position. The first bin of the pulse height distribution was excluded since the errors are not well determined.

In this new analysis we have also used data from the MPC for which > 500 net counts were detected. Apart from early studies by Halpern (1981) and Elvis *et al.* (1986), the MPC has been little used for quasars until now due to systematic uncertainties in the background subtraction process for these faint sources. These uncertainties have now been reduced and quantified for all observations prior to Oct 1980 (Arnaud 1991 and see below) allowing simultaneous fitting of IPC and MPC data.

The MPC data have the advantage of covering a higher energy range with the counts distributed into 8 pulse height channels extending from 1.2 to 20 keV. Channels 7 and 8 (> 10 keV) were not used in this analysis as they provide no additional constraint on the spectral fits. The energy range of our study generally covers the two decades 0.1−10 keV. In most cases the MPC and IPC data were obtained simultaneously. The exceptions are PG 0026+129, II Zw 136 and PKS 0637−752 where no significant variation was detected between the two dates and non-simultaneous data were used to maximize the signal-to-noise ratio.

2.2 The Monitor Proportional Counter (MPC).

The MPC was a collimated proportional counter filled with Argon and sealed with a 38 μm window of beryllium foil. Its effective area was 667 cm^2 with a triangular field of view having full width at half maximum of 43′ and a flattened top ~ 6′ wide. Counts were collected in 8 pulse height (PI) channels from 1.2−20 keV with an energy resolution of ~ 20% at 6 keV. The instrument was mounted on the outside of the *Einstein* Observatory telescope and aligned within 1′ of the optical axis. The MPC is described in detail by Gaillardetz *et al.* (1978) and Grindlay *et al.* (1980).

We used the latest, Rev1, time-ordered MPC processing with data extracted following the method of Arnaud (1991). Briefly, all data taken during points in the orbit with McIlwain l> 1.2, B< 0.25, which includes South Atlantic Anomaly passage, were discarded. The background consists of two components. A background

model for the cosmic background was constructed using source-free observations. The background is estimated using correlations with the pulse risetime discriminator rates and McIlwain *l,B*, parameters modified by long-term time variability which includes the decay of the in-flight calibration source (Cd^{109}), modeled as an exponential with a half-life of 450.4 days). In addition the response matrix was modified following the discovery that the earlier, Rev0, processing system assumed an energy resolution $\sim$ 10 times better than reality. The resulting effective area curve is shown by Vrtilek *et al.* (1990) and Arnaud (1991).

2.3 IPC/MPC Relative Normalization.

The IPC and MPC instruments were calibrated independently and the estimated accuracy of these calibrations are about 10% and 20% respectively. Before combining data from the IPC and MPC, the relative accuracy of their calibrations must be determined. Since the instruments have very different sensitivities they did not observe the same calibration sources. Instead we made a comparison utilizing the quasar data under the assumption (consistent with *Ginga* results, Pounds 1990) that quasar spectra do not change drastically ($\Delta\alpha > \pm 0.5$) in the 0.6–10 keV energy range.

A single power law model, with the line-of-sight absorbing column density fixed at the Galactic value, was fitted to the high-energy band of the IPC (0.6–3.5 keV) to minimize the effects of any soft excess. A power law model with the IPC best fit slope and Galactic N_H was then fitted to the MPC data but with the normalization (flux density at 1 keV) free. These fits should give comparable normalization in both instruments. In all but the highest S/N observations, those of 3C273, the ratio of MPC to IPC normalization (Figure 2) is consistent with unity. However a weighted mean gives a value of IPC/MPC = 1.14$\pm$0.04, similar to those for 3C273 and implying that the MPC calibration is too low relative to the IPC. This conclusion is reinforced by a comparison of the best fit power law slopes determined by fitting the IPC and MPC data individually and in combination for the two 3C273 observations where this is possible (Table 2b and Wilkes & Elvis 1987). The IPC/MPC combination gives a steeper slope ($\alpha_E \sim$ 0.6) than either instrument individually, which each gave $\alpha_E \sim$ 0.4. The latter is in better agreement with measurements of 3C273 by other experiments (Worrall *et al.* 1979, Turner *et al.* 1990a,b). Since the ratio of IPC to MPC normalization is not sensitive to the spectral slope assumed, our result does not critically depend on the accuracy of the spectral fit.

We conclude that the relative normalization of the MPC is systematically low relative to the IPC by a factor of 1.14. This is within the absolute accuracy of the calibration of each instrument. The MPC data were corrected accordingly in our subsequent analysis and all numbers presented here include this correction. We note that the decision of which instrument to correct is arbitrary.

2.4 Spectral Analysis.

The results of conventional, single power law models, with N_H fixed at the Galactic value, are presented in Table 3. They are poor ($P(\chi^2) \leq 10\%$) for 9 observations of 7 of the 13 quasars analyzed here. In 11 observations the residuals clearly show the lowest 1 or 2 PHA (pulse height analysis) channels to be significantly above the fit, suggesting the presence of a soft excess.

Conventional two-component fits give poorly constrained parameters (slope and normalization at 1.0 keV, f(1.0 keV)) for the low energy excess (***e.g.*** Arnaud ***et al.*** 1985, Pounds ***et al.*** 1986). However, the excess flux can be much better determined than its spectrum since a small change in flux at 0.2 keV results in a large change in slope and normalization (f(1.0 keV)). We have therefore applied broken power-law fits to the data, minimizing χ^2 with respect to the 0.2 keV flux in each component and to the 1.0 keV flux of the high energy component (f_{XS}(0.2 keV), f_{HE}(0.2 keV), f(1.0 keV) respectively) instead of the more conventional spectral slope. The results are given in Figure 3 and Table 3, with errors quoted at 1σ for one interesting parameter, $\Delta\chi^2 = 1.0$ (Avni 1976). N_H was again fixed at the Galactic value. The energy resolution and S/N of the data are insufficient to warrant the addition of a fourth free parameter and thus it is not possible to determine the break energy between the two power laws. The IPC is best suited to detecting soft excesses in its lowest independent energy band *i.e.* with break energy in the range 0.4−0.6 keV. The break energy was thus fixed at 0.6 keV, yielding a conservative estimate of the observed flux in any detected excess. Decreasing this value to 0.4 typically results in a small but insignificant ($< 2\sigma$) increase in the deduced flux of the soft excess.

Fits with power-law plus black-body components were also applied, leaving free the 0.2 keV flux in each component and the normalization of the high energy component. The energy resolution is not sufficient to fit the black-body temperature, which was therefore fixed at 0.05 keV. Both the high energy component and the soft excess flux are consistent with corresponding results from the broken power law fits as shown in Figure 4. Our discussion will be confined to the results of the broken power law model.

An F-test for the significance of an additional parameter shows that a broken power law model represents a significant improvement over a single power law fit for 8 of the 16 observations (5 of the 10 with MPC data) at 5% (0.05) confidence or better (Table 3). Including PG 1211+143, this leads to a total of 9 excesses detected in observations of 8 quasars from our sample of 14. Upper limits at 3σ are given for the remaining 8 observations for which no significant excess was detected.

2.5 The Effect of Additional Absorption.

The presence of any additional absorbing material (molecular and partially ionized Galactic or material intrinsic to the quasar) along the line of sight to a quasar would increase the requirement for a soft excess. We have quantified this effect for the case of partially ionized hydrogen in the Galaxy. Reynolds (1989) estimated that 37% of the gas along a high latitude line of sight through the Galaxy is ionized. Increasing the metal contribution to our X-ray opacities by 37% results in the detection of 4 more excesses for 3 quasars: (3C273 (9310), 1426+015 (both observations) and 1613+658). For those quasars with a detected excess, the 0.2 keV flux of the excess increased by 20-43%.

2.6 Notes on Individual Objects.

PG 1211+143.

PG 1211+143 is already known to have a steep low energy spectrum (Elvis, Wilkes & Tananbaum 1985, Bechtold *et al.* 1986, Czerny & Elvis 1987). This soft excess is unusual since it is reported to display a break energy around 2 keV, much higher than the 0.3−0.6 keV generally seen. The MPC data for this object are unreliable, as are all MPC observations made after October 1980, due to a change in instrument configuration on that date[1]. The lack of higher energy data combined with the 2 keV break energy between the excess and the high energy component make it impossible to constrain the spectral parameters and so it is not analyzed here. Since it is part of the sample, we include it in our discussion. A detailed discussion of its spectrum both from ***Einstein*** and EXOSAT data is given by Elvis *et al.* (1991a) and from ***Ginga*** data by Turner *et al.*(1990a).

3C273.

There are three observations of 3C273 over 17 months. The first observation has a weak excess (Table 3). In the second, 6 months later, the excess has almost twice the flux level of the first and in the third, 11 months later than the second, the upper limit is consistent with both the earlier measurements. The high energy flux density also varies but is uncorrelated with a 20% decrease over 6 months followed by a 93% increase over 11 months. Similar, uncorrelated low and high variations were found in ***Ginga*** and EXOSAT observations of 3C273 (Turner *et al.* 1990b).

PHL 1657 (2135−148).

The X-ray spectrum is not fitted well by a power law or a black body form. A good fit was obtained with a partial covering model (see ***e.g.*** Turner and Pounds

[1]This change in state of the MPC was not known at the time of the earlier IPC/MPC study by Bechtold *et al.* (1986)

1989): α_E=2.1±0.5, N_H(additional)=7.1±1.6 10^{20} cm^{-2} (fraction 92±7%), f(1.0 keV)=4.1±1.6 μJy (χ^2=15, n=16).

Optical images of this source show two nearby companions and surrounding nebulosity (Hutchings *et al.* 1984) extending to $> 6''$ so that additional X-ray absorption is likely to be present. X-ray spatial structure at this level cannot be confirmed at the resolution of the IPC and indeed the IPC image shows no evidence for extended emission. There is a possibility that the closest companion, a fainter quasar at the same redshift only 1".9 away, may contribute to the X-ray flux leading to the complex spectrum. Two, higher energy, EXOSAT observations of this quasar show no evidence for a complex spectrum. A single power law fit gives an energy spectral index ~ 0.7 (Singh, Rao and Vahia 1990). However, these authors also report a variation in the (0.2−1.0 keV) soft X-ray flux during this time which might indicate complexity at lower energies.

2.7 Excess above an IR−X-ray Baseline.

Under the hypothesis that the soft X-ray excess is the high energy tail of the blue bump, we would expect its flux to correlate with the strength of the blue bump. However, the soft X-ray excess is measured with respect to the higher-energy X-ray power law while the blue bump is generally estimated relative to the IR emission. While it has been suggested that the IR and X-ray emission is related (Malkan 1985, Carleton *et al.* 1987), it is by no means proven and the lack of any relation could invalidate a search for a blue bump/soft excess correlation due to the large continuum range involved. Alternatively, both components could be measured above the common baseline of an effective IR/X-ray power-law. We have therefore estimated the soft X-ray excess above this power law as a check on our earlier results.

An estimate of the spectral slope from IR to X-ray was made from luminosities integrated between $1-2\mu m$ and 0.6 keV using data from Elvis *et al.*(1991b, and Figure 8), with the exception of 1253−055 (3C279) for which we have little multi-wavelength data. The monochromatic luminosity at 0.2 keV in the rest frame, for a soft X-ray excess above the IR−X-ray power law was computed. Such an excess is present at $> 1\sigma$ for 7 of the 8 quasars which show an excess above the high energy X-ray power law. One quasar, 3C273, no longer shows an excess. The fitted results for all objects and upper limits for the remainder are given in Table 4.

3 Results.

3.1 Soft Excess above the High Energy X-ray Power Law.

The flux density in the soft X-ray excess at 0.2 keV ranges from $\sim 1-6$ times that in the high energy component at the same energy (Table 4). It is clearly

very strong, dominating the energy output in the soft X-ray region ($\lesssim$0.3keV) in quasars.

The soft excess was detected, at $\gtrsim$90% confidence, in 7 of the 13 quasars analyzed here and also in PG 1211+143. Five of these were reported by Wilkes & Elvis (1987), the remaining two, NAB 0205+024 and B2 1028+313, are new detections in this analysis. Including PG 1211+143, this yields 8 of 14 quasars with an excess. Studies of lower luminosity Seyfert 1 galaxies (Turner & Pounds 1989, Kruper, Urry & Canizares 1990) show a similar $\sim$ 50% detection rate. This number is likely to increase if, as discussed above, a significant fraction of the hydrogen in our galaxy is ionized (Reynolds 1989). Our results confirm that soft excess components are common in many types of active galaxies and over a wide range in luminosity.

3.2 Soft Excess above an IR−X-ray Baseline.

When measured relative to an IR−X-ray power law, 7 of the 8 quasars earlier found to have an excess still have one at $> 1\sigma$ (Table 4). 3C273 is the exception, leaving 1 radio-loud and 6 radio-quiet quasars with soft X-ray excesses. Figure 5 shows the comparison of the excess determined by the two methods with the line of equality shown. With the exception of 3C273, the soft excesses determined according to the two different methods agree. Although insignificant, the sense of any difference is that the excess strength decreases when measured with respect to the IR−X-ray power. This implies that the IR−X-ray slope is generally steeper than the high energy X-ray power law (see Tables 3, 4).

A decrease in the apparent strength of the soft X-ray excess when it is measured relative to an IR−X-ray power law is expected for radio-loud objects such as 3C273. They are stronger X-ray sources than their radio-quiet counterparts, this is thought to be due to presence of an additional, radio-linked, high energy, X-ray component (Zamorani *et al.* 1981, Wilkes & Elvis 1987). This picture also predicts flatter IR−X-ray power law slopes for radio-loud quasars, though for our small sample the difference is only 2σ: $\alpha_{\rm IRX} = 1.18\pm0.02$ (radio-loud), $= 1.22\pm0.02$ (radio quiet).

3.3 Relation to other Properties.

The magnitude and errors of our detected flux densities at 0.2 keV suggest that a redshift of 0.5 would be sufficient to make it undetectable in most cases. The lack of a detected excess in the two highest redshift objects in our sample (z>0.5), PKS 0637−752 and 3C279, is consistent with this prediction.

In the current sample, 2 of the 5 radio-loud and 6 of the 9 radio-quiet quasars show excesses. The probability of seeing such a distribution if the parent populations of these two samples are the same is 28% (Fisher test), *i.e.* there is no evidence from this small sample that radio-loud and radio-quiet objects are

different in either the presence or the strength of their excess properties. This conclusion does not change if we instead determine the soft excess above the IR−X-ray baseline. It is strengthened if we omit the two higher redshift quasars which are both radio-loud.

No relation was found between the soft X-ray excess, measured in either way, and the high energy X-ray luminosity density (at 1.0 keV) (16% probability of a chance occurrence).

3.4 The High Energy Component.

Figure 6 shows a comparison of the high energy slopes determined from the broken power law fits with those reported by Wilkes and Elvis (1987) for a single power law fit with free N_H. The results are consistent in all cases, confirming Wilkes and Elvis (1987) conclusion that allowing free N_H in a single power law fit with the IPC successfully models the soft X-ray excess. We confirm and extend their primary result that a range of slopes is present in the soft X-ray region, 0.2-10 keV, with the slopes for radio-loud and radio-quiet quasars being $\alpha_E \sim 0.5, 1.0$ respectively.

A synchrotron self-Compton origin for the $\alpha_E \sim 0.5$ X-ray component in radio-loud quasars is generally accepted (Zamorani *et al.* 1981, Wilkes and Elvis 1987). For radio-quiet quasars and Seyfert 1 galaxies, the currently popular reflection model, in which the X-rays are reflected off cool, optically thick, matter surrounding the central continuum source (Lightman and White 1988, Guilbert and Rees 1988), nicely explains all the available X-ray spectra. The model predicts $\alpha_E \sim 1.0$ at low energies, $\lesssim 5$ keV, as seen for radio-quiet quasars with ***Einstein*** (Table 3), and a broad hump of emission extending from $\sim$ 10 keV to high energy ($\sim$ 300 keV). It was the detection of this hump by ***Ginga***, for a sample of Seyfert 1 Galaxies (see Pounds 1990 for a review), which first brought this model to the fore. The intermediate, $\alpha_E \sim 0.7$, $2-10$ keV slope, frequently reported for Seyfert 1 galaxies by HEAO1-A2 (Mushotzky 1985) and EXOSAT (Turner and Pounds 1989), is the natural result of fitting a single power law to the complex spectrum predicted by the reflection model. Data for individual Seyfert 1s observed with both HEAO1-A2 and the ***Einstein*** IPC (0.2−3.5 keV) confirm this conclusion in that the HEAO1-A2 ($\sim$ 0.7) slopes are flatter than the IPC ($\sim$ 1.0, Kruper, Urry and Canizares 1990). Although we see no evidence for a reflection component in the current quasar sample, the S/N of the MPC data is so low that it is unlikely to be detected.

3.5 Relation to the Blue Bump.

The far-infrared to X-ray energy distributions for those quasars with a soft excess are shown in Figure 8. These distributions are corrected for Galactic reddening and emission lines have been subtracted. The data are being presented in detail by Elvis *et al.* (1991b) and so will be discussed no further here.

It is clear from the figures (*e.g.* NAB 0205+024) that the blue bump generally dominates the energy output of these quasars and that the soft X-ray excess may well be its high energy tail. However, we found no evidence for a correlation between the strength of the blue bump (Figure 7), as measured by the ratio of blue bump to IR−X-ray power law flux at $0.1 - 0.2\mu m$ (f_{BB}),[2] and that of the excess, measured by its ratio to the high energy component at 0.2 keV, (f_{XS}(0.2 keV)/f_{HE}(0.2 keV), Table 4). This is true even when the two higher redshift >0.5 objects are removed and when radio-loud and quiet objects are considered separately. While this result is disappointing in view of the popular interpretation of the soft excess as the high energy tail of the blue bump, it is clear from the figure that the uncertainties in the soft excess measurement are sufficiently large to mask any existing correlation. Further uncertainty is added by the possibility of variability and the possible presence of intrinsic, absorbing material.

No firm conclusions on the identity of the soft excess can be made until more data, in particular simultaneous UV and soft X-ray data with improved X-ray spectral resolution, have been obtained. This will be possible with ROSAT.

3.6 Comparison with the Czerny−Elvis Model.

Accretion disk models have generally not attempted to predict the soft X-ray flux in addition to the UV/optical regime, primarily due to the large uncertainties in the parameters of the inner regions of an accretion disk where this emission originates. Czerny & Elvis (1987) do include the soft X-ray and successfully reproduce the strong soft excess in PG 1211+143 using an electron scattering atmosphere surrounding the disk itself. In comparison with this result, column 8 ("CE87 ratio") in Table 4 gives the ratio (multiplied by 10) of the product energy-luminosity of the luminosity in excess of the IR−X-ray power law at 0.2 keV to that at 10^{15} Hz. This is similar to the parameter defined by Czerny & Elvis (1987, their equation 28). They predict that, assuming the accretion disk parameters for every quasar are the same and their inclinations are random, $\sim$ 15% of quasars will have observed values for this parameter > 1.0. Six of the quasars with a soft X-ray excess, *i.e.* 40% of our sample, exceed this value implying that, for this model to apply, either the quasars in this sample are predominantly viewed face-on, or a range of model parameters is present.

4 Conclusions.

Two component spectral fits to IPC/MPC quasar data show that the soft X-ray excess dominates the X-ray flux $\lesssim$0.3 keV in half our sample. The fluxes in the excess at 0.2 keV cover the range 1−6 times that in the high energy component at

[2]This ratio is strongly correlated with the bump measure, C_{UV}/C_{IR}, McDowell *et al.* (1989) but is used in its place to be consistent with the X-ray measurement.

the same energy. The lack of spectral information combined with uncertainty in the line-of-sight absorption makes it impossible to draw any definite conclusions concerning its identity. The high energy tail of the blue bump remains the most attractive candidate and the common presence of both components, regardless of the class of AGN, might be considered as circumstantial support for this picture. However, we cannot rule out such extreme alternatives as a completely new component or a single X-ray component which steepens below $\sim$ 0.3 keV (Band and Grindlay 1986, Schwartz, Qian & Tucker 1990).

The high energy slopes determined for the broken power-law fits presented here are consistent with those reported earlier by Wilkes and Elvis (1987). Our results are fully consistent with the reflection model popularized by recent ***Ginga*** results for radio-quiet quasars and Seyfert 1 galaxies. For radio-loud quasars, the flatter ($\alpha_E \sim$ 0.5) slopes is consistent with the presence of a synchrotron self-Compton (SSC) radio-linked component (Zamorani *et al.* 1981, Wilkes & Elvis 1987) which probably dominates any reflection component in these quasars.

Measurements of the soft excess relative to an IR−X-ray power law agree well with those relative to the higher energy X-ray in all objects except 3C273. This confirms that our soft excess measurements are valid for comparison with the blue bump flux which is measured with respect to the IR. Some weakening of the excess flux for radio-loud objects, such as 3C273, is consistent with their additional SSC component and stronger X-ray flux. Measurement with respect to the high energy X-ray is the most sensitive way to detect the soft X-ray excess in radio-loud quasars. It is once again clear that radio-loud and radio-quiet quasars should be treated as distinct in X-ray studies.

Comparison of the observed ratio of the luminosity in excess of the IR−X-ray power law at 0.2 keV to that at 10^{15} Hz with that predicted by an accretion disk model, imply that a range of parameters is necessary to explain the whole sample. However, large uncertainties in line-of-sight absorption (Galactic or intrinsic to the quasar) and the lack of simultaneous UV data preclude detailed modeling. More, higher resolution, soft X-ray observations (*e.g.* with ROSAT) are clearly necessary, preferably simultaneously with UV data, in order to delineate the blue bump unambiguously.

Acknowledgements.

The authors would like to thank Jules Halpern, Ken Pounds, Meg Urry and Saeqa Vrtilek for useful discussions. JLM wishes to thank the High Energy Astroph· ·s Division, Harvard-Smithsonian Center for Astrophysics for their hospitality · ing short term visits for this work. BJW would like to thank her friend· · d colleagues at the Observatoire de Paris−Meudon for their kind hospitality and support during her visits. This research was partially supported by NASA grant NAS 8−30751. JLM and BJW acknowledge the support of the French Ministère des Affaires Etrangères. Mrs Xenia Lasareff is acknowledged for assistance in

preparing the figures.

5 References.

Arnaud, K. A. 1991 in preparation

Arnaud, K. A., Branduardi-Raymont, G., Culhane, J. L., Fabian, A. C., Hazard, C., McGlynn, T. A., Shafer, R. A., Tennant, A. F. and Ward, M. J. 1985 *MNRAS* **217**, 105

Avni, Y. 1976 *ApJ* **210**, 642

Band, D. L. and Grindlay, J. E. 1986 *ApJ* **308**, 576

Barvainis, R. 1990 *ApJ* **353**, 419

Bechtold, J., Czerny, B., Elvis, M., Fabbiano, G. and Green, R. F. 1986 *ApJ* **314**, 699

Branduardi-Raymont, G., Mason, K. O., Murdin, P. G. and Martin, C. 1985 *MNRAS* **216**, 1043

Brown, R. L. and Gould, R. J. 1970 *Phys. Rev. D* **2**,2252

Carleton, N. P, Elvis, M., Fabbiano, G., Wilner, S. P., Lawrence, A. and Ward, M. 1987 *ApJ* **318**, 595

Czerny, B. and Elvis, M. 1987 *ApJ* **321**, 305

Dickey, J. M., Salpeter, E. E. and Terzian, Y. 1978 *ApJS* **36**, 77

Elvis, M., Wilkes, B. J. and Tananbaum, H. 1985 *ApJ* **292**, 357

Elvis, M., Green, R. F., Bechtold, J., Schmidt, M., Neugebauer, G., Soifer, B. T., Matthews, K. and Fabbiano, G. 1986 *ApJ* **310**, 291

Elvis, M., Lockman, F. J. and Wilkes, B. J. 1989 *AJ* **97**, 777

Elvis, M., Wilkes, B. J. and McDowell, J. C. 1989 in *Extreme Ultraviolet Astronomy*, R. F. Malina and S. Bowyer *in press*

Elvis, M, Giommi, P., Wilkes, B. J. and McDowell, J. 1991a *ApJ* 10 September

Elvis, M., Wilkes,B . J., McDowell, J. C., Green, R. F., Bechtold, J., Willner, S. P., Cutri, R., Oey, M, S., and Polomski, E. 1991b *ApJS in preparation*

Ferland, G. F., Korista, K. T. and Peterson, B. M. 1990 *ApJ* **363**, L21

Gaillardetz *et al.* 1978 *IEEE Trans. on Nuc. Sci.* **NS-25**, 437

Grindlay *et al.* 1980 *ApJL* **240**, L121

Guilbert, P. W. and Rees, M. J. 1988 *MNRAS* **233**,475

Halpern, J. 1981 PhD. Thesis, Harvard University.

Heiles, C. and Cleary, M. N. 1979 *Aust. J. Phys. Suppl.* **47,1**

Hutchings, J. B., Crampton, D., Campbell, B., DUncan, D. and Glandenning, B. 1984 *ApJS* **55**,319

Kruper, J. S., Urry, C. M. and Canizares, C. R. 1990 *ApJS* **74**,347

Lightman, A. P. and White, T. R. 1988 *ApJ* **335**,57

Malkan, M. 1985 in *X-ray and UV Emission from Active Galactic Nuclei* eds. W. Brinkmann and S. Trümper p. 121

Malkan, M. A. and Sargent, W. L. W. 1982 *ApJ* **254**, 22

McDowell, J. C., Elvis, M., Wilkes, B. J., Willner, S. P., Oey, M. S., Polomski, E., Bechtold, J. and Green, R. F. 1989 *ApJL* **345**, L11

Morrison, R. and McCammon, D. 1983 *ApJ* **270**, 119

Mushotzky, R. F. 1985 *Adv. Sp. Res.* **3**,157
Pounds, K. A., Stanger V. J., Turner, T. J., King, A. R. and Czerny B. 1986 *MNRAS* **224**, 443
Pounds, K. A. 1990 in Proceedings of the 23rd ESLAB Symposium ed. Nick White [ESA Publications Division], **2**, 753
Reynolds, R. J. 1989 *ApJ* **339**, L29
Schwartz, D. A., Qian, Y. and Tucker, W. 1990 in Proceedings of the 23rd ESLAB Symposium ed. Nick White [ESA Publications Division], **2**, 1043
Shields, G. A. 1978 *Nature* **272**, 706
Singh, K. P., Garmire, G. P. and Nousek, J. 1985 *ApJ* **297**, 333
Singh, K. P., Rao, A. R. and Vahia, M. N. 1990 *A&A* in press
Turner, M. J. L., Williams, O. R., Saxton, R., Stewart, G. C., Courvoisier, T. J-L, Ohashi, T., Makishima, K., Kli, T. and Inoue, H. 1990a, in Proceedings of the 23rd ESLAB Symposium ed. Nick White [ESA Publications Division], **2**,769
Turner, M. J. L. *et al.* 1990b *MNRAS* **244**,310
Turner, T. J. and Pounds, K. A. 1989 *MNRAS* **240**,769
Vrtilek, S. D., McClintock, J. E., Seward, S. D., Kahn, S. M. and Wargelin, B. J. 1990 *ApJS* in preparation
Wilkes, B. J. and Elvis, M. 1987 *ApJ* **323**, 243
Worrall, D. M., Mushotzky, R. F., Boldt, E. A., Holt, S. S. and Serlemitsos, P. J. 1979 *ApJ* **232**,683
Zamorani, G. *et al.* 1981 *ApJ* **245**, 357

6 Figure Captions.

Figure 1: 68%, 90% and 99% confidence contours for α_E and N_H for single power law (Wilkes and Elvis (1987)–style) fits to observations of 3C273, sequence numbers: a) 5692 and b) 9310. These are included for comparison with the earlier results.

Figure 2: A histogram of IPC relative to MPC normalization for single power law fits using the IPC best fitted slope.

Figure 3: Results of broken power law fits to the IPC plus MPC data.

Figure 4: Comparison of the 0.2 keV flux density in the soft excess component as determined using a power law and a black body as the spectral form for the soft component.

Figure 5: Comparison of the soft X-ray excess determined relative to the high energy X-ray power law and the IR–X-ray power law.

Figure 6: Comparison of the IPC/MPC slopes determined here with the IPC only results of Wilkes and Elvis (1987).

Figure 7: The strength of the blue bump vs. that of the soft X-ray excess relative to the higher energy X-ray power law.

Figure 8: Far-infrared to X-ray energy distributions for those quasars in our sample with a detected soft X-ray excess. The data are fully presented and discussed by Elvis *et al.* (1991b). The scale of log νF_νvslogν gives the energy output as a function of frequency.

Table 1: Observational Details.

Name	Redshift N_H[a]	I/MPC	Seq.No.	Date	Net Counts[b]	T_{exp}
0026+129	0.142	IPC	5417[c]	1981 Jan 4	2678±55	11152
PG	4.93	MPC	518	1979 Jan 7	1279±265	2826
0054+145	0.171	IPC	5418	1980 Jul 19	1289±39	11735
PHL 909	4.20	IPC	4248	1979 Jul 2	424±23	3717
0205+024	0.155	IPC	3978	1979 Jul 20	1237±38	7608
NAB	2.99					
0637−752	0.656	IPC	8494	1980 Dec 14	1199±39	7480
PKS	8.4[d]	MPC	5404	1979 Nov 30	546±138	860
1028+313	0.177	IPC	4256	1979 May 24	1167±37	6595
B2	1.98	MPC	4256[e]		561±275	3768
1219+756	0.07	IPC	5424	1980 Apr 20	6434±107	13113
MKN 205	2.74	MPC	5424		8399±543	11305
1226+023	0.158	IPC	2037	1979 Jun 20	4523±68	1740
3C273	1.80[f]	MPC	2037		4015±152	737
		IPC	5692	1980 Jan 1	9362±98	3911
		MPC	5692		16297±379	3482
		IPC	9310	1980 Dec 13	6687±83	1668
1253−055	0.538	IPC	4645	1980 Jul 14	3279±65	25095
3C279	2.22	MPC	4645		1775±604	14828
1426+015	0.086	IPC	5348[g]	1980 Aug 3	1231±36	2034
PG	2.64	MPC	5348		1585±210	1925
		IPC	10374[h]	1981 Jan 5	4748±91	13210
1501+106	0.036	IPC	6713	1980 Jan 18	1663±42	1475
MKN 841	2.23	MPC	6713		1153±155	1024

Name	Redshift N_H^a	I/MPC	Seq. No.	Date	Net Counts[b]	T_{exp} (s)
1613+658	0.129	IPC	10375[i]	1981 Feb 6	2217±51	7209
PG	2.66					
2130+099	0.061	IPC	1972	1980 May 3	862±33	4987
II Zw 136	4.20	IPC	1971	1981 Apr 20	485±23	1429
2135−148	0.20	IPC	5426	1980 May 10	2521±54	12902
PHL 1657	4.45	MPC	5426		2037±464	8560

a: Galactic equivalent hydrogen column density in units of 10^{20} atoms cm^{-2} from Elvis, Lockman and Wilkes (1989) (unless otherwise noted).
b: 0.15−3.5 keV (IPC, bin 1 excluded) and 2−10 keV (MPC, bins 1 to 6)
c: Sum of sequence numbers 5417,9550,9551,9552,9553
d: Heiles and Cleary (1979)
e: Excluding bins 1,2 due to their low counts.
f: Dickey *et al.* (1978)
g: Spectral results reported by Elvis *et al.* (1986)
h: sum of sequence numbers: 10374,10390,10391,10392,10393
i: sum of sequence numbers: 10375,10394,10395,10396,10397

Table 2: Fits to 3C273 a: Wilkes and Elvis (1987) style, single power law fits (1σ error bars); b: Comparison of single power law fits to MPC only and IPC/MPC.

a:

Seq. No.	PH Channels	α_E	N_H (10^{20} atms cm^{-2})	χ^2_{min}/d.o.f[a]	f(1.0 keV)[b]
5692	2-11	$0.34^{+0.09}_{-0.07}$	$0.3^{+0.4}_{-0.3}$	10.7/8	9.4 ± 1.1
9310	2-9	$0.46^{+0.11}_{-0.11}$	$1.0^{+0.6}_{-0.6}$	6.3/6	18.7 ± 3.0

b:

Seq. No.	MPC α_E	MPC f^b_{1keV}	α_E(IPC/MPC)	f^b_{1keV}(IPC/MPC)
2037	0.42±0.09	10.8±1.3	0.55±0.02	12.6±0.2
5692	0.43±0.05	9.4±0.6	0.62±0.02	11.3±0.1

a: Degrees of Freedom
b: Normalization in μJy, errors are quoted at 1σ for one interesting parameter.

Table 3: Parameters of Spectral Fits.

		Single Power Law			Broken Power Law					
Name	IPC MPC	α_E	f(1.0 keV)[a]	χ^2 Bins	f(1.0 keV)[a]	f_{HE}(0.2 keV)[b]	f_{XS}(0.2 keV)[c]	α^d_{HE} α^d_{LE}	χ^2 Bins	Sig[e]
0026+129	I5417	0.88 ± 0.05	1.41 ± 0.03	10.0	$1.41^{+0.07}_{-0.07}$	$5.9^{+1.4}_{-1.1}$	<13.5	0.88	10.0	-
PG	M518			14				0.87	14	
0054+145	I5418	0.74 ± 0.07	0.61 ± 0.02	18.8	$0.52^{+0.04}_{-0.04}$	$1.02^{+0.33}_{-0.26}$	$4.16^{+1.63}_{-1.58}$	0.41	11.5	0.01
PHL 909	I4248			21				1.89	21	
0205+024	I3978	1.80 ± 0.07	0.70 ± 0.03	14.6	$0.58^{+0.06}_{-0.06}$	$4.0^{+2.4}_{-1.5}$	$14.8^{+4.4}_{5.0}$	1.2	8.4	0.05
NAB				11				2.61	11	
0637−752[f]	I8494	0.46 ± 0.10	0.98 ± 0.05	6.4	$0.97^{+0.05}_{-0.09}$	$2.0^{+0.5}_{-0.5}$	<32.8	0.44	6.4	-
PKS	M5404			15				0.97	15	
1028+313	I4256	0.96 ± 0.06	0.91 ± 0.03	9.4	$0.76^{+0.07}_{-0.07}$	$2.1^{+0.5}_{-0.5}$	$5.4^{+2.0}_{-2.1}$	0.62	3.8	0.01
B2	M4256			12				1.79	12	
1219+756	I5424	0.96 ± 0.03	2.49 ± 0.04	25.9	$2.24^{+0.08}_{-0.08}$	$7.8^{+1.0}_{-0.9}$	$8.9^{+2.4}_{-2.5}$	0.78	14.3	0.01
MKN 205	M5424			16				1.47	16	
1226+023	I2037	0.55 ± 0.02	12.6 ± 0.2	23.6	$11.8^{+0.4}_{-0.4}$	$25.0^{+2.1}_{-2.0}$	$16.6^{+6.0}_{-6.0}$	0.47	16.0	0.05
3C273	M2037			15				0.93	15	
	I5692	0.62 ± 0.01	11.3 ± 0.1	83.3	$9.8^{+0.2}_{-0.2}$	$20.1^{+1.1}_{-1.1}$	$28.8^{+3.3}_{-3.3}$	0.45	14.5	0.01
	M5692			16				1.26	16	
	I9310	0.63 ± 0.03	20.2 ± 0.3	10.6	$18.9^{+0.7}_{-0.7}$	$41.5^{+6.1}_{-5.4}$	<71.2	0.49	5.6	-
				8				1.00	8	

		Single Power Law			Broken Power Law					
Name	IPC MPC	α_E	f(1.0 keV)[a]	χ^2 Bins	f(1.0 keV)[a]	f_{HE}(0.2 keV)[b]	f_{XS}(0.2 keV)[c]	α^d_{HE} α^d_{LE}	χ^2 Bins	Sig[e]
1253−055	I4645	0.62 ± 0.04	0.63 ± 0.01	27.0	$0.67^{+0.02}_{-0.04}$	$2.2^{+0.2}_{-0.5}$	<1.8	0.74	26.1	-
3C279	M4645			16				0.29	16	
1426+015	I5348	1.19 ± 0.05	3.05 ± 0.09	16.8	$2.94^{+0.2}_{-0.2}$	$17.9^{+5.9}_{-4.7}$	<32.5	1.12	16.5	-
PG	M5348			15				1.37	15	
	I10374	1.16 ± 0.04	1.91 ± 0.04	11.4	$1.73^{+0.09}_{-0.09}$	$7.8^{+2.0}_{-1.6}$	<21.3	0.94	7.2	-
				8				1.65	8	
1501+106	I6713	1.27 ± 0.04	4.82 ± 0.14	15.2	$4.2^{+0.3}_{-0.3}$	$18.7^{+5.0}_{-4.0}$	$30.6^{+8.3}_{-9.3}$	0.93	7.1	0.01
MKN 841	M6713			16				1.82	16	
1613+658	I10375	1.21 ± 0.04	1.40 ± 0.04	7.0	$1.33^{+0.07}_{-0.07}$	$7.0^{+2.4}_{-1.8}$	<12.4	1.10	6.3	-
PG				11				1.39	11	
2130+099	I1971	1.41 ± 0.07	1.14 ± 0.04	14.7	$0.91^{+0.08}_{-0.08}$	$3.4^{+1.5}_{-1.1}$	$19.4^{+5.4}_{-5.3}$	0.81	3.2	0.01
II Zw 136	I1972			10				2.55	10	
2135−148	I5426	0.73 ± 0.05	1.10 ± 0.02	24.6	$1.10^{+0.05}_{-0.05}$	$3.4^{+0.5}_{-0.5}$	<6.3	0.71	24.5	-
PHL 1657	M5426			16				0.81	16	

a: Normalization in μJy. Errors are quoted at 1σ for one interesting parameter.
b: Flux density of high energy component at 0.2 keV (observed frame) in μJy, corrected for Galactic absorption
c: Flux density in excess at 0.2 keV (observed frame) in μJy, corrected for Galactic absorption. Upper limits are at 3σ
d: α_{HE}, α_{LE}: high and low energy power law energy indices respectively resulting from the fitted X-ray fluxes.
e: Significance of the soft X-ray excess as determined by an F test.
f: 0637−752 has no accurate Galactic N_H measurement due to its southern declination. Fits were performed at the Galactic value $\pm 1 \times 10^{20}$ and no evidence for a soft excess was found in either case.

Table 4: Luminosity of the excess :

Name	IPC MPC	$f_{XS}(0.2)/^a$ $f_{HE}(0.2)$	α^b_{IRX}	L^c 1 keV	L^d_{XS-HE} 0.2 keV	L^e_{XS-IRX} 0.2 keV	CE87[f] ratio	$R_L{}^g$ f^h_{BB}
0026+129	I5417	< 2.3	1.17	0.14	< 1.88	< 1.07		0.34
PG	M518							4.7
0054+145	I5418	$4.1^{+1.9}_{-2.0}$	1.33	0.07	$0.75^{+0.28}_{-0.27}$	$0.48^{+0.28}_{-0.27}$	3.76	−0.01
PHL909	I4248							2.3
0205+024	I3978	$3.7^{+1.8}_{-2.6}$	1.24	0.07	$2.35^{+0.67}_{-0.76}$	$2.33^{+0.67}_{-0.76}$	5.87	−0.40
NAB								6.7
0637−752	I8494	< 16.3	1.14	2.35	< 110	< 98.6		3.52
PKS	M5404							8.0
1028+313	I4256	$2.6^{+0.9}_{-0.9}$	1.17	0.11	$1.05^{+0.38}_{-0.36}$	$0.77^{+0.38}_{-0.36}$	42.6	2.14
B2	M4256							4.7
1219+756	I5424	$1.1^{+0.3}_{-0.4}$	1.19	0.05	$0.22^{+0.06}_{-0.06}$	$0.11^{+0.06}_{-0.06}$	2.5	−0.31
MKN 205	M5424							1.6
1226+023	I2037	$0.7^{+0.3}_{-0.3}$	1.21	1.36	$2.26^{+0.74}_{-0.74}$	$-1.85^{+0.74}_{-0.74}$	-0.36	3.06
3C273	M2037							5.7
	I5692	$1.4^{+0.2}_{-0.2}$	1.24	1.13	$4.03^{+0.43}_{-0.43}$	$0.42^{+0.43}_{-0.43}$	0.08	
	M5692							
	I9310	< 1.7	1.15	2.19	< 14.1	< 3.6		
1426+015	I5348	< 1.8	1.13	0.10	< 1.80	< 1.16		−0.55
PG	M5348							6.4
	I10374	< 2.7	1.21	0.06	< 1.06	< 0.69		

Name	IPC MPC	$f_{XS}(0.2)/^{a}$ $f_{HE}(0.2)$	α^{b}_{IRX}	L^{c} 1 keV	L^{d}_{XS-HE} 0.2 keV	L^{e}_{XS-IRX} 0.2 keV	CE87[f] ratio	R_L[g] f^{h}_{BB}
1501+106 MKN 841	I6713 M6713	$1.6^{+0.6}_{-0.7}$	1.18	0.02	$0.19^{+0.05}_{-0.05}$	$0.15^{+0.05}_{-0.05}$	3.4	−0.67 3.9
1613+658 PG	I10375	< 1.6	1.21	0.11	< 1.72	< 0.98		−0.10 3.3
2130+099 II Zw 136	I1971 I1972	$5.7^{+3.9}_{-3.0}$	1.35	0.02	$0.37^{+0.10}_{-0.10}$	$0.32^{+0.10}_{-0.10}$	2.40	0.37 6.0
2135−148 PHL 1657	I5426 M5426	< 1.9	1.18	0.22	< 1.95	< 0.77		1.70 2.4

a: Ratio of excess and high energy X-ray power law contributions at 0.2 keV. Upper limits are at 3σ and errors at 1σ for one interesting parameter.

b: Index of the power law connecting the infrared ($1\mu m - 2\mu m$) flux to the X-ray flux at 0.6 keV

c: Luminosity of the high energy power law component at 1 keV in units of 10^{28} ergs s^{-1} Hz^{-1} ($H_o = 50$ km s^{-1} $Mpc^{-1}, q_o = 0$)

d: Luminosity of the excess value above the high energy X-ray power law in units of 10^{28} ergs s^{-1} Hz^{-1}. Upper limits are at 3σ and errors at 1σ for one interesting parameter.

e: Luminosity of the excess observed above the IR−X-ray power law connecting the infrared ($1\ \mu m - 2\ \mu m$) to the X-ray spectrum at 0.6 keV in units of 10^{28} ergs s^{-1} Hz^{-1} Upper limits are at 3σ and errors at 1σ for one interesting parameter.

f: E.L(0.2 keV) / E.L(10^{15}Hz), see section 3.5

g: Radio−loudness (Wilkes & Elvis 1987)

h: Ratio of blue bump to IR−X-ray power law in the range $0.1 - 0.2\ \mu m$

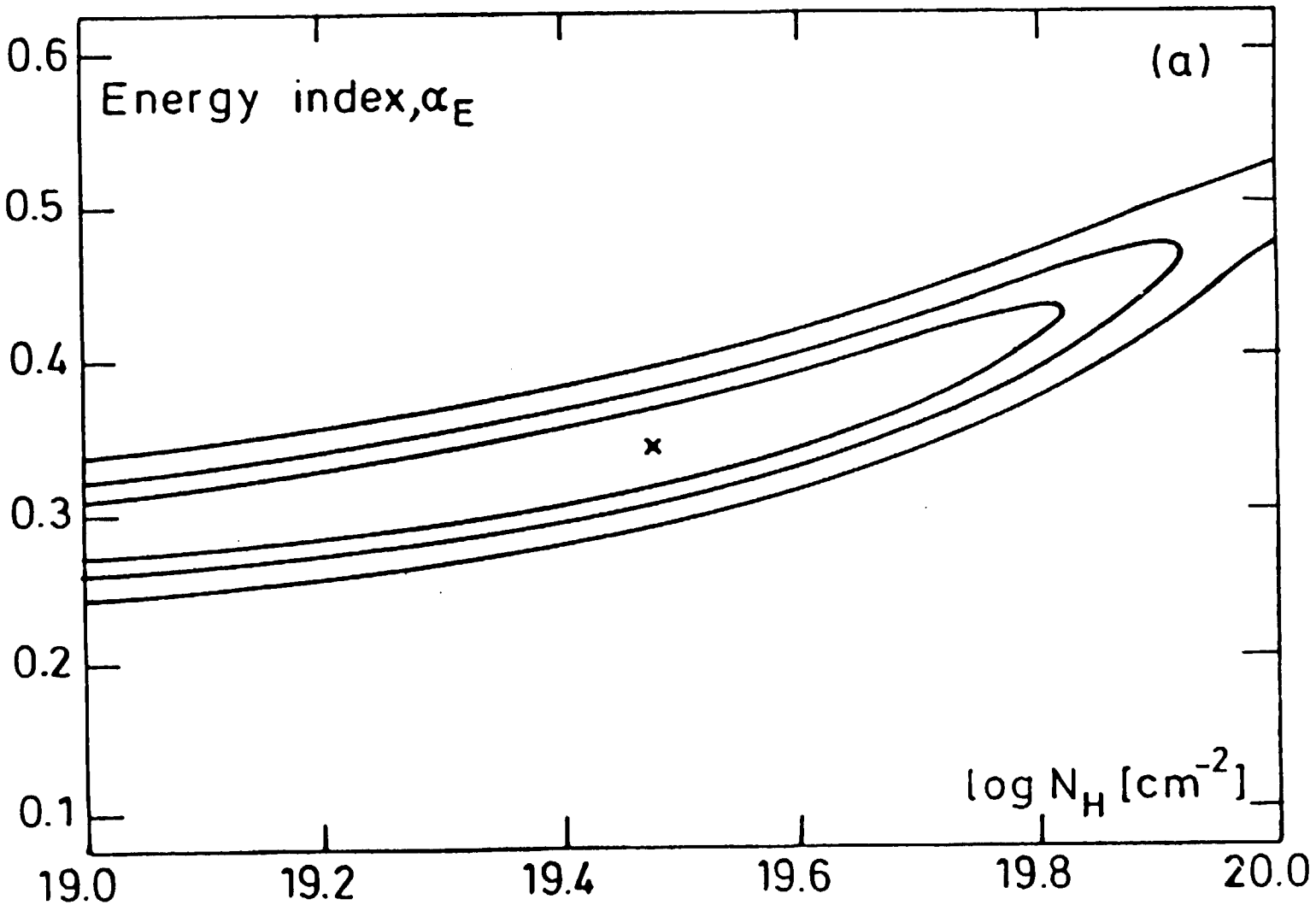
(a)
Energy index, α_E
0.6
0.5
0.4
0.3
0.2
0.1
19.0
19.2
19.4
19.6
19.8
20.0
log N_H [cm^{-2}]

Fig. 1a

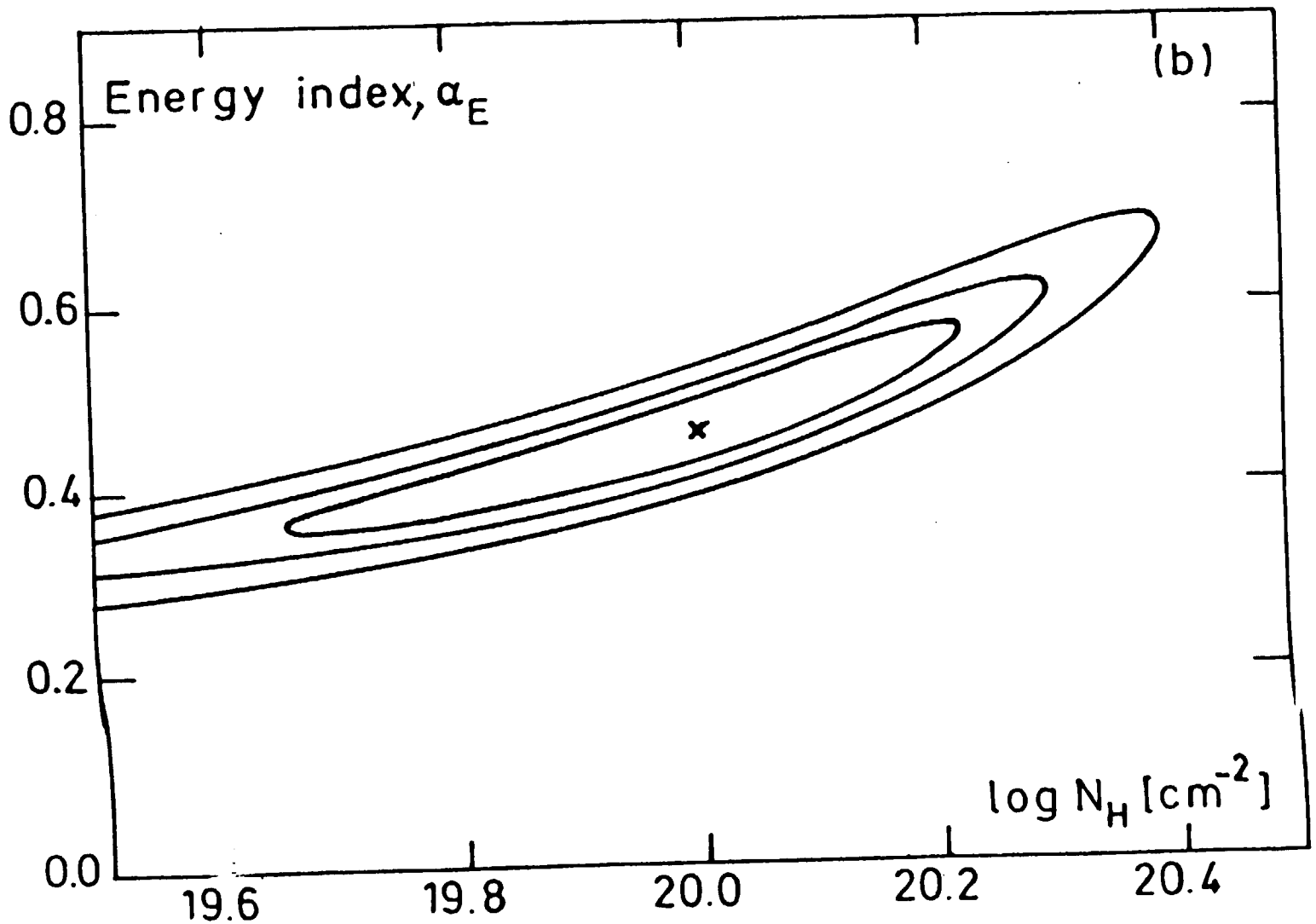
(b)
Energy index, α_E
0.8
0.6
0.4
0.2
0.0
19.6
19.8
20.0
20.2
20.4
log N_H [cm^{-2}]

Fig. 1b

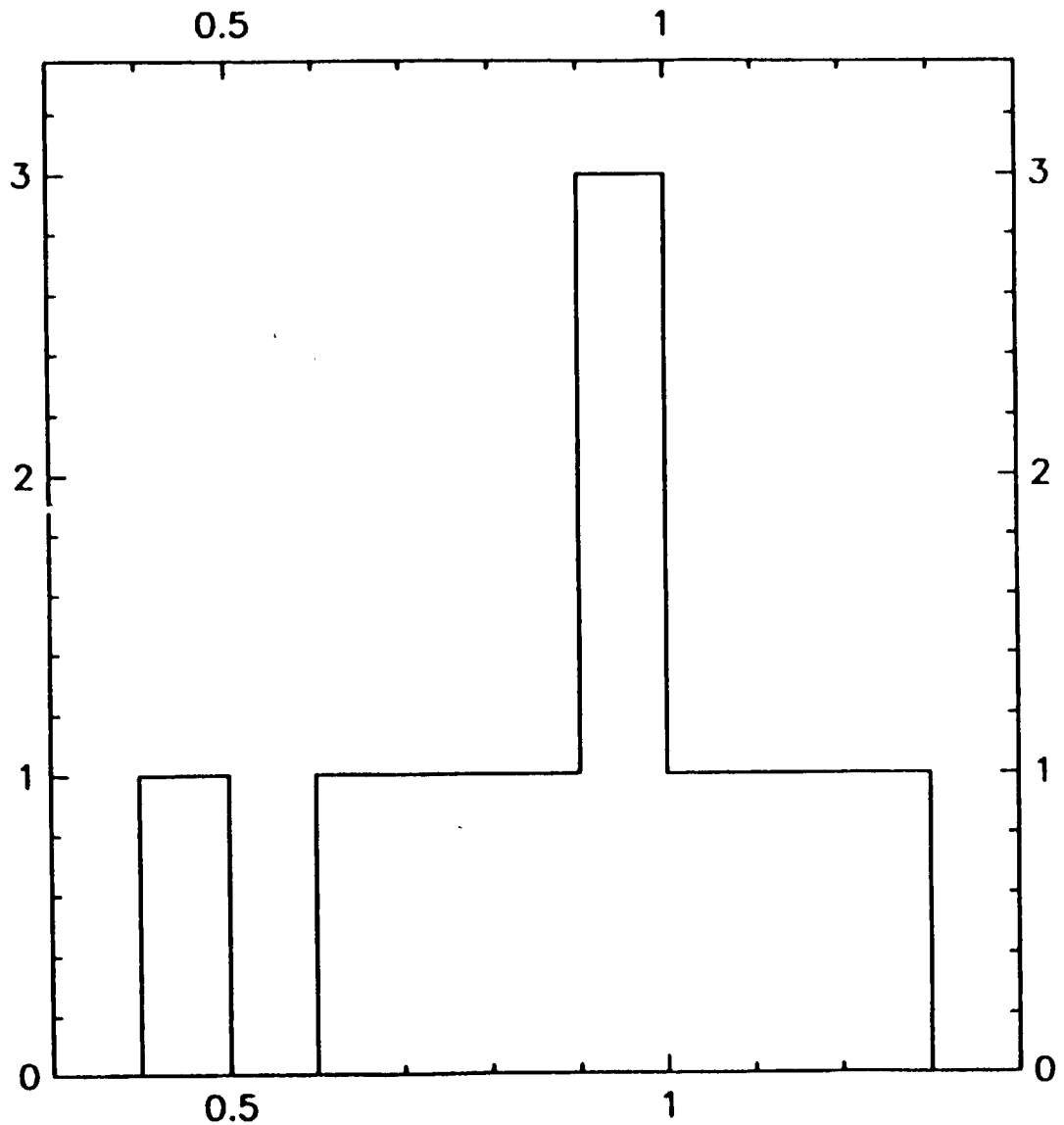

Ratio MPC/IPC Normalisation

Fig. 2

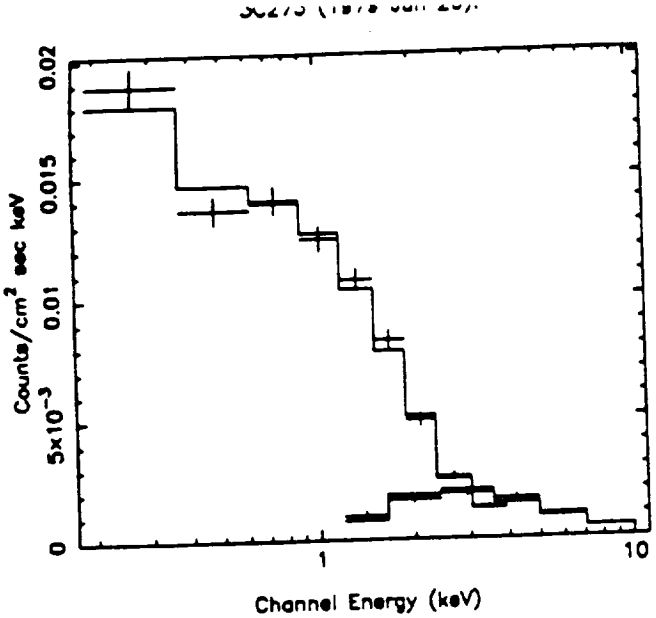

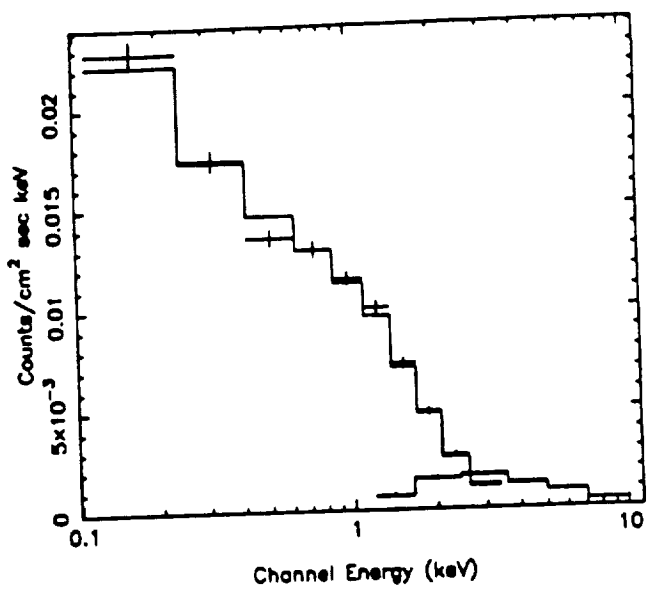

3C273 (1980 Dec 13):

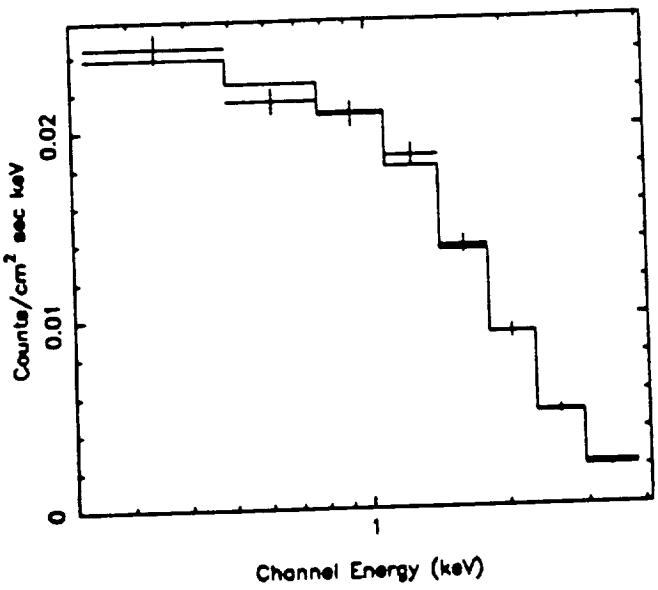

3C279:

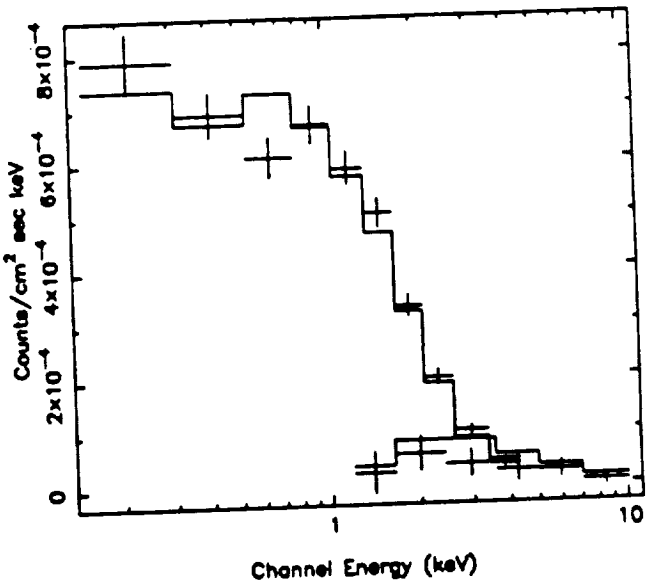

PG 1426+015 (1980 Aug 3):

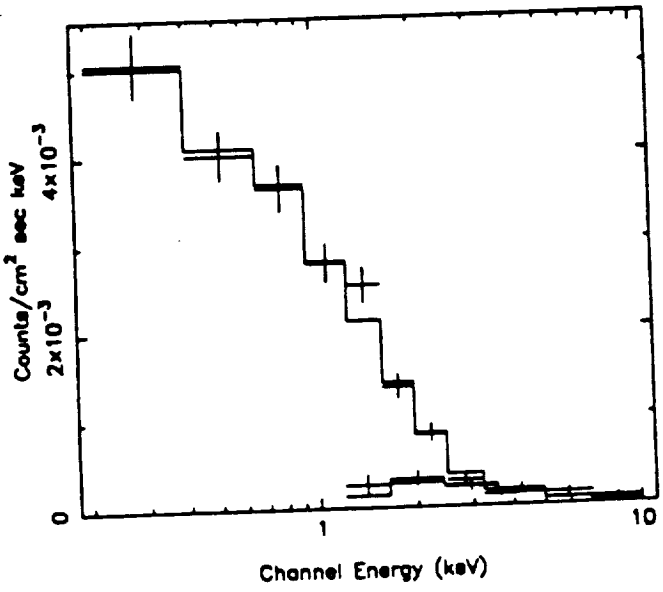

PG 1426+015 (1981 Jan 5):

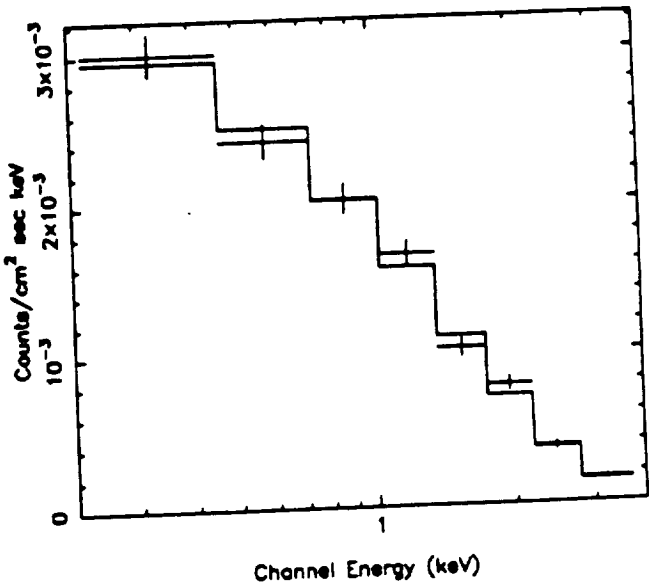

Fig. 3

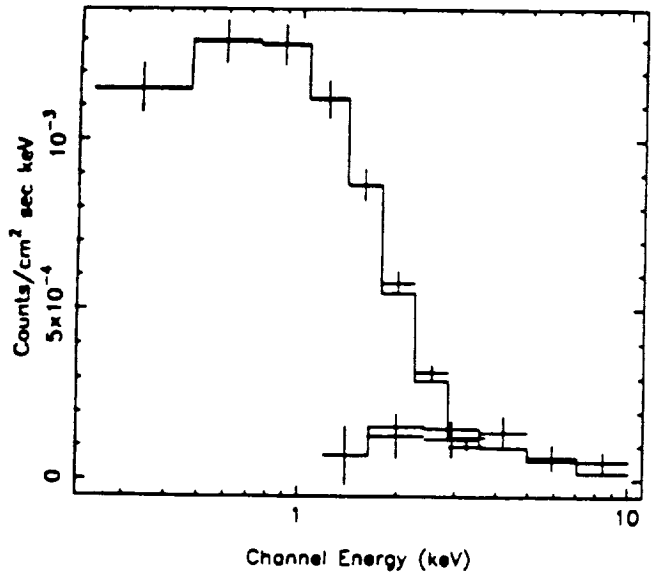

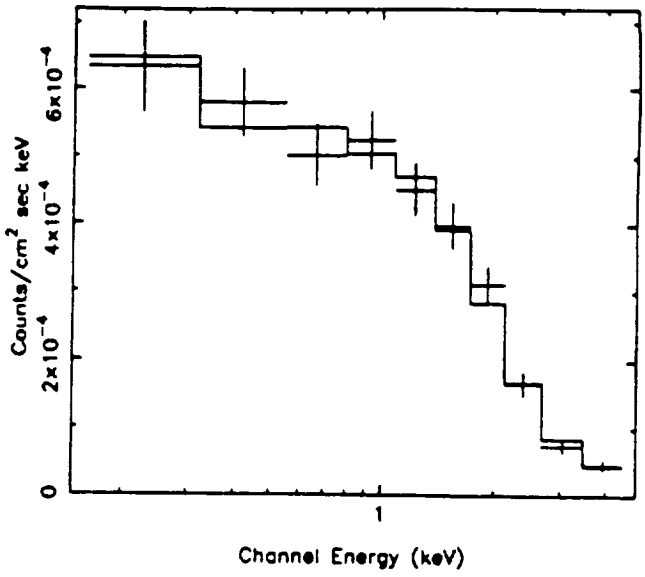

NAB 0205-024:

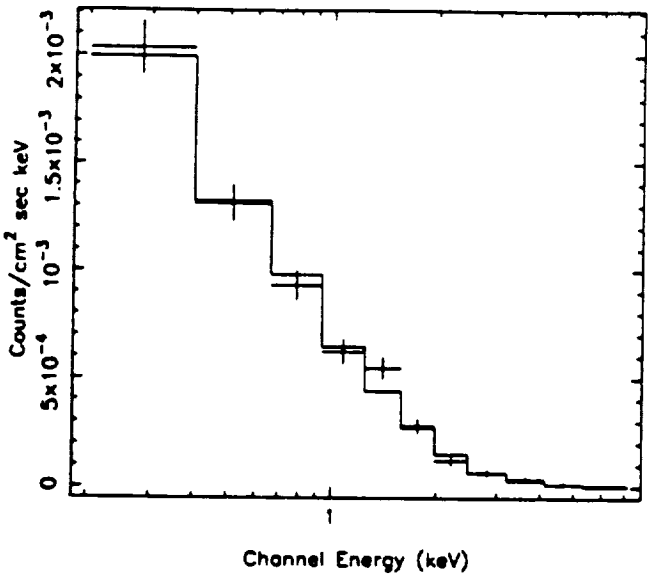

PKS 0637-752:

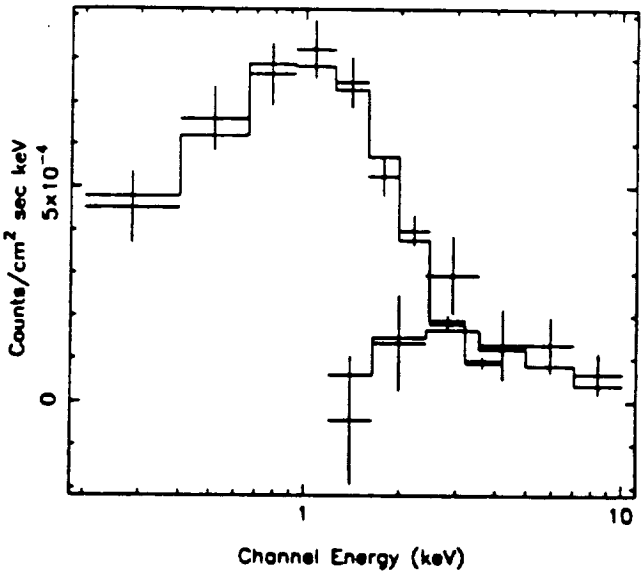

B2 1028+313:

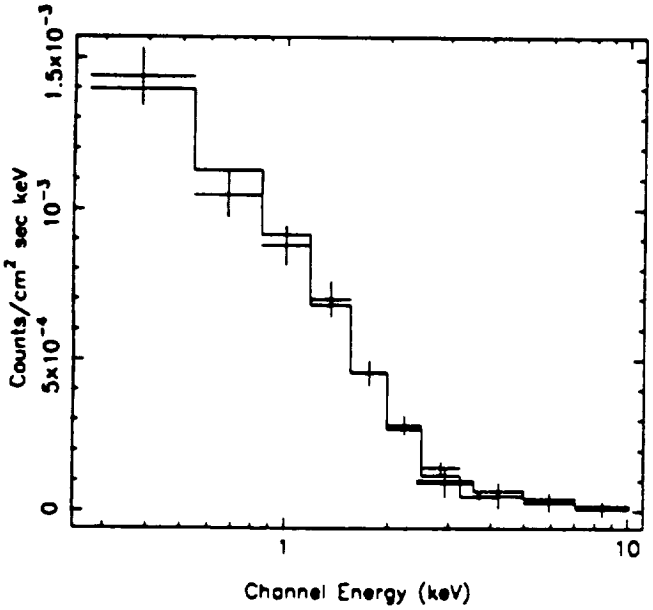

MKN 205:

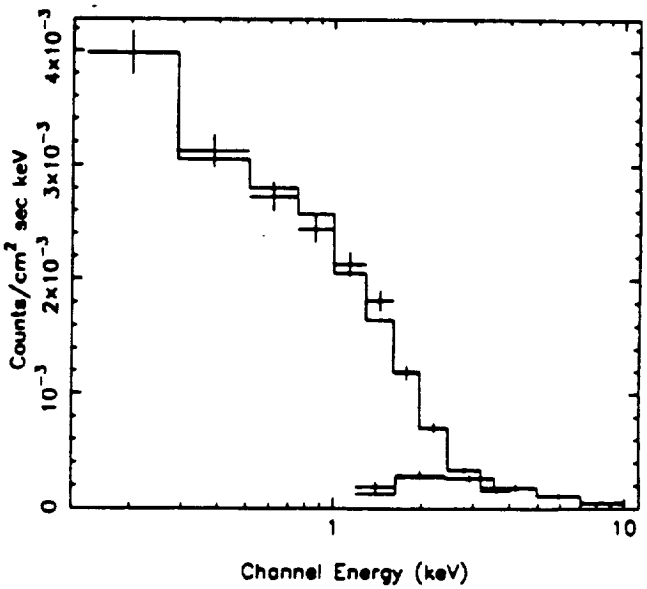

Fig. 3 A.

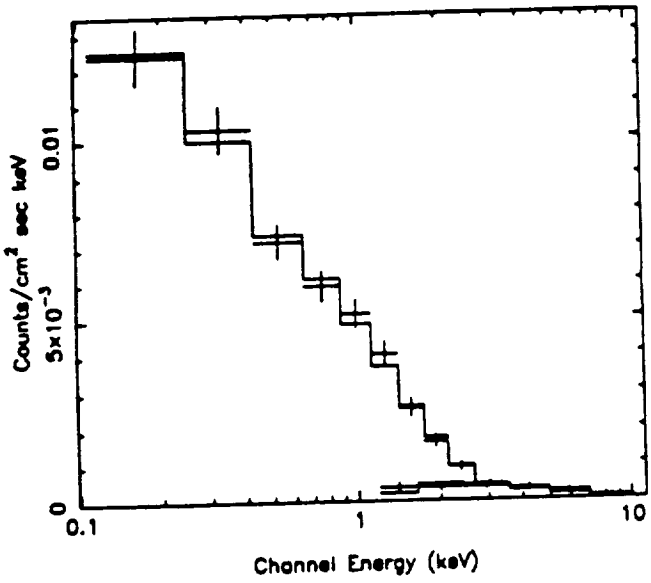

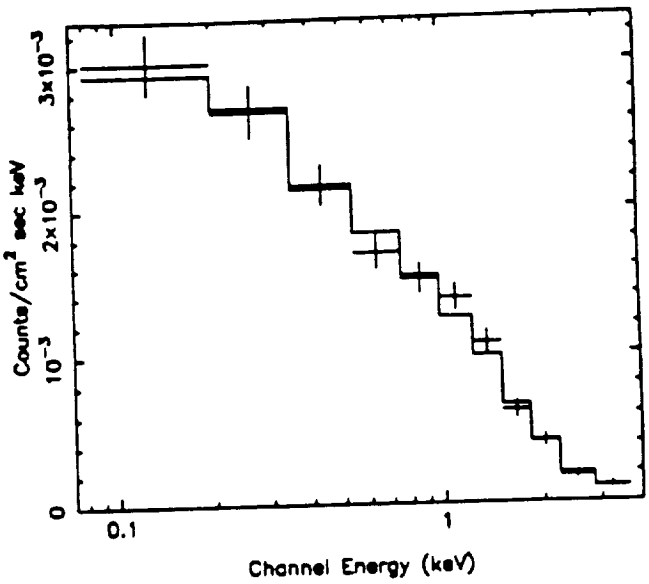

II Zw 138:

PHL 1657:

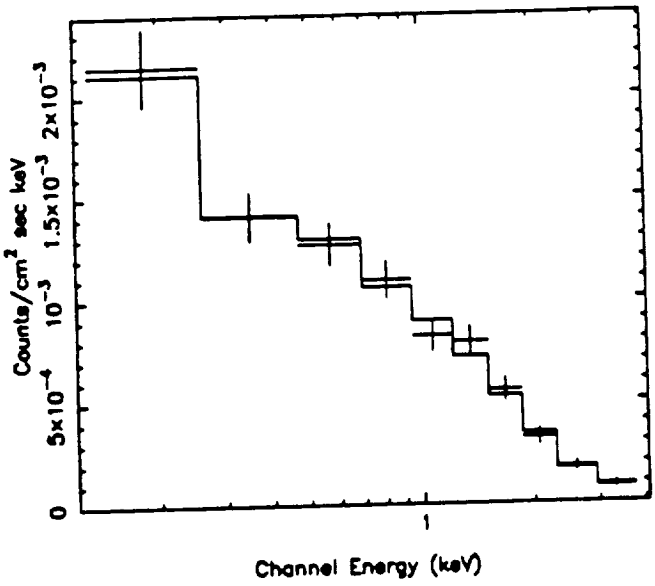

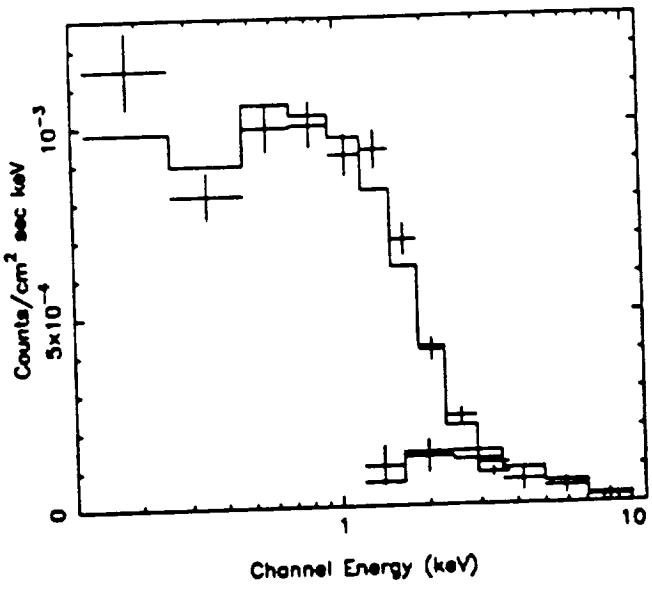

Fig. 3

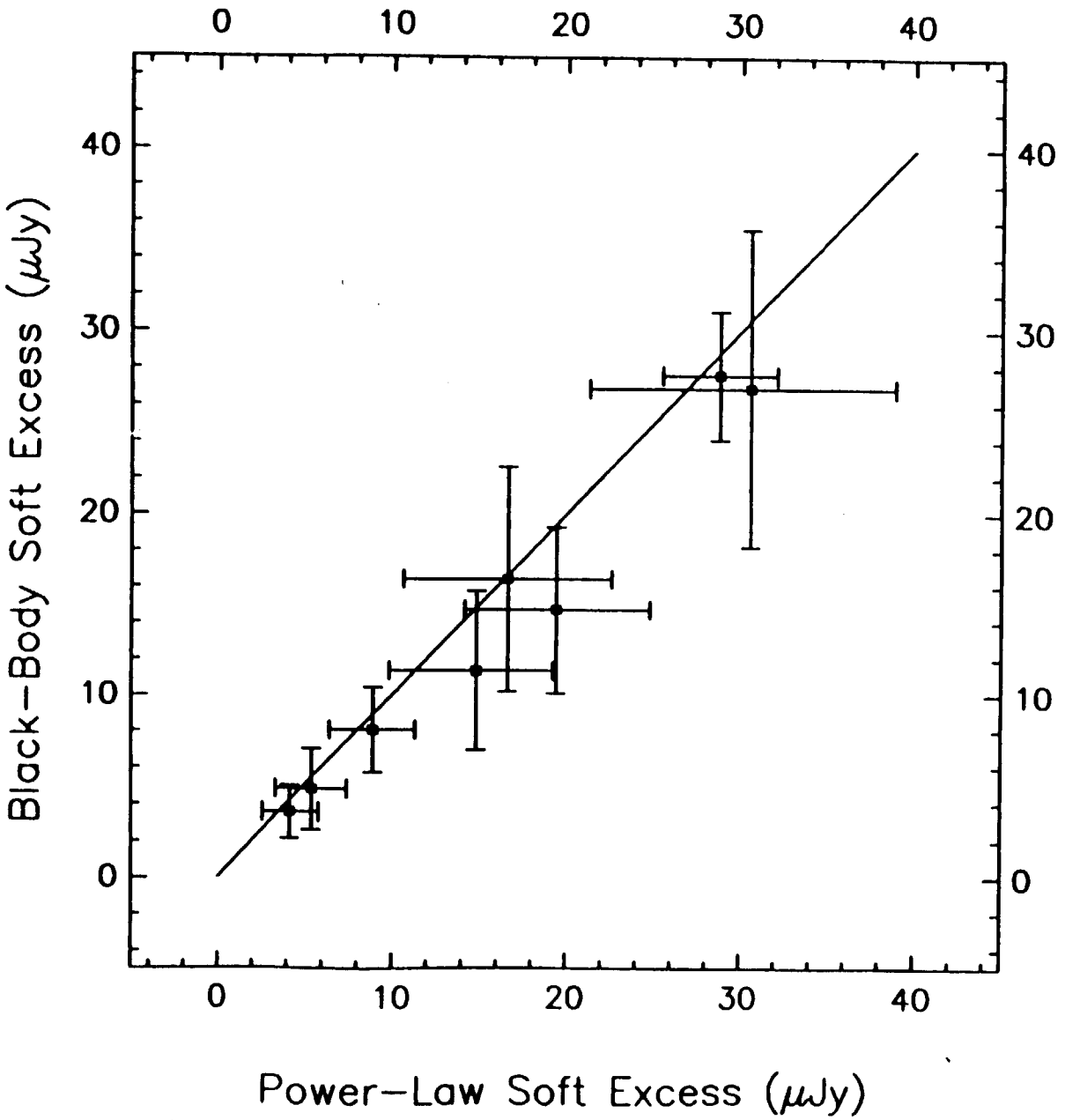
0
10
20
30
40
Black–Body Soft Excess (μJy)
Power–Law Soft Excess (μJy)

Fig. 4

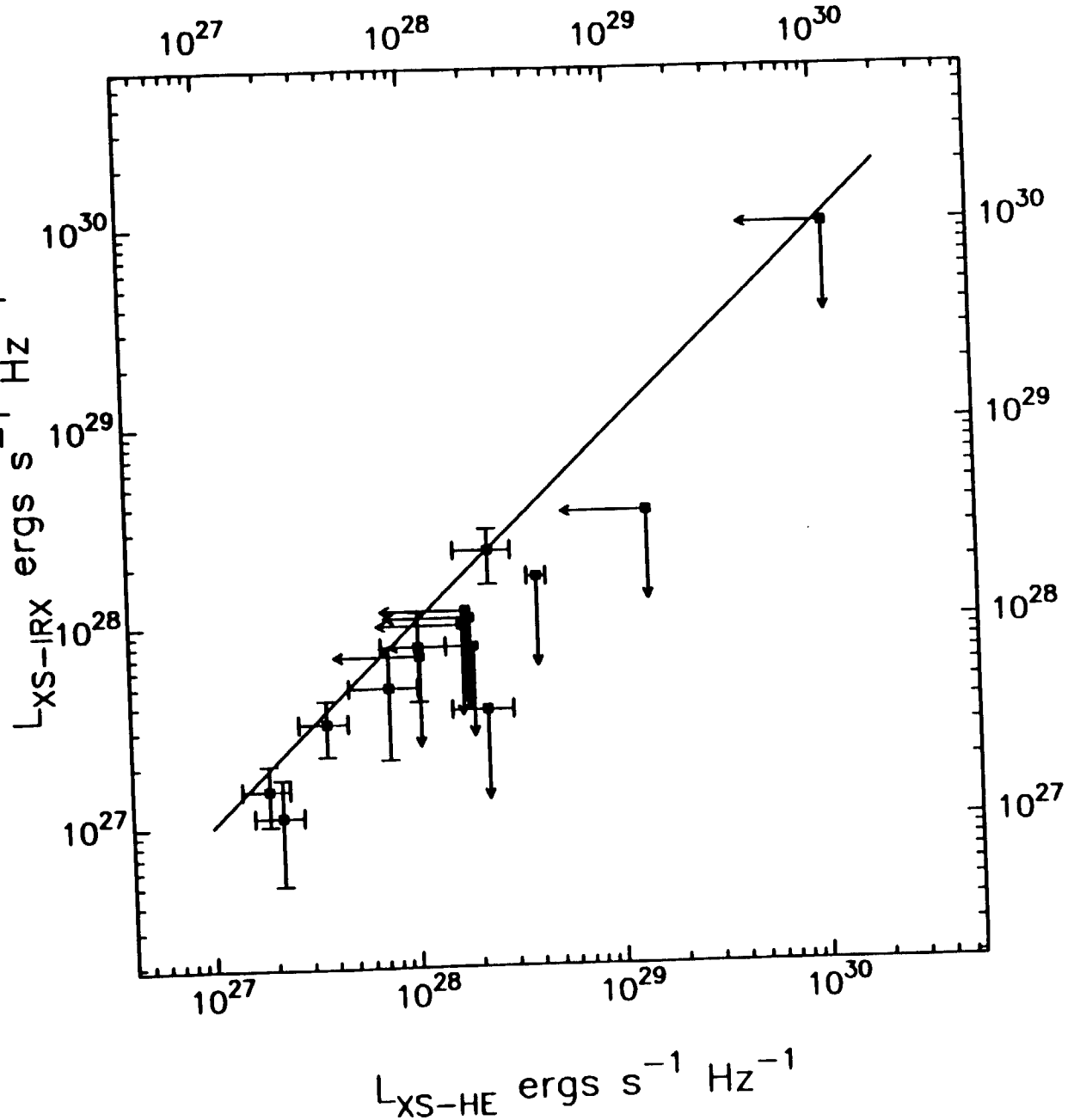

Fig. 5

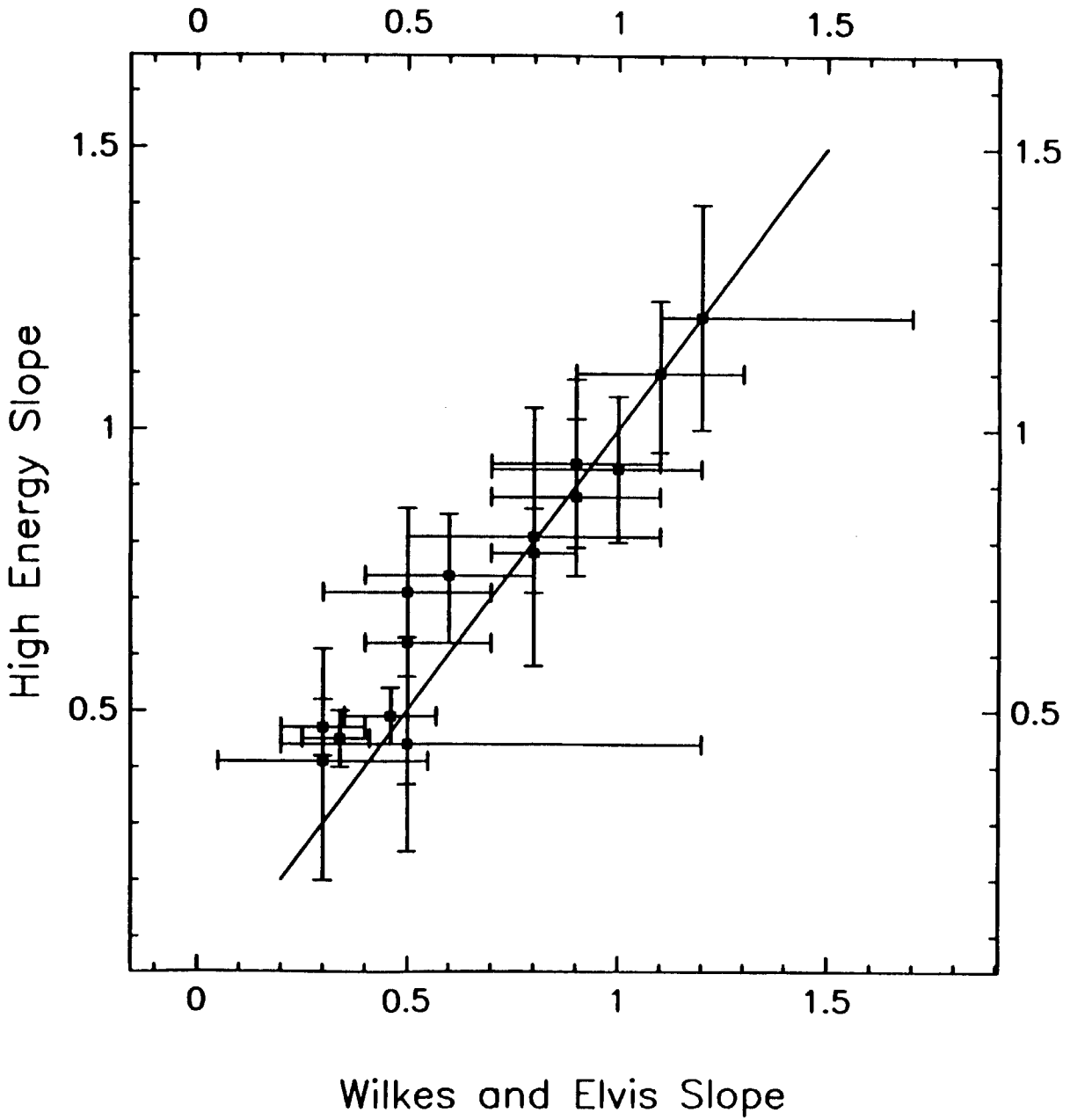

Fig. 6

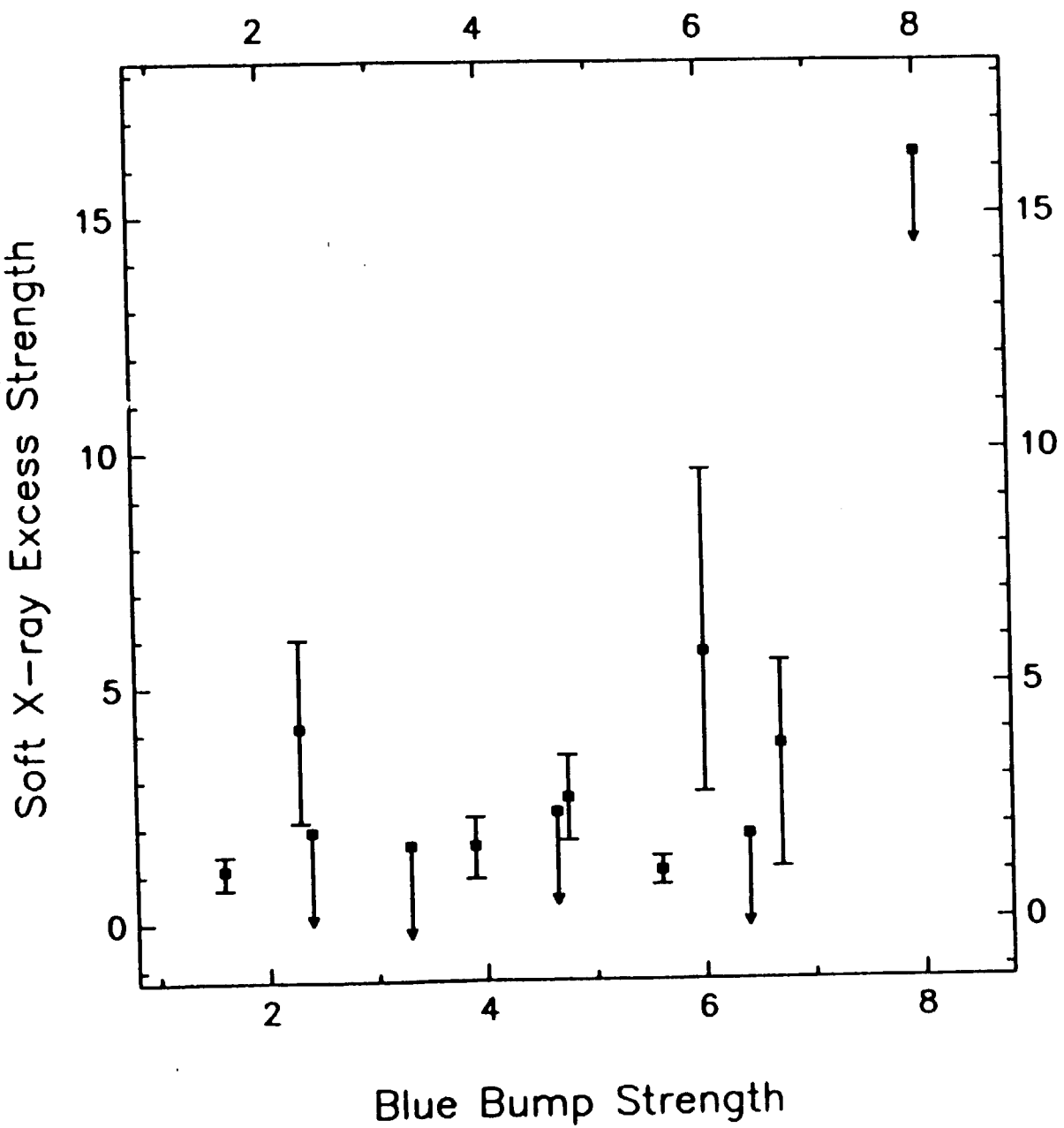

Fig. 7

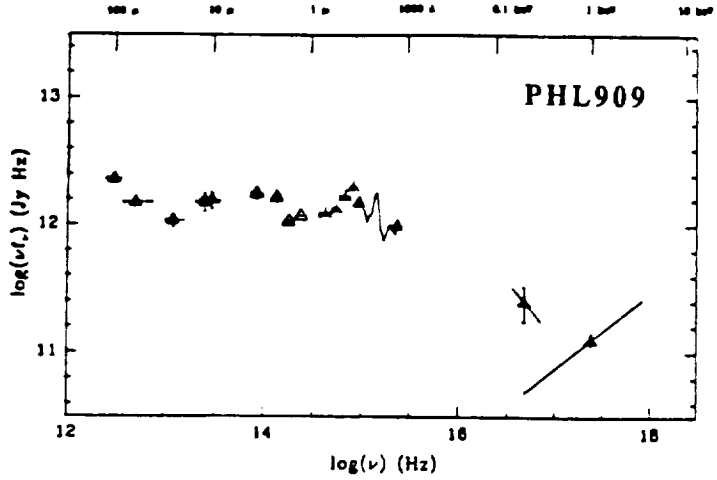
PHL909
log(νf_ν) (Jy Hz)
log(ν) (Hz)

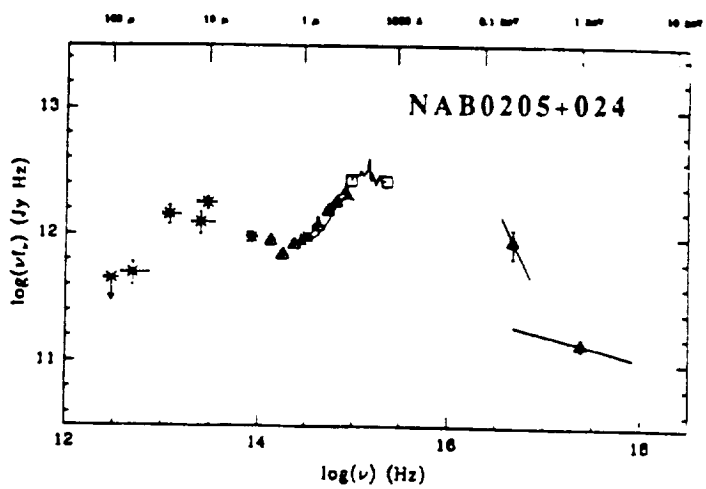
NAB0205+024
log(νf_ν) (Jy Hz)
log(ν) (Hz)

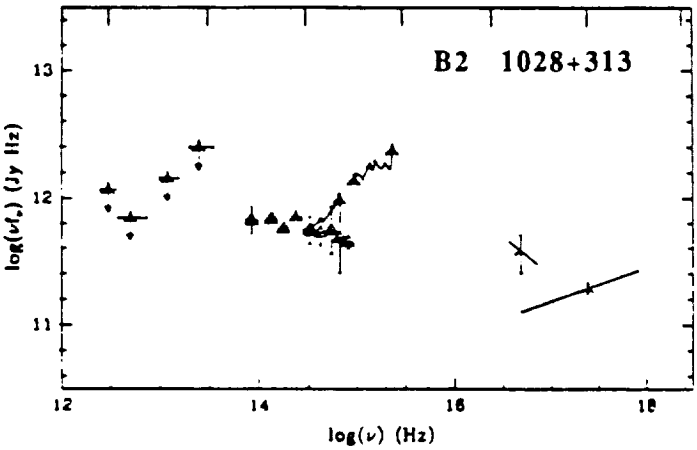
B2 1028+313
log(νf_ν) (Jy Hz)
log(ν) (Hz)

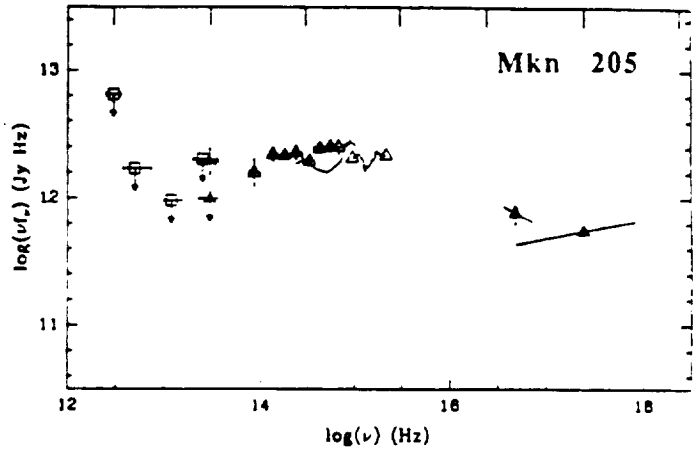
Mkn 205
log(νf_ν) (Jy Hz)
log(ν) (Hz)

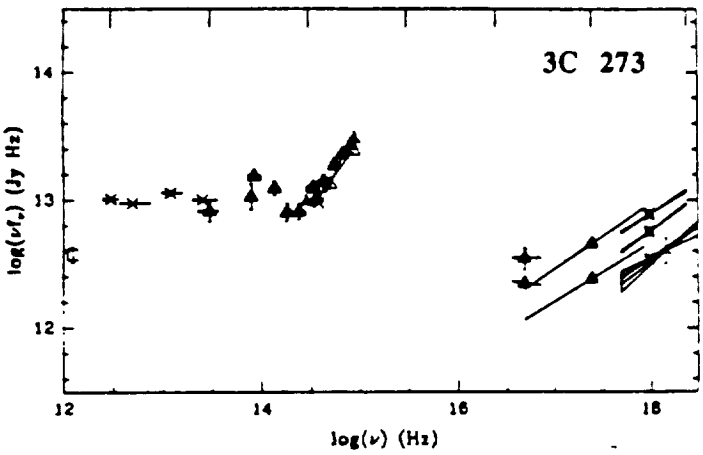
3C 273
log(νf_ν) (Jy Hz)
log(ν) (Hz)

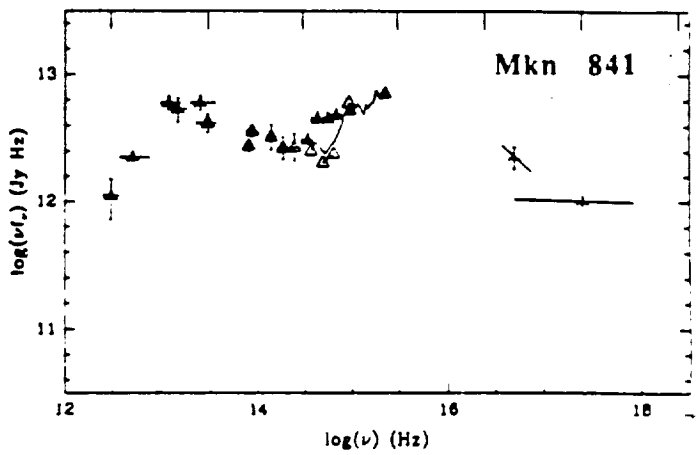
Mkn 841
log(νf_ν) (Jy Hz)
log(ν) (Hz)

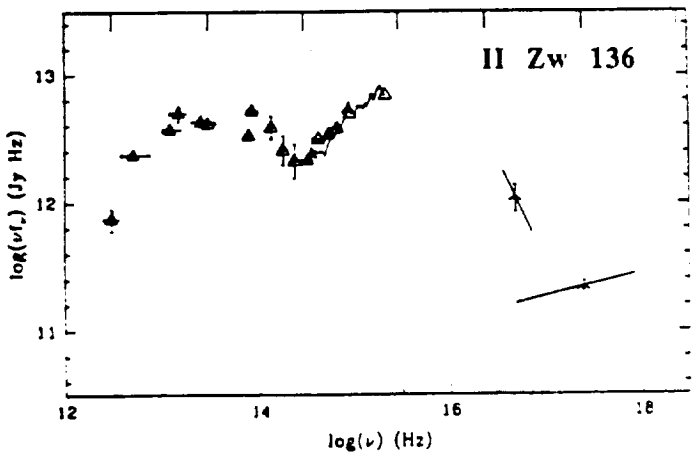
II Zw 136
log(νf_ν) (Jy Hz)
log(ν) (Hz)

Fig. 8

EXOSAT X-ray Spectra of Quasars

Andrea Comastri[1,2], Giancarlo Setti[1,2,3], Giovanni Zamorani[4,2]
Martin Elvis[5], Paolo Giommi[6,7]
Belinda J. Wilkes[5], Jonathan C. McDowell[5]

1 Dipartimento di Astronomia, Universita' di Bologna, Italy
2 Istituto di Radioastronomia del CNR, Bologna, Italy
3 European Southern Observatory, Garching bei Munchen, FRG
4 Osservatorio Astronomico di Bologna, Italy
5 Center for Astrophysics, Cambridge, MA, USA
6 EXOSAT observatory, Astrophysics Division, Space Science Dept. of ESA, ESTEC, The Netherlands
7 On leave of absence from Istituto di Fisica Cosmica del CNR, Milano, Italy

Submitted to Astrophysical Journal 2/21/91

ABSTRACT

We have measured the X-ray spectra in the 0.1-10 keV energy range for 17 AGNs (mostly PG quasars) using the EXOSAT Low and Medium-Energy arrays. The sample has been selected on the basis of soft X-ray flux, and includes **all** the AGNs in Zamorani et al. (1981) and Tananbaum et al. (1986) with an ***Einstein*** flux greater than $6 \times 10^{-12} ergs\ cm^{-2} sec^{-1}$.

For each object we have determined the best fit spectral parameters in the medium energy range ($\sim 2 - 10$ keV), i.e. the power law slope, the normalization and the absorbing column density. In this energy range all the spectra are well described by a single power law model, with a wide distribution of energy spectral indices in the range $0.4 < \alpha < 1.3$. The average spectral index is $< \alpha >= 0.89 \pm 0.06$, but most of the objects are distributed around $\alpha \simeq 1.0$. The overall distribution of spectral indices is significantly displaced toward steeper spectra, when compared to that found in the same energy band by Turner and Pounds (1989),for a large sample of hard X-ray selected Seyfert galaxies. This difference can be understood in terms of the different selection criteria of the two samples (soft versus hard X-ray selection) and it is concluded that the **true** distribution of hard X-ray spectral indices in AGNs is probably wider than previously suggested.

Inclusion of lower energy data ($\sim 0.1 - 2.0\ keV$) shows the presence of **significant** soft excess in 6 out of 17 cases. This soft excess emission can be modeled by either a steep power law with α ranging from 2.7 to 4.2 or the high energy tail of a blackbody with temperatures in the range 40-80 eV. The intersection of this soft excess emission with the hard X-ray power law is in the energy interval 0.35-0.75 keV, in the source rest frame.

A correlation analysis performed on our data set does not reveal any correlation between the medium energy spectral properties and other physical parameters of the sources. However, fits performed in the energy range 0.1-4.0 keV (comparable with the *Einstein* IPC energy range) show a significant correlation between radio-loudness and X-ray spectral properties, with the radio-loud objects having, on average, flatter slopes than the radio-quiet ones, in agreement with Wilkes and Elvis (1987) findings. The fact that the same correlation is not seen in our data at higher energy seems to be explained by a correlation between presence and strength of soft excess and "radioquietness": the objects with significant soft excess emission tend to be the most radio-quiet quasars in our sample.

Subject headings: quasars-Seyfert nuclei-X-rays:spectra

I. INTRODUCTION

Quasars and Seyfert 1 galaxies are well known to be powerful sources of X-rays which constitute an important, and sometimes even dominant, fraction of their total energy output. Although the nature of the X-ray emission is still uncertain, it is widely believed that it might be associated with the activity induced by a central compact object, perhaps a massive black hole. The study of the X-ray spectra and their time variability, together with an intercomparison of the spectral behaviour in other portions of the emitted radiation spectrum, may therefore provide important clues to understanding the nature of the emission mechanisms and the physical conditions of the regions surrounding the central compact object.

In addition, the study of the X-ray spectra of quasars and Seyfert 1 galaxies is important to set constraints to the integrated contribution of these objects to the extragalactic X-ray background (XRB), whose origin is still the subject of debate (e.g. Setti 1990 for a recent review). Since the average spectrum in the 2-10 keV energy interval of a close-by, bright sample of Seyfert 1 galaxies is significantly steeper than that of the XRB in the same energy interval, it appears that this class of objects cannot contribute the dominant fraction of the XRB unless there is a positive cosmological evolution in the number density and/or luminosity of Seyfert 1 nuclei accompanied by a flattening of the average spectrum (in the observer's frame) as a function of cosmic epoch (Setti and Woltjer, 1989; Fabian et al., 1990; Morisawa et al., 1990).

Early surveys in the 2-20 keV range of X-ray bright AGNs (mostly low-luminosity and low-redshift Seyfert 1 galaxies) suggested the existence of a "universal" energy spectrum described by a power law of the form $S(E) \propto E^{-\alpha}$, where E is the photon energy and $\alpha \simeq 0.7$. The small spread in the observed distribution of the spectral indices was consistent with the expected dispersion introduced by the observational uncertainties only (Mushotzky 1984). Recently, Turner and Pounds (1989, hereafter TP89) reported EXOSAT observations of a larger sample of 48 hard X-ray selected AGNs (again mostly Seyfert 1 nuclei) and confirmed that the energy spectra in the 2-10 keV range are described by simple power-laws, with a narrow distribution (dispersion $\sigma = 0.16$) of spectral indices around a mean energy index of about 0.7. There are however some significant exceptions (NGC4151, 3C273, MKN335, AKN120), which suggest a real spread in spectral slopes over the X-ray band (TP89 and references therein).

Hard X-ray spectra of quasars have been recently measured with the Japanese satellite GINGA in the energy range 2-10 keV (Turner et al. 1989). For this small sample of 8 objects (5 radio-loud and 3 radio-quiet) they found a mean spectral slope of 0.69, but with a relatively high dispersion of about 0.29. In fact, two objects show spectra significantly flatter than the average: $\alpha = 0.48$ for 3C273 and $\alpha = 0.05$ for PG1416-129. For this sample no correlation between radio loudness and the 2-10 keV spectral slope is found.

The X-ray spectra of a sample of 20 Seyfert 1 galaxies observed over a broader energy range ($\sim 0.15 - 10$ keV; IPC and MPC instruments of the ***Einstein*** Observatory) show the "canonical" average energy index of 0.7 at energies > 2 keV (Urry et al. 1989). From the combined IPC/MPC data it is concluded that, although

a single power law model is generally acceptable, in most cases a power law plus a soft excess emission modeled by a blackbody give a significantly better description of the data.

The simplicity of the X-ray spectra of AGNs at hard energies (*i.e.* single power laws) apparently breaks down at softer X-ray energies. At these energies there are at least two effects which may complicate the description of the X-ray spectra. The first, intrinsic absorption, has been shown to be important mainly in low luminosity AGNs (Reichert et al. 1985, Lawrence and Elvis 1982). The second, soft excess, has been quite clearly seen in the study of the ***Einstein*** IPC data of a sample of 33 quasars (Wilkes and Elvis 1987, hereafter WE87) and then confirmed to be a common feature in EXOSAT data of Seyfert galaxies (TP89). The same ***Einstein*** Observatory IPC data (0.3-3.5 keV) showed (Elvis et al. 1986; WE87) that, although the soft X-ray spectra of AGNs (with both low and high intrinsic luminosity) have a wide range of power-law spectral indices ($-0.2 < \alpha < 1.8$), they are strongly grouped around $\alpha \sim 0.5$ for radio loud objects and $\alpha \sim 1.0$ for radio quiet objects. This difference of the soft X-ray spectra as a function of the radio properties has been confirmed and extended by the results obtained by Canizares and White (1989) on a larger sample of quasars, covering a wide redshift range. They also find that the X-ray spectral index shows no evidence of dependence on redshift.

A recent analysis of *Einstein* IPC observations of a large sample of mostly radio-quiet Seyfert 1 galaxies (75 objects) performed by Kruper, Urry and Canizares (1990) shows a mean spectral index $\alpha = 0.81 \pm 0.03$, significantly steeper than the "universal" hard energy slope. Although the number of radio-loud objects in their sample is small, their results are consistent with the correlation seen in quasars (WE87, Canizares and White 1989) between soft spectral indices and radio loudness. A weak correlation between the X-ray power law index and the X-ray luminosity ($\Delta\alpha \sim 0.2$ for $\Delta log L_X \sim 5$ decades) has been found by these authors for the sub-sample of well determined spectra of radio-quiet Seyfert 1 and quasars, with the higher-luminosity objects having a steeper spectral index.

Elvis et al. (1986) discussed various possibilities which may explain the observed difference in the spectral index distributions between the IPC results and those obtained at harder energies. They concluded that, while the lower energy range of the IPC is relevant in a fraction of the objects, the most likely explanation for the observed difference is biases induced by the selection of the samples to be compared. To further investigate this effect we have used EXOSAT Low and Medium Energy data to determine the energy spectral index of a number of AGNs, selected on the basis of soft (i.e. ***Einstein***) X-ray flux. In §II we define the selection criteria of our sample, we give the observation log and describe in detail our spectral analysis. The results of our analysis are presented and discussed in §III, the conclusions are given in §IV.

II. OBSERVATIONS AND ANALYSIS

We present new X-ray data for a sample of X-ray bright Seyfert 1 nuclei and

quasars (hereafter AGNs) observed with the EXOSAT Observatory. The objects in the sample were selected on the basis of soft (*Einstein*) X-ray flux. In particular, the sample includes all the AGN in Zamorani et al. (1981) and Tananbaum et al. (1986) with an *Einstein* flux greater than $6 \times 10^{-12} ergs\ cm^{-2} sec^{-1}$, or equivalently 0.2 IPC counts per sec , which appeared in the EXOSAT database as of May 1990. A total number of 17 AGNs satisfy this selection criterion; most of them are PG quasars (Schmidt and Green 1983). Table 1 lists some relevant data for these objects. The successive columns give : coordinates and alternate names of each object, redshift, absolute B magnitude, *Einstein* flux, luminosity and spectral index, α_{ox}, and radio-loudness index. The definitions and/or the references for these data are given in the footnotes to the table. $H_0 = 50\ km\ sec^{-1}\ Mpc^{-1}$ and $q_0 = 0.0$ are used throughout this paper.

For all the objects in our sample the EXOSAT data were obtained with both the low energy (LE) imaging telescopes (De Korte et al. 1981) and the medium energy (ME) detector array (Turner, Smith and Zimmerman 1981). Although the ME detector was in principle sensitive up to about 50 keV, the signal/noise ratio becomes very poor above $\sim$ 8 keV for the relatively weak sources of our sample. Details on the instrumentation can be found in White and Peackock (1988).

Table 2 gives the observing log for the 17 objects of the sample. The various columns list the source name, the date of the observations, the detector used (ME or LE filter), the exposure time (in seconds) and, finally, the count rate (in counts per second for ME and 10^{-2} counts per sec for LE observations). When more than one observation was available in the EXOSAT database for the same objects, we have used the data-set with the longer exposure time and/or higher quality. As seen in Table 2, most of the objects have been observed with at least two low energy filters (3000 Lexan and Al/p), the only exception being PKS 0637-75 for which there is only one observation with the Lexan filter. For ten objects additional LE data with the Boron filter are also available, while for one object (PG1229+204) we have also one observation with the PPL filter. For all filters (with the exception of the boron) we have used vignetting corrected and background subtracted data from the EXOSAT database. The Boron case is special since the point spread function in this filter strongly depends on the source spectral shape. For this reason a careful re-analysis of all the original image data has been performed using the interactive analysis system of the EXOSAT Observatory.

The effective areas of the LE filters can be found in Figure 2 of White and Peackock (1988). While the Boron filter has a narrow energy response peaked at around 1 keV, the Lexan and Al/p filters are still sensitive at much lower energies, well below the C-band (0.28 keV). The combination of the count rates in the low energy filters with the more detailed spectral information given by the medium energy detector at higher energies not only provides a better determination of the spectral slope, but also allows to constrain the degree of interstellar and/or intrinsic absorption and to detect, if present, additional soft components.

a) ME Spectral Fitting

For all our objects the ME analysis has been performed only in the energy range where a net signal above the background was detected. The highest PHA channel used ranges from channel 25, corresponding to about 7 keV, to channel 35 (about 9-10 keV). For each object the pulse height spectrum was fitted with a simple model corresponding to a source power law spectrum corrected for absorption due to interstellar gas of solar composition (Morrison and McCammon, 1983). For the fitting procedure we used the standard χ^2 minimization technique available in the EXOSAT spectral fitting package (XSPEC; Shafer, Haberl, Arnaud 1989).

In a first fitting run both the slope of the power law spectrum and the amount of absorbing hydrogen were considered as free parameters and the 90 % confidence limits on each parameter were calculated (see Avni 1976; Lampton, Margon and Bowyer 1976). Because of the relative faintness of our objects, with typical fluxes in the range 4 to $8 \times 10^{-12} ergs\ cm^{-2} sec{-}1$, the allowed region in the $N_H - \alpha$ plane is almost always very large (Figure 1). With the only exception of PG0049+171 the values of Galactic N_H are well inside the allowed regions and mostly very close to the best fit values, so that we have decided to keep N_H fixed at the Galactic values. The results of these fits are shown in Table 3 where for each object we give the channels used in the fit, the flux in the 2-8 keV energy range, the power law spectral index with associated 90 % errors ($\Delta\chi^2 = 2.71$ for one interesting parameter, Avni 1976), the Galactic N_H from the accurate radio measurement performed by Elvis, Lockman and Wilkes (1989), and, finally, the reduced χ^2 and degrees of freedom.

As seen from the last column of Table 3, the simple power law model with absorption from our own Galaxy provides an acceptable fit for essentially all the objects (reduced χ^2 of the order of unity). The overall distribution of the reduced χ^2 for the entire sample (with $N_H = N_{Hgal}$) is consistent with that expected by chance according to a Kolmogorov - Smirnov test ($p \sim 0.2$). Therefore our data do not indicate the presence of any substantial amount of intrinsic absorbing cold matter. PG0049+171, with a reduced χ^2 of 1.98 (17 degrees of freedom), appears to be the only object for which a substantial N_H in excess of Galactic N_H seems to be required. For this object we give in the footnote of Table 3 the parameters corresponding to the best fit with free N_H. Inspection of the data for this object shows that an important contribution to the large χ^2 is due to a single channel (channel 15 at about 4.2 keV) which is significantly higher than the adjacent channels. Excluding this "peculiar" channel from the fit, the reduced χ^2 with $N_H = N_{Hgal}$ becomes 1.31. We also note that PG0052+251 is the only object for which the best fit column density is higher than the Galactic value at 68 % confidence interval, however this value is consistent with the Galactic N_H at 90 %.

Thermal bremsstrahlung models were also tried, but they generally provided significantly worse fits to the data.

b) LE and ME Combined Spectral Fitting

The same simple model (single power law + cold gas absorption) was then fitted to the combined LE and ME data. The results of these fits are shown in Table 4, where for each object we give two sets of results, the first with both the

spectral slope (column 2) and the amount of N_H (column 3) considered as free parameters and the second with N_H kept fixed at the Galactic value. Column 4 gives the reduced χ^2 and degrees of freedom of the combined fit, while column 5 gives, for each case, the increment in the χ^2 value resulting from the addition to the ME data of the data for the LE filters. In the same column also the number of the LE filters is given for each object.

In order to check whether the addition of the LE data is consistent with the model of a single power law, we have applied the F-test, i.e. for each object we have computed the F statistics defined as (Bevington, 1969):

$$F(\chi^2, \nu_1, \nu_2) = \frac{\Delta\chi^2/\Delta\nu_1}{\chi^2_{ME}/\nu_2}$$

where $\Delta\nu_1$ = number of additional data points (i.e. number of LE filters) and ν_2 = number of degrees of freedom in the ME filters. Adopting as a critical value for F the value corresponding to the probability of 5 %, we find that for six objects (all of them PG quasars : 0003+199, 1211+143, 1226+023, 1229+204, 1426+015, 1501+106) the F value in the case $N_H = N_{Hgal}$ is larger than F_{crit} ($F_{crit} \sim 3$ for the relevant number of degrees of freedom). This suggests that for these objects a single power law model is not an acceptable description of the spectrum over the energy range 0.1 - 8 keV. For all these objects the best fit value for N_H is significantly smaller than the measured value of N_{Hgal} and, moreover, for all of them the best fit slope (at $N_H = N_{Hgal}$) of the LE + ME data is steeper than the corresponding slope of ME data only. On the basis of these independent checks, we conclude that we have detected the presence of a soft excess in these six objects for which a more detailed spectral analysis is reported below.

For the other eleven objects the F-value for $N_H = N_{Hgal}$ is well below the value of F_{crit} and N_{Hgal} is always within the allowed N_H range. This is true also for PG 0049+171, for which the ME data seemed to require a substantial amount of $N_H(> 10^{22} atoms\ cm^{-2})$. In light of the possible problems with at least one ME channel for this object (see §II.a) we tentatively conclude that the combined LE and ME data are consistent with a single power law spectrum over the entire energy range 0.1 - 8 keV, with no significant absorption in addition to the Galactic one.

For the six objects classified as "soft excess" in Table 4, we have tried more complex fits to the data. In Table 5 we report the best fit results for two models, one described by two power laws and the other by a blackbody plus a power law with the high energy slope and normalization fixed at the value found from the ME fit. In order to find a lower limit for the strength of the soft excess emission we have fixed the amount of N_H at the minimum value, i.e. $N_H = N_{Hgal}$. The entries in Table 5 give the low energy best fit results (α_{steep} and blackbody temperature) with the 90 % error intervals, together with the value of reduced χ^2 and corresponding probability and, finally, an estimate of the break energy, defined as the intersection, in the source rest frame, between the soft excess emission fit and the hard X-ray power law. To test the statistical significance of the models used to fit the soft excess emission, we have performed an F-test. The addition of two free parameters (α_{steep} or the blackbody temperature with the relative normalizations) gives a statistically better fit for all six objects.

For some of the objects in our soft X-ray selected sample there are already published EXOSAT spectral data with which we can compare our results. These objects are MKN335, IIIZW2, 3C273 (TP89), PG0026+129 (Treves et al. 1988), MKN841 (Arnaud et al. 1985). In most cases our fits are in good agreement, within the errors, with the published results. This is true both for the slopes of the power law and for the presence or absence of soft excess emission. The only discrepancy is in the temperature of the fitted blackbody for MKN841; the value found by Arnaud et al. (1985) ($\sim 17\ eV$) is significantly lower than our best fit value (57 eV). It must be noted, however, that Arnaud et al. fitted the blackbody emission combining data in the ultraviolet and in the soft X-ray ranges. Additional comparisons with other non EXOSAT, results will be discussed in the next section.

III. DISCUSSION

a) ME Results

The hard X-ray emission spectra of all the 17 AGNs in our sample can be well described by a single power law. The distribution of the ME spectral indices is shown in Fig. 2, where the dashed part of the histogram represents objects with a one sigma error on the slope smaller than 0.20. In the same figure we show also the gaussian which best fits the data in TP89. The distribution of spectral indices of our objects shows a wide range of slopes centered around $\alpha \sim 1.0$ and with a pronounced tail toward flat slopes. The average spectral index for our 17 objects is $< \alpha >= 0.89 \pm 0.06$, with an observed dispersion $\sigma = 0.25$. In this case the weighted mean is somewhat meaningless because it is dominated by the slopes of two objects (3C273 and IIIZW2) which, having a significantly higher ME flux, also have 1σ errors on the slope much smaller than the rest of the objects. Since both these objects happen to be among the flattest of the entire sample, the weighted mean would be artificially displaced toward flat slopes.

Our distribution of observed ME spectral indices is significantly different (at 98% confidence level, according to the Kolmogorov-Smirnov test) from that obtained with the same instrument by TP89 for hard X-ray selected AGNs. In their sample the percentage of Seyfert 1 galaxies with α steeper than 1.0 is 7 %, to be compared with 41 % in our sample. Figure 3 shows the spectral indices of the Seyfert 1 and quasars in the two samples as a function of the X-ray luminosity. Two differences between the samples are immediately clear from the figure: first, our objects are on average more X-ray luminous; second, in the range of overlapping luminosities our objects tend to have a steeper spectral index (even if a few flat spectrum objects are present also in our sample). Part of the latter difference may be explained by the different selection criteria of the two samples, as Elvis et al. (1986) concluded. While ours is a flux limited sample selected in the soft X-ray domain, the TP89 sample comprises objects which have been primarily selected in the hard X-ray domain. Each of the two selections has its own biases, ours against flat spectra, theirs against steep spectra.

However, essentially the same difference is present between our data and the *Einstein* MPC data of 20 Seyfert 1 galaxies of Urry et al. (1989), who claim that

their sample, like ours, is soft X-ray flux limited. This is probably not completely true, because the original IPC Seyfert sample from which this subsample has been derived (Kruper et al. 1990) contains four objects (i.e. about 20 % of the Urry at al. (1989) sample) with an IPC flux greater than their stated threshold, for which, however, no MPC spectra are presented. It is likely that the spectra of these objects are, on average, steeper than the others, thus explaining the lack of useful MPC data. Assuming that the spectral slope of these four objects are of the order of the steepest object of the sample the mean of their entire distribution would change from 0.70 to 0.79, thus becoming almost consistent with ours.

A variety of models and emission mechanisms have been proposed to explain the X-ray spectral properties of AGN, and in particular the "universal" hard spectral index of 0.7 (e.g. Mushotzky, 1984). Our results, which show that the distribution of the observed spectral indices is a function of the selection criteria of the samples, lead us to suggest that the true distribution of hard X-ray (above ~ 2 keV) spectral indices is wider than previously suggested and probably shifted toward steeper spectra.

Recent observations with the Japanese satellite GINGA of some bright Seyfert 1 galaxies (Pounds et al. 1990) have revealed new features in the high energy spectra of these objects: an iron fluorescence line near 6.4 keV, a large dip between 8 and 12 keV due to Fe K-shell absorption and a flattening of the spectrum for energies ≥ 12 keV. Models which can account for these features have been discussed by Lightman and White (1988) and Guilbert and Rees (1988). These models predict that a significant fraction (about one half) of X-rays coming from the central source should be reprocessed by cold matter (in form of a disk or clouds) through Compton scattering and fluorescence: assuming an intrinsic slope $\alpha \sim 0.9$ this model can reproduce the "universal" observed slope of $\alpha \simeq 0.7$. In this framework our results ($< \alpha > \sim 0.9$) can be interpreted in two different ways: either the reflected component is almost absent in the objects of our sample and we see mainly the direct component, or, if the reflection model holds also for these objects, their intrinsic emission spectrum has to be steeper.

b) ME + LE Results

The addition of the low energy (LE) data has allowed the analysis of the X-ray spectra over an energy interval spanning about two orders of magnitude (0.1 - 8 keV). We find that for about 2/3 of the sample (11/17) a single power law fit is consistent with the data over the entire energy range. The remaining 6 objects show a clear indication of soft excess emission in the low energy filters. This percentage of objects with significant soft excess is consistent with that (31 %) found by TP89 for Seyfert 1 galaxies. The X-ray spectra of a sample of 14 quasars have been recently measured by Masnou et al. (1991), over approximately the same energy range, with the IPC and MPC instruments of the ***Einstein*** Observatory. They find a higher percentage (57%) of objects with soft excess emission at low energy (below 0 keV). Four of the six objects for which we detect soft excess emission are in common with this sample: for three out of these four objects the soft excess

emission has been also recovered by Masnou et al. (1991). Vice versa they find soft excess in two out of five of the remaining objects in common for which a single power law gives a good fit to our data.

We note that the objects with soft excess in our sample tend to lie in regions of lower Galactic N_H than those which are consistent with a single power law. For example, soft excess is detected in 5 out of 8 objects with a Galactic N_H lower than 3.5×10^{20}, and in 1 out of 9 objects with Galactic N_H greater than this limit. The same effect is present at some level also in the TP89 data: the percentage of Seyfert 1 galaxies with soft excess in their sample increases to 55 % when the objects with Galactic $N_H < 3.5 \times 10^{20}$ are considered. Some correlation between detection of soft excess and Galactic N_H is qualitatively expected because the same amount of soft excess is more easily detected in the absence of any kind of intervening absorption. To obtain a more quantitative estimate of the possible importance of this effect we have performed the following test: first, we have created simulated data for the six objects with soft excess emission (Table 5) assuming that the true spectrum of each source is the one found from the best fit with a double power law, or with the blackbody plus a power law models. For each source we have assumed the actually observed background. Then we have applied our fitting procedure on these simulated data through the actually used filters searching for the minimum amount of Galactic N_H above which there would be no statistically significant difference between the single and the double power law (or blackbody plus power law) fits: had these objects been in a region of Galactic N_H greater than this minimum value, we would have classified their spectra as consistent with a single power law. For five objects we find that this minimum value of N_H lies between 8×10^{20} and 1.4×10^{21} *atoms* cm^{-2}. For the remaining object (PG1229+204) the minimum value of N_H is about 4×10^{20}. These minimum values of N_H have been computed choosing the appropriate $\Delta\chi^2$ with an associated probability of 95 % according to the F-test. ($F_{crit} \sim 4$ for the relevant number of d.o.f.). Since these values (with the exception of PG1229+204) are much higher than the Galactic N_H of all the objects in our sample, we can conclude that a strong soft excess, if present, would have been detected in the objects classified as single power law, all of which have a Galactic N_H lower than 6×10^{20} *atoms* cm^{-2}. A more marginal excess, however, (see the case of PG1229+204) could have escaped detection in objects with Galactic $N_H > 4 \times 10^{20}$. As a consequence, the fact that a large fraction of soft excess objects in our sample is located in regions of low Galactic N_H appears to be accidental (see also §III.c) even if the probability of observing this distribution by chance is low ($\sim 4.2\%$ according to the Fisher test).

To give a more quantitative estimate of the number of objects for which the detection of a weak excess could have been missed by our fitting procedure, we have computed for each object the quantity R_{ex} (last Column of Table 4) defined as the ratio of the observed minus predicted counts in the low energy filters to the predicted counts where the predicted counts have been computed by extrapolating to low energy the ME best fit. For the six objects classified "soft excess" the value of R_{ex} is significantly larger than zero, thus confirming the previous classification. For six out of eleven objects for which a single power law gives an acceptable fit

over the entire energy range, we find an excess of counts (*i.e.* $R_{ex} > 0$) with a significance between 1σ and 2σ, while for the remaining 5 we find a deficit of counts (*i.e.* $R_{ex} < 0$). We have then considered the six objects which have $R_{ex} > 0$ and whose spectra are well fitted by a single power law and have fitted their data with a double power law model with the high energy parameters fixed from the ME fit and a steep low energy power law. To be consistent with the results shown in Table 5, we varied α_{steep} in the range 2.5-4.0 leaving as a free parameter the low energy normalization or, equivalently, the break energy. The results show that the break energies above which the fits become significantly worse than the single power law fits lie between 0.2 and 0.5 keV depending on the adopted steepness of the low energy power law and on the value of R_{ex}. These values have to be compared with the break energies derived for the objects with soft excess emission, which are in the energy range 0.35 - 0.75 keV. The partial overlap between the energy range of the break energies for objects with and without detected soft excess suggests that we cannot exclude that also some of the AGNs in our sample whose spectra are consistent with a single power law do really have some kind of soft excess, although confined to softer X-ray energies.

Also it should be noted that the objects with detected soft excess emission tend to have better constrained ME spectra, *i.e.* smaller error on α. For this reason they have, on average, smaller errors on the expected extrapolated counts at soft energy so that the soft excess, if present can be more easily detected. On the basis of the results of the two previous tests and of this consideration we conclude that the observed percentage (35 %) of soft excess objects in our sample should be considered as a lower limit on the true frequency of such objects. Even more so if we consider that the presence of a possible absorption intrinsic to the objects, which was assumed to be absent in our fitting procedure, would cause a systematic underestimate of the soft excess strength. We have quantified the effect of additional absorbing material assuming an intrinsic column density at the source of 2×10^{20} *atoms* cm^{-2}. The corresponding increase of the X-ray opacity results in the detection of soft excess in one more quasar, *i.e.* PG2130+099.

An independent indication of the possible presence of some excess emission at low energies in most of the objects is seen in Fig. 4. which shows the distribution of ΔN_H, defined as the difference between the best N_H value obtained through the fit of a single power law to the ME and LE data and the Galactic one. If all the objects had a negligible intrinsic absorbing column, this distribution would be symmetric about zero with a spread consistent with the expected small-scale fluctuations of N_H in our Galaxy and the measurement errors. Even excluding the six objects with detected soft excess (marked with an S in the histogram), the distribution is significantly displaced toward negative values of ΔN_H: only two objects have $N_H(EXOSAT) > N_H(21cm)$. Following WE87, this can be taken as an evidence of a general presence of some soft excess in the population, although not detectable in the analysis of the spectra of the single objects. Moreover, this is consistent with the average steepening of the fits to the ME + LE data with respect to the ME ones: for the 11 objects fitted with a single power law we find an average LE+ME spectral index $< \alpha >= 1.01 \pm 0.08$, while for the same objects the mean of the ME

spectral indices are 0.95 ± 0.05.

For the objects with a significant soft excess the resulting parameters from the fits with two power laws or a blackbody plus a power law are qualitatively similar to each other. Because of the lack of detailed energy resolution of the LE detectors the spectral shape of the soft excess is not well constrained, and for most of these objects we cannot discriminate between the power law and the blackbody models. However, it is interesting to note that for five out of six objects the blackbody model gives a better fit than the power law model and the difference between the two models is statistically significant (see columns 4 and 8 of Table 5) for 3C273 and MKN335, *i.e.* the two sources with the highest soft flux. In particular, for each of the objects we find that:

a) For the two power law model the best fit slope at low energy falls in the range 2.7-4.2, much steeper than the high energy slope.

b) For the blackbody plus power law model the best fit blackbody temperatures are in the range of 45 to 80 eV, with associated errors of the order of 30 %. This range of temperatures is at variance with the bimodal distribution of the preferred temperatures ($kT < 10$ eV or $kT \simeq 200 - 300$ eV) of the fitted blackbody suggested by Urry et al. (1989), on the basis of an analysis of IPC data of Seyfert 1 galaxies. However they note that this result is affected by the discontinuous response of the IPC in the energy range 250-600 eV.

c) For both fitting models the nominal energy of intersection of the soft and hard component is in the range 0.35 - 0.75 keV.

c) X-RAY SPECTRA VS. RADIO-LOUDNESS

We have searched for correlations between the hard X-ray spectral index and other physical parameters of the sources, but none has been found. Specifically, no significant correlation has been found with the intrinsic optical luminosity nor with the redshift spanning from 0.025 to 0.25 (with one object at z=0.65) nor with the X-ray luminosity of the objects, which encompasses about three decades. As discussed in §III.a, the fact that the mean spectral slope of our sample, containing mostly high luminosity objects, is steeper than the one found by TPS9 for lower luminosity AGNs, is probably due to selection effects.

In agreement with the findings of TPS9 no obvious correlation is evident also between the ME spectral indices (α_{ME}) and the strength of the radio emission (R_L), defined as $R_L = log(f_R/f_B)$ where f_R and f_B are the flux densities at 5 GHz and 2500 Å (Fig. 5a). Such a correlation was found by WE87, although at lower energies (0.3-3.5 keV), with the radio-loud objects grouped around $\alpha \simeq 0.5$ and the radio-quiet ones around $\alpha \simeq 1.0$. Following WE87 we define a quasar radio-loud when $R_L > 1$. In order to understand the reason for this apparent discrepancy (note that 11 out of 17 objects in our sample are in common with the WE87 sample) we have performed spectral fits to our data in the 0.1-4.0 keV energy range (similar to the IPC range, 0.2-3.5 keV). The results (Fig. 5b) show that in this softer energy range there is a clear trend with radio-quiet quasars having steeper slopes than radio-loud quasars, in agreement with the WE87 work. However, for the 11 objects in common

with WE87 we find that our (0.1-4.0 keV) slopes are systematically steeper, with an average $\Delta\alpha = \alpha_{ours} - \alpha_{WE87}$ of the order of 0.3. This difference, which is also seen in Fig. 5b where most of our data points lie above the line representing the WE87 correlation could be due to either a systematic effect between the two detectors (IPC and LE/ME), or the slightly softer energy interval considered for our spectral fit results. Here we point out the existence of four objects with extremely EXOSAT steep slopes ($\alpha > 1.6$) in the 0.1-4.0 keV energy range (PG0003+199, PG1211+143, PG1229+204, PG2130+099). One of them (PG1211+143) was the only object with a very steep slope ($\alpha = 1.8$) also in the IPC energy range and was classified as exceptional by WE87. Our results indicate that these steep slopes are probably a diffuse feature in the quasars spectra.

The other apparently significant correlation in our data is between the presence of soft excess and radio loudness. Five out of six objects with detected soft excess emission are radio quiet and four of these are among the last five most radio-quiet objects in the sample (see column 8 in Table 1). The only radio-loud object with soft excess (3C273) is somewhat peculiar with respect to the other objects in the same class in that its value of R_{ex} is significantly lower than the mean value of the other five objects ($R_{ex} \sim 3$), so that the detection of the soft excess in 3C273 is mainly due to its high X-ray flux, about one order of magnitude larger than the average flux of the other objects in the sample.

In the previous Section we have discussed the apparent correlation between the soft excess and the amount of Galactic N_H. Therefore the soft excess (or equivalently, the excess counts R_{ex}) appears to be correlated with both N_H and R_L. In order to determine which of the two correlations is the fundamental one we have computed the Kendall partial rank-order correlation coefficient $T_{xy.z}$ (Siegel and Castellan 1988), which allows one to compute the probabilities of correlation for each pair of variables with the other one held constant. The only significant (anti-) correlation resulting from this test is that between the excess of counts, R_{ex}, and the radio-loudness, R_L. This result is consistent with the conclusion reached in §III.b, that the apparent correlation between soft excess and N_H is mostly accidental.

The different spectral behaviour of the radio-loud and radio-quiet quasars is also shown in Figure 6 where we plot the ME spectral slopes versus the 0.1-4.0 keV slopes. Two facts are immediately clear from the figure: first, the radio-loud objects are spread around the line of equal spectral indices and do not show any change of slope over the entire energy range; second, the radio-quiet objects tend to have systematically steeper slopes in the 0.1-4.0 keV energy range. This is true also for those objects without soft excess.

The observed anti-correlation between R_L, R_{ex} and the data shown in Figure 6 can be interpreted in two physically different ways by adopting simple two-components models. Either the radio-quiet objects may have an enhanced soft emission on the top of the power law component, which in this case would be the same in both radio-quiet and radio-loud quasars; or, alternatively, the radio-loud ones may have a relatively stronger power law component with a constant slope from low to medium energy (see triangles in Figure 6). The existence of this enhanced power law component would make more difficult the detection of the soft excess in

their spectra and would be consistent with the fact that the radio-loud quasars are stronger X-ray emitters (about a factor 3) than the radio-quiet ones (Zamorani et al. 1981). These alternative pictures are perfectly self-consistent within our EXOSAT data sample. However if the explanation of the systematically steeper 0.1-4.0 keV spectral slopes found in our sample is not due to instrumental calibration differences between EXOSAT and the *Einstein* IPC, but rather only to the softer spectral extension of EXOSAT, then the emission spectra of the sources become much more complex and the simple modelling described above need to be modified.

IV. CONCLUSIONS

We have analyzed simultaneous LE and ME EXOSAT data to determine the X-ray spectra of 17 objects selected by their soft X-ray flux (mostly PG Quasars and Seyfert 1s nuclei). The most important results of our spectral survey can be summarized as follows :

1) The hard X-ray emission spectra (above $\sim$ 2 keV) of all the AGNs in our sample can be described by a single power law model. These measured spectral indices show a wide variety of power law slopes with α spanning from 0.4 to 1.3. The average slope is $< \alpha >= 0.89 \pm 0.06$, but the distribution is centered around $\alpha = 1.0$. The narrow observed range of slopes around $\alpha \simeq 0.7$ in high energy selected samples is a result of their tendency to select the most "2-10 keV bright" AGN, which tend to be those with the flattest X-ray spectra over the whole 0.2-10 keV range. These results suggest that the true distribution of hard X-ray spectral indices is wider and probably steeper than previously suggested.

2) Approximately 1/3 (6 out of 17) of the sources in our sample show evidence for soft excess emission in the low energy filters (below 1 keV). For these objects a power law plus a soft excess modeled by steep power law or by the high energy tail of a blackbody is a significantly better description of the data than a single power law over the energy range 0.1-10 keV. Although the poor energy resolution of the LE filters precludes an accurate description of the spectral shape of the soft excess emission the blackbody model seems to be preferred to the two power law model.

3) The best fit slopes of the steep power law fits at low energies are in the range $\alpha = 2.7 - 4.2$, while the preferred temperatures of the fitted blackbodies are in the range 40-80 eV. The "break" energy between the soft and hard component is in the range 0.35-0.75 keV at the source.

4) There is no obvious dependence of ME energy index with the other physical parameters of the sources such as the optical and X-ray luminosity, the redshift, and the radio-loudness.

5) Spectral fits in the 0.1-4.0 keV energy range confirm the correlation between the X-ray slope in this band and the radioloudness, with the radio-loud quasars having flatter slopes than the radio-quiet ones.

6) Five out of six objects with detected soft excess emission are radio-quiet. The detection of soft excess emission in one radio-loud object (3C273) is probably due to its much higher X-ray flux.

Acknowledgements

This work was partially supported by NASA contract NAS8-30751 (HEAO-2) and NAS grant NAG5-1201 (ADI). AC acknowledge hospitality and support from Center for Astrophysics where part of this work has been done. EXOSAT team and in particular Frank Haberl and Gianpiero Tagliaferri are also thanked for help with the EXOSAT data reduction.

REFERENCES

Arnaud,K.A.,et al. 1985, *M.N.R.A.S.*, **217**, 105.

Avni Y. 1976, *Ap. J.*,**210**, 642.

Bevington,P.R. 1969, *Data Reduction and Error Analysis for the Physical Sciences*, McGraw-Hill Book Company, New York.

Canizares,C.R.,White,J.L. 1989, *Ap. J.*,**339**, 27.

De Korte,P.A.J.,et al. 1981, *Space Sci. Rev.*,**30**, 495.

Elvis,M.,et al. 1986, *Ap. J.*, **310**, 291.

Elvis,M.,Lockman,F.J.,Wilkes,B.J. 1989, *A. J.*, **97**, 777.

Elvis,M.,et al. 1991, *Ap. J. Suppl.*, in press

Fabian,A.C.,et al. 1990, *M.N.R.A.S.*, **242**, 14P.

Guilbert P.W.,and Rees M.J. 1988, *M.N.R.A.S.*, **233**, 475.

Kellerman,K.I.,et al. 1989, *A. J.*, **98**, 1195.

Kruper,J.S.,Urry,C.M.,Canizares,C.R. 1990, *Ap. J. Suppl.*, **74**, 347.

Lampton,M.,Margon,B.,Bowyer,S. 1976, *Ap. J.*, **208**, 177.

Lawrence,A.,and Elvis,M. 1982, *Ap. J.*, **256**, 410.

Lightman A.P.,and White T.R. 1988, *Ap. J.*, **335**, 57.

Masnou J.L.,Wilkes B.J.,Elvis M.,McDowell J.C.,Arnaud K. 1991, *Astr. Ap.*, submitted.

Morisawa,K.,et al. 1990, *Astr. Ap.*, **236**, 299.

Morrison,R.,and McCammon,D. 1983, *Ap. J.*, **270**, 119.

Mushotzky,R.F. 1984, *Adv.Space Res.*, **3**, 157.

Pounds K.A.,Nandra K.,Stewart G.C.,George I.M.,Fabian A.C. 1990, *Nature*, **344**, 132.

Reichert,G.A.,et al. 1985, *Ap. J.*, **296**, 69.

Schimdt,M.,Green,R.F. 1983, *Ap. J.*, **269**, 352.

Setti,G., 1990. in IAU Symposium No. 139 *"The Galactic and Extragalactic Background Radiation"*, ed. S. Bowyer and C. Leinert, p. 345.

Setti,G.,and Woltjer,L. 1989, *Astr. Ap. Letters*, **224**, L21.

Shafer,R.A.,Haberl,F.,Arnaud,K.A. 1989, *XSPEC User's Guide*.

Siegel,S., and Castellan,N.J. 1988, *Nonparametric Statistics for the Behavioral Sciences* 2^{nd} *edition*. McGraw-Hill Book Company, New York.

Tananbaum,H.,et al. 1986, *Ap. J.*, **305**, 57.

Treves,A.,et al. 1988, *Ap. J.*, **330**, 178.

Turner,M.J.L.,Smith, A.,Zimmerman,H.V. 1981, *Space Sci. Rev.*, **30**, 513.

Turner,M.J.L.,et al. 1989, in *Proceedings of the* 23^{rd} *ESLAB Symposium on Two Topics in X-ray Astronomy*, ed. J. Hunt and B. Battrick (Noordwijk : ESA), ESA SP-296, p.769.

Turner,T.J.,Pounds,K.A. 1989, *M.N.R.A.S.*, **240**, 833. **(TP89)**

Urry,C.M., et al. 1989, in *Proceedings of the* 23^{rd} *ESLAB Symposium on Two Topics in X-ray Astronomy*, ed. J. Hunt and B. Battrick (Noordwijk : ESA), ESA SP-296, p.789.

White,N.E.,Peackock,A. 1988, *Mem. Soc. Astr. It.*, **59**, 7.

Wilkes,B.J.,Elvis,M. 1987, *Ap. J.*, **323**, 243. **(WE87)**
Zamorani,G.,et al. 1981. *Ap. J.*, **245**, 357.

Table 1								
THE SAMPLE								
Coordinate	Name	z	M_B	S_X^a	L_X^b	α_{IPC}^c	α_{ox}^d	R_L^e
0003+199	PG, Mkn 335	0.025	−22.55	76.6	2.0	—	1.25	0.55
0007+106	PG, III Zw 2	0.089	−22.93	19.0	9.0	$0.4^{+1.2}_{-0.4}$	1.06	2.24
0026+129	PG	0.142	−25.13	7.0	7.6	$0.9^{+0.8}_{-0.9}$	1.43	0.34
0049+171	PG, Mkn 1148	0.064	−22.45	9.0	2.0	$0.7^{+2.0}_{-0.4}$	1.24	−0.49
0052+251	PG	0.155	−24.95	7.1	9.5	$1.1^{+2.3}_{-0.7}$	1.36	−0.61
0637−752	PKS	0.651	−27.65	6.9	230.0	$0.5^{+0.9}_{-0.4}$	1.25	3.52
0804+761	PG	0.100	−24.30	10.9	5.8	—	1.34	−0.21
0923+129	PG, Mkn 705	0.029	−21.70	8.2	0.4	—	1.41	0.32
1211+143	PG	0.085	−24.25	32.3	11.8	$1.8^{+0.8}_{-0.4}$	1.22	−0.72
1217+023	PKS	0.240	−24.60	8.6	26.0	$0.5^{+0.5}_{-0.2}$	1.14	2.38
1219+756	Mkn 205	0.070	−22.95	17.0	2.9	$0.8^{+0.2}_{-0.2}$	1.25	−0.31
1226+023	PG, 3C273	0.158	−27.43	83.4	117.0	$0.3^{+0.2}_{-0.1}$	1.32	3.06
1229+204	PG, Ton 1542	0.064	−23.58	6.5	1.5	—	1.47	−0.96
1426+015	PG, Mkn 1383	0.086	−23.90	16.0	6.7	$0.9^{+0.2}_{-0.2}$	1.26	−0.55
1501+106	PG, Mkn 841	0.036	−21.93	28.5	2.0	$1.0^{+0.4}_{-0.4}$	1.16	−0.67
2130+099	PG, II Zw 136	0.061	−23.75	8.8	1.8	$0.8^{+0.6}_{-0.4}$	1.46	0.37
2135−147	PKS, PHL 1657	0.200	−25.18	7.1	17.0	$0.5^{+0.4}_{-0.2}$	1.30	1.70

Notes:

[a] units of $10^{-12} ergs\ sec^{-1} cm^{-2}$ in the energy range 0.3-3.5 keV. Zamorani et al. (1981), Tananbaum et al. (1986).

[b] units of $10^{44} ergs\ sec^{-1}$ in the energy range 0.5-4.5 keV (the same references as S_X).

[c] from Wilkes and Elvis (1987), except for PG0049+171 (from Elvis et al. 1986) and PG0052+251 (from Elvis et al. 1991).

[d] defined in Zamorani et al. (1981).

[e] from Wilkes and Elvis (1987), when available, or computed from Kellerman et al. (1989) data.

Table 2				
Observations Log				
Objects	*Date*[a]	*Detector*	*Exposure Time*[b]	*Count Rate*[c]
0003+199	84.341	ME	32370	1.25 ± 0.03
		3lx	4732	20.00 ± 0.90
		Al/p	5321	9.39 ± 0.56
		Boron	19770	0.93 ± 0.09
0007+106	85.354	ME	22870	2.60 ± 0.04
		3lx	15671	3.50 ± 0.20
		Al/p	2291	2.65 ± 0.43
0026+129	84.198	ME	34540	0.51 ± 0.04
		3lx	5520	1.61 ± 0.22
		Al/p	5930	1.16 ± 0.18
		Boron	21008	0.43 ± 0.15
0049+171	85.334	ME	20100	0.71 ± 0.04
		3lx	18888	1.43 ± 0.12
		Al/p	3472	0.82 ± 0.21
0052+251	85.354	ME	22170	0.30 ± 0.04
		3lx	10841	1.65 ± 0.16
		Al/p	5863	0.92 ± 0.17
0637-752	84.252	ME	15030	0.41 ± 0.04
		3lx	14340	0.50 ± 0.08
0804+761	85.075	ME	26090	0.81 ± 0.03
		3lx	4237	3.30 ± 0.30
		Al/p	5563	2.50 ± 0.30
		Boron	10735	0.35 ± 0.13
0923+129	85.129	ME	12220	1.02 ± 0.08
		3lx	3110	2.70 ± 0.40
		Al/p	6568	1.80 ± 0.20
		Boron	13026	0.43 ± 0.15
1211+143	85.164	ME	24470	0.88 ± 0.04
		3lx	1257	20.2 [illegible] 1.50
		Al/p	3539	8.8[illegible] 0.62
		Boron	16560	0.88 ± 0.25
1217+023	84.029	ME	17880	0.44 ± 0.09
		3lx	5052	2.54 ± 0.28
		Al/p	7968	1.17 ± 0.16

Table 2 (cont.)				
Observations Log				
Objects	*Date*[a]	*Detector*	*Exposure Time*[b]	*Count Rate*[c]
1219+756	84.027	ME	9950	0.57 ± 0.07
		3lx	1679	2.94 ± 0.51
		Al/p	5293	1.34 ± 0.21
1226+023	85.138	ME	22820	6.27 ± 0.04
		3lx	5424	26.00 ± 1.00
		Al/p	3332	13.30 ± 0.82
		Boron	10546	2.20 ± 0.19
1229+204	85.159	ME	49730	0.40 ± 0.02
		Al/p	11194	2.95 ± 0.21
		Boron	21197	0.56 ± 0.17
		4lx	2824	6.21 ± 0.57
		PPL	3156	6.97 ± 0.58
1426+015	85.187	ME	21810	0.83 ± 0.04
		3lx	4689	4.63 ± 0.39
		Al/p	3599	2.71 ± 0.35
		Boron	10056	0.27 ± 0.12
1501+106	86.053	ME	19860	1.14 ± 0.04
		3lx	1998	9.55 ± 0.86
		Al/p	3713	3.92 ± 0.41
2130+099	85.318	ME	26130	0.49 ± 0.03
		3lx	4090	5.64 ± 0.47
		Al/p	3325	3.26 ± 0.39
		Boron	15327	0.54 ± 0.17
2135-147	84.133	ME	28560	0.71 ± 0.05
		3lx	4863	2.14 ± 0.27
		Al/p	8033	1.20 ± 0.16
		Boron	11691	0.34 ± 0.12

Notes:

[a] Year and Day

[b] Seconds

[c] Counts per second (units of 10^{-2} for the LE filters).

Table 3					
Single Power Law fits to the ME Data assuming Galactic N_H					
Objects	Channels	*Flux*[a]	α	$N^b_{H_{gal.}}$	$\chi^2_\nu/d.o.f.^c$
0003+199	7-35	12.6	$1.11^{+0.13}_{-0.13}$	4.00	1.01/27
0007+106	7-35	29.6	$0.68^{+0.08}_{-0.07}$	6.09	0.75/27
0026+129	7-25	5.7	$0.86^{+0.39}_{-0.38}$	4.93	0.67/17
0049+171[d]	7-25	7.6	$1.03^{+0.30}_{-0.29}$	4.26	1.98/17
0052+251	7-26	3.7	$0.84^{+0.58}_{-0.52}$	4.50	1.26/18
0637-752	7-29	4.1	$0.93^{+0.64}_{-0.60}$	4.80	0.61/21
0804+761	7-25	8.3	$0.92^{+0.23}_{-0.23}$	3.12	0.93/17
0923+129	7-24	10.0	$0.75^{+0.44}_{-0.44}$	4.03	0.98/16
1211+143	7-25	8.5	$1.02^{+0.23}_{-0.22}$	2.83	1.38/17
1217+023	7-25	4.3	$1.16^{+1.35}_{-1.11}$	1.97	1.00/17
1219+756	7-28	6.0	$1.17^{+0.67}_{-0.60}$	2.74	0.84/20
1226+023	7-35	68.8	$0.53^{+0.03}_{-0.03}$	1.80	1.00/27
1229+204	7-29	3.8	$1.14^{+0.33}_{-0.31}$	2.58	1.07/21
1426+015	7-35	8.5	$0.46^{+0.25}_{-0.25}$	2.64	0.81/27
1501+106	7-35	14.3	$0.42^{+0.16}_{-0.16}$	2.23	1.53/27
2130+099	7-30	4.8	$1.27^{+0.36}_{-0.36}$	4.20	0.84/22
2135-147	7-30	7.6	$0.83^{+0.33}_{-0.31}$	4.45	0.99/22

Notes:

[a] units of $10^{-12} ergs\ cm^{-2} sec^{-1}$ in the energy range 2-8 keV

[b] units of $10^{20} atoms\ cm^{-2}$, from Elvis Lockman and Wilkes (1989), except for 0003+199 (TP89), and 1226+023 (WE87)

[c] degrees of freedom

[d] For PG0049+171 the Galactic N_H is excluded at more than 99 % confidence by the fit to the data. Leaving N_H free to vary, the best fit parameters are $\alpha \simeq 3.5$ and $N_H \sim 8 \times 10^{22} atoms\ cm^{-2}$, with a reduced χ^2 of 1.29 with 16 d.o.f. (see discussion in the test).

Table 4						
Single Power Law fits to the ME+LE Data						
Objects	α	$\frac{N_H^a}{N_{Hgal.}^a}$	$\chi^2_\nu/d.o.f.^b$	$\Delta\chi^2/n.o.f^c$	Classification	R_{cs}^d
0003+199	$0.68^{+0.03}_{-0.03}$	0.0-0.007	2.30/29	39.75/3	Soft Excess	$2.74^{+0.48}_{-0.38}$
	$1.64^{+0.05}_{-0.05}$	4.00	6.47/30	167.05/3		
0007+106	$0.68^{+0.10}_{-0.10}$	$6.0^{+2.4}_{-1.8}$	0.72/28	4.86/2	Single P.L.	$0.00^{+0.09}_{-0.09}$
	$0.68^{+0.04}_{-0.04}$	6.09	0.70/29	0.08/2		
0026+129	$1.00^{+0.44}_{-0.38}$	$4.0^{+7.3}_{-2.8}$	0.65/19	1.04/3	Single P.L.	$0.49^{+0.57}_{-0.39}$
	$1.07^{+0.10}_{-0.11}$	4.93	0.63/20	1.21/3		
0049+171	$1.72^{+0.44}_{-0.40}$	$8.1^{+10.0}_{-5.5}$	1.91/18	13.66/2	Single P.L.	$-0.39^{+0.23}_{-0.18}$
	$0.79^{+0.07}_{-0.08}$	4.26	1.90/19	2.45/2		
0052+251	$0.95^{+0.52}_{-0.42}$	$2.1^{+5.3}_{-2.1}$	1.22/19	3.65/2	Single P.L.	$1.14^{+1.40}_{-0.77}$
	$1.23^{+0.12}_{-0.12}$	4.50	1.25/20	2.01/2		
0637-752	$0.95^{+0.06}_{-0.82}$	$11.9^{+33.5}_{-11.2}$	0.61/21	0.04/1	Single P.L.	$-0.45^{+0.60}_{-0.28}$
	$0.61^{+0.10}_{-0.17}$	4.80	0.62/22	0.80/1		
0804+761	$1.02^{+0.22}_{-0.22}$	$2.7^{+2.3}_{-1.4}$	1.18/19	6.72/3	Single P.L.	$0.42^{+0.34}_{-0.27}$
	$1.07^{+0.06}_{-0.06}$	3.12	1.14/20	6.99/3		
0923+129	$0.87^{+0.36}_{-0.31}$	$2.9^{+5.0}_{-1.9}$	0.94/18	1.12/3	Single P.L.	$0.51^{+0.71}_{-0.44}$
	$0.97^{+0.10}_{-0.11}$	4.03	0.91/19	1.57/3		
1211+143	$1.48^{+0.13}_{-0.06}$	$1.4^{+0.6}_{-0.3}$	2.63/19	28.44/3	Soft Excess	$3.87^{+1.10}_{-0.83}$
	$1.76^{+0.06}_{-0.06}$	2.83	3.12/20	38.99/3		
1217+023	$0.94^{+0.81}_{-0.38}$	$1.5^{+4.1}_{-1.5}$	0.96/18	0.12/2	Single P.L.	$-0.27^{+1.96}_{-0.40}$
	$1.02^{+0.19}_{-0.14}$	1.97	0.92/19	0.32/2		
1219+756	$0.89^{+0.75}_{-0.36}$	$1.7^{+11.7}_{-1.7}$	0.83/21	0.72/2	Single P.L.	$-0.28^{+0.62}_{-0.29}$
	$1.02^{+0.22}_{-0.19}$	2.74	0.81/22	1.10/2		
1226+023	$0.53^{+0.05}_{-0.05}$	$0.6^{+0.2}_{-0.2}$	2.63/29	49.59/3	Soft Excess	$1.00^{+0.11}_{-0.09}$
	$0.66^{+0.03}_{-0.04}$	1.80	5.79/30	146.50/3		
1229+204	$1.39^{+0.19}_{-0.18}$	$1.3^{+0.8}_{-0.9}$	1.05/24	2.64/4	Soft Excess	$1.88^{+0.91}_{-0.59}$
	$1.64^{+0.06}_{-0.05}$	2.58	1.38/25	11.97/4		
1426+015	$0.38^{+0.08}_{-0.06}$	0.0-0.023	0.90/29	4.41/3	Soft Excess	$3.26^{+1.17}_{-0.88}$
	$1.10^{+0.07}_{-0.07}$	2.64	1.65/30	27.54/3		
1501+106	$0.46^{+0.10}_{-0.08}$	0.0-0.051	1.49/28	0.41/2	Soft Excess	$3.94^{+0.84}_{-0.70}$
	$1.10^{+0.07}_{-0.07}$	2.23	3.34/29	55.53/2		
2130+099	$1.45^{+0.32}_{-0.30}$	$2.6^{+2.8}_{-1.4}$	0.85/24	1.97/3	Single P.L.	$1.19^{+0.92}_{-0.59}$
	$1.66^{+0.08}_{-0.08}$	4.20	0.90/25	3.93/3		
2135-147	$0.78^{+0.34}_{-0.28}$	$2.4^{+4.3}_{-1.7}$	0.92/24	0.11/3	Single P.L.	$0.32^{+0.43}_{-0.31}$
	$0.96^{+0.09}_{-0.10}$	4.45	0.95/25	1.81/3		

Notes:

[a] units of 10^{20} *atoms* cm^{-2}

[b] degrees of freedom

[c] drop on χ^2 from ME to ME+LE over the number of LE filters

[d] ratio of the observed minus predicted counts to the predicted counts in the Al/p and 3000Lex filters. The predicted counts are computed by extrapolating the ME best fit. The errors are 1σ.

Table 5								
DOUBLE POWER LAW AND BLACKBODY + POWER LAW FITS								
Object	α_{steep}	$\chi^2_\nu/d.o.f.^a$	$P(\chi^2)$	E^b_{break}	$kT\ (eV)$	$\chi^2_\nu/d.o.f.^a$	$P(\chi^2)$	E^b_{break}
0003+199	$4.22^{+0.58}_{-0.49}$	1.62/30	0.018	0.48	46^{+10}_{-7}	1.01/30	0.45	0.49
1211+143	$3.33^{+0.66}_{-0.42}$	1.45/20	0.085	0.67	57^{+19}_{-14}	1.18/20	0.26	0.61
1226+023	$2.66^{+0.45}_{-0.34}$	1.98/30	0.001	0.35	70^{+16}_{-14}	1.32/30	0.12	0.50
1229+204	$3.32^{+1.30}_{-0.87}$	0.92/25	0.580	0.46	45^{+15}_{-12}	0.94/25	0.56	0.44
1426+015	$2.66^{+1.09}_{-0.49}$	0.91/30	0.610	0.66	79^{+32}_{-27}	0.77/30	0.81	0.76
1501+106	$2.87^{+1.07}_{-0.48}$	1.45/29	0.057	0.64	57^{+39}_{-19}	1.43/29	0.064	0.54

Notes:

[a] degrees of freedom

[b] keV (at the source)

FIGURE CAPTIONS

Fig. 1

The χ^2 contours for the power law spectral fit to the ME data. The X axis is the logarithm of the absorbing column density of neutral hydrogen (units of 10^{22} *atoms* cm^{-2}) and the Y axis is the power law photon index. The contours are 68 %, 90 %, 99 %, joint confidence limits. The vertical line marks the column density expected due to absorption in our galaxy as measured by 21 cm emission (Elvis, Lockman and Wilkes 1989).

Fig. 2

Distribution of the hard X-ray (2-10 keV) spectral energy indices of our sample. The dashed part of the hystogram represents objects with 1σ error on the slope smaller than 0.20. The gaussian curve is taken from Turner and Pounds (1989) and describes the best fit energy index distribution of their sample.

Fig. 3

ME spectral energy index values versus the logarithm of the X-ray luminosity (*ergs* sec^{-1}). We have marked with filled circles the objects of our sample, with open circles the Seyfert 1 galaxies and quasars in the Turner and Pounds (1989) sample and with open triangles the three objects in common.

Fig. 4

Distribution of ΔN_H (in units of 10^{20} *atoms* cm^{-2}) defined as the difference between the N_H value obtained through the fit of a single power law over the full energy range ($\sim 0.1 - 10$ *keV*) and the Galactic value obtained by radio measurements (Elvis, Lockman and Wilkes 1989). The objects with detected soft excess emission are marked with an S.

Fig. 5

a) ME spectral energy index values versus the radio-loudness index R_L.

b) 0.1-4.0 keV energy index values versus the radio-loudness index R_L.

We have marked with open circles the objects with soft excess emission and with filled circles the others. The line gives the WE87 correlation.

Fig. 6

ME spectral energy index values versus the 0.1-4.0 keV ones. Circles and triangles represent radio-quiet and radio-loud objects respectively. The objects with soft excess are represented with open symbols.

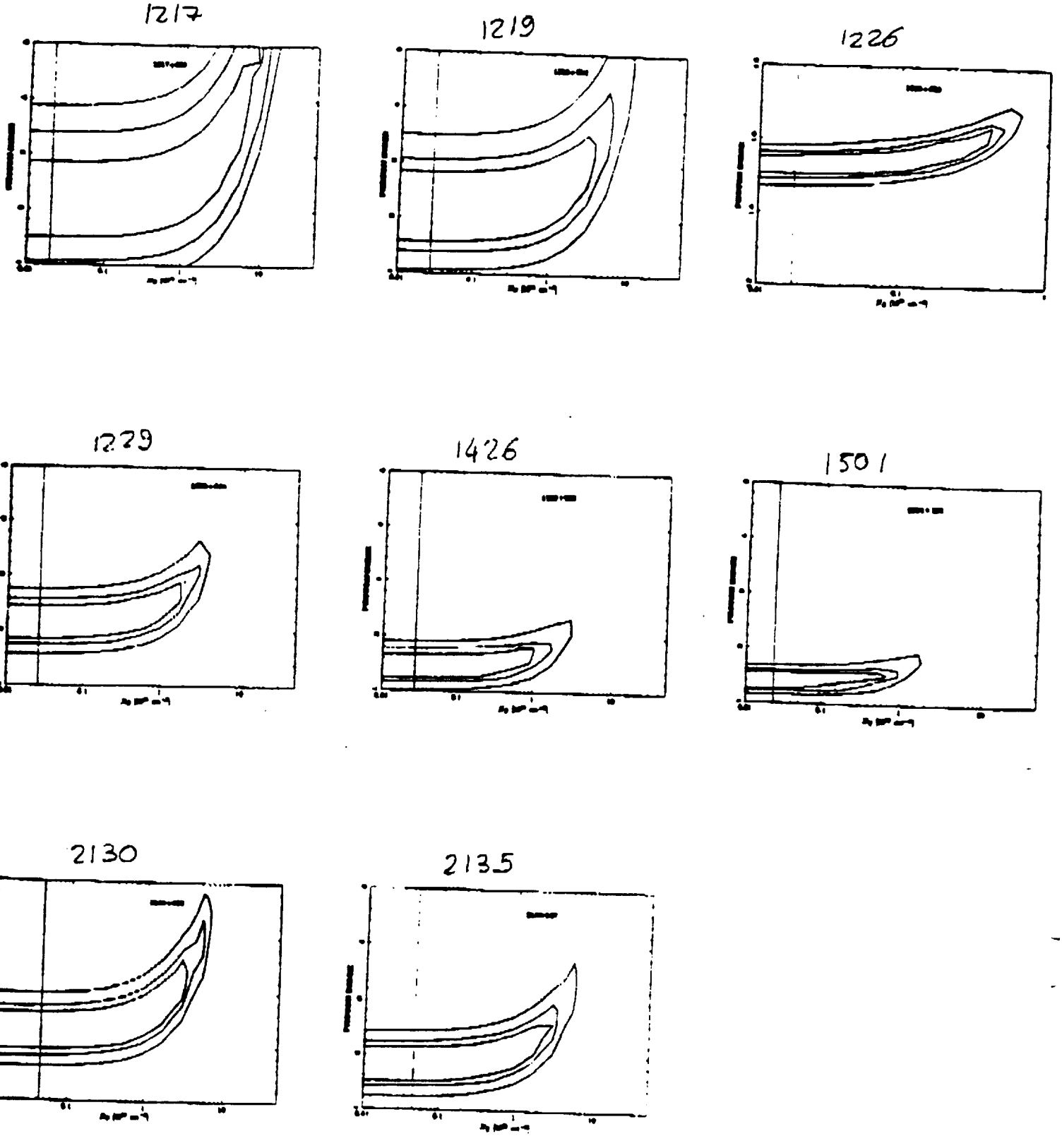

FIGURE 1

ORIGINAL PAGE IS
OF POOR QUALITY

0003

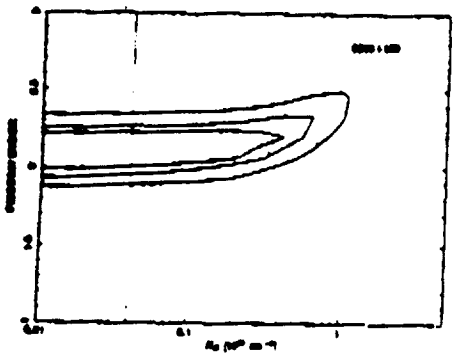

0007

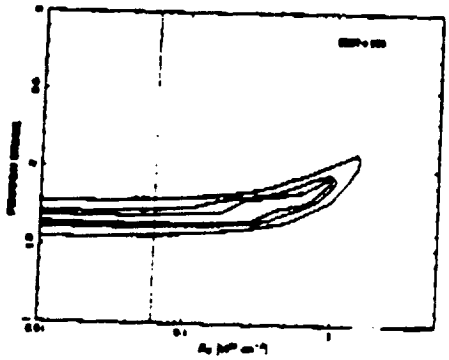

0026

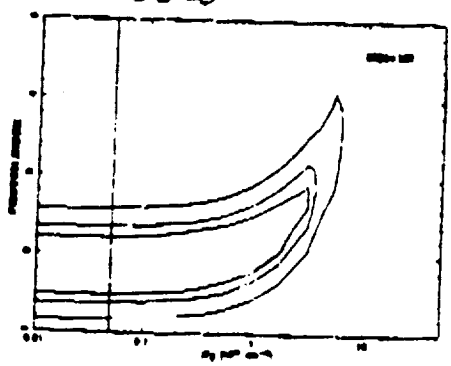

0049

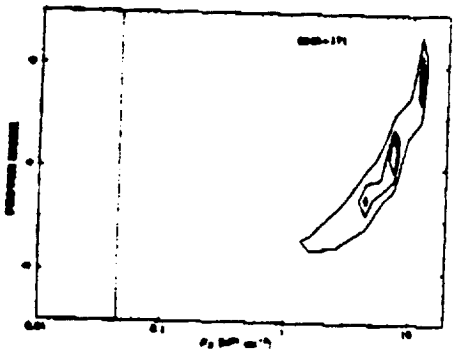

0052

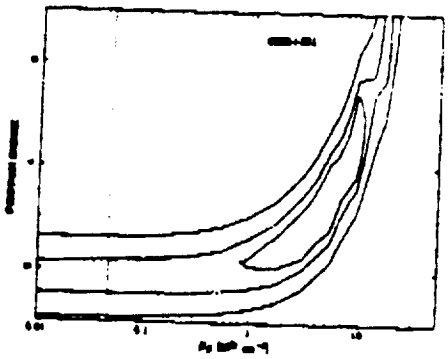

0637

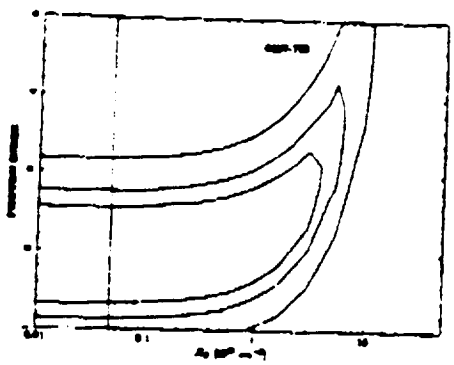

0804

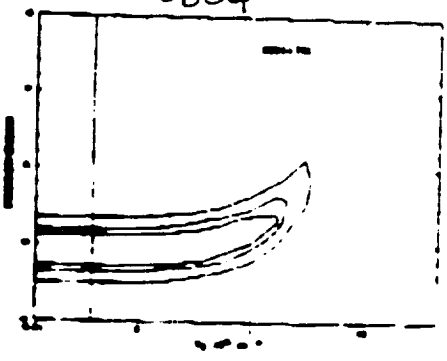

0923

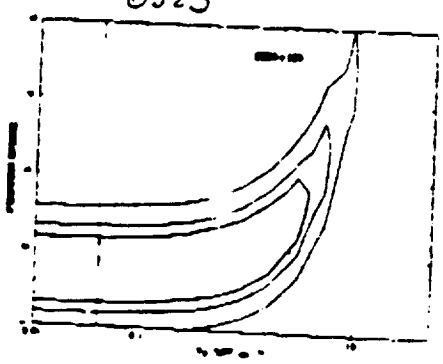

1211

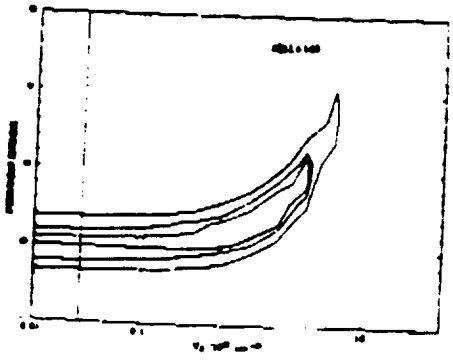

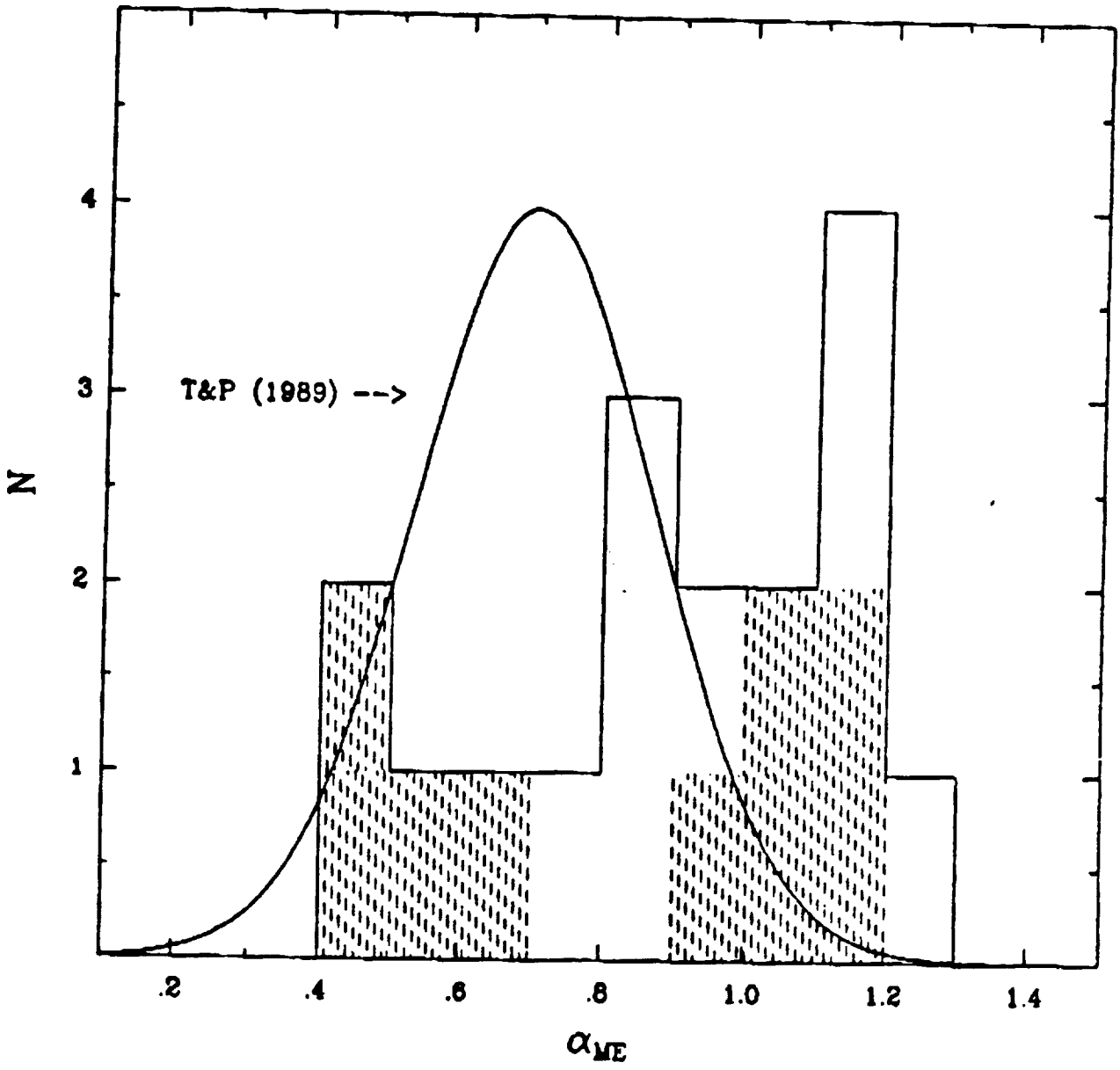

FIGURE 2

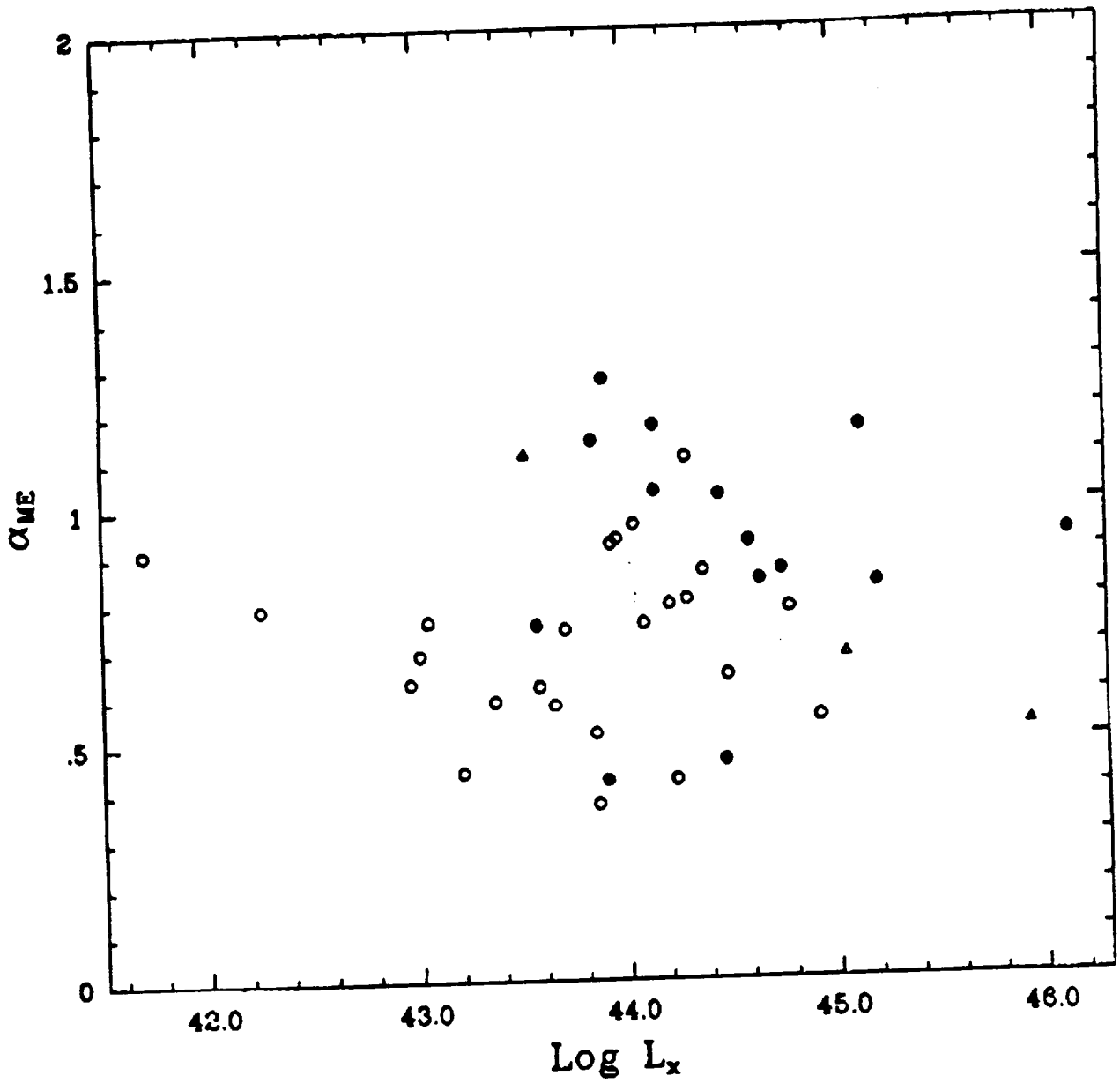

FIGURE 3

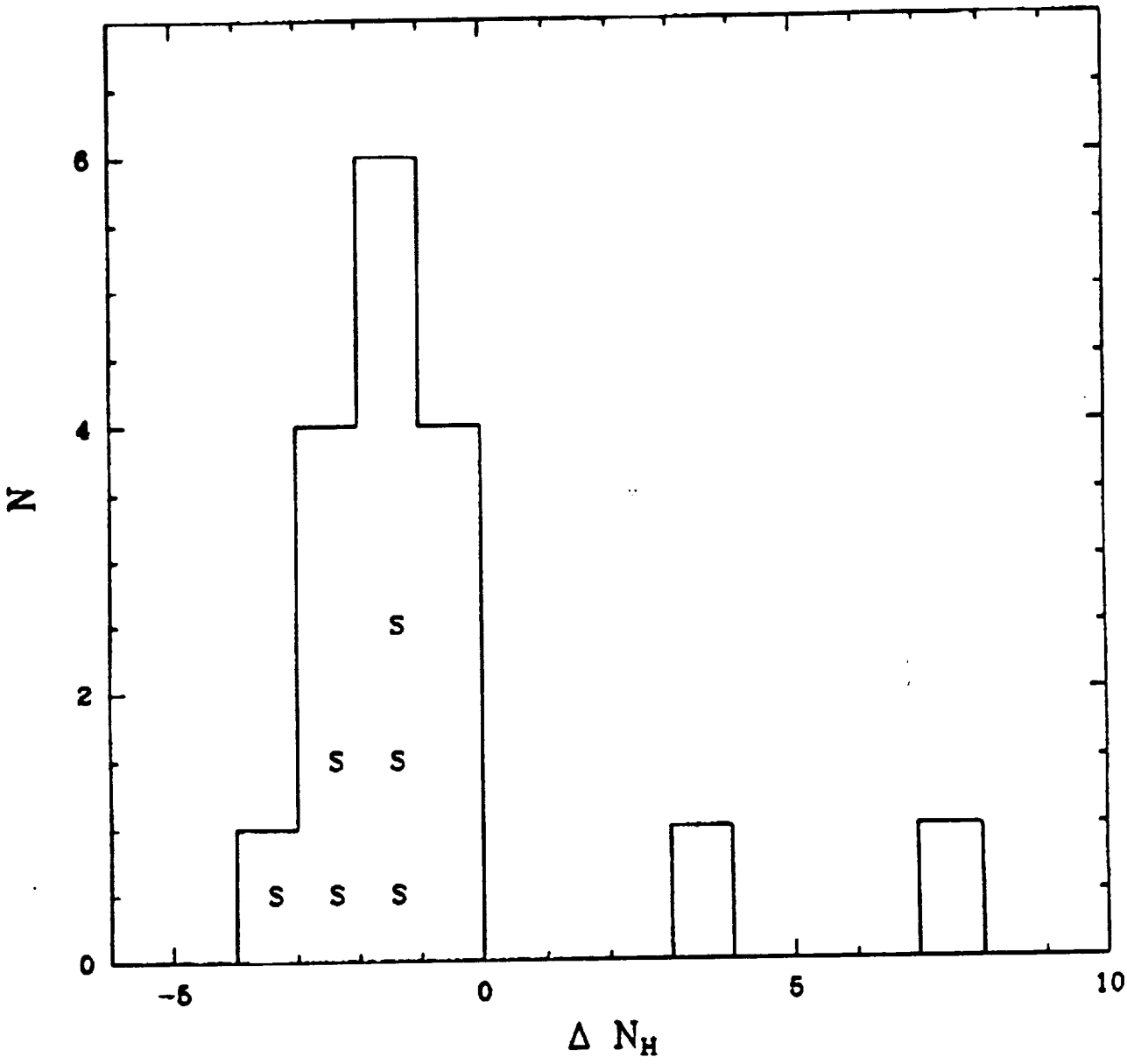

FIGURE 4

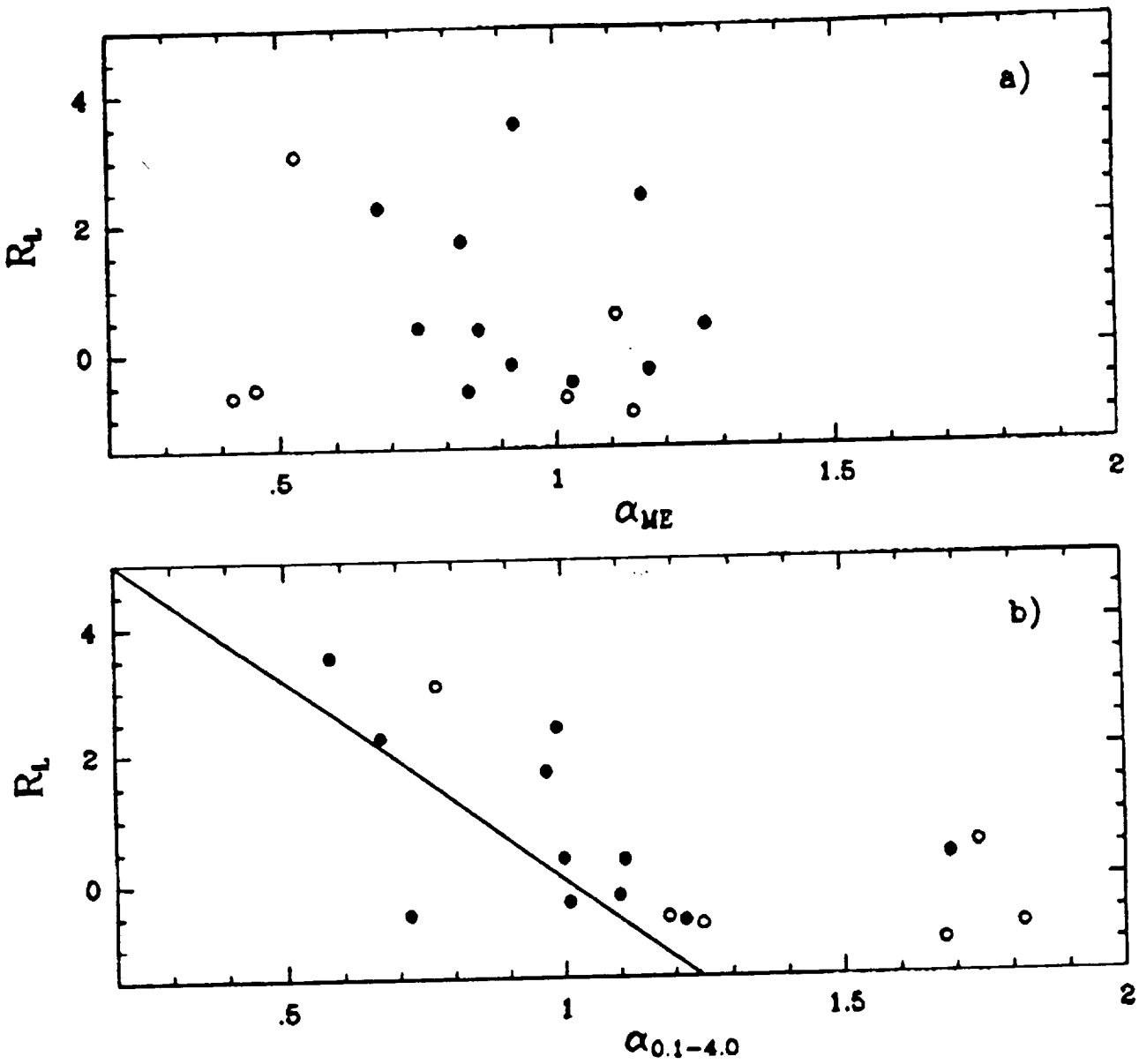

FIGURE 5

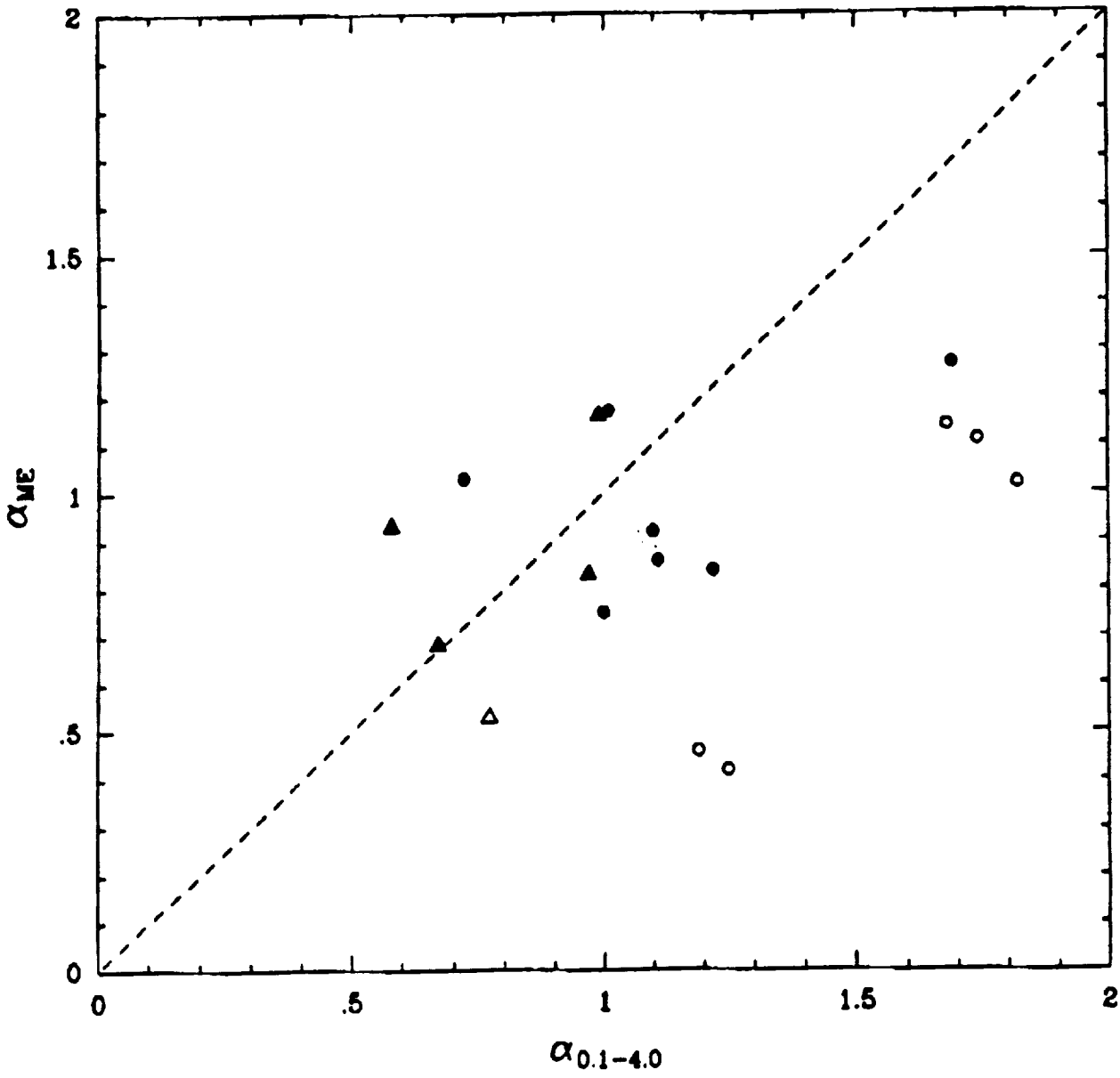

FIGURE 6

AUTHORS' ADDRESSES

A. COMASTRI, and G. SETTI:
Istituto di Radioastronomia del CNR, via Irnerio 46, 40126 Bologna, Italy
G. ZAMORANI:
Osservatorio Astronomico, via Zamboni 33, 40126 Bologna, Italy
M. ELVIS, B. J. WILKES, J. C. MCDOWELL:
Harvard-Smithsonian Center for Astrophysics, 60 Garden Street, Cambridge, MA 02138
P. GIOMMI:
Code SAE, ESTEC, Postbus 229, 2200 AG Noordwijk, The Netherlands